Genetic inactivation of Alzheimer's disease risk gene CD33 in human macrophages causes changes in gene signalling and cell function

SHUANG PU

A thesis submitted in partial fulfilment of the requirements of Manchester Metropolitan University for the degree of Doctor of Philosophy

Department of Life Sciences

Manchester Metropolitan University

2023

Table of Contents

List of Figures

List of Abbreviations

AD: Alzheimer's disease
ADtg: AD transgenic models
Aβ: Amyloid-β protein
APP: Amyloid precursor protein
ApoE: Apolipoprotein E
AV: Autophagic vacuole
BACE1: β-secretase 1
BBB: Blood–brain barrier
BNIP3: BCL2/adenovirus E1B 19 kDa protein-interacting protein 3
CD33: Sialic acid binding Ig-like lectin 3
CCR2: c-c chemokine receptor type 2
CNS: Central nervous system
CAA: Cerebral amyloid angiopathy
CSF: Cerebrospinal fluid
CMA: Chaperone-mediated autophagy
DAMPs: Damage-associated molecular patterns
ECE-1: Endothelin-converting enzyme 1
ER: endoplasmic reticulum
FAD: Familial Alzheimer's disease
GWAS: Genome-wide association study
GFP: Green fluorescent protein
pTau: Hyperphosphorylated tau
ITIM: Immunoreceptor tyrosine-based inhibition motif
IL-1β: Interleukin-1β
IL-10: Interleukin-10
ISF: Interstitial fluid
Iba1: Ionized calcium binding adapter molecule 1
JAK1: Janus kinase 1
JAK2: Janus kinase 2
JAK3: Janus kinase 3
STAT3: signalling transducer and activator of transcription 3
LOAD: Late-onset AD
LPS: Lipopolysaccharide
LRP-1: Low-density lipoprotein-related protein 1
LDLR: Low-density lipoprotein receptor
LC3b: Microtubule-associated protein 1 light chain 3
LAMP2: Lysosomal-associated membrane protein 2
M-CSF: Macrophage colony-stimulating factor
SCARA1: Macrophage scavenger receptor 1
mTOR: Mammalian target of rapamycin
MMP-9: Matrix metalloproteinase-9
MCP-1: Monocyte chemotactic protein 1
MSR1: Macrophage scavenger receptor 1
NFTs: Neurofibrillary tangles
PBMC: Peripheral blood monocyte

PICALM: Phosphatidylinositol binding clathrin assembly protein
PS1; PS2: Presenilin-1 and -2
PAMPs: Pathogen-associated molecular patterns
ptau: Hyperphosphorylated tau protein
p62: sequestosome 1(SQSTM1)
ROS: Reactive oxygen species
RFP: Red fluorescent protein
CD33: Sialic acid-binding immunoglobulin-like lectin 3
SNP: Single nucleotide polymorphism
TLR: Toll-like receptor
TGF-β: Transforming growth factor β
TREM2: Triggering receptor on myeloid cells 2
TNFα: Tumor necrosis factor
Tyk2: Tyrosine kinase 2
UPS: Ubiquitin–proteasome system
APP: Amyloid precursor protein
BACE1: Beta-site amyloid precursor protein cleaving enzyme 1
PEN2: Presenilin enhancer 2
NFTs: Neurofibrillary tangles
PHFs: Paired helical filaments
SFs: Straight filaments
p38-MAPK: P38 mitogen-activated protein kinase
PRRs: Pattern-recognition receptors
DAMPs: Damage-Associated Molecular Patterns
TLRs: Characterization of Toll-like receptors
FcR: Fc receptors
CR: Complement receptors
MAPK: Mitogen-activated protein kinase
NLRs: Nucleotide oligomerization domain (NOD)-like receptors
NLRPs: Pyrin domain-containing protein
CARD domain-containing protein (NLRC) subfamily
NAIP: Apoptosis inhibitory protein
CIITA: NLRX1 and Class II major histocompatibility complex transactivator
LRRs: Leucine-rich repeats
CARDs: Caspase recruitment domains
ASC: Apoptosis associated speck-like protein containing a CARD domain
RIG-I: Retinoic acid-inducible gene I
MDA-5: Melanoma differentiation-associated gene-5
LGP-2: Laboratory of genetics and physiology-2
dsRNA: Double-stranded RNA
IFN: Type-I interferon
CLRs: C-type lectin receptors
CTLD: C-type lectin-like domain
Fcγs: Fc receptor common gamma chain
GPI: Glycosylphosphatidylinositol
LAMP-2A: Membrane protein 2A
RTK: Receptor tyrosine kinase

DAPK: Death-associated protein kinase
mTORC1: mTOR Complex 1
mTORC2: mTOR Complex 2
Rheb: Ras homolog enriched in brain
FOXO: Forkhead box O
EMT: Epithelial–mesenchymal transition
GM-CSF: Macrophage colony-stimulating factor
G-CSF: Granulocyte colony-stimulating factor
EGF: Epidermal growth factor
TNF: Tumor necrosis factor
μm: Micrometer
mM: Millimolar
mg: Milligram
μg: Microgram
°C:Degree Celsius

Declaration

This thesis is the result of my own work and includes nothing which is the outcome of work done in collaboration except as specified in the text and declared here:

- CD33 knockout U937 human monocyte using CRISPR/Cas9 technology was performed in collaborating lab at the University of Alberta, Canada and cells were kindly provided by Prof Matthew S. Macauley (University of Alberta, Canada).
- RNA deep sequencing analysis was performed by BGI Genomics (Shenzhen, China).

This thesis is not substantially the same as any work that has already been submitted before for any degree or other qualification.

Acknowledgements

First and foremost, I would like to thank my supervisors Professor Mark Slevin and Dr Baoqiang Guo for giving me the opportunity to do a PhD at MMU, and thank Professor Xianwei Zeng for funding this project, and for their endless support and invaluable guidance throughout the course of my study. I doubt I will ever be able to convey my appreciation fully, but I dedicate to both of you all the success I had or will have in my future career life. To my director of studies Dr.Baoqiang Guo; without your expertise, friendship, encouragement, and guidance, I could never have completed this PhD and become the scientist I am today. And I would like to especially thank the great efforts Dr. Baoqiang Guo devoted to our cell model in this project. It was a real privilege to be part of your research team during the last three years. We have shared some great moments inside and outside the labs, and now that I am submitting my thesis, I feel so proud of what we have achieved together.

To Professor Mark Slevin; thank you for offering me the chance to pursue my research studies and be a member of your fantastic research group. I would like to express my sincere appreciation and thanks to you for all the experimental advice, help, and continuous support.

To Professor Xianwei Zeng; thank you for the generous funding for the RNA deep sequencing which provided our group with a promising insight for future work.

Special thanks to Dr. Matthew Macauley (Department of Medical Microbiology and Immunology, University of Albert, Canada) for generously providing the U937CD33WT and U937 CD33KO cell lines, and thanks to Professor Sonia Correa-Muller for providing the antibodies for my work, without which I could never finish my work in such a limited period.

To Professor Zhenbo Hu and all colleagues in China, thank you all for offering me a chance to carry on the research work in your lab during the lockdown of the COVID-19 pandemic.

Special thanks to the MMU staff and my friends (Jiandong, Zhimin, Runze, Leijin, Sana, Razan, Maria, Marta and Subhan) who worked together on the second and third floors,

without your help and support, I can never finish this. My time at MMU could never have been the same without you guys. I have learned so much with you guys and wish you every success in your career.

To the most important and inspirational persons in my life, my mum and dad who always support me. I can never thank you enough and will be eternally grateful to you for everything you have done for me. I hope reading this thesis will make you feel proud of your daughter.

Finally, I would like to express my heartfelt gratitude to everyone who supported me whenever I encountered challenges beyond my own capabilities to solve. Without your unwavering assistance, I would not have been able to complete this PhD journey. This achievement is dedicated to all of you.

Abstract

Late-onset sporadic AD (LOAD), the most common form of dementia, is influenced by multiple risk genes identified by Genome-Wide Association Studies (GWAS). Among these, the sialic acid receptor CD33 has emerged as a significant factor due to its strong negative correlation with phagocytic capabilities, which is essential for the clearance of AD hallmark—amyloid β (Aβ). Current understanding of CD33 in Aβ plaque clearance and AD pathology is insufficient. Thus, in this project, the human U937 monocyte-derived macrophage model was developed to investigate CD33 signaling pathway in Aβ plaque clearance and its implications for LOAD.CRISPR/Cas9 technology was used to generate human CD33KO-U937 monocytes. Both CD33 wild type (CD33WT) and knockout (CD33KO) U937 monocytes were differentiated into macrophages using PMA treatment and total RNA was extracted for RNA deep sequencing. Key gene expression changes were validated by RT-qPCR and Western blot assays. Phagocytosis assays using fluorescent beads and pre-aggregated $A\beta_{40}$ and $A\beta_{42}$, were analyzed by flow cytometry and confocal microscopy to assess the impact of CD33 on phagocytic capacity. Holomonitor and scanning electron microscopy were applied to examine changes in macrophage mobility and morphology following CD33 knockout. The results demonstrated significant changes in multiple signaling pathways due to CD33 knockout, impacting immune response, cell proliferation, differentiation, apoptosis, autophagy, phagocytosis, and cell migration. Key findings, validated by RT-qPCR, Western blot, and fluorescence confocal microscopy indicated that CD33 knockout :(i) enhanced Aβ clearance through phagocytosis and autophagy-mediated Aβ degradation;(ii)resulted in dramatic increase of phagocytosis related gene MSR1 expression;(iii)elevated LAMP2 and LC3b expression, indicating enhanced lysosomal degradation; (iv)inhibited both JAK/STAT3 signaling, and PDK1/PI3K/AKT signalling, then promoted autophagy activity in macrophages;(v)exhibited increase in IL-1β, TNF-α, and NOX2, accompanied by increased anti-inflammatory IL-1RN expression to counterbalance pro-inflammatory effects;(vi) enhanced cell motility resulting from elevated chemokines (CCL2, CCL3, CCL7) to boost Aβ clearance. In summary, this thesis provides insights into the signalling changes related to Aβ clearance in CD33KO-U937 monocyte-derived macrophage model,and sheds new light on possible future therapeutic strategies for Alzheimer's disease.

Chapter 1 Introduction

1. Alzheimer's disease
1.1 Overview of Alzheimer's disease

Alzheimer's disease (AD) is a progressive neurological disorder first discovered by Alois Alzheimer in 1907, and it remains the most prevalent form of dementia(Ballard et al., 2011).AD affects at least 27 million people worldwide, which accounts for 60 -70% of all dementia cases(Ferreira et al., 2014).It is a neurodegenerative disorder that primarily impacts the brain and leads to a progressive decline in neuronal function and cognitive deficits(Lane et al., 2018, Weller and Budson, 2018, McKhann et al., 2011).Two forms of AD have been classified: early-onset familial AD(FAD) and late-onset sporadic AD (LOAD). The incidence of FAD accounts for less than 10% of all AD cases(Wu et al., 2012), characterized by an early age typically before 65 years old with a well-defined familial inheritance pattern, however, LOAD constitutes the majority, accounting for approximately 90% of all AD cases(Dorszewska et al., 2016). LOAD, mainly occurring after the age of 65, is sporadic and exhibits a non-mendelian inheritance pattern. FAD has a well-characterized familial inheritance caused by mutations of amyloid precursor protein (APP) on human Chromosome 21, presenilin 1(PSEN1) on human Chromosome 14, and presenilin 2 (PSEN2) on human Chromosome 1(Cacace et al., 2016).

LOAD is the most prevalent form of AD cases induced by a complex of causes of gene mutation, age, and environmental and lifestyle factors, such as smoking and excessive alcohol etc, however, early onset AD is more likely to be linked and influenced by mutation of AD-risk genes and tends to be familiar-inheritance compared to sporadic occurrence of LOAD. Over decades, researchers have focused on the study of pathogenesis, risk factors and treatments for LOAD, great progress has been made from their contribution, however, a full understanding of its mechanism for pathogenesis as well as treatment remains elusive.

1.2 Causes and risk factors of AD

AD is characterized by two key pathological hallmarks: amyloid plaques and neurofibrillary tangles(Ballard et al., 2011). It is recognized as a multifactorial disease, with two primary hypotheses proposed to explain its etiology: the cholinergic hypothesis and the amyloid

hypothesis. Additionally, numerous other risk factors have been identified, including aging, genetics, environmental influences, diet, metals, infections, obesity, diabetes, head injuries, and vascular diseases(Breijyeh and Karaman, 2020).

Currently, the leading theories regarding the primary cause of AD pathology focus on the excessive deposition and impaired clearance of amyloid-beta plaques, as well as damage to cholinergic function. Based on these insights, researchers have developed two major hypotheses: the Amyloid Hypothesis and the Cholinergic Hypothesis.

1.2.1 Amyloid Hypothesis

Over the decades, the amyloid hypothesis has remained a widely accepted theory to explain AD pathology. Initially proposed through studies on early-onset familial AD, this hypothesis has since been extended to encompass all forms of AD(R, 2019). The amyloid hypothesis is mainly illustrated as the aggregation and deposition of Aβ peptides (Aβ_{40} and Aβ_{42}), especially Aβ_{42}. The peptides, particularly A$\beta_{42,}$ tend to form into soluble aggregates and insoluble fibrils. As these insoluble fibrils accumulate, an imbalance arises between the production and clearance of amyloid peptides, eventually resulting in dense amyloid plaques in the brain. These plaques further trigger a cascade of pathological processes, including neuroinflammation and Tau pathology. This ultimately leads to neuronal dysfunction, synaptic loss, kinase deregulation, and progressive neurodegeneration, which culminates in the cognitive deficits observed in AD patients(Karran and De Strooper, 2022, Breijyeh and Karaman, 2020, Jeremic et al., 2021)(**Figure 1**).
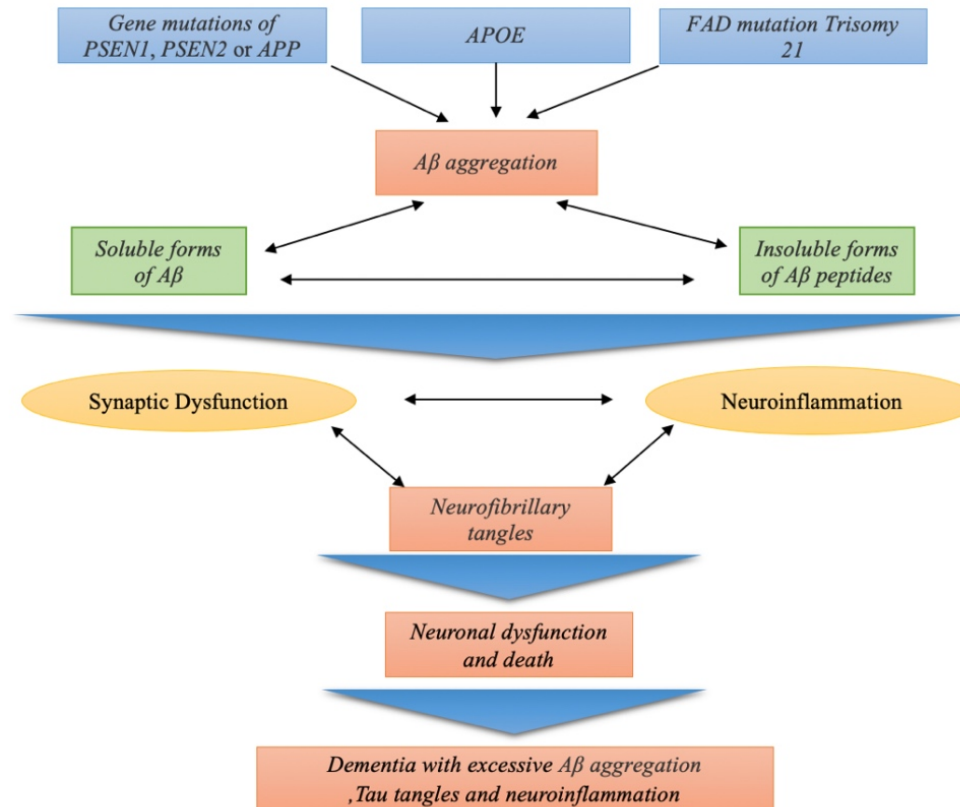
Figure 1. The illustration of the Amyloid Hypothesis in AD. Gene mutations such as PSEN1, PSEN2, and APOE disrupt amyloid beta metabolism, particularly affecting Aβ42, which aggregates into insoluble fibrils. Accumulation of these fibrils in the brain creates an imbalance in amyloid peptide production and clearance, forming dense plaques that trigger neuroinflammation and Tau pathology. This cascade leads to neuronal dysfunction, synaptic loss, kinase deregulation, and progressive neurodegeneration, culminating in the cognitive deficits seen in Alzheimer's Disease. Figure drawn based on information in (Ballard et al., 2011) (Breijyeh and Karaman, 2020).

1.2.2 Cholinergic Hypothesis

In the 1970s, researchers discovered that deficits in neocortical and presynaptic cholinergic systems were linked to the enzyme choline acetyltransferase (ChAT), which is essential for the synthesis of acetylcholine (ACh). Given the crucial role of ACh in cognitive function, the cholinergic hypothesis of Alzheimer's disease was proposed(Breijyeh and Karaman, 2020). ACh is involved in key physiological processes including memory, learning, and various other critical functions. In the brains of AD patients, the synthesis of ACh is compromised due to the degradation and loss of cholinergic neurons. This leads to reduced ACh release, resulting in cholinergic dysfunction, memory loss, and cognitive impairment.The involvement of Aβ in AD pathology has been associated with disturbances in cholinergic neurotransmission, which leads to decreased choline uptake and ACh release. Studies have shown that cholinergic synaptic loss and amyloid fibril formation are linked to the neurotoxicity of Aβ oligomers and the interactions between acetylcholinesterase (AChE) and Aβ peptides(Breijyeh and Karaman, 2020, Hampel et al., 2021).

1.2.3 Age

AD can be classified into two types based on the age-related risk factor. Patients who develop AD before the age of 60-65 years are recognized as having early-onset AD, while those who develop the disease after the age of 65 have late-onset AD. Aging is an irreversible risk factor with a strong correlation to AD, and LOAD is particularly associated with aging. It is reported that younger individuals rarely develop AD, and the majority of AD cases have a late onset, occurring after the age of 65(Riedel et al., 2016)).AD can be classified into two types based on the age-related risk factor. Patients who develop AD before the age of 60-65 years are recognized as having early-onset AD, while those who develop the disease after the age of 65 have late-onset AD. Aging is an irreversible risk factor with a strong correlation to AD, and LOAD is particularly associated with aging. It is reported that younger individuals rarely develop AD, and the majority of AD cases have a late onset, occurring after the age of 65(Doruk et al., 2010) and the development of AD(Herrup, 2010).

1.2.4 Genetics

Extensive studies have demonstrated a strong correlation between Alzheimer's disease (AD) and gene mutations. Researchers have identified 230 mutations in the presenilin (PS1, PS2) and amyloid precursor protein (APP) genes in Familial Alzheimer's disease (FAD), which lead to dysfunction in APP-related pathways and ultimately result in the excessive production of amyloid beta(Wu et al., 2012).Large-scale genome-wide association studies (GWAS) have shown a correlation between late-onset AD and a complex group of genes, including membrane-spanning 4-domains subfamily A member 4 (MS4A4), Apolipoprotein E (ApoE), sialic acid binding Ig-like lectin 3(CD33), complement receptor 1 (CR1), and ATP-binding cassette transporter A7 (ABCA7) (Liu et al., 2014).

1.2.4.3 Sialic acid binding Ig-like lectin 3(CD33)

Sialic acid binding Ig-like lectin 3(CD33) is a member of the sialic acid-binding immunoglobulin-like superfamily (Siglec) and is exclusively expressed on hematopoietic and phagocytic cells, including macrophages, dendritic cells, monocytes, and microglia in the brain(Zhao, 2019, Crocker et al., 2007).It is one of the top-ranked risk genes for AD identified by genome-wide association studies (GWAS).

CD33 has been reported to exhibit increased expression on microglial cells in the post-mortem brains of AD patients, and high levels of CD33 have been found to hinder the uptake and clearance of Aβ in microglial cell cultures. A study demonstrated that the knockout of CD33 reduces amyloid plaque burden in mouse models of AD(Griciuc et al., 2020).Two single nucleotide polymorphisms (SNPs) in CD33, rs3826656(Bertram et al., 2008) and rs3865444 (Hollingworth et al., 2011, Naj et al., 2011) have been associated with late-onset AD (LOAD).CD33 is expressed on the surface of immune cells—including myeloid progenitor cells, monocytes, and macrophages—where it regulates the inflammatory responses of the innate immune system(Griciuc et al., 2020). In the research conducted by A. Griciuc and colleagues, the amyloid plaque burden was markedly reduced in APP/PS1 transgenic mice in which CD33 had been knocked out (Griciuc et al., 2013), This finding was further confirmed in their later research in 2020, which targeted CD33 as a gene therapy approach. They concluded that primary microglial cells from CD33 knockout mice displayed an increased uptake of $Aβ_{42}$ compared to wild-type (WT) microglia(Griciuc et al., 2020).

1.2.4.3.1 Structure of CD33

The human CD33 gene, located on chromosome 19q13.33, encodes a 67 kDa transmembrane glycoprotein. As shown in **Figure 3,** CD33 is a type I transmembrane protein with several domains: an extracellular N-terminus, a transmembrane domain, and an intracellular C-terminus(Avril et al., 2004).

The CD33 gene consists of seven coding exons that separately encode different domains, ranging from the extracellular N-terminus to the intracellular C-terminus, each with distinct functions(Bhattacherjee et al., 2021, Butler et al., 2021). Structurally, CD33 can be divided into three parts: the extracellular domain, the transmembrane domain, and the cytoplasmic domain. The extracellular domain of the CD33 protein, located on the cell's outer surface, includes functional domains of IgC and IgV. The IgV domain, encoded by exon 2, contains a conserved sialic acid-binding motif vital for sialic acid binding functions. Below the IgV domain, there are two IgC domains encoded by exons 3 and 4. Siglec family members vary in the number of C2-Ig domains they contain. Some Siglecs have multiple C2-Ig domains, allowing them to extend prominently from the cell surface and interact with trans-ligands. However, CD33 has only one C2-Ig domain, making it the shortest member within the Siglec family(Crocker et al., 2007, Griciuc et al., 2020).

The transmembrane domain is encoded by exon 5, while exons 6 and 7 encode the intracellular domain. Exon 6 encodes an immunotyrosine inhibitory motif (ITIM), and exon 7 encodes a membrane-distal ITIM-like motif. The ITIM motif is exclusively expressed in humans and acts as an inhibitory motif for downstream signaling. Conversely, the ITIM-like motif is expressed in both humans and mice, likely maintaining its regulatory role related to endocytosis and involvement in immunoreceptor tyrosine-based inhibitory signaling (Griciuc et al., 2020, Crocker et al., 2007, Avril et al., 2004).

1.2.4.3.2 Function of CD33

CD33 acts as an inhibitory receptor involved in immune responses and can be activated through cell surface receptor-ligand binding. It is widely accepted that CD33 mediates immune activities, including phagocytosis, the regulation of cytokine production, and cell growth(Griciuc et al., 2019). Binding of CD33 to ligands containing sialic acid (e.g., sialic acid-bearing glycoproteins and glycolipids in amyloid beta plaques) results in the activation of CD33. Upon activation, the tyrosine residues within the immunotyrosine inhibitory motif (ITIM) can be phosphorylated by SRC kinases. These phosphorylated motifs act as docking sites for Src homology 2 domain-containing phosphatases(SHPs), leading to the

dephosphorylation of cellular proteins(Zhao, 2019, Eskandari-Sedighi et al., 2022, Gonzalez-Gil et al., 2022).The activation of CD33 signaling contrasts sharply with the activating signals induced by immunotyrosine activation motifs (ITAMs), and it exerts an inhibitory effect on cellular functions such as phagocytosis(Zhao, 2019, Eskandari-Sedighi et al., 2022, Gonzalez-Gil et al., 2022) (**Figure 2**).CD33 is a member of the Siglec family and transmits signals through its immunotyrosine inhibitory motif (ITIM) and ITIM-like motifs. Studies have demonstrated that suppressor of cytokine signaling 3 (SOCS3) efficiently binds to the phosphorylated ITIMs of CD33 and Siglec-7, competing with SHP1 and SHP2 for ITIM-dependent inhibition of cytokine-induced proliferation (Orr et al., 2007b, Orr et al., 2007a). Recruited SOCS3 functions as an E3 ligase, leading to proteasome-dependent degradation of both Siglec and SOCS3. SOCS3 is a key negative regulator of cytokine signaling in myeloid cells(Wong et al., 2006).The SH2 domain of SOCS3 shares approximately 39-41% homology with the SHP-1 and SHP-2 domains, suggesting competition with SHP-1 and SHP-2 for binding to the ITIM and ITIM-like motifs of CD33(Orr et al., 2007b)).This indicates a delicately balanced mechanism of leukocyte activation involving CD33-related Siglecs and underscores the important roles of SHP1, SHP2(Crocker et al., 2007),shown as in **Figure 4**.
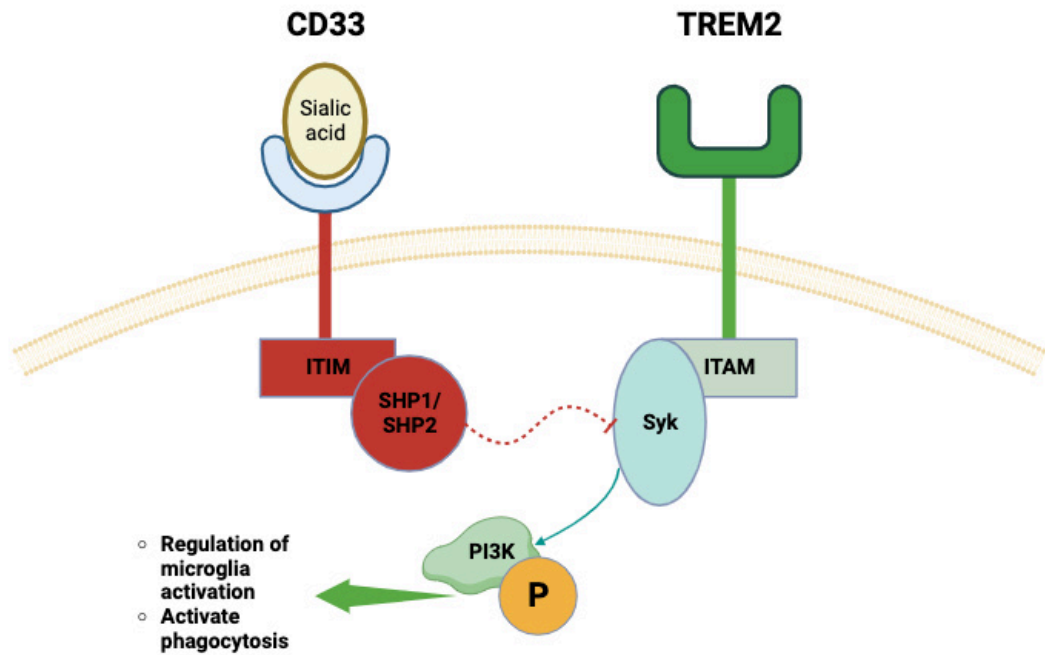
Figure 2. Illustration of phagocytosis is regulated via TREM2- and CD33-signalling pathways. CD33 functions as an inhibitory receptor involved in immune responses and is activated through the binding of cell surface receptors to their ligands. In contrast to the activating signals mediated by immunotyrosine activation motifs (ITAMs), CD33 signaling exerts an inhibitory effect on cellular processes, such as phagocytosis. Figure drawn based on information in(Salminen et al., 2021)). Created with BioRender.com
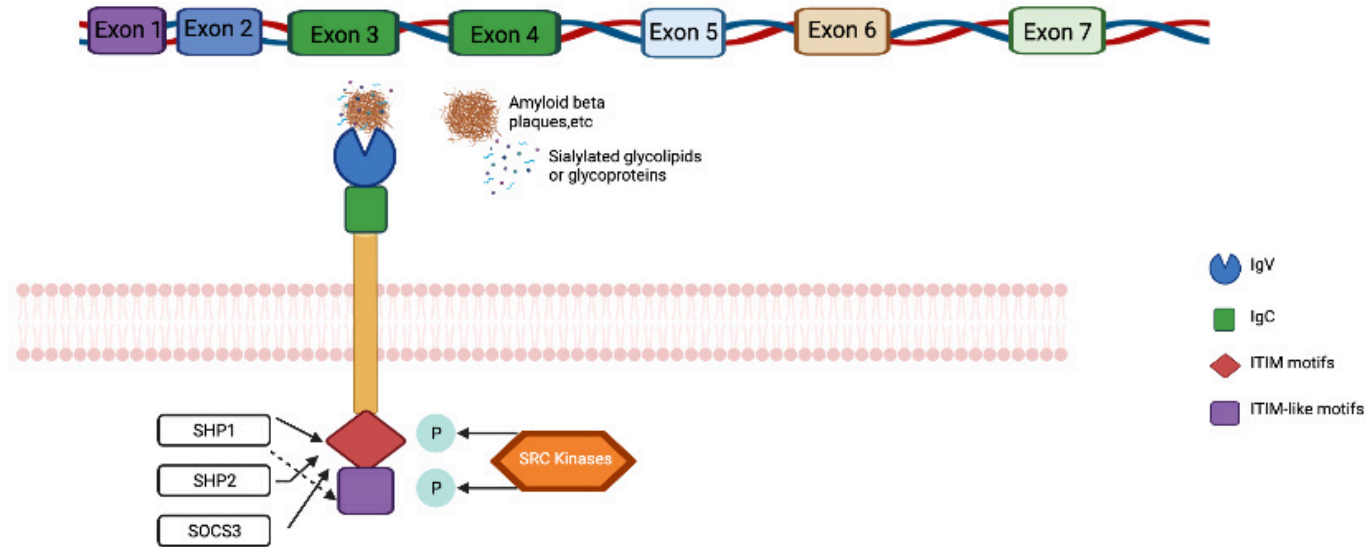
Figure 3. Depiction of CD33 gene structure and CD33 receptor structure. The type I transmembrane protein CD33 consists of seven coding exons, each corresponding to distinct functional domains, ranging from the extracellular N-terminus to the intracellular C-terminus. Structurally, CD33 can be divided into three main sections: the extracellular domain, the transmembrane domain, and the cytoplasmic domain. (a) Extracellular domain: Located on the cell's outer surface, this region contains one IgV domain (blue), encoded by exon 2, and two IgC domains (green), located below the IgV domain, which are encoded by exons 3 and 4.(b) Transmembrane domain: This domain spans the cell membrane and is encoded by exon 5.(c) Intracellular domain: Comprising an immunotyrosine inhibitory motif (ITIM) and a membrane-distal ITIM-like motif, the intracellular domain is encoded separately by exons 6 and 7.Created by BioRender.com.
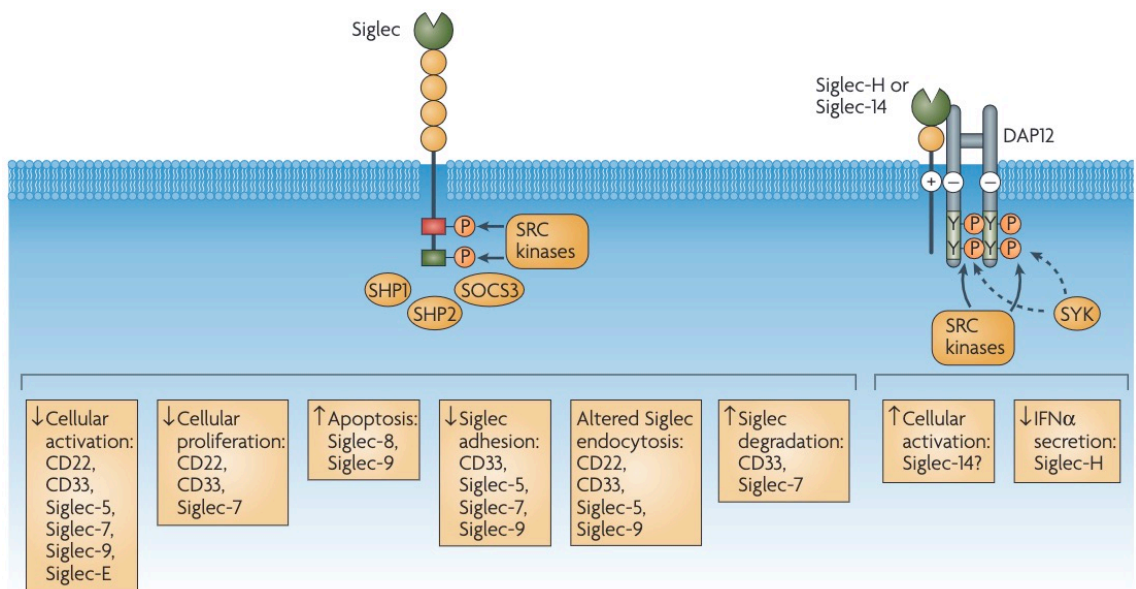
Figure 4. The functional activities of Siglecs activated via inhibitory ITIM signalling and positive ITAM signallilng.CD33, a member of the Siglec family, transmits signals through its immunotyrosine inhibitory motif (ITIM) and ITIM-like motifs. Upon activation, the tyrosine residues within the ITIM can be phosphorylated by SRC kinases, creating docking sites for Src homology 2 domain-containing phosphatases (SHPs). These phosphatases dephosphorylate cellular proteins, mediating inhibitory signaling. CD33 plays a role in immune functions, including phagocytosis, cytokine production regulation, and cell growth. Activation occurs upon binding to sialic acid-containing ligands, such as sialic acid-bearing glycoproteins and glycolipids (e.g., in amyloid beta plaques). This ligand binding triggers ITIM phosphorylation by SRC kinases, recruiting SHPs and modulating downstream immune responses (Zhao, 2019, Eskandari-Sedighi et al., 2022, Gonzalez-Gil et al., 2022)).

1.2.4.4 Sortilin-related receptor 1(SORL1)

Sortilin-related receptor 1 (SORL1), commonly referred to as LR11 is a 250 kDa membrane protein with seven different domains that is found on human chromosome 11q23.2-q24.2 and spans 121452203-121633762 base pairs (bp)(Mishra et al., 2022, Gao et al., 2014)). SORL1 is a type I transmembrane protein which belongs to both the low-density lipoprotein receptor (LDLR) family and the vacuolar protein sorting 10 (VPS10) domain receptor family(Yin et al., 2015).SORL1 is expressed extensively in the brain, mainly in neurons in the hippocampus. At the subcellular level, SORL1 is predominantly present in early endosomes and the trans-Golgi network (TGN). The SORL1 protein is regarded as a hybrid receptor, consisting of structural elements from various proteins. SORL1 plays multiple physiological roles in cell function such as transporting cellular cargo, exhibiting chaperone-like activity, participating in signaling pathways, and facilitating intracellular sorting processes. SORL1 is a novel candidate gene that was first found to be associated with AD in 2004(Cong et al., 2018, Yin et al., 2015)). Subsequent Genome-Wide Association Studies (GWAS) published in recent years have further confirmed the genetic association of the SORL1 gene with AD (Meng et al., 2007, Miyashita et al., 2013)). Additionally, investigations in a transgenic mouse model of AD and familial AD brains demonstrated consistent SORL1 expression, unaffected by genotype, β-amyloid (Aβ) accumulation, or other AD neuropathological changes(Dodson et al., 2008)). The level of SORL1 was found to be decreased in the AD brain which positively correlated with Aβ accumulation. SORL1 plays a complex role in AD pathogenesis, despite its indirect contribution to Aβ destruction, SORL1 also influence the recycling or degradation of APP leading to enhanced Aβ production; the other one is that SORL1 can interfere with the AD risk gene of the APOE pathway by affecting the intracellular trafficking and process of APOE, disrupting lip homeostasis and clearance.

1.2.4.5 Membrane spanning 4 domains A(MS4A)

The MS4A gene cluster spans~800 kb on chromosome 11q12–13 and has been proved to contain at least 16 human and mouse genes which share common structural features and similar intron/exon splice boundaries (Liang et al., 2001, Ma et al., 2015, Liang and Tedder,

2001).The MS4A gene cluster, which encodes cell membrane proteins involved in the regulation of calcium signalling, has been extensively explored in the process of neurodegeneration and AD. Many researchers confirmed that dysregulation of intracellular calcium signalling plays an important role in the pathogenesis of AD(Ma et al., 2015). As demonstrated by Liang et al.(Liang et al., 2001), MS4A4A and MS4A6A were detected in the normal brain and MS4A6A also was detected in the central nervous system (CNS). Previous studies have provided evidence suggesting an increase in the expression level of MS4A4A and MS4A6A in brain tissue obtained from autopsied AD patients (Deming et al., 2019)), supporting the expression of these genes in the cerebellum and frontal cortex, and confirming that the expression levels potentially correlated with disease status. In other researchers' study, along with MS4A6A, MS4A4A and MS4A6E, MS4A4E is also confirmed to be associated with AD by GWAS analysis (Lin et al., 2017, Karch et al., 2012)). MS4A4A can modulate another Ad risk gene of TREM2. MS4A4A and TREM2 co-localized on lipid rafts at the plasma membrane. The increased sTREM2 level was observed with MS4A4A overexpression, whereas silencing of MS4A4A led to a reduction in sTREM2 production (Deming et al., 2019).

1.2.5 Other risk factors

Despite the predominant risk factors illustrated as above, there are still some risk factors also have an effect in the process of AD cases, such as air pollution, diet, metals, chronic infections to central nervous system (CNS), medical factors(Cardiovascular Disease, obesity and diabetes, etc.)and many others may induce oxidative stress and inflammation and increase the risk for developing AD(Breijyeh and Karaman, 2020).

1.3 Biomarkers and pathogenesis

The neuropathological hallmarks of AD consist of two major components: amyloid plaques and neurofibrillary tangles (NFTs).Amyloid plaques, composed of aggregated Aβ,accumulate during the early stages of AD. NFTs, which consist of hyperphosphorylated tau proteins, accumulate later and are more closely correlated with clinical impairment

(Horie et al., 2020).The two isoforms of amyloid beta that are widely studied as hallmarks of AD are $A\beta_{40}$ and $A\beta_{42}$. Both are generated from the amyloid precursor protein (APP) by enzymes known as beta-secretase and gamma-secretase. APP is a transmembrane protein initially processed by beta-secretase, also known as BACE1. This cleavage produces a large soluble fragment, soluble APP-beta (sAPPβ), and a membrane-bound fragment, C99 (the C-terminal 99 residues). C99 is further cleaved by a complex of enzymes known as gamma-secretase.The gamma-secretase complex, composed of several proteins — including presenilin, nicastrin, APH1, and PEN2—cleaves C99 at its extracellular domain into various amyloid beta peptides, such as $A\beta_{38}$, $A\beta_{40}$, $A\beta_{42}$, and $A\beta_{43}$, which consist of 38, 40, 42, and 43 amino acids, respectively(Thinakaran and Koo, 2008). $A\beta_{40}$ is more abundant in the brain compared to $A\beta_{42}$. However, $A\beta_{42}$ is more prone to aggregation and is considered more toxic than $A\beta_{40}$. It is widely believed that the accumulation of $A\beta_{42}$ in the brain plays a critical role in the pathogenesis of AD.

Another key pathological feature in Alzheimer's disease is neurofibrillary tangles (NFTs), which are composed of hyperphosphorylated tau proteins(Horie et al., 2020, Wegmann et al., 2021)), shown as in **Figure 5**.Tau is a crucial microtubule-associated protein that plays a vital role in stabilizing and supporting the structure of nerve cells. Under healthy neuronal conditions, tau carries multiple phosphate groups in its microtubule assembly domain. However, in AD, elevated levels of phosphorylated and aggregated tau are found in the brain and are recognized as pathological hallmarks of the disease(Wegmann et al., 2021). Under normal biological conditions, tau stabilizes microtubules by binding to them, facilitating the transport of nutrients and cellular components along the nerve cell axons. In AD, tau undergoes improper modifications, such as hyperphosphorylation. The hyperphosphorylated tau protein loses its ability to bind to microtubules, leading to the detachment of tau from microtubules. This detachment results in the disruption of microtubule stability and function. The detached tau proteins aggregate with other tau molecules,forming paired helical filaments(PHFs) and straight filaments(SFs), which further aggregate to form NFTs(Jie et al., 2021).
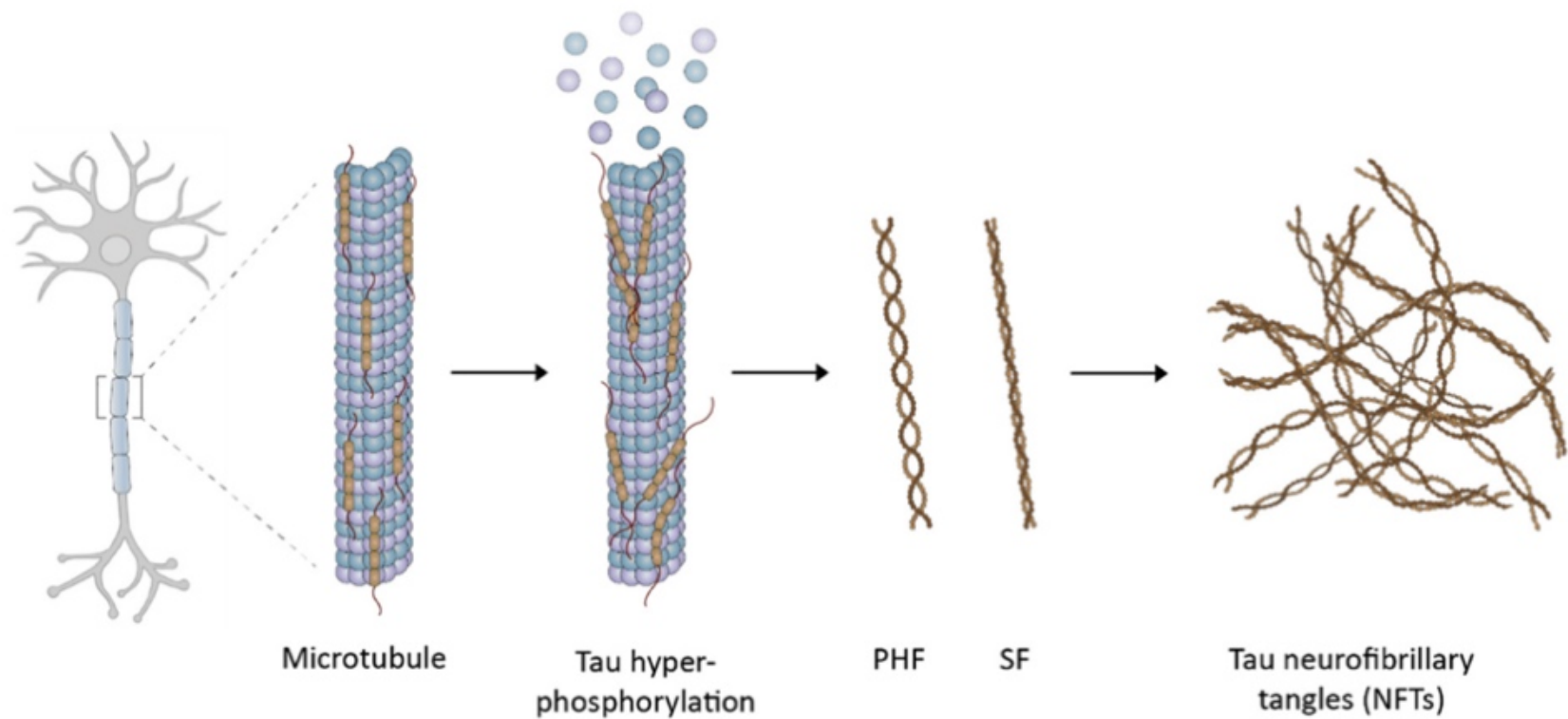
Figure 5.The development of tau neurofibrillary tangles (NFTs). Tau proteins self-aggregate to form loosely intertwined paired helical filaments (PHFs) and the tightly wrapped straight filaments (SFs), which then leads to the formation of NFTs(Jie et al., 2021).

1.4 Diagnosis and treatment of Late-Onset Alzheimer's Disease (LOAD)

The diagnosis of AD currently relies on a comprehensive clinical approach, which includes clinical assessments, medical history evaluation, cognitive and neuropsychological testing (Bier et al., 2015),brain imaging techniques like magnetic resonance imaging (MRI) to confirm hippocampal atrophy(Bjerke and Engelborghs, 2018),and laboratory tests for biomarkers such as $A\beta_{42}$, tau, and phospho-tau in cerebrospinal fluid (CSF). Precise differentiation between AD and other forms of dementia is critical, as their early symptoms can be remarkably similar, but treatment strategies differ significantly.

Over the years, AD treatment has focused mainly on drug development to slow cognitive decline. Symptomatic drugs such as donepezil, rivastigmine, galantamine, and memantine have been employed to moderate symptom progression(Tolar et al., 2020, Wu et al., 2012). Currently, clinical research is progressing in reducing amyloid beta among mild AD patients. A significant breakthrough in treatment research is theFDA-approved anti-amyloid beta antibody, which, in phase II trials, successfully reduced amyloid beta load. Concurrently, researchers are exploring the potential of curing AD by targeting risk genes for knockout or editing. Studies have shown that knocking out CD33 in mice reduces amyloid beta plaque burden, hinting at the possibility of preventing AD at the genetic level as gene-editing technologies rapidly advance.

2. Neuroinflammation in AD

2.1 Overview of neuroinflammation and AD

Inflammation is widely accepted as a pervasive process throughout all stages of AD. Neuroinflammation is a complex process in the central nervous system (CNS), characterized by the activation and recruitment of immune cells and the release of inflammatory cytokines. Like peripheral inflammation, neuroinflammation acts as a fundamental defense mechanism to protect the CNS from harmful insults such as pathogens, toxic molecules (e.g., amyloid beta), and tissue damage (e.g., stroke). Extensive research has identified neuroinflammation as a prominent feature in AD and other chronic

neurodegenerative disorders, where it exacerbates underlying pathologies by generating numerous inflammatory mediators and neurotoxic compounds(McGeer and McGeer, 2010).The presence of elevated inflammatory markers in AD patients and the association of AD risk genes with innate immune functions underscore the significant role of neuroinflammation in AD pathogenesis(Leng and Edison, 2021).

Mounting evidence indicates that inflammation influences amyloid beta and tau in AD pathology. To effectively respond to these, microglia and macrophages are recruited to the CNS through pro-inflammatory signaling pathways(Newcombe et al., 2018) to response to injury, infection, or autoimmune reactions(Li et al., 2021b, Cui et al., 2021) .Upon activation, these cells can engage in various activities, including promoting vascularization, recruiting additional immune cells, and initiating phagocytosis of debris and pathogens(Newcombe et al., 2018). Activation of the IL-1β signaling pathway triggers kinases GSK3β, CDK5, and p38-MAPK, leading to tau hyperphosphorylation and cognitive impairment in the 3xTg-AD mouse model(Kitazawa et al., 2011).Uncontrolled inflammation due to elevated deposition of Aβ plaques and tangles is a primary cause of neurodegeneration in AD, rather than the accumulation of these misfolded proteins alone(Newcombe et al., 2018).CD33 has been linked to inflammatory activity, as demonstrated by studies using CD33 knockout models(Griciuc et al., 2020, Wißfeld et al., 2021).Furthermore, some researchers propose that neuroinflammation in AD brains occurs independently of Aβ accumulation or precedes Aβ plaque formation (Wright et al., 2013).Elevated levels of pro-inflammatory cytokines such as IL-1α, IL-1β, IL-6, IL-8, IL-12, and particularly TNFα, have been reported in the AD brain. Conversely, anti-inflammatory cytokines IL-4 and IL-10 also show corresponding increases(Heneka et al., 2015, McGeer and McGeer, 2010) .

2.2 Microglia/Macrophage in AD

Microglia are the brain's tissue macrophages, accounting for approximately 5% of the total cell population in the cerebral cortex of mice, though their abundance varies significantly across different brain areas(Kirkitadze et al., 2001, Cui et al., 2021).As resident phagocytes and primary immune effector cells in the central nervous system (CNS), microglia originate

from peripherally derived myeloid lineage progenitors and migrate into the CNS during embryogenesis, before the maturation of the blood-brain barrier (BBB)(Lee and Landreth, 2010).Microglia are considered tissue-resident macrophages of the CNS, playing a crucial role in maintaining the stability and plasticity of neuronal circuits. Upon activation by pathological triggers such as neuronal death or protein aggregates, microglia extend their processes to the site of injury, migrating to the lesion and initiating innate immune responses(Heneka et al., 2015, Cornell et al., 2022).In AD, Aβ can activate microglia. Studies have shown that when microglia co-cultured with hippocampal brain slices are exposed to aggregated Aβ, there is an increase in pro-inflammatory molecules and neuronal death(Butovsky et al., 2005).Microglial activation is a cornerstone of neuroinflammation in AD(Leng and Edison, 2021).Microglia were traditionally thought to exist in two states: resting and activated. However, research suggests that microglia can be polarized into pro-inflammatory(M1) or anti-inflammatory(M2) states, depending on the stimuli encountered. Aggregated Aβ and lipopolysaccharide can induce microglia into the M1 state, while interleukins like IL-4 or IL-10 promote the M2 state(Schwab and McGeer, 2008). Once activated, microglia's response—whether M1 or M2—is influenced by the type of cytokines present. The M1 phenotype produces pro-inflammatory cytokines, reactive oxygen species, and nitric oxide, which can contribute to CNS dysfunction. In contrast, the M2 phenotype involves the expression of cytokines and receptors that help inhibit inflammation and restore homeostasis(Nakagawa and Chiba, 2014)(**Figure 6**).

Macrophages, originating from either embryonic precursors or bone marrow(BM) hematopoietic stem/progenitor cells, are the most prevalent immune cells across nearly all tissues, playing a crucial role in maintaining homeostatic function under normal physiological conditions(Qu et al., 2022). Despite residing in different tissues, microglia and macrophages share key functions in preserving homeostasis, such as regulating inflammation, facilitating tissue repair, and phagocytosing pathogens and cellular debris. Research has shown that human peripheral blood mononuclear cells(PBMCs) are important in mitigating disease(Zuroff et al., 2017). In Alzheimer's Disease (AD) patients, PBMCs exhibit a reduced phagocytic capability while showing an increased release of pro-inflammatory cytokines in response to soluble amyloid beta(Fiala et al., 2005, Saresella et

al., 2014, Tian et al., 2014a, Tiribuzi et al., 2014). Monocyte-derived macrophages, known for their effectiveness as professional phagocytes, play a crucial role in the AD brain, similar to microglia(Zuroff et al., 2017).

Microglia and non-parenchymal macrophages are mononuclear phagocytes that play vital roles in the development, homeostasis, and pathology of the central nervous system (CNS)(Li and Barres, 2018).In Alzheimer's Disease, peripheral macrophages can be recruited to migrate into the brain by crossing the blood-brain barrier (BBB). While resident microglia can target amyloid aggregates, their capacity to prevent further Aβ plaque formation is limited. In contrast, increasing evidence suggests that peripheral phagocytes possess enhanced Aβ clearance and immune response capabilities(Rezai-Zadeh et al., 2011).The migration of peripheral macrophages into the brain is a complex process with mechanisms that remain incompletely understood. Disruption of the BBB is a critical factor for macrophage infiltration into the CNS. In AD pathology, activated microglia and damaged neurons release cytokines that aid in recruiting peripheral macrophages into the brain. Additionally, monocytes from the bloodstream can differentiate into macrophages within brain tissue. This recruitment process is facilitated by chemotactic signals and adhesion molecules expressed by endothelial cells in brain blood vessels(Leng and Edison, 2021, Qu et al., 2022, Cui et al., 2021).
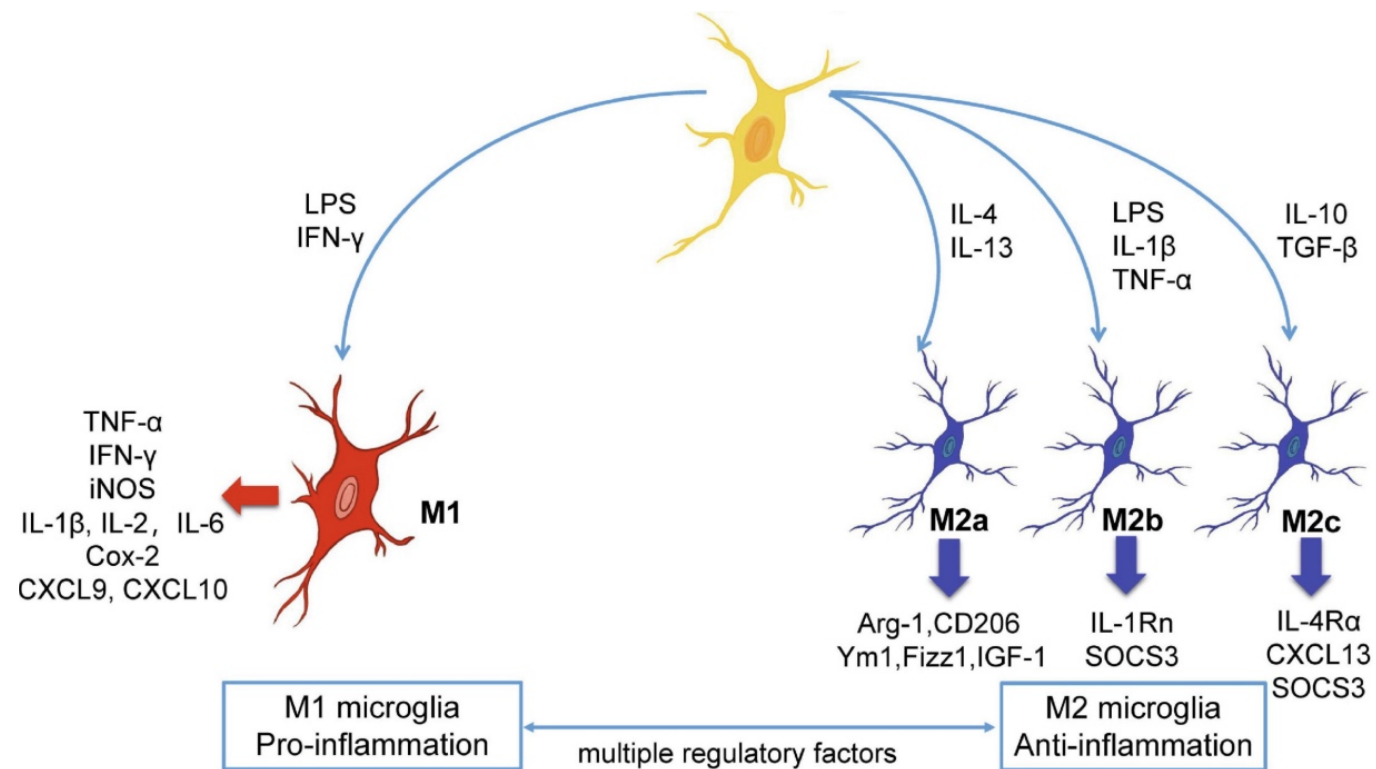
Figure 6. The polarization and phenotypic transition of microglia. Resting microglia/macrophages can be transformed into two distinct phenotypes: the pro-inflammatory M1 phenotype and the anti-inflammatory M2 phenotype. Toxic amyloid beta and other stimuli activate microglia/macrophages, inducing a shift toward either the M1 or M2 phenotype, which respectively release pro-inflammatory and anti-inflammatory cytokines. Importantly, these two phenotypes can convert into one another under specific conditions(Li et al., 2021).

2.3 Inflammatory mediators

2.3.1 Lipopolysaccharide (LPS)

Lipopolysaccharide (LPS), a component of the outer membrane of Gram-negative bacteria, is a potent activator of the immune system. It strongly activates various downstream signaling pathways by binding to Toll-like receptor 4 (TLR4). LPS is recognized as a primary stimulant for the production of pro-inflammatory cytokines such as TNFα, IL-1β, and IL-6 (Wen et al., 2022, Orecchioni et al., 2019, Catorce and Gevorkian, 2016).Consequently, LPS is widely used in inflammation studies as an inducer. Additionally, LPS can stimulate monocytes to produce cytokines like IL-19, IL-20, and IL-24.

2.3.2 Liver X Receptor (LXR) agonist GW3965

GW3965 is a synthetic agonist of liver X receptors (LXRs), a subgroup of nuclear hormone receptors (NHRs) that play a role in cellular activation. LXR activation exhibits anti-inflammatory effects by inhibiting the NF-κB pathway, suppressing pro-inflammatory cytokine expression, and inducing the production of anti-inflammatory cytokines like IL-10 (Schmuth et al., 2014)). In macrophages, LXR activation also upregulates phagocytic receptors (MER, CD36, and AxI) and opsonins (C1qb, Gas6, MFG-E8)(Heckmann et al., 2017). LXRs are involved in lipid metabolism and cholesterol homeostasis, critical factors in Alzheimer's disease. Genome-wide association studies (GWAS) have linked polymorphisms in lipid metabolism genes, such as ApoE(Krasemann et al., 2017)) and ABCA7(Reitz et al., 2013)) to increased AD risk. As a synthetic ligand, GW3965 activates LXR to regulate cholesterol and fatty acid metabolism, offering potential therapeutic benefits for treating AD by suppressing the production of pro-inflammatory cytokines and chemokines.

2.3.3 C-reactive protein (CRP)

C-reactive protein (CRP) is a homopentameric acute-phase inflammatory protein first identified in 1930 by Tillet and Francis(Tillett and Francis, 1930).Produced primarily by liver hepatocytes, CRP is also synthesized by smooth muscle cells, macrophages, endothelial

cells, lymphocytes, and adipocytes.It is widely recognized as a marker of acute inflammation and plays roles in apoptosis, phagocytosis, nitric oxide release (NO), and cytokine production, particularly of interleukin-6 and TNFα (Sproston and Ashworth, 2018). CRP exists as a pentameric protein (nCRP), composed of five monomeric subunits (mCRP). While nCRP exhibits anti-inflammatory effects and promotes phagocytosis and apoptosis through caspase-mediated mechanisms, particularly through enhanced caspase-3 activity, mCRP is associated with promoting inflammation(Sproston and Ashworth, 2018). CRP has been shown to promote IL-8 production via activation of the ERK, p38 MAPK, and JNK pathways(Kibayashi et al., 2005). CRP is also detected in neurodegenerative diseases, including AD(Mulder et al., 2010, Slevin et al., 2017)) and amyotrophic lateral sclerosis (Ryberg et al., 2010)).

2.3.4 Monomeric C -reactive protein(mCRP)

Monomeric C-reactive protein (mCRP) is subunit of nCRP which is irreversibly dissociated from (nCRP) during inflammation. mCRP accumulates at inflammatory sites, gathering in the extracellular matrix (ECM) to amplify and localize the inflammatory response(Di Napoli et al., 2018)),inducing chemotaxis, recruiting circulating leukocytes to inflammatory areas, and inhibiting apoptosis(Sproston and Ashworth, 2018).In terms of cytokine production, mCRP enhances the synthesis of IL-8 and MCP-1, while nCRP induces IL-6 and TNF-α production(Sproston and Ashworth, 2018). mCRP is specifically capable of enhancing inflammation in both in vitro and in vivo settings and has been found to accumulate within the brain after intracerebral hemorrhage (ICH) (Di Napoli et al., 2018)). In the brain, mCRP is produced in substantial quantities following ischemic insults and in response to inflammation, leading to its persistent binding within the ECM(Slevin et al., 2010)). In endothelial cells, mCRP binds to membrane-associated lipid rafts and stimulates cellular activation via MAP kinase and NF-κB signaling pathways (Ji et al., 2009)).

2.4 Pro-inflammatory cytokines
2.4.1 Tumor necrosis factor alpha (TNF-α)

Tumor necrosis factor alpha (TNF-α) is a potent pro-inflammatory cytokine encoded by a gene located on chromosome 6 (6p21.32). It is produced by a diverse range of cells, including NK cells, B cells, neutrophils, endothelial cells, smooth muscle cells, fibroblasts, astrocytes, dendritic cells, and microglial cells(Zelová and Hošek, 2013).However, the primary producers are microglia-macrophages and T cells(Zelová and Hošek, 2013).

Chronic production of TNF-α by microglia is linked to neuroinflammatory responses associated with neurodegenerative disorders such as Alzheimer's disease, Parkinson's disease, multiple sclerosis, and amyotrophic lateral sclerosis(Olmos and Lladó, 2014, Brás et al., 2020)). Beyond its role in inflammation, TNF-α is involved in cell proliferation, differentiation, and apoptosis(Baud and Karin, 2001). TNF-α-mediated inflammation may contribute to amyloid beta (Aβ) plaque development in AD(Decourt et al., 2017)). TNF-α exerts its biological effects by binding to TNF receptor type 1 (TNFR1) and TNF receptor type 2 (TNFR2)(Zelová and Hošek, 2013). Activation of TNFR1 triggers complex signaling pathways that can lead to either cell survival or apoptosis(Zelová and Hošek, 2013). TNFR1 activation activates classical signaling pathways, including NF-κB and MAPK(Zelová and Hošek, 2013, Mitoma et al., 2018), which involve extracellular signal-regulated kinases (ERKs), c-Jun N-terminal kinase (JNK), and p38 MAPK(Sethi et al., 2008, Montgomery and Bowers, 2012).The activation of these pathways results in the production of pro-inflammatory cytokines and other inflammatory mediators. The activation of these pathways results in the production of pro-inflammatory cytokines and other inflammatory mediators.Conversely, TNFR2 activation not only triggers the MAPK pathway but also engages the phosphoinositide 3-kinase (PI3K)/Akt pathway, which regulates cell survival, proliferation, and migration(Montgomery and Bowers, 2012).

2.4.2 Interleukin 1 beta (IL-1β)

Interleukin 1 beta (IL-1β) is a key pro-inflammatory cytokine belonging to the interleukin-1 (IL-1) family. It is primarily produced by pathogenic lymphocytes, blood myeloid cells, and CNS-resident microglia and astrocytes(Mendiola and Cardona, 2018). IL-1β is synthesized as an inactive precursor protein, and its secretion relies entirely on the activation of

caspase-1(Yazdi and Ghoreschi, 2016). Pro-IL-1β can be induced by various stimuli, including inflammatory signals such as TNF, TLR activation, PMA, or stimulation of the IL-1 receptor by mature IL-1β or IL-1α(Burns et al., 2003).Once processed by caspase-1, pro-IL-1β is converted into its active form, engaging in inflammation and other immune responses. To exert its effects, IL-1β binds to its receptor IL-1R1, part of the TIR superfamily. Similar to toll-like receptors (TLRs), IL-1R1 transmits signals via the adaptor protein MyD88, activating the transcription factor NF-κB to initiate the inflammatory process(Burns et al., 2003). Conversely, the intracellular soluble IL-1R2 acts as an inhibitor of IL-1 signaling (Re et al., 1994).Research indicates that sustained expression of IL-1β in the hippocampus can decrease amyloid plaque accumulation in APPswe/PS1dE9 (APP/PS1) and 3xTg-AD mouse models(Shaftel et al., 2007, Matousek et al., 2012), suggesting that IL-1β presence in AD brains is associated with amyloid beta (Aβ) plaque pathology(Ghosh et al., 2013).

2.5 Anti-inflammatory cytokines and factors
2.5.1 Interleukin-1 receptor antagonist (IL-1RN)

Interleukin-1 receptor antagonist (IL-1RN) is a crucial regulatory protein encoded by the IL-1RN gene. It functions as an antagonist by competitively binding to IL-1 receptors, thereby regulating inflammatory activities(Dinarello, 1996, Vamvakopoulos et al., 2002).Unlike interleukin-1 (IL-1), the binding of IL-1RN to IL-1 receptors does not initiate signal transduction. Instead, it mitigates the inflammatory response by preventing IL-1 from binding to these receptors(Dinarello, 1996, Vamvakopoulos et al., 2002).IL-1RN is synthesized and secreted by various cell types, including monocytes, macrophages, and epithelial cells(Vamvakopoulos et al., 2002, Dinarello, 1996). As a competitive antagonist, IL-1RN acts as a counterbalance to IL-1, inhibiting downstream signaling cascades associated with inflammation.This competitive binding effectively prevents IL-1 from promoting inflammation. Thus, maintaining a delicate balance between IL-1 and IL-1RN is essential for immune homeostasis and preventing excessive inflammation, shown as in **Figure 7**.

2.5.2 Interleukin 10(IL-10)

Interleukin 10 (IL-10), which was identified by Mosmann and colleagues(Mosmann and Coffman, 1987) in 1989, is one of the anti-inflammatory cytokines produced by various immune cells, including T cells, B cells, macrophages, dendritic cells, and regulatory T cells (Tregs).IL-10 is a 160 amino-acid protein, acting as a major suppressor of the immune response and a key player in human disease. As an anti-inflammatory cytokine, IL-10 can inhibit the production of pro-inflammatory cytokines such as IL-1, IL-6, and TNF alpha. Janus kinase 1 (JAK1) and Tyrosine kinase 2 (Tyk2) are associated with two receptor chains of IL-10R1 and IL-10R2, respectively(Ho et al., 1995, Finbloom and Winestock, 1995)), resulting in phosphorylation of JAK1 and Tyrosine kinase 2 (Tyk2), which further becoming as docking sites for signalling transducer and activator of transcription 3 (STAT3).This is due to that IL-10 can activate Jak-STAT signaling.STAT3 is the key downstream transcription factor utilized by IL-20 and IL-10 subfamily (Ouyang et al., 2011).IL-10 can activates STAT1, STAT3, and sometimes STAT5; and STAT3 is critical in mediating the function of IL-10 in immune cells (Meraz et al., 1996, Takeda et al., 1999).The inhibitory impacts of IL-10 on the generation of pro-inflammatory cytokines are completely deficient in macrophages and neutrophils which is lacking STAT3 (Takeda et al., 1999). Generally, STATs are recognized as fundamental transcriptional regulators of IL-10(Ouyang et al., 2011):STAT1, STAT3, and STAT4 have all been implicated in IL-10 regulation(Fitzgerald et al., 2007, Meyaard et al., 1996))(**Figure 7**).In Th1 cells, IL-10 expression depends on STAT4 and ERK singalling pathways (Saraiva et al., 2009).IL-10 expression can be potently induced by IL-21 and IL-27 sigannling (Fuqua et al., 2008, Owaki et al., 2006). On the other hand, IL-10 regulates and suppresses the production of proinflammatory cytokines during the recovery phase of infections, minimizing tissue damage caused by proinflammatory cytokines(Ouyang et al., 2011),which could be regarded as a promising therapeutic target.

.
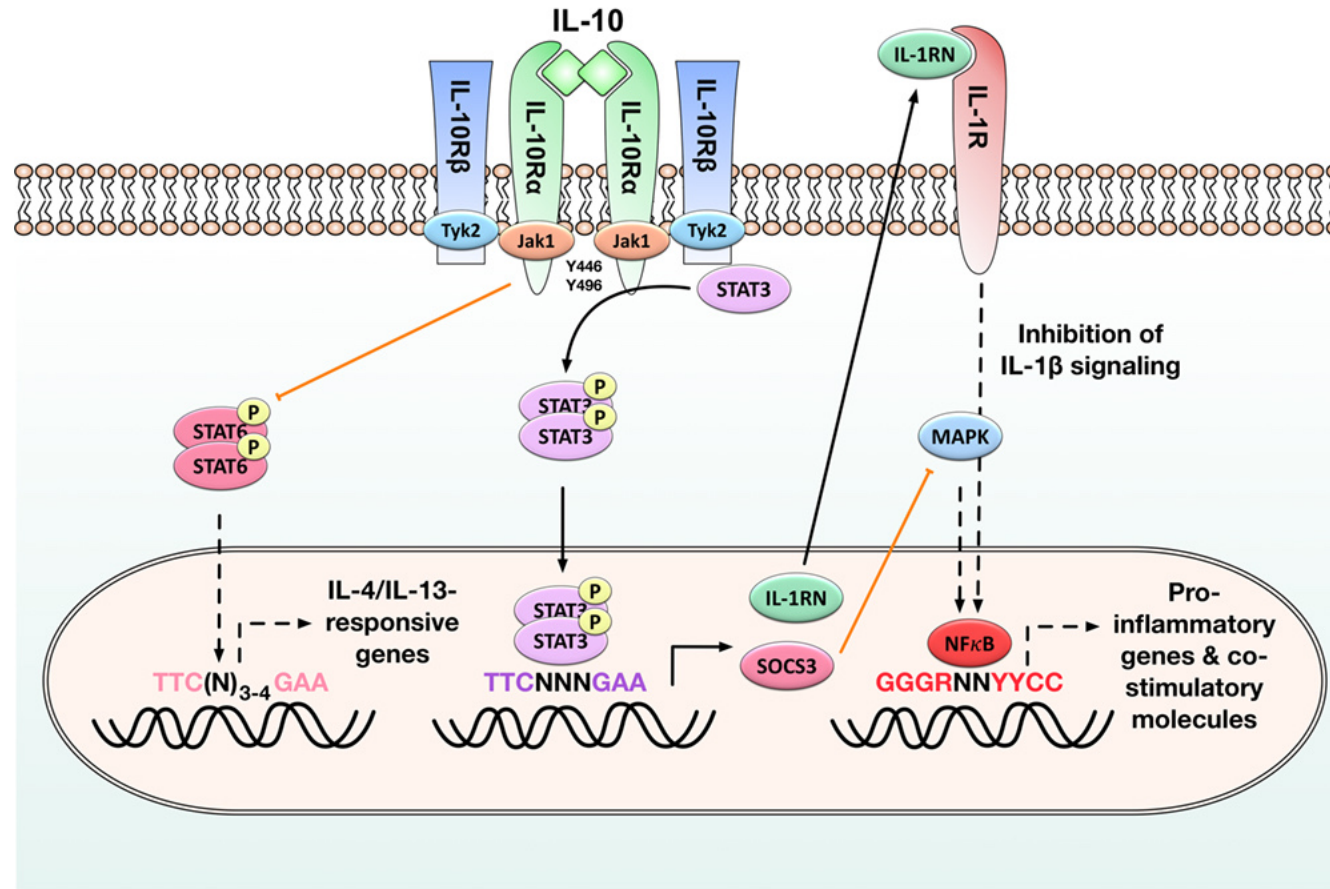
Figure 7. Illustration the role of IL-1RN and IL-10 in inflammatory signalling. IL-1RN is produced by cell types such as monocytes, macrophages, and epithelial cells, functioning as a competitive antagonist to IL-1 by inhibiting inflammatory signaling pathways. In contrast, IL-10 interacts with its receptor to activate the Jak-STAT signaling pathway, involving JAK1 and Tyk2, which associate with IL-10R1 and IL-10R2 respectively. This pathway leads to the phosphorylation and activation of STAT3, a crucial transcription factor for mediating IL-10's anti-inflammatory effects on immune cells (Ouyang et al., 2011) (Dinarello, 1996, Vamvakopoulos et al., 2002)) (Vamvakopoulos et al., 2002, Dinarello, 1996)) (Schülke, 2018).

3. Phagocytosis

3.1 Overview of Phagocytosis

Phagocytosis is a fundamental process for nutrition in nearly all cell types of multicellular organisms, primarily responsible for engulfing and internalizing a wide range of particles larger than 0.5 µm in diameter, including pathogens and apoptotic cells such as bacteria and dead cells(Uribe-Querol and Rosales, 2020, Freeman and Grinstein, 2014). Among all the cell types that perform phagocytosis, a specific group of cells is characterized as professional phagocytes.These professional phagocytes—including neutrophils, macrophages, dendritic cells, and monocytes—execute phagocytosis with high efficiency (Rabinovitch, 1995, Gordon, 2016).In the immune response, professional phagocytes collaborate to recognize, engulf, and eliminate pathogens, contributing to acute and precise responses to invading pathogens and infections. They also play a critical role in initiating adaptive immune responses by presenting antigens to T cells.

Professional phagocytes play a crucial role in eliminating microorganisms and presenting antigens to lymphocytes, thereby activating an adaptive immune response. In contrast, fibroblasts, epithelial cells, and endothelial cells with low efficiency of phagocytosis are ranked as non-professional phagocytes(Uribe-Querol and Rosales, 2020).While non-professional ph100YAEQagocytes lack the ability to ingest microorganisms, they are essential for eliminating dead cells and maintaining cellular homeostasis(Gordon, 2016). The process of phagocytosis can be summarized in six distinct steps: i) detection of the target cargo, ii) activation of specific signaling pathways to induce internalization, iii) formation of the phagosome, iv) fusion and maturation of the phagolysosome, v) pathogen killing or degradation of molecules, and vi) elimination and exocytosis(Rosales and Uribe-Querol, 2017).Phagocytosis is a complex process involving multiple specified steps, and the biological characteristics of the particles engulfed by phagocytes lead to different outcomes. For instance, macrophages that phagocytose bacteria typically promote pro-inflammatory responses, whereas those that ingest apoptotic cells can generate anti-inflammatory responses(Li and Underhill, 2020).The intricate mechanisms employed by phagocytes ensure the appropriate clearance of various particles and defense against

pathogens, thereby maintaining both an effective immune response and tissue homeostasis.

3.3 Mechanism of phagocytosis

Phagocytosis is a complex and multifaceted process involving various signaling pathways critical for immune responses and tissue homeostasis. Professional phagocytes, such as macrophages, typically exhibit pro-inflammatory effects upon bacterial ingestion while generating anti-inflammatory responses when digesting apoptotic cells(Li and Underhill, 2020). The recognition of target particles and the initiation of signaling pathways in phagocytosis are mediated by distinct receptors(Uribe-Querol and Rosales, 2020).Phagocytosis begins with the internalization step, wherein phagocytes recognize particles through the binding of pattern recognition receptors (PRRs). This binding activates signaling pathways that lead to actin cytoskeleton remodeling and changes in membrane lipid composition regulated by PI3K (Uribe-Querol and Rosales, 2020). These changes cause membrane invagination, forming a structure known as the phagocytic cup. The cup extends pseudopods around the target particle until it is fully enclosed. Subsequently, the phagocytic cup membranes fuse distally to form a phagosome, a vesicle that detaches from the plasma membrane (Uribe-Querol and Rosales, 2020).Phagosome maturation involves a series of processes that transform phagosomes into phagolysosomes, culminating in particle degradation. Initially, phagosomes fuse with early endosomes, a process facilitated by the GTPase Rab5. Rab5 recruits EEA1, promoting the fusion between phagosomes and early endosomes(Christoforidis et al., 1999). EEA1 functions as a bridge, connecting early endosomes and endocytic vesicles and facilitating the recruitment of Rab7(Callaghan et al., 1999).As maturation progresses, Rab5 is replaced by Rab7, which mediates the fusion of phagosomes with late endosomes. Additionally, the accumulation of V-ATPase molecules on the phagosome membrane helps acidify the phagosome interior to a pH of 5.5-6.0 by translocating protons (H+) into its lumen(Kinchen and Ravichandran, 2008, Marshansky and Futai, 2008).Through a series of reactions and fusions with early and late endosomes, phagosomes mature and eventually fuse with lysosomes to form phagolysosomes. These phagolysosomes are essential microbicidal organelles equipped with various hydrolytic

enzymes, including cathepsins, proteases, lysozymes, and lipases, which play critical roles in degrading the ingested material(Uribe-Querol and Rosales, 2020, Kinchen and Ravichandran, 2008). Phagolysosomes possess a highly acidic environment (pH 4.5) due to the high concentration of V-ATPases on their membranes. Furthermore, the phagolysosome membrane harbors the NADPH oxidase complex, responsible for producing reactive oxygen species (ROS) such as superoxide (O_2-)(Chocry and Leloup, 2020, Uribe-Querol and Rosales, 2020). Superoxide dismutates to hydrogen peroxide (H_2O_2), which can subsequently react with chloride ions ($Cl-$) to form hypochlorous acid, a potent microbicidal substance(Nauseef, 2014).In the final stage of phagocytosis, depending on the nature of the ingested material, phagocytes may either release the digested contents through exocytosis or present antigenic fragments on their surface to activate other immune cells.

3.2 Receptors of phagocytosis
3.2.1 Pattern-recognition receptors (PRRs)

Phagocytosis begins with the detection of target particles through pattern-recognition receptors (PRRs), which recognize pathogen-associated molecular patterns (PAMPs) and damage-associated molecular patterns (DAMPs) (Amarante-Mendes et al., 2018, Walsh et al., 2013).PRRs, including Toll-like receptors (TLRs) and other subfamilies such as NOD-like receptors (NLRs), RIG-like receptors (RLRs), and C-type lectin receptors (CLRs), are crucial in stabilizing gut homeostasis and detecting pathogens(Walsh et al., 2013).

TLRs are type-I transmembrane glycoproteins classified into 10 functional types in humans that initiate inflammatory responses upon recognizing microbial PAMPs and DAMPs(Kawai and Akira, 2010). Most TLRs activate downstream signaling through the adaptor protein MyD88(Walsh et al., 2013, Fukata et al., 2007),leading to the activation of signaling cascades of NF-kB, MAPK, and AP-1 through the MyD88-dependent pathway, and the interferon regulatory factors 3 and 7 (IRF-3/-7) through MyD88-independent pathways(Li and Underhill, 2020).NLRs, comprising 22 cytosolic receptors, function as cytosolic sentinels, regulating immune responses by recognizing molecular motifs (Rosenstiel et al., 2007, Shaw et al., 2011, Walsh et al., 2013).RLRs are a subgroup of intracellular pattern

recognition receptors (PRRs) responsible for detecting viral infections by recognizing viral RNA molecules. They identify viral pathogen-associated molecular patterns (PAMPs), such as double-stranded RNA (dsRNA), and induce signaling cascades that include the NF-kB and interferon regulatory factor 3 and 7 (IRF-3/-7) pathways(Meylan et al., 2006, Szabo and Rajnavolgyi, 2013).CLRs are calcium-dependent(Rabinovich et al., 2012) receptors that perform a diverse range of functions in vivo, including complement activation, modulation of inflammatory signaling, and phagocytosis(Geijtenbeek and Gringhuis, 2009, Li and Underhill, 2020).

3.2.2 Fcγ receptors(FcγRs)

Fcγ receptors (FcγRs) are glycoproteins that specifically bind to the Fc region of IgG molecules, serving as opsonins to coat target particles(Freeman and Grinstein, 2014, Uribe-Querol and Rosales, 2020). Humans express six types of Fcγ receptors: FcγRI, FcγRIIA, FcγRIIB, FcγRIIC, FcγRIIIA, and FcγRIIIB(Bruhns et al., 2009). These receptors exhibit diverse affinities for various IgG subclasses in both soluble and immune-complexed forms(Bruhns et al., 2009). Macrophages express activating FcγRs equipped with either ITAMs or ITIMs(Anthony et al., 2012, Meylan et al., 2006). Activation involves receptor clustering and subsequent ITAM phosphorylation mediated by Src-family kinases, to create docking sites for spleen tyrosine kinase (Syk) through SH2 domains. Syk activation phosphorylates adjacent ITAM tyrosines,initiating downstream signaling pathways essential for phagocytosis(Takai, 2002).Syk phosphorylation is crucial for triggering phagocytosis, activating signaling molecules such as phosphatidylinositol 3-kinase (PI3K), phospholipase C (PLC), and GTPase-activating proteins(Edwards and Watson, 1995). Meanwhile, ITIM-phosphorylated tyrosines can recruit phosphatases, attenuating activation signals from ITAM-bearing receptors. FcγRIIA, predominantly found on phagocytic cells, lacks association with the FcR common γ-chain and possesses an activating ITAM motif. Conversely, FcγRIIB, containing an ITIM motif, acts as a negative regulator of phagocytosis. FcγRIIIA is a transmembrane receptor with a cytoplasmic tail associated with FcRγ chain dimers, while FcγRIIIB is a GPI-linked receptor without a cytoplasmic tail or associated subunits(Willcocks et al., 2009). Cytokines modulate the surface expression of FcγRs: pro-

inflammatory cytokines typically elevate activating FcγRs relative to inhibitory ones, whereas anti-inflammatory signals downregulate activating FcγRs and boost FcγRIIB expression(Bournazos et al., 2017)(**Figure 8**).
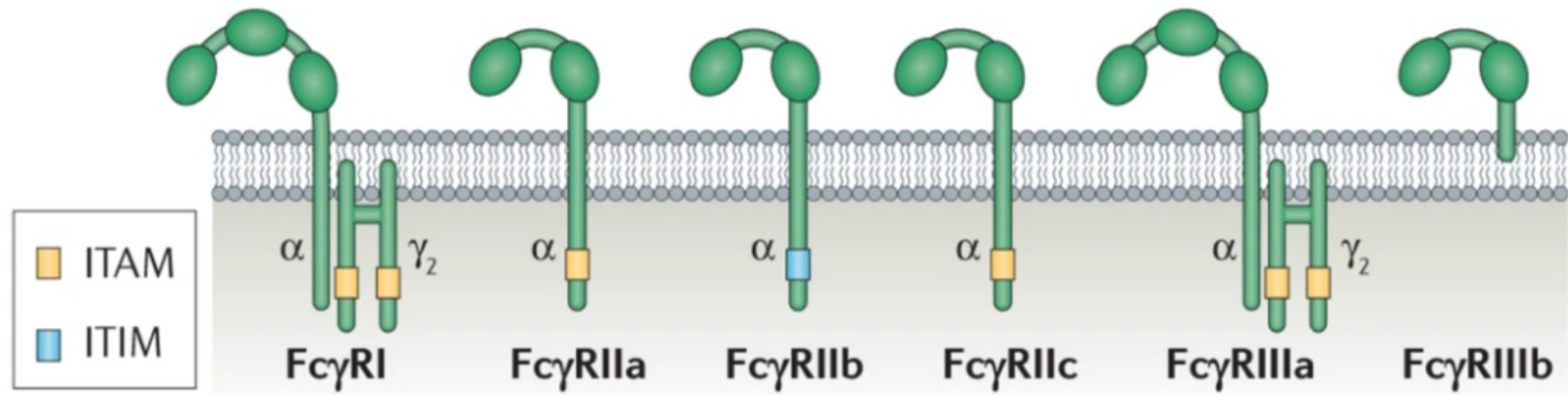
Figure 8. Subtypes of FC gamma receptors. Humans express six types of Fcγ receptors: FcγRI, FcγRIIA, FcγRIIB, FcγRIIC, FcγRIIIA, and FcγRIIIB. These receptors exhibit diverse affinities for various IgG subclasses in both soluble and immune-complexed forms Macrophages express activating FcγRs equipped with either immunoreceptor tyrosine-based activation motifs (ITAMs) or inhibitory motifs (ITIMs) (Anthony et al., 2012, Meylan et al., 2006)) (Bruhns et al., 2009).

3.2.3 Complement receptors

Complement receptors (CRs) play a crucial role in binding activated complement molecules deposited on microorganisms or cells(Edwards and Watson, 1995, Uribe-Querol and Rosales, 2020, Dustin, 2016). CRs are categorized into three subgroups: i) CR1 and CR2, which consist of short consensus repeat (SCR) elements; ii) CR3 and CR4, part of the β2 integrin family; and iii) CRIg, a member of the immunoglobulin Ig-superfamily (van Lookeren Campagne et al., 2007, Dustin, 2016) . The complement pathway can be activated via three distinct pathways, which converge at the activation of C3 and C5 convertases, initiating a cascade of proteins that aid in binding microbial surfaces, thereby facilitating immune recognition and activation of phagocytosis(Li et al., 2007a, Trial et al., 2016). Despite differing triggers, these pathways merge at the crucial step of C3 and C5 convertase activation(Sproston and Ashworth, 2018). In Alzheimer's disease pathology, complement pathways are vital for clearing amyloid beta. Evidence indicates that circulating $A\beta_{42}$ adheres to complement component C3b on erythrocytes, utilizing classic mechanisms by which pathogens and foreign proteins are cleared from the bloodstream(Rogers et al., 2006).

3.4 phagocytosis-related Signalling pathways

Phagocytosis involves multiple signaling pathways, some of which overlap in their activation or inhibition processes and can be triggered by the same receptors. Additionally, phagocytosis intersects with other cellular responses such as the formation of reactive oxygen species (ROS), the release of pro-inflammatory cytokines, and the degranulation of antimicrobial molecules(Freeman and Grinstein, 2014, Rosales and Uribe-Querol, 2017)).SYK(spleen tyrosine kinase) signaling is crucial for phagocytosis and mediates various other pathways. For instance, when the Fcγ receptor (FcγR) is activated, Src-family kinases co-localize with the clustered FcγR, leading to the phosphorylation of tyrosine residues within the immunoreceptor tyrosine-based activation motifs. SYK then binds to these phosphorylated ITAMs and becomes activated(Rosales and Uribe-Querol, 2017, Freeman and Grinstein, 2014). Activated SYK phosphorylates multiple substrates, initiating

various signaling pathways associated with cellular responses such as phagocytosis and transcriptional activation(Meylan et al., 2006, Gordon, 2016).Key substrates include phosphatidylinositol 3-kinase (PI3-K) and phospholipase Cγ (PLCγ). PI3-K regulates phosphatidylinositol (3,4,5)-trisphosphate (PIP3) and GTPase Rac. Activated Rac participates in the activation of signaling molecules such as c-Jun N-terminal kinase (JNK) and the nuclear factor NF-κB. Additionally, other signaling pathways, including extracellular signal-regulated kinase (ERK) and p38, intersect with phagocytic pathways via the activation of protein kinase C (PKC). Different PRRs can trigger distinct signaling pathways, further illustrating the complexity and crosstalk within the phagocytic process.

3.4.1 Immunoreceptor tyrosine-based activation motif (ITAM) and immunoreceptor tyrosine-based inhibitory motifs (ITIM) siganlling

Functional immune responses undergo a highly controlled process that involves interactions between activating and inhibitory receptors expressed on the surface of immune cells(Billadeau and Leibson, 2002). These complex interactions are orchestrated by two critical motifs: immunoreceptor tyrosine-based activation motifs (ITAMs) and immunoreceptor tyrosine-based inhibitory motifs (ITIMs),which mediate opposing signaling processes, promoting activation and inhibition within the immune system, respectively(Billadeau and Leibson, 2002). These motifs, located within the intracellular domains of signaling proteins, are key determinants of the quality and magnitude of immune responses(Billadeau and Leibson, 2002). Transmembrane receptors containing ITIMs are found on nearly all immune cells and even some non-hematopoietic cells(Ravetch and Lanier, 2000).These motifs regulate cellular activities in immune cells in a distinct but balanced manner. ITAM-mediated signaling promotes immune activation through the activation of SYK kinases. Conversely, ITIM signaling negatively regulates this activation by facilitating the dephosphorylation of SYK through the action of phosphatases such as SHP-1 and SHP-2, thereby maintaining immune homeostasis (**Figure 9**).
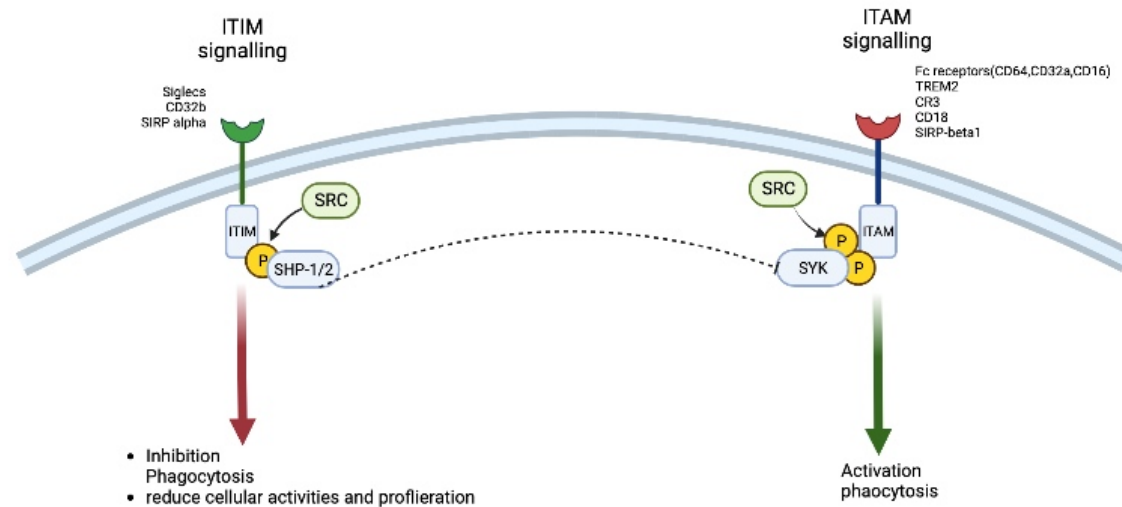
Figure 9. ITAM-signalling and ITIM-signaling cascade counterbalance description. The interplay between immunoreceptor tyrosine-based activation motifs (ITAMs) and immunoreceptor tyrosine-based inhibitory motifs (ITIMs) is critical for regulating immune signaling. ITAMs mediate pro-inflammatory signals by activating SYK kinases, thereby promoting immune cell activation. Conversely, ITIMs negatively regulate immune responses by facilitating the dephosphorylation of SYK through the recruitment of phosphatases such as SHP-1 and SHP-2. This balance between ITAM and ITIM signaling is essential for maintaining immune homeostasis within the immune system. Figure drawn based on the information in(Linnartz-Gerlach et al., 2014).

3.4.2 ITAM signalling

The positive immunoreceptor tyrosine-based activation motif (ITAM) is characterized by the consensus sequence YXXL/I(X6-8) YXXL/I. This conserved amino acid sequence is located in the cytoplasmic domains of various surface receptors primarily involved in immune responses (Cambier, 1995, Billadeau and Leibson, 2002)).ITAM signaling amplifies positive downstream signaling cascades and relies on associated receptors, including the T cell receptor (TCR), B cell receptor (BCR), certain Fc receptors like FcεRI (Fc epsilon receptor I) and CD16 (Fc gamma receptor IIIA), and natural killer (NK) cell receptors such as NKG2D(Billadeau and Leibson, 2002).Upon receptor activation and conformational changes, Src family kinases phosphorylate the tyrosine residues within ITAM motifs (Pasquier et al., 2005)). These phosphorylated tyrosines serve as docking sites for downstream signaling molecules such as SYK (Spleen Tyrosine Kinase) or ZAP-70 (Zeta-Chain-Associated Protein Kinase 70)(Billadeau and Leibson, 2002).The phosphorylation process is facilitated by the binding of the SH2 domain in Src kinases to phosphotyrosine residues and the interaction of the SH3 domain with other signaling proteins. The activation of Src family protein tyrosine kinases (PTKs) lead to the phosphorylation of both tyrosine residues within the ITAM, which subsequently recruits and activates the tandem SH2 domain-containing kinases SYK and ZAP-70. These kinases then engage and phosphorylate multiple downstream signaling molecules. The integrated activation of ITAMs is critical for amplifying downstream cascades, including the MAPK (mitogen-activated protein kinase) signaling pathway and the NF-κB signaling pathway(Ivashkiv, 2009)).Additionally, ITAM signaling positively regulates processes like phagocytosis and other biological activities, such as cell survival(Pasquier et al., 2005, Ivashkiv, 2009)).

3.4.3 Inhibitory immunoreceptor tyrosine-based inhibitory motif (ITIM) signalling

Inhibitory immunoreceptor tyrosine-based inhibitory motifs (ITIMs) are short amino acid sequences typically found in the cytoplasmic domains of certain immune cell receptors, such as those on macrophages and natural killer (NK) cells. These sequences are characterized by the consensus sequence (I/V/L/S)-X-Y-X-X-(L/V)(Billadeau and Leibson,

2002)and are crucial for mediating inhibitory functions in cellular activities. Receptors associated with ITIM motifs include FcγRIIB, SIGLEC family receptors, and killer cell immunoglobulin-like receptors (KIRs). Upon ligand engagement,inhibitory receptors undergo phosphorylation of the tyrosine residues within their ITIM motifs by Src family kinases. This phosphorylation facilitates the recruitment of SH2 domain-containing negative regulators such as the phosphatase SHIP (Src homology 2−containing inositol polyphosphate 5-phosphatase) and phosphotyrosine phosphatases (PTPs) like SHP-1 and SHP-2 (Ravetch and Lanier, 2000, Barrow and Trowsdale, 2006, Burshtyn et al., 1996).SHP-1 is widely recognized as a negative regulator of signaling events, while SHP-2 can sometimes amplify signaling pathways by dephosphorylating inhibitory phosphotyrosine residues, thus promoting downstream cascades like the RAS-RAF-ERK pathway(Liu et al., 2021). Meanwhile, SHIP and SHP-1 initiate inhibitory signals via different mechanisms. SHP-1 removes phosphate groups from various substrates, while SHIP hydrolyzes the membrane phosphoinositide PIP3 to PIP2, counteracting PI3K-induced pathways and leading to the suppression of calcium signaling(Damen et al., 1996).Additionally, phosphorylated SHIP can associate with the RasGAP-binding protein Dok, facilitated by Dok's phosphotyrosine-binding domain, ultimately inhibiting Ras and ERK(Tamir et al., 2000)). Activation of ITIM motifs modulates various signaling pathways, such as the Ras-MAPK, JAK-STAT, and PI3K-AKT pathways, through the actions of SHP-1 and SHP-2.This regulatory mechanism is essential for preventing excessive immune activation and maintaining immune homeostasis.

4. Autophagy

4.1 Overview of Autophagy

Autophagy, a term coined by Christian de Duve, refers to the process of self-degradation first observed in rat liver perfused with glucagon, wherein lysosomes degrade intracellular structures such as mitochondria(Deter and De Duve, 1967).This highly conserved process is present in all eukaryotes and is crucial for balancing energy sources during development and in response to nutrient stress(Glick et al., 2010, Parzych and Klionsky, 2014). Autophagy functions as a housekeeping mechanism to remove misfolded proteins, aggregated proteins, damaged organelles, and intracellular pathogens, representing a self-cannibalization process(Zhou et al., 2015).Research over the years has demonstrated that autophagy plays significant roles in various conditions, including neurodegenerative diseases, tumor progression, and inflammatory diseases(Levine and Kroemer, 2008).Autophagy can be either non-selective or selective in the removal of specific organelles, ribosomes, and protein aggregates(Glick et al., 2010).There are three major forms of autophagy: macroautophagy, chaperone-mediated autophagy (CMA), and microautophagy. These forms facilitate the proteolytic degradation of cytosolic components within the lysosomes(Lamark and Johansen, 2021, Parzych and Klionsky, 2014)) **(Figure 10)**. Macroautophagy, the most common type, delivers cytoplasmic cargo to lysosomes for degradation and can process large structures through selective or non-selective mechanisms. CMA involves translocating targeted proteins across the lysosomal membrane in complex with chaperone proteins recognized by lysosomal-associated membrane protein 2A (LAMP-2A), leading to substrate protein degradation(Eskelinen, 2006, Rothaug et al., 2015, Arias and Cuervo, 2011). Macroautophagy, compared to CMA and microautophagy, encompasses various subtypes, including mitophagy, reticulophagy, nucleophagy, lipophagy, and xenophagy. The process initiates with the formation of phagophores, which enclose target cargo and deliver it to lysosomes for degradation. Phagophores are double-membrane structures derived from the endoplasmic reticulum (ER), the trans-Golgi network, and/or endosomes (Parzych and Klionsky, 2014, Nakatogawa et al., 2009).However, the exact origin of the phagophore remains controversial. Phagophores expand to enclose target cargo within spherical vesicles called

autophagosomes, sequestering it from the cytoplasm. The target cargo typically includes misfolded or aggregated proteins, damaged organelles, and ribosomes(Glick et al., 2010).In mammals, autophagosomes fuse with lysosomes to form autolysosomes, where the cargo encounters the acidic environment and lysosomal hydrolases for degradation(Parzych and Klionsky, 2014) (Yorimitsu and Klionsky, 2005).The resulting byproducts and components are then exported back into the cytoplasm for use in biosynthetic processes or to generate energy(Yorimitsu and Klionsky, 2005).
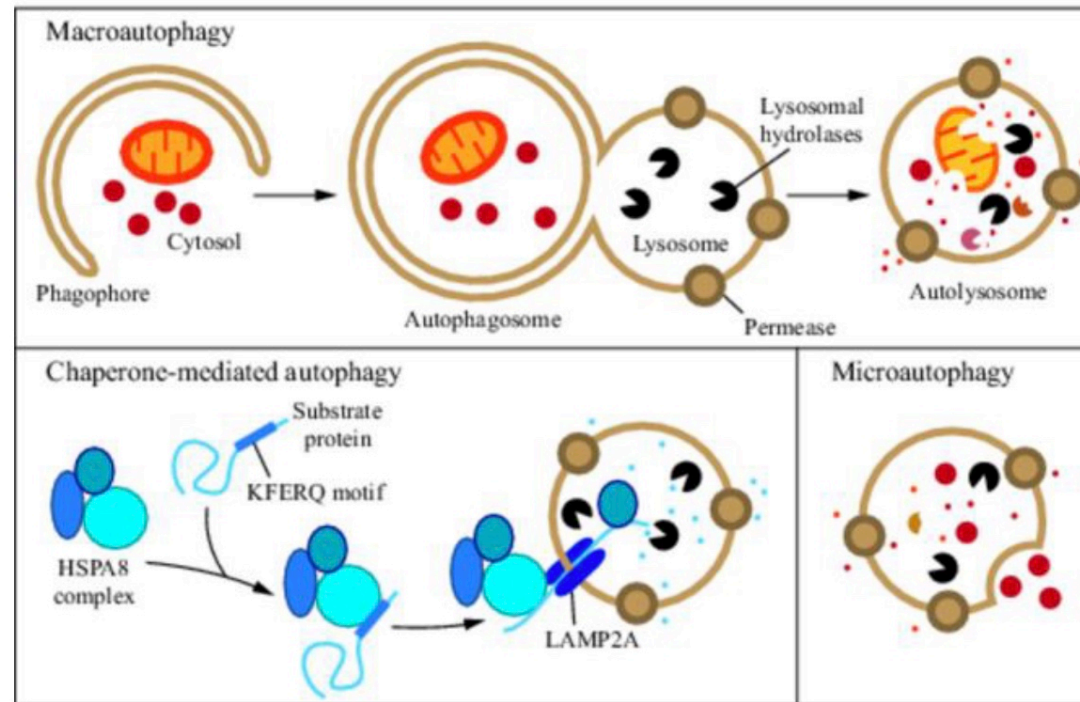
Figure 10.Three types of autophagy in mammalian cells. Autophagy functions as a housekeeping mechanism to remove misfolded proteins, aggregated proteins, damaged organelles, and intracellular pathogens, representing a self-cannibalization process. It is categorized into three major forms: macroautophagy, chaperone-mediated autophagy (CMA), and microautophagy (Parzych and Klionsky, 2014) (Zhou et al., 2015).

4.2 Mechanism of Macroautophagy

The completion of the autophagy process relies on a series of enzyme complexes and other proteins that play key roles in promoting this process. Autophagy is tightly controlled by a group of Autophagy Related Genes (ATGs), which are evolutionarily conserved and present in higher species, including mammals. These ATGs encode proteins that interact and form multi-molecular complexes within cells, regulating various stages of autophagy. The process of macroautophagy can be broken down into distinct steps: induction and nucleation, elongation, closure and maturation, as well as fusion and degradation, as depicted in **Figure 11** and **Figure 12**.
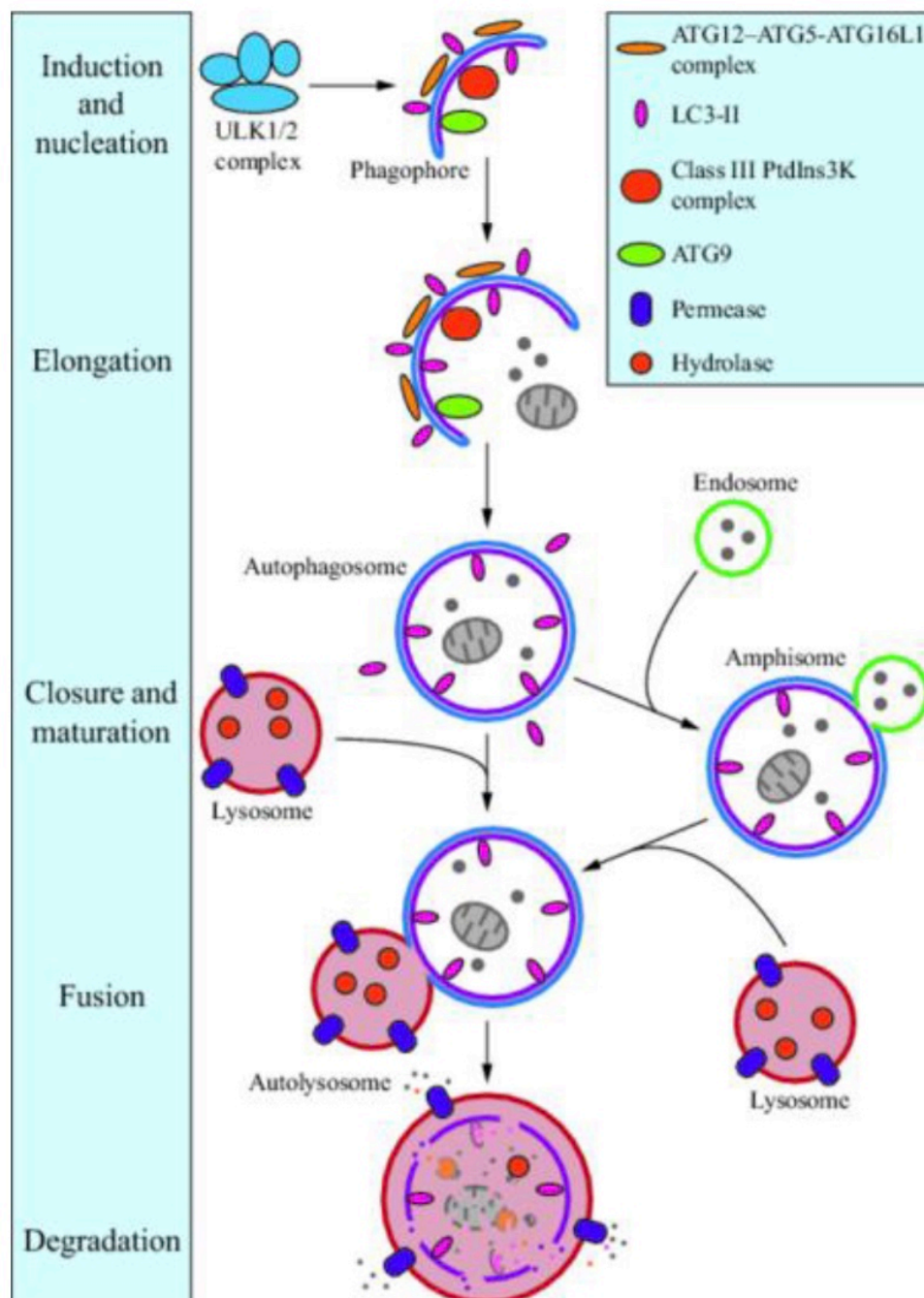
Figure 11. Morphology of macroautophagy. The process initiates with the formation of phagophores. Phagophores are double-membrane structures derived from the endoplasmic reticulum (ER), the trans-Golgi network, and/or endosomes. Phagophores then expand to enclose target cargo within spherical vesicles called autophagosomes, sequestering it from the cytoplasm. The target cargo typically includes misfolded or aggregated proteins, damaged organelles, and ribosomes. In mammals, autophagosomes fuse with lysosomes to form autolysosomes, where the cargo encounters the acidic environment and lysosomal hydrolases for degradation. The resulting byproducts and components are then exported back into the cytoplasm for use in biosynthetic processes or to generate energy (Parzych and Klionsky, 2014, Nakatogawa et al., 2009)).

4.2.1 Induction and nucleation

The process of autophagy begins with the formation of phagophores, which later expand into double-membrane vesicles called autophagosomes(Uddin et al., 2019)). In mammals, autophagosome membranes originate from the ER in dynamic equilibrium with other cytosolic membranes(Glick et al., 2010).This induction is promoted by comlpex of ULK1-ATG13-ATG101-FIP200 by phosphorylation of ATG13 and FIP200(He and Klionsky, 2009).In selective autophagy, cargos are recognized through interactions with specific receptor proteins(He and Klionsky, 2009). In mammals, p62 functions similarly to yeast Atg19 as a receptor for ubiquitinated proteins or organelles in selective autophagy (He and Klionsky, 2009, Noda et al., 2008)). P62 acts as a scaffold by interacting with both LC3-II and ubiquitin chains on target cargo to facilitate autophagosome elongation and degradation (He and Klionsky, 2009, Noda et al., 2008)). This is facilitated by its LC3-interacting region (LIR) domain, which allows it to interact with LC3-II, and its ubiquitin-associated (UBA) domain, which enables p62 to bind to ubiquitin chains on ubiquitinated substrates. The Class III phosphatidylinositol 3-kinase (PI3K) complex, known as the PIK3C3 complex, is also vital for the nucleation and formation of the initial phagophore membrane(Itakura et al., 2008)).In mammalian cells, the PIK3C3 complex, consisting of Beclin1, Vps34, and p150, generates phosphatidylinositol 3-phosphate (PI3P), which is crucial for autophagosome nucleation(Itakura et al., 2008)).Beclin1 regulates autophagosome formation and maturation through different complexes, promoting nucleation(Beclin1-hVps34-Atg14L) or positively regulating maturation(Beclin1-hVps34-UVRAG) (Liu et al., 2020)).

4.2.2 Elongation

Elongation, a complex process in autophagy, involves the recruitment and activation of various ATGs responsible for membrane dynamics and lipid modifications(Weidberg et al., 2011).this is the process which the phagophore membrane extends and grows to wrap the cytoplasmic targets. In both yeast and mammals, two conjugation systems with ubiquitin-like (UBL) proteins contribute to phagophore expansion(Weidberg et al., 2011). The first one is Atg12–Atg5-Atg16(Atg16L in mammalian orthologs) complex. In yeast, Atg12 is

covalently linked to Atg5 through a catalyzed reaction by E1-like enzyme/Atg7 and E2-like enzyme/Atg10. Atg16 then noncovalently binds to Atg12–Atg5, forming the complete Atg12–Atg5-Atg16 complex (Atg12–Atg5-Atg16L in mammals) at the outer membrane of the expanding phagophore, the site of autophagosome formation. In mammals, the ATG12–ATG5-ATG16L1 complex dissociates from the phagophore membrane when the formation of autophagosome is completed(Mizushima et al., 2003, Mizushima et al., 2001)). The second UBL system involved in phagophore expansion is the Atg8/LC3 system(Parzych and Klionsky, 2014). LC3 is the counterpart homologue in mammals of Atg8 in yeast. In mammals, LC3-I is generated through processing by the cysteine protease Atg4, followed by activation through the E1-like enzyme Atg7. LC3-I is then transferred to E2-like enzyme Atg3, resulting in covalent binding with phosphatidylethanolamine (PE) and LC3-II, which associates with autophagosomal membranes from both inside and out, is regarded as a marker to dynamically monitor autophagy flux(Parzych and Klionsky, 2014). During elongation, LC3-II interacts with the Atg5-Atg12-Atg16L1 complex and Atg9 to facilitate autophagosome expansion and curvature, as well as cargo sequestration(Cao et al., 2021). P62/SQSTM1 functions as a bridge, binding ubiquitinated cargo and LC3-II for precise target recognition(He and Klionsky, 2009).LC3-II remains associated with the autophagosome until degradation in the autolysosome, where it is recycled for new autophagy.

4.2.3 Fusion and Degradation

The fusion of the autophagosome and lysosome is a critical step in autophagy, forming the autolysosome, where cargoes are degraded(Glick et al., 2010). Autophagosomes undergo processes such as fusion with early and late endosomes, facilitated by VTIIB and lowered pH levels, to mature before fusing with lysosomes. This fusion is promoted by the lysosomal membrane protein LAMP-2 (Tanaka et al., 2000)), which helps autophagosomes recognize and tether lysosomes, allowing physical contact between their membranes. The trans-SNARE (soluble N-ethylmaleimide-sensitive factor attachment protein receptor) complex is crucial for the membrane fusion process. After fusion, autolysosomes undergo acidification through proton pumps that transport H+ into lysosomes. This acidification activates lysosomal enzymes, such as proteases, nucleases, and lipases, which degrade the cargo.
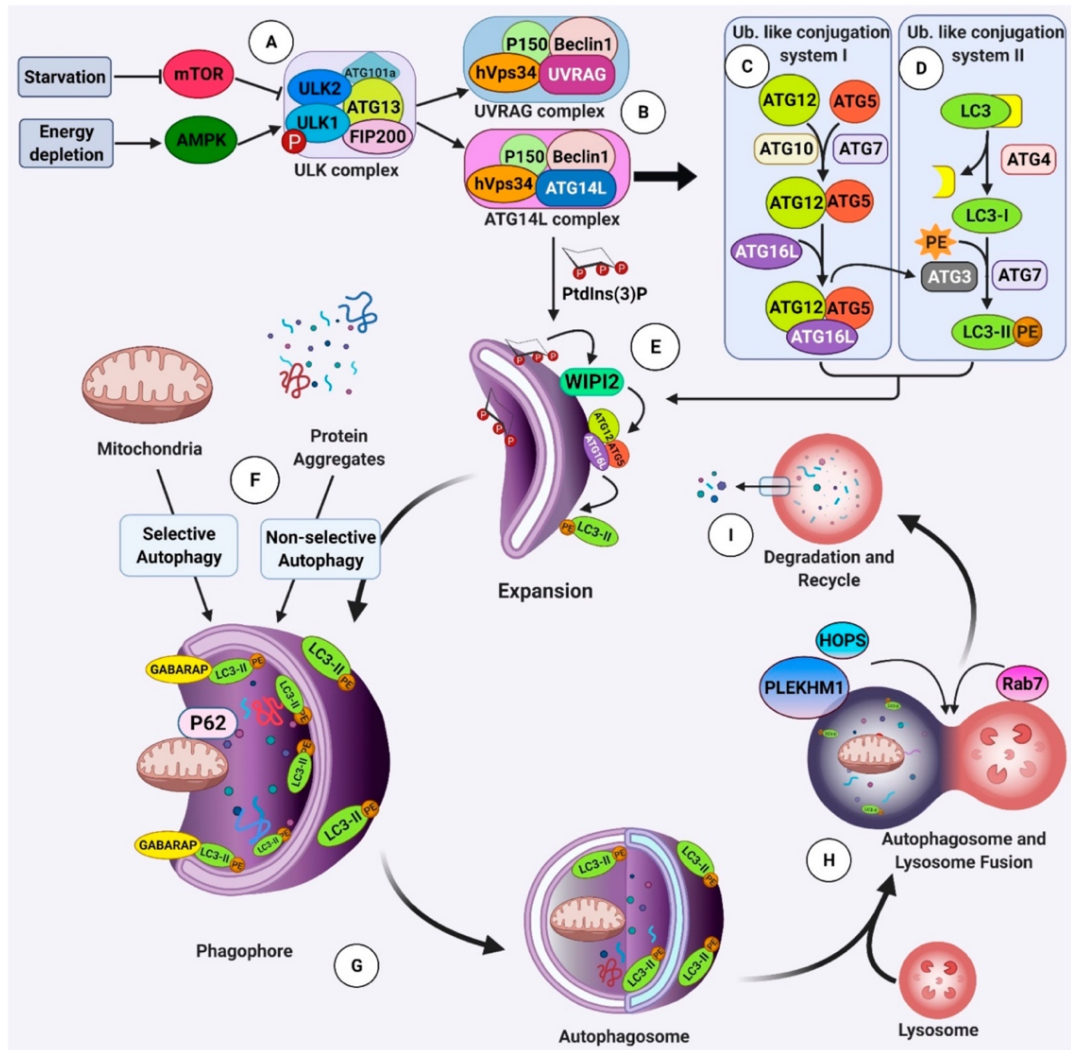
Figure 12. Brief molecular mechanisms of macroautophagy. The Class III phosphatidylinositol 3-kinase (PI3K) complex and ULK1-ATG13-ATG101-FIP200 complex play a pivotal role in autophagosome nucleation. P62 functions as a molecular scaffold by interacting with LC3-II and ubiquitin chains, thereby facilitating autophagosome elongation and degradation. Beclin1 modulates autophagosome formation and maturation through distinct complexes: Beclin1-hVps34-Atg14L promotes nucleation, whereas Beclin1-hVps34-UVRAG is involved in maturation. Elongation is promoted by wo conjugation systems with ubiquitin-like (UBL) proteins of Atg12–Atg5-Atg16(Atg16L in mammalian orthologs) complex at the outer membrane of the expanding phagophore and the Atg8/LC3 system. During elongation, LC3-II interacts with the Atg5-Atg12-Atg16L1 complex and Atg9 to facilitate autophagosome expansion, curvature, cargo sequestration. The fusion of autophagosomes with lysosomes is facilitated by the lysosomal membrane protein LAMP-2, which helps autophagosomes recognize and tether lysosomes, allowing physical contact between their membranes. Following fusion, autolysosomes undergo acidification through proton pumps that transport H+ into lysosomes to promote cargo degradation(He and Klionsky, 2009) (Cao et al., 2021) (Weidberg et al., 2011) (Eshraghi et al., 2021)).

5.Thesis aims

The overall aim of this PhD study was to explore the effect of CD33 knockout on the clearance of the AD hallmark amyloid beta plaques, and the effect of this knockout on other biological features and key signalling pathways.

To address this aim, as well as provide novel insights into the cellular and molecular mechanisms of Alzheimer's disease, the overall aim was divided into smaller aims, addressed in each experimental chapter. These were as follows:

Aim 1) To investigate the effects of CD33 knockout on autophagy flux and the signalling pathways regulating autophagy in a model cell line.

This was done by specifically comparing human CD33WT U937 monocyte-derived macrophages and CD33KO-U937 monocyte-derived macrophages, differentiated using PMA. For this aim, the CRISPR/CAS9 gene editing technique was performed to knock out CD33 in human U937 monocytes, to establish a model cell line in collaboration with a lab at Albert University, Canada. RNA deep sequencing was performed to identify and validate genes associated with autophagy, as well as their signaling pathways in the presence and absence of CD33. The impact of CD33 knockout on the autophagy marker LC3b in a modelled AD inflammatory microenvironment was then evaluated, induced by inflammatory mediators such as LPS, GW3965, mCRP, and TNF-alpha.

Aim 2) To investigate the impact of CD33 knockout on phagocytosis and to validate changes in phagocytosis-related gene expression following CD33 deletion.

This aim was achieved by verifying changes in phagocytosis-related gene expression resulting from CD33 knockout using qRT-PCR and RNA deep sequencing. Expression of MSR1 and LAMP2 in CD33WT-U937 and CD33KO-U937 macrophages was further confirmed through Western blot analysis. The changes in phagocytic capability as well as LC3-associated phagocytic capability of CD33WT-U937 and CD33KO-U937 macrophages

were visualized under confocal microscope by using fluorescent beads and the Alzheimer's disease markers of amyloid beta$_{40}$ and amyloid beta$_{42}$ and engulfment was validated by FCM.

Aim 3) To validate the effects of CD33 knockout on the production of cytokines associated with inflammation and cell movement.

This aim was achieved by investigating the impact of CD33 knockout on cytokine production, and cell movement in the presence and absence of the Alzheimer's disease pathological hallmark of amyloid beta$_{42}$ plaques, and in the presence and absence of lipopolysaccharide (LPS).

Chapter 2 Materials and Methods

1. Materials table 1

Details of all reagents used in this thesis are presented in Table 1 below

Reagents and chemicals	*Company*
U937 Human monocytic cell line	ATCC® CRL-1593.2
Roswell Park Memorial Institute Medium (RPMI)	Lonza, UK
Dulbecco's phosphate buffered saline	Lonza, UK
Dulbecco's modified eagle medium	Sigma Aldrich
Foetal bovine Serum (FBS)	Sigma Aldrich
Phorbol myristate acetate (PMA)	Sigma Aldrich
GW3965	Sigma Aldrich
Lipopolysaccharides (LPS)	Sigma Aldrich
Tris base	Thermo Fisher Scientific, UK
Tween-20	Thermo Fisher Scientific, UK
Bovine serum albumin (BSA)	Thermo Fisher Scientific, UK
Ethylenediaminetetraacetic acid (EDTA)	Thermo Fisher Scientific, UK
Bicinchoninic acid assay (BCA)	Thermo Fisher Scientific, UK
Dimethyl sulfoxide (DMSO)	Thermo Fisher Scientific, UK
IgG 568 goat anti mouse	Thermo Fisher Scientific, UK
Alexafluro 488 goat anti-rabbit IgG	Thermo Fisher Scientific, UK
RNAeasy mini kit	Norgen
QuantiTect Reverse Transcription Kit	Qiagen
QuantiNova Syber green qPCR	Qiagen
Bio-Rad 27-plex human cytokine kit	Biorad
Endotoxin Removal Kit - (Rapid)	ABCAM
Native C reactive protein	My BioSource
Trypsin EDTA	Lonza, Belgium
Ethanol	Fisher chemicals
Invitrogen™ UltraPure™ Urea	Invitrogen
p-STAT3	Cell signalling
LC3b	Cell signalling
p-ERK1/2	Cell signalling
P62	Cell signalling
Total ERK	Cell signalling
GADPH	Abcam
Tubulin	Abcam
Protein ladder	Thermo Fisher Scientific, UK
HRP linked substrate	Thermo Fisher Scientific, UK

DAPI	Thermo Fisher Scientific, UK
Goat serum	Gibco
Triton	Sigma Aldrich
Glycine	Sigma Aldrich
Anti-Mouse HRP linked antibody	Cell signalling
Anti-Rabbit HRP linked antibody	Cell signalling
RIPA buffer	Thermo Fisher Scientific, UK
0.22um PVDF	Millipore
Mounting medium (without DAPI)	Vector Laboratories
PE-CD33 Monoclonal Antibody (WM53)	Thermo Fisher Scientific, UK
FITC-Amyloid beta1-42	BACHEM
Amyloid beta1-42	BACHEM
TAMRA-Amyloid beta1-40	AnaSpec
1 um Yellow-green fluorescent beads	Sigma Aldrich
Poly-D-Lysine	Sigma Aldrich
Goat anti-rabbit IgG (H+L) superclonal secondary antibody, alexa fluor® 488	Abcam
Goat anti-rabbit IgG (H+L) superclonal secondary antibody, alexa fluor® 568	Abcam
Goat anti-rabbit IgG (H+L) superclonal secondary antibody, alexa fluor® 647	Abcam
Goat anti-Mouse IgG (H+L) superclonal secondary antibody, alexa fluor® 488	Abcam
Goat anti-Mouse IgG (H+L) superclonal secondary antibody, alexa fluor® 568	Abcam
Goat anti-Mouse IgG (H+L) superclonal secondary antibody, alexa fluor® 647	Abcam

2. Methods

2.1 Tissue culture

2.1.1 Complete growth medium growth RPMI-1640

The base medium for culturing the U937 cell line is Roswell Park Memorial Institute (RPMI)

1640 medium, which includes L-glutamine and 25 mM HEPES. To prepare the complete

growth medium, fetal bovine serum (FBS) is added to the RPMI-1640 to achieve a final concentration of 10%. Additionally, the medium is supplemented with 1% penicillin-streptomycin. The complete RPMI-1640 growth medium is stored at 4 degrees Celsius before use.

2.1.2 Cell culture of Human promonocytic leukemia U937 cells

Cell cultures were performed in a cell culture hood. Prior to use, all items placed inside were sterilized with a 70% ethanol spray, and the interior surfaces were cleaned with 70% ethanol. Following each session, the cabinet was subjected to 30 minutes of ultraviolet (UV) irradiation to ensure decontamination.

To thaw U937 cells stored in liquid nitrogen, cryovials were rapidly warmed in a 37°C water bath until approximately 80% thawed, then transferred to a biosafety cabinet. The partially thawed cells were gently transferred to a 15 mL Falcon tube containing 9 mL of RPMI-1640 medium and mixed thoroughly. The suspension was centrifuged at 500 g for 5 minutes, and the resulting cell pellet was gently resuspended in fresh RPMI-1640 medium. The cells were then cultured in a T-25 flask under aseptic conditions at 37°C in a 5% CO_2 atmosphere. Cell viability and confluence were monitored daily, with the growth medium replaced every 2 days until subculture was necessary.

Cells were subcultured upon reaching 80% confluence or when density exceeded 0.5×10^6 cells/mL. Subculturing was conducted within a biosafety cabinet. For subsequent experimental purposes, cell viability was assessed using 0.4% trypan blue dye mixed at a 1:1 ratio, and cell counting was performed using a TC10 automated cell counter (Bio-Rad, USA).

2.2 Establishment of CD33KO-U937 cell model system

The human CD33-knockout U937 monocyte model cell line used in this project was generated via CRISPR/Cas9 gene editing at a collaborating lab at the University of Alberta, Canada. Custom crRNA was designed to target human CD33, with the target sequence GAACACCCCCGATCTTCTCC. Cells were seeded in 6-well plates at a density of 500,000 cells per well one day prior to transfection. For each well, the transfection mixture contained

6.25 µg of Cas9 nuclease (IDT), 1.2 µg of ATTO-550-labeled crRNA:tracrRNA (IDT) duplex, 12.5 µg of Cas9 Plus reagent (IDT), and 7.5 µL of CRISPRMAX reagent in 250 µL Opti-MEM medium (Bhattacherjee et al., 2019)). Following transfection, the cells were harvested and resuspended in 300 µL of cell sorting medium (HBSS, 10% FBS, 1 mM EDTA). Flow cytometry was used to sort cells, selecting the top 5% brightest ATTO-550 stained cells, which were then plated into three 96-well plates. These cells were allowed to grow for approximately 3 weeks until the colonies were sufficiently large to be transferred into 12-well plates. Once the cells reached 90% confluence, they were screened by flow cytometry using a PE-conjugated antibody for human CD33 (clone WM53) (Bhattacherjee et al., 2019)). In this study, the wild-type U937 monocytes were designated as CD33WT-U937, while the gene-edited monocytes were labeled as CD33KO-U937.

2.3 Differentiation of Monocytes into M0 Macrophages

To differentiate CD33WT-U937 and CD33KO-U937 monocytes into macrophages, cells were first harvested and centrifuged at 1500 rpm for 5 minutes. The cell pellet was retained and gently resuspended in complete RPMI-1640 growth medium. The cells were then seeded into a 6-well plate at a density of 1 x 10^6 cells/mL. For differentiation, cells were incubated with phorbol 12-myristate 13-acetate (PMA) at a concentration of 50 ng/mL in complete RPMI-1640 medium for 24 hours at 37 °C in a 5% CO_2 atmosphere. After 24 hours, the PMA-containing medium was removed and replaced with PMA-free complete RPMI-1640 medium, and the cells were incubated for an additional 48 hours to ensure further differentiation.

2.4 Flow Cytometry

2.4.1 Verification for CD33 expression on U937monocyte by FCM

The expression levels of CD33 on CD33WT-U937 and CD33KO-U937 monocytes were analyzed using flow cytometry. Both cell types were cultured separately in T75 flasks with complete RPMI-1640 growth medium, with the medium replaced every 2-3 days until cells reached 80% confluence. The cell density was adjusted to 1 x 10^6 cells/mL after counting, and 500 µL of each cell suspension was collected from each flask (n=4 for each monocyte type) and properly labeled. Cells were centrifuged at 1500 rpm for 5 minutes at room

temperature, then resuspended in cold FACS buffer. The suspension was transferred to labeled Falcon tubes and washed three times with FACS buffer at 1500 rpm for 5 minutes. The cell pellets were resuspended in 300 µL of FACS buffer and stained with PE-conjugated antibodies, including an isotype control (isotype-PE) and a specific antibody (CD33-WM53-PE) at a dilution of 1:100. One tube was left unstained as a negative control. Cells were incubated at 4 °C for 30 minutes in the dark. After incubation, the cells were washed three times with FACS buffer and resuspended in 200 µL of cold FACS buffer, then kept on ice for flow cytometry analysis.

2.4.2 Validation of phagocytic ability difference in CD33WT-U937 macrophage and CD33KO-U937 macrophage by FCM

To assess the phagocytic capability of CD33WT-U937 and CD33KO-U937 macrophages, a phagocytosis assay was performed using yellow-green fluorescent beads. Both CD33WT-U937 and CD33KO-U937 cells were seeded in 6-well plates at a density of 5 x 10^5 cells/mL and differentiated into macrophages using PMA stimulation according to the protocol described in section 2.3. Fluorescent latex beads (1 µm diameter; Sigma-Aldrich) were diluted in RPMI-1640 complete growth medium to a final concentration of 0.05% (v/v). The bead suspension was incubated at 37 °C for 1 hour in the dark and vortexed thoroughly before use.

The culture medium was replaced with 1 mL of bead-containing medium, and the cells were incubated at 37 °C in a 5% CO_2 atmosphere for 3 hours to facilitate engulfment. After incubation, the medium was gently aspirated, and the cells were washed 2-3 times with ice-cold PBS. The cells were trypsinized with 0.25% trypsin-EDTA (Gibco, catalog number: 25200056). The trypsin activity was neutralized with growth medium containing FBS, followed by centrifugation at 1500 rpm for 5 minutes. The resulting cell pellet was resuspended in ice-cold FACS buffer, and the cells were washed three times with FACS buffer to remove excess fluorescent beads, minimizing bias in flow cytometry measurements.

After the final wash, cells were resuspended in 300 µL of ice-cold FACS buffer and immediately subjected to flow cytometry analysis. Before trypsinization, images were

captured using a fluorescent microscope at 20x magnification to visually document phagocytosis.

2.5 RNA analysis

2.5.1 RNA extraction

CD33WT-U937 and CD33KO-U937 monocytes were seeded in 6-well plates at a density of 1×10^6 cells/mL in complete RPMI-1640 growth medium. Phorbol 12-myristate 13-acetate (PMA) was added to the culture medium at a concentration of 50 ng/mL, and the cells were incubated at 37 °C in a 5% CO_2 atmosphere for 24 hours. After the initial incubation, the medium was replaced with PMA-free complete growth medium, and incubation continued for an additional 48 hours to achieve full differentiation.

Following differentiation, cells were treated with 100 ng/mL lipopolysaccharide (LPS) after replenishing the fresh growth medium and incubated for another 6 hours at 37 °C in a 5% CO_2 atmosphere. RNA extraction for RNA sequencing analysis was then performed according to the manufacturer's instructions using the RNeasy Mini Kit.

2.5.2 RNA deep sequencing and RT-qPCR

RNA concentrations were measured using a Nanodrop spectrophotometer. The RNA was then converted to cDNA using the High-Capacity cDNA Reverse Transcription Kit (Applied Biosystems), following the manufacturer's instructions. The reaction was prepared on ice and then placed into a thermal cycler. The cycling parameters were set as follows: Step 1 at 25 °C for 10 minutes, Step 2 at 37 °C for 120 minutes, Step 3 at 85 °C for 5 minutes. After completing the cycle, the cDNA plates could be stored at -20 °C for long-term storage or at 4 °C for short-term use.

Real-time quantitative RT-PCR was conducted using the Bio-Rad CFX Connect™ Real-Time PCR Detection System and the KAPA SYBR® FAST qPCR Kit (Kapa Biosystems, Boston, MA, USA). Each reaction consisted of 0.5 µL of cDNA and 1 µL of each primer in a 20 µL total reaction volume. The PCR cycling conditions were 95 °C for 2 minutes, followed by 40 cycles of 95 °C for 5 seconds, and 61 °C for 5 seconds for annealing and extension. Relative gene

expression was quantified using the ΔΔCT method with GAPDH as the internal control. All values were normalized to the wild-type control condition.

RNA samples, designated as CD33WT-macrophage, CD33KO-macrophage, CD33WT-macrophage with 6 hours of LPS treatment, and CD33KO-macrophage with 6 hours of LPS treatment, were sent to BGI Genomics (Shenzhen, China) for deep sequencing analysis. The experimental analysis utilized the NOISeq method, a nonparametric approach for identifying differentially expressed genes (DEGs) with thresholds set at log2-fold change > 1, probability ≥ 0.80, and false discovery rate (FDR) ≤ 0.001. Subsequent data analysis was performed online by Dr. Tom at the Beijing Genomics Institute.

2.6 Western blot assay

2.6.1 Cell preparation

CD33WT-U937 and CD33KO-U937 monocytes were seeded in 6-well plates at a density of 1 x 10^6 cells/mL. Phorbol 12-myristate 13-acetate (PMA) was dissolved in complete growth medium to a working concentration of 50 ng/mL to induce monocyte differentiation into macrophages, following the protocol described in section 2.3. The day before treatment, the medium was replaced with fresh complete growth medium.On the following day, cells were replenished with either serum-free or complete RPMI-1640 medium, preparing samples for further experiments with different conditions. Lipopolysaccharide (LPS), GW3965, and amyloid beta42 were added individually to achieve working concentrations of 100 ng/mL, 1 μM, and 2 μg/mL, respectively. The plates were incubated at 37 °C in a 5% CO2 atmosphere for 12 hours.

treatment	Working concentration	Culture condition	Incubation period
LPS	100ng/ml	Serum free	12h
GW3965	1mM	Serum free	12h
LPS+GW3965	100ng/ml+1mM	Serum free	12h
mCRP	25ug/ml	Serum free	12h
TNF alpha	10ng/ml	Serum free	12h
Amyloid beta 42	2ug/ml	Serum free	12h

2.6.2 Protein Extraction

For protein extraction, the cell lysis buffer was prepared by mixing RIPA buffer with Protease Inhibitor Cocktails 1 and 2, each at a final working concentration of 1:100, made fresh for immediate use. After removing the treatment-containing medium, cells were gently washed twice with cold PBS. Then, 150 µL of the lysis buffer was added to each well of the 6-well plates. The plates were incubated on ice for 30 minutes to ensure complete cell lysis.

Cells were then scraped, and the lysates were collected into 1.5 mL Eppendorf tubes, properly labeled for identification. The tubes were centrifuged at 14,000 rpm for 20 minutes at 4 °C. The supernatants, containing the extracted proteins, were collected and stored at -80 °C for subsequent analysis. Protein concentrations were determined using a BCA assay prior to conducting Western blotting.

2.6.3 BCA assay

The protein concentration in each sample was determined using the Bicinchoninic Acid (BCA) Protein Quantification Assay, following the manufacturer's instructions (Thermo Scientific, catalog number 23227). A 2 mg/mL solution of bovine serum albumin (BSA) was used to prepare the protein standards. The BSA was diluted with RIPA buffer according to the manufacturer's instructions to create a set of standards with concentrations of 0, 25, 125, 250, 500, 750, 1000, 1500, and 2000 µg/mL.A working BCA reagent was prepared and added to each of the BSA standards, followed by incubation at 37 °C for 30 minutes. The absorbance of each sample was measured at 562 nm, and a standard curve was constructed using the BSA standards. This standard curve was then used to determine the protein concentration in the cell lysates by interpolation. The protein samples were stored at -80 °C for subsequent analyses.

2.6.4 Detection of proteins (LC3, MSR1, LAMP2, P-ERK, P-STAT3, total STAT3)

To detect target proteins LC3b, MSR1, LAMP2, P-ERK, P-STAT3, and total STAT3, an SDS-PAGE gel system was set up with 15% acrylamide concentration. GAPDH was used as a loading control. Protein samples were prepared based on BCA assay results and diluted with 4X loading buffer according to the manufacturer's instructions. Samples were heated at 95°C for 5 minutes, then briefly centrifuged before loading onto SDS-PAGE gels. A protein

ladder (5 µl) was loaded on the left side of the gel, and 20 µg of each sample was loaded per lane. Electrophoresis was conducted at a constant voltage of 100V until the loading dye reached the bottom of the gels.

A wet transfer was performed using 0.22 µm PVDF membranes at a constant 100V for 60 minutes. Membranes were blocked with 5% non-fat milk in 0.1% PBST (PBS containing 0.1% Tween-20) at room temperature with gentle rocking for 1 hour. Primary antibody solutions were prepared following the blocking step. Target primary antibodies and GAPDH were diluted in 5% non-fat milk in 0.1% PBST based on the manufacturer's recommendations. Membranes were incubated with primary antibodies at 4°C overnight.The next morning, primary antibodies were removed, and membranes were washed three times with 0.1% PBST for 10 minutes each at room temperature. HRP-conjugated secondary antibodies for anti-mouse IgG and anti-rabbit IgG were diluted in 5% non-fat milk in 0.1% PBST and incubated with the membranes for 1 hour at room temperature. Following incubation, membranes were washed three times with 0.1% PBST for 10 minutes each at room temperature on a fast speed shaker.HRP chemiluminescence detection was conducted by preparing a 1:1 mix of reagents A and B. Approximately 500 µL of the HRP solution was applied to the target protein area and incubated for 1 minute at room temperature. Membranes were then visualized using the Li-Cor Odyssey software with exposure times of 0.5 minutes for GAPDH and 10 minutes for LC3b, MSR1, P-ERK, P-STAT3, and total STAT3. Blots were quantitatively analyzed using ImageJ software.

2.7 Scanning Electron Microscopy to detect morphology of CD33WT-U937 macrophage and CD33KO-U937 macrophage stimulated by PMA.

Sterile silicon wafers, each 1 cm² in diameter, were washed with PBS for 10 minutes and sterilized with 70% ethanol, followed by 15 minutes of UV irradiation before being placed in 12-well plates. Adherent CD33WT-U937 and CD33KO-U937 macrophages were cultured on the silicon wafers using the methods described in section 2.3. Once the cells were fully differentiated into M0 macrophages, the silicon wafers were collected from each well and fixed with 2.5% glutaraldehyde in PBS.The wafers were then washed twice with PBS and sequentially soaked in increasing concentrations of ethanol: 20% for 30 minutes, 40% for 30 minutes, 60% for 30 minutes, 80% for 30 minutes, and finally 100% ethanol for 30

minutes twice. The wafers were dried overnight in a vacuum-assisted desiccator (Sigma-Aldrich, UK). Scanning electron microscopy (SEM) was performed using a Supra 40VP scanning electron microscope (Zeiss, Germany) with SmartSEM software (Carl Zeiss Ltd, Germany) to compare morphological changes in M0 macrophages following CD33 knockout.

2.8 confocal microscopy observation assay

2.8.1 Preparation of cells

Coverslips were pre-autoclaved and placed in 12-well plates. To coat the coverslips, 1% gelatin was added, and the plates were incubated at 37 °C for 1 hour or at room temperature for 2 hours, allowing the gelatin to solidify and create a sticky surface. The excess gelatin was gently washed off with PBS twice before proceeding with cell seeding.CD33WT-U937 and CD33KO-U937 monocytes were seeded onto the gelatin-coated coverslips in 12-well plates at a density of 5 x 10^5 cells per well in complete RPMI-1640 growth medium. They were then differentiated into macrophages following the protocol described in section2.3. Once the cells were fully differentiated, the medium was replenished with fresh complete growth medium to prepare for further assays.

2.8.2 Preparation of fluorescent amyloid beta

Fluorescently labeled amyloid beta40 and amyloid beta42 were dissolved in DMSO according to the manufacturer's instructions. TAMRA-labeled amyloid beta40 and FITC-labeled amyloid beta42 were prepared in DMSO to stock concentrations of 0.1 mM and 1 μg/μL, respectively, and stored at -80 °C.

For experiments, TAMRA-amyloid beta40 was further diluted in complete RPMI-1640 growth medium to a final working concentration of 2500 nM, and FITC-amyloid beta42 was diluted to a final concentration of 2 μg/mL. The amyloid beta solutions were incubated at 37 °C for 1 hour in the dark to promote aggregation.

2.8.3 Preparation for confocal microscope slides

After incubation, the coverslips were washed three times with PBS. Using tweezers, the coverslips were gently removed, and the edges were dried with tissue. A drop of 10 μL of

hard-set mounting medium was placed onto the surface of a microscope slide, and the coverslip was applied with the cell side down onto the mounting medium. The slides were left to dry completely in the dark.Once dried, the slides were ready for examination under a confocal microscope. Images were captured using a Leica STELLARIS 5 Confocal Microscope at 100X magnification. Z-stack analysis was performed to capture images of fluorescent beads or amyloid beta proteins within macrophages. The prepared slides can be stored at -20 °C for several weeks.

2.8.4 Observation of phagocytosis of amyloid beta$_{1-40}$ and amyloid beta$_{1-42}$ by CD33WT-U937 macrophage and CD33KO-U937 macrophage

To study amyloid beta uptake, cells were incubated in RPMI-1640 culture medium containing either amyloid beta40 or amyloid beta42. In a 12-well plate, 1 mL of amyloid beta-containing medium was added to each well, and cultures were incubated at 37 °C in a 5% CO2 atmosphere for 3 hours. Following incubation, cells were washed gently twice with PBS and then fixed in 4% paraformaldehyde (PFA) for 15 minutes at room temperature. The cells were subsequently washed twice with PBS and permeabilized with 0.5% Triton X-100 in PBS for 15 minutes at room temperature. After permeabilization, a PBS wash was performed prior to blocking.Cells were blocked with a buffer containing 3% goat serum and 5% BSA in PBS for 1 hour at room temperature. During blocking, primary antibody staining solutions were prepared. For FITC-amyloid beta42, DAPI stain and phalloidin were dissolved in PBS at dilutions of 1:1000 and 1:500, respectively, along with goat serum. After washing off the blocking buffer with PBS, 300 μL of the staining solution was added to each well, and the plates were incubated overnight at 4 °C in the dark.

The next morning, the DAPI and phalloidin solution was gently removed, and cells were washed three times with ice-cold PBS before performing further immunohistochemistry. For TAMRA-amyloid beta40, DAPI stain and anti-alpha-tubulin antibodies, diluted 1:1000 and 1:500, respectively, along with goat serum, were used, and the plates were incubated overnight at 4 °C in the dark.

On the second day, secondary staining was performed using Alexa Fluor 488 goat anti-mouse antibody for tubulin, diluted 1:500 in PBS containing 3% BSA. The staining was conducted at room temperature on a gentle shaker for 1 hour.

2.8.5 Observation of autophagy marker LC3b in CD33WT-U937 macrophage and CD33KO-U937 macrophage

To observe LC3b expression in CD33WT-U937 and CD33KO-U937 macrophages, cells were seeded in 12-well plates as described in Section 2.8 and differentiated into macrophages following the protocol outlined in Section 2.3. After full differentiation, the plates were replenished with fresh serum-free RPMI-1640 medium and incubated at 37 °C with 5% CO_2 for 6 hours. Subsequently, the cells were gently washed twice with warm PBS.Cells were then fixed with 4% paraformaldehyde (PFA) at room temperature for 15 minutes, followed by two PBS washes. Permeabilization was performed using 0.5% Triton X-100 in PBS for 15 minutes at room temperature. After permeabilization and a PBS wash, cells were blocked with a solution containing 3% goat serum and 5% BSA in PBS for 1 hour at room temperature.During blocking, a primary antibody staining solution was prepared: DAPI stain, LC3b primary antibody, phalloidin, and goat serum were diluted in PBS at 1:1000, 1:500, 1:500, and 1:300, respectively. This solution was added to each well after washing off the blocking buffer with PBS, and the plates were incubated overnight at 4 °C in the dark.The following morning, the primary antibody solution was gently removed, and cells were washed twice with PBS. Cells were then stained with Alexa Fluor® 488-conjugated goat anti-rabbit IgG (H+L) secondary antibody, dissolved in 3% BSA in PBS. The plates were incubated on a gentle rocker for 1 hour at room temperature. After incubation, cells were washed three times with PBS.Carefully remove the coverslips using tweezers and dry the edges with tissue. Add 10 µL of hard-set mounting medium to a microscope slide, and place the coverslip, cell side down, onto the mounting medium. Allow the slides to dry completely in the dark.The slides were observed using a Leica STELLARIS 5 Confocal Microscope at 40X and 100X magnification. Z-stack analysis was performed to capture LC3b proteins in the macrophages. The slides can be stored at -20 °C for several weeks.

2.9 Single-cell tracking by holo-monitor assay

CD33WT-U937 and CD33KO-U937 monocytes were seeded in a 24-well plate at 5% confluence, corresponding to approximately 5,000 cells per well. These cells were fully differentiated into macrophages using the method described in Section 2.3 prior to setting up the holomonitor assay. The cells were then replenished with fresh complete RPMI-1640 growth medium and treated with 100 ng/mL lipopolysaccharide (LPS) 30 minutes before initiating the holomonitor assay. The holomonitor was situated in a humidified chamber maintained at 37.5 °C with 5% CO_2. The device was calibrated with sterilized HoloLids for 30 minutes inside the incubator. Holographic imaging was configured according to the manufacturer's instructions, with a minimum of three fields of view selected for each well. Parameters measured included single cell tracking, cell morphology, confluence percentage, average volume (μm^3), motility distance and speed, and migration distance.

Chapter 3 CD33 and Autophagy

1. Autophagy and Alzheimer's disease (AD)

Subsequent studies have demonstrated that activating autophagy has beneficial effects across nearly all neurodegenerative diseases. This is primarily achieved by eliminating cytoplasmic aggregates, such as alpha-synuclein in Parkinson's disease and tau protein in various other neurodegenerative conditions.Autophagy is a crucial player in neuroinflammation and plays an essential role in maintaining protein homeostasis within neurons. It goes beyond basic housekeeping functions to perform specific tasks that stabilize neuronal conditions, such as facilitating synaptic transmission, ensuring proper neuronal connectivity, and guiding axonal development (Alizadeh et al., 2019, Hwang et al., 2019)). Similar to other cell types, neuronal cells accumulate intracellular toxins and damaged organelles, such as mitochondria, as part of the aging process, which necessitates clearance via autophagy to maintain cellular homeostasis(Li et al., 2017). However, unlike other cell types, neurons are post-mitotic, meaning their toxic burden cannot be reduced through cell division, making autophagy-dependent clearance of proteins and organelles particularly crucial (Mariño et al., 2011, Li et al., 2017).Autophagy serves a housekeeping role by removing misfolded or aggregated proteins, clearing damaged organelles like mitochondria, the endoplasmic reticulum, and peroxisomes, and eliminating intracellular pathogens(Parzych and Klionsky, 2014).

AD is the most prevalent neurodegenerative disorder, characterized by the loss of memory and cognitive abilities. Autophagy is one of three critical pathways responsible for degrading amyloid beta (Aβ),alongside the endosomal/lysosomal pathway and the ubiquitin–proteasome system (UPS)(Zuroff et al., 2017). Early evidence indicates that both macroautophagy and chaperone-mediated autophagy (CMA) dysfunctions are implicated in AD (Koga and Cuervo, 2011, Zare-Shahabadi et al., 2015).This is further supported by findings of significant impairment in autophagy in both AD patients and transgenic AD models, evidenced by the accumulation of unprocessed, Aβ-rich autophagic vacuoles (AVs) in dystrophic neurites (Boland et al., 2008, Nixon, 2007).Consistent evidence of autophagic dysregulation has been documented in both AD animal models and patients. In 1967, researchers observed aggregated tau protein and subcellular vesicles in the dystrophic neurites of AD patient brains(Suzuki and Terry, 1967).In 2005, Nixon and colleagues

identified these vesicles as AVs using electron microscopy(Nixon et al., 2005).That same year, PS-1/APP double transgenic mice showed AV accumulation in neuronal dendrites before amyloid beta plaques appeared, indicating early autophagy involvement in AD pathology(Nixon et al., 2005).Further studies have demonstrated changes in the expression of autophagy-related proteins, highlighting dysfunction in the early stages of AD. A recent study reported downregulation of autophagy-related genes atg1, atg8a, and atg18 in Drosophila melanogaster, accompanied by reduced autophagic activity and increased Aβ generation. This suggests a link between age-related reductions in autophagy-related gene expression and late-onset neuronal dysfunction(Omata et al., 2014, Li et al., 2017). Emerging findings suggest complex relationships between autophagy and amyloid beta metabolism, with autophagy being a major pathway for amyloid beta clearance alongside amyloid-degrading enzymes.

A recent study reported that enhancing LC3-associated endocytosis, a pathway similar to LC3-associated phagocytosis (LAP), promotes amyloid beta (Aβ) clearance and alleviates neurodegeneration in murine models of AD (Heckmann et al., 2019).Autophagy plays a crucial role in degrading amyloid precursor protein (APP) and its cleavage products, such as amyloid beta and APP-cleaved C-terminal fragments (APP-CTFs)(Son et al., 2012 ,Tian et al., 2014). In microglia, autophagy facilitates amyloid beta degradation(Zhou et al., 2011). The autophagy-lysosome system has been identified as a novel mechanism for amyloid beta degradation(Nixon et al., 2005).

Emerging studies have shown that amyloid beta can be detected within autophagic vacuoles following autophagy activation(Mizushima, 2005).Immunostaining has revealed $A\beta_{1\text{-}42}$ in autophagy–endosomal–lysosomal (AEL) vesicles in Drosophila neurons (Ling et al., 2014)). Interestingly, amyloid beta can also regulate autophagy. $A\beta_{1\text{-}42}$ has been reported to induce autophagy in endothelial cells and impair neurovascular regeneration(Hayashi et al., 2009).Aβ-induced autophagic vacuole formation is regulated through the RAGE-calcium-CaMKKb-AMPK pathway (Son et al., 2012).

The classic pathological hallmarks of AD include excessive toxic amyloid beta plaques, neurofibrillary tangles in neurons, and progressive loss of synapses and neurons. Studies indicate that autophagy deficits occur early in AD. Autophagy serves as a mechanism to self-clear misfolded and aggregated proteins, such as amyloid beta, and remove damaged organelles, thus playing an important role in amyloid beta metabolism. Among the three types of autophagy—macroautophagy, microautophagy, and chaperone-mediated autophagy—macroautophagy is considered most relevant to AD. Nonetheless, the mechanisms underlying autophagy pathway disruption in AD are not fully understood.

Dysregulation of the PI3K/AKT/mTOR pathway has been associated with autophagy disruption in AD and Parkinson's Disease (PD)(Heras-Sandoval et al., 2014)). Autophagosomes are abundant in AD brains, and hyperactivation of the PI3K/AKT/mTOR pathway correlates with reduced autophagic flux by phosphorylating the ULK1–ATG13–FIP200 complex, which contributes to Aβ deposition (Heras-Sandoval et al., 2014).

2. Autophagy-associated genes

To date, 32 autophagy-related genes have been identified in yeast, with many of these genes being conserved in mammals(Nakatogawa et al., 2009).These genes encode protein complexes that play crucial roles in the autophagy process in mammals. Key complexes involved include the ULK1/2-ATG13-FIP200 complex, the PtdIns3K complex, and the ubiquitin-like conjugation system comprised of Atg12, Atg5, and ATG16L(Eshraghi et al., 2021, Otomo et al., 2013).The detailed mechanisms through which these complexes facilitate autophagy are thoroughly discussed in Chapter 1.

2.1 LC3/ Microtubule-associated protein 1 light chain 3 (LC3)

The LC3 protein, encoded by the MAP1LC3 gene (Microtubule-associated protein 1 light chain 3), is synthesized as a precursor form known as LC3-I. During autophagy, LC3-I is enzymatically lipidated to form LC3-II. LC3-II serves as a key marker of autophagy flux, particularly under starvation conditions.The detailed mechanisms by which LC3-II functions in autophagy and LC3-associated phagocytosis (LAP) are thoroughly discussed in Chapter 1.

2.2 P62/sequestosome 1(SQSTM1)

P62 also referred as sequestosome 1(SQSTM1) is a multifunctional adaptor protein that aids in the turnover of polyubiquitinated protein aggregates by interacting with LC3-II at the autophagosome and plays roles in oxidative stress and other cellular functions (Caccamo et al., 2017, Glick et al., 2010)). This protein consists of 440 amino acids and includes eight distinct domains, notably the ubiquitin-binding domain (UBA) and the LC3-interacting region (LIR)(Caccamo et al., 2017).P62 facilitates selective autophagy by binding LC3 via its LIR domain. As detailed in Chapter 1, p62 acts as a bridge between ubiquitinated cargo and LC3-II, binding to ubiquitin chains on substrates and serving as a scaffold to integrate cargo with the autophagosome until degradation. P62 is associated with AD, as it strongly binds to neurofibrillary tangles and Tau to target them for degradation(Kuusisto et al., 2002, Caccamo et al., 2017). Additionally, p62 is recognized as a marker for detecting autophagy flux; unlike LC3b, p62 expression typically inversely correlates with autophagic activity due to its self-degradation through autophagy. However, assessing autophagic activity using p62 requires careful consideration of multiple factors, as p62 is involved in crosstalk with other signaling pathways that can affect its transcription (Liu et al., 2016).

2.3 LAMP2/ Lysosomal-associated membrane protein 2(LAMP2)

Lysosomal-associated membrane protein 2(LAMP2) is a protein found in late endosomes and lysosomes(Eskelinen et al., 2002, Eskelinen et al., 2004). It comprises a large luminal portion, a proline-rich hinge region, a single transmembrane-spanning segment, and a short cytoplasmic tail of 11 amino acids(Eskelinen et al., 2002, Eskelinen et al., 2004). LAMP2 is crucial for the fusion of autophagosomes with lysosomes during autophagy(Glick et al., 2010) . Additionally, it serves as a receptor for the selective import and degradation of cytosolic proteins in chaperone-mediated autophagy(CMA)(Eskelinen et al., 2002). Specifically, the LAMP2A isoform functions as a docking site for the chaperone complex, facilitating the translocation of target cargo into the lysosome(Crotzer and Blum, 2008).

2.4 BCL2/adenovirus E1B 19kDa interacting protein 3(BNIP3)

BCL2/adenovirus E1B 19kDa interacting protein 3 (BNIP3) is a protein involved in several cellular processes, including autophagy and apoptosis. It is inducible under various stress

conditions, such as oxygen deprivation. BNIP3 interacts with Beclin-1 during the early stages of autophagosome formation and collaborates with p62 in the degradation of damaged mitochondria through mitophagy. Both BNIP3 and its homolog BNIP3L are non-canonical members of the Bcl-2 family, which are known regulators of cell death(Glick et al., 2010).The Bcl-2 protein has been reported to inhibit Beclin1-dependent autophagy in both yeast and mammalian cells by preventing the formation of the Beclin1–hVps34–PI3K complex, subsequently inhibiting Beclin1-related PI3K III activity and downregulating autophagy (Pattingre et al., 2005) (Zhou et al., 2015). In mitophagy, BNIP3/BNIP3L plays a crucial role in de-repressing Beclin-1 and promoting mitochondrial clearance through interactions with proteins such as GABARAP and Rheb(Tracy and Macleod, 2007) (Zhang et al., 2008) (Schwarten et al., 2009) (Li et al., 2007b). Upon activation, BNIP3 can form heterodimers with BCL2 and BCL-XL, promoting autophagy and enhancing cell survival (Zhang and Ney, 2009) (Redza-Dutordoir and Averill-Bates, 2021).

3. Signalling pathways related to autophagy

Autophagy is tightly regulated by a complex network of signaling pathways, which can be broadly categorized into mechanistic target of rapamycin (mTOR)-dependent and mTOR-independent pathways. mTOR-dependent pathways primarily include the AMPK pathway, the RTK/PI3K/AKT pathway, the stress-responsive c-Jun N-terminal kinase 1 (JNK1) pathway, the death-associated protein kinase (DAPK) pathway, and the RAS-MAPK-ERK1/2 pathway. Notably, while AMPK is a key regulator within the mTOR-dependent framework, it can also modulate ULK1 activity independently of mTOR. Other mTOR-independent pathways involve regulators such as calcium ions (Ca²+), MAPK/JNK, and reactive oxygen species (ROS), among others(Al-Bari and Xu, 2020).

3.1 mechanistic target of rapamycin (mTOR)-dependent pathway

mTOR signaling plays a pivotal role in regulating not only autophagy but also cell growth and metabolism. As a serine/threonine kinase from the PI3K-related kinase (PIKK) family, mTOR forms two distinct complexes: mTOR Complex 1 (mTORC1) and mTOR Complex 2

(mTORC2)(Saxton and Sabatini, 2017)).While mTORC1 primarily drives cell growth and proliferation, mTORC2 is crucial for cytoskeletal organization and cell survival, with mTORC1 influencing mTORC2 signaling through a feedback loop involving insulin/PI3K pathways (Sabatini, 2017, Al-Bari and Xu, 2020)). Nutrient availability is a key regulator of mTORC1 activity. Under nutrient-rich conditions, mTORC1 is activated to stimulate cell growth and protein synthesis. Conversely, nutrient deprivation inhibits mTORC1, triggering autophagy to provide energy resources. This regulation is mediated through the ULK1 complex, which is essential for initiating autophagy. In the presence of nutrients, mTORC1 phosphorylates ULK1, inhibiting autophagosome formation.During starvation, dephosphorylation of ULK1 occurs, activating the complex and promoting autophagy.

The mTORC1 complex is composed of mTOR, Raptor, mLST8, PRAS40, and DEPTOR (Saxton and Sabatini, 2017). Its activation is controlled by the small GTPase Rheb, which resides on the lysosomal membrane. Intralysosomal amino acids, through Rag GTPases, facilitate the translocation of mTORC1 to the lysosome, where active, GTP-bound Rheb can engage with mTORC1 to promote signaling. When energy is low, Rheb with GDP fails to activate mTORC1, enhancing autophagy instead. Rheb activity is negatively regulated by the tuberous sclerosis complex TSC1/2, where TSC2's GTPase-activating function converts Rheb to its inactive form(Rosset et al., 2017)(Al-Bari and Xu, 2020).This inhibition of mTORC1 by TSC1/2 is modulated by upstream pathways, including RTK/RAS–MAPK-ERK1/2 and RTK/PI3K/AKT pathways, as well as the AMPK-mTORC1 pathway, which together orchestrate the cellular response to a wide array of metabolic cues.This intricate regulatory framework underscores the diverse roles of mTOR signaling in cellular homeostasis, making it a focal point of study for understanding metabolic diseases and potential therapeutic interventions.

3.2 AMP-activated protein kinase (AMPK) pathway

The AMPK pathway plays a crucial role in regulating autophagy through both mTORC1-dependent and mTORC1-independent mechanisms. As a cellular energy sensor, AMPK detects changes in ATP/AMP ratios, activating in response to metabolic stress(Meijer and

Codogno, 2007). AMPK activation, triggered by molecules such as liver kinase B1, Ca2+/calmodulin-dependent protein kinase kinase-β, and transforming growth factor-β-activated kinase, influences autophagy by phosphorylating TSC2 under nutrient deprivation or low energy conditions(Al-Bari and Xu, 2020).This phosphorylation stabilizes the TSC1-TSC2 complex, detaches it from the lysosomal membrane, and subsequently inhibits mTORC1 activity, thereby promoting autophagy (Saxton and Sabatini, 2017). Moreover, AMPK can regulate autophagy independently of mTORC1. In nutrient-poor conditions, AMPK directly phosphorylates ULK1 at Ser317 and Ser777, activating the ULK1/2-ATG13-FIP200 complex and initiating autophagy. Conversely, when nutrients are abundant, mTOR activity may phosphorylate ULK1 at Ser757, blocking its activation by AMPK and inhibiting autophagy(Wang and Zhang, 2019).

3.3 Receptor tyrosine kinase (RTK)/PI3K/AKT signalling

The AKT signaling pathway regulates autophagy via TSC-dependent and independent mechanisms, as depicted in **Figure 13**. Growth factors, cytokines, Wnt proteins, energy levels, hypoxia, and DNA damage influence mTORC1 through the PI3K-AKT-TSC1/2-Rheb pathway, thereby modulating autophagy(Sabatini, 2017, Al-Bari and Xu, 2020, Saxton and Sabatini, 2017). Growth factors like insulin activate the PI3K pathway through autophosphorylation of receptor tyrosine kinases(RTKs) and phosphorylation of insulin receptor substrates (IRSs)(Al-Bari and Xu, 2020). Phosphorylated IRSs recruit and activate PI3K, converting phosphatidylinositol 4,5-bisphosphate (PIP2) to phosphatidylinositol (3,4,5)-trisphosphate (PIP3), which then recruits PDK1 to phosphorylate AKT at Thr308(Rabanal-Ruiz et al., 2017) (Ziemba et al., 2013).Activated AKT phosphorylates and inhibits TSC2, leading to the activation of mTORC1 and inhibition of autophagy. AKT also independently transmits signals to mTORC1 by phosphorylating PRAS40, releasing it from Raptor, a component of mTORC1(Vander Haar et al., 2007).Additionally, AKT can phosphorylate the forkhead box O (FOXO) family transcription factors, including FOXO1, FOXO3a, and FOXO4, inhibiting autophagy-related proteins such as LC3. AKT can also directly inhibit ULK1 activity by phosphorylating it, disrupting the ULK1 complex.
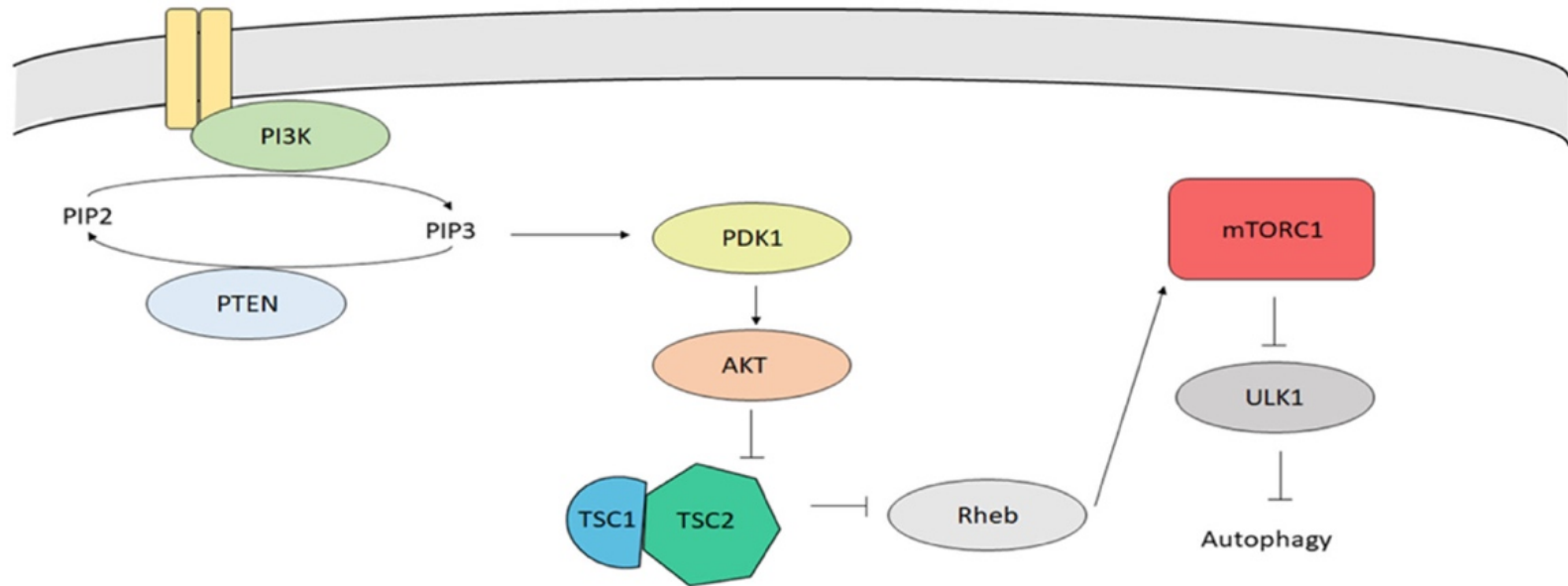
Figure 13. PI3K-mTOR autophagy pathway utilizes PIP3 lipid signaling. The AKT signaling pathway regulates autophagy via TSC-dependent and independent mechanisms. Growth factors like insulin activate the PI3K pathway through autophosphorylation of receptor tyrosine kinases (RTKs). The activated PI3K play a role in converting phosphatidylinositol 4,5-bisphosphate (PIP2) to phosphatidylinositol (3,4,5)-trisphosphate (PIP3), which then recruits PDK1 to phosphorylate AKT at Thr308.Activated AKT phosphorylates and inhibits TSC2, leading to the activation of mTORC1 and inhibition of autophagy (Soto-Avellaneda and Morrison, 2020)).

3.4 MAPK-JNK signalling in autophagy

The c-Jun NH2-terminal kinase (JNK) pathway plays a significant role in regulating various forms of autophagy, particularly under conditions such as nutrient deficiency, decreased cytokines and growth factors, and exposure to neurotoxic drugs (Zhou et al., 2015)). JNK is a stress-activated protein kinase that responds to a variety of stress-related signals, including oxidative and endoplasmic reticulum (ER) stress.

The MAPK-JNK signaling pathway intersects with autophagy signaling by modulating the activity of Bcl-2 family proteins, such as Bcl-2 itself. When JNK phosphorylates Bcl-2, it leads to the dissociation of Bcl-2 from Beclin 1, subsequently influencing PIK3C3 activity, which is crucial for the induction and nucleation of autophagosomes.

Additionally, JNK can interact with mTOR signaling pathways. It phosphorylates and inhibits TSC2, a negative regulator of mTORC1, resulting in increased levels of active Rheb-GTP. This activation of Rheb enhances mTORC1 activity, promoting cellular growth and proliferation while concurrently inhibiting autophagy.

3.5 JAK-STAT siganlling

The Janus kinase/signal transducer and activator of transcription (JAK/STAT) signaling pathway is a central communication node in cellular functions such as cytokine production, tissue repair, inflammation, and apoptosis (Hu et al., 2021)(Owen et al., 2019)(**Figure 14**).This pathway involves over 50 cytokines and growth factors, including hormones, interferons (IFNs), interleukins (ILs), and colony-stimulating factors. Evolutionarily conserved, the JAK/STAT pathway comprises ligand-receptor complexes, Janus kinases (JAKs), and STAT proteins (Hu et al., 2021)).The JAK family includes four subtypes: JAK1, JAK2, JAK3, and TYK2, which are expressed in nearly all tissues except JAK3, which is primarily found in the bone marrow, lymphatic system, endothelial cells, and vascular smooth muscle cells(Lai et al., 1995), (Verbsky et al., 1996, Hu et al., 2021). The STAT family consists of seven members: STAT1, STAT2, STAT3, STAT4, STAT5a, STAT5b, and STAT6. The

JAK/STAT signaling pathway is negatively regulated by the intracellular SOCS/CIS family, the PIAS family, and protein tyrosine phosphatases (PTPs) (Hu et al., 2021). JAK/STAT signaling interacts with other vital pathways, such as TGFβ, MAPK, PI3K/AKT/mTOR, and NF-κB (primarily via STAT3), to regulate cellular processes like proliferation, survival, and differentiation (Hu et al., 2021).The pathway is initiated when activated JAKs cause tyrosine phosphorylation of the bound receptors, creating docking sites for STATs. Phosphorylated STATs dissociate from the receptor, dimerize via SH2-domain–phosphotyrosine interactions, and translocate to the nucleus to regulate target gene transcription(Durham et al., 2019). JAK-STAT signal transduction can be categorized into canonical and non-canonical signaling. In canonical signaling, ligand-receptor binding and receptor dimerization are prerequisites. Key receptors include gp130(Tenhumberg et al., 2006),EpoR(Livnah et al., 1999),TNF-R1(Naismith et al., 1995), IL-17R (Kramer et al., 2006), IL-10R(Krause et al., 2006) and GH receptor.The connection between the ligand and the receptor induces transphosphorylation of JAK. The activated STAT binds to its DNA target site to regulate transcription(Hu et al., 2021)). Dysregulation of JAK/STAT signaling is implicated in various diseases, including inflammatory and immune conditions like systemic lupus erythematosus (SLE) and age-related diseases characterized by chronic inflammation.
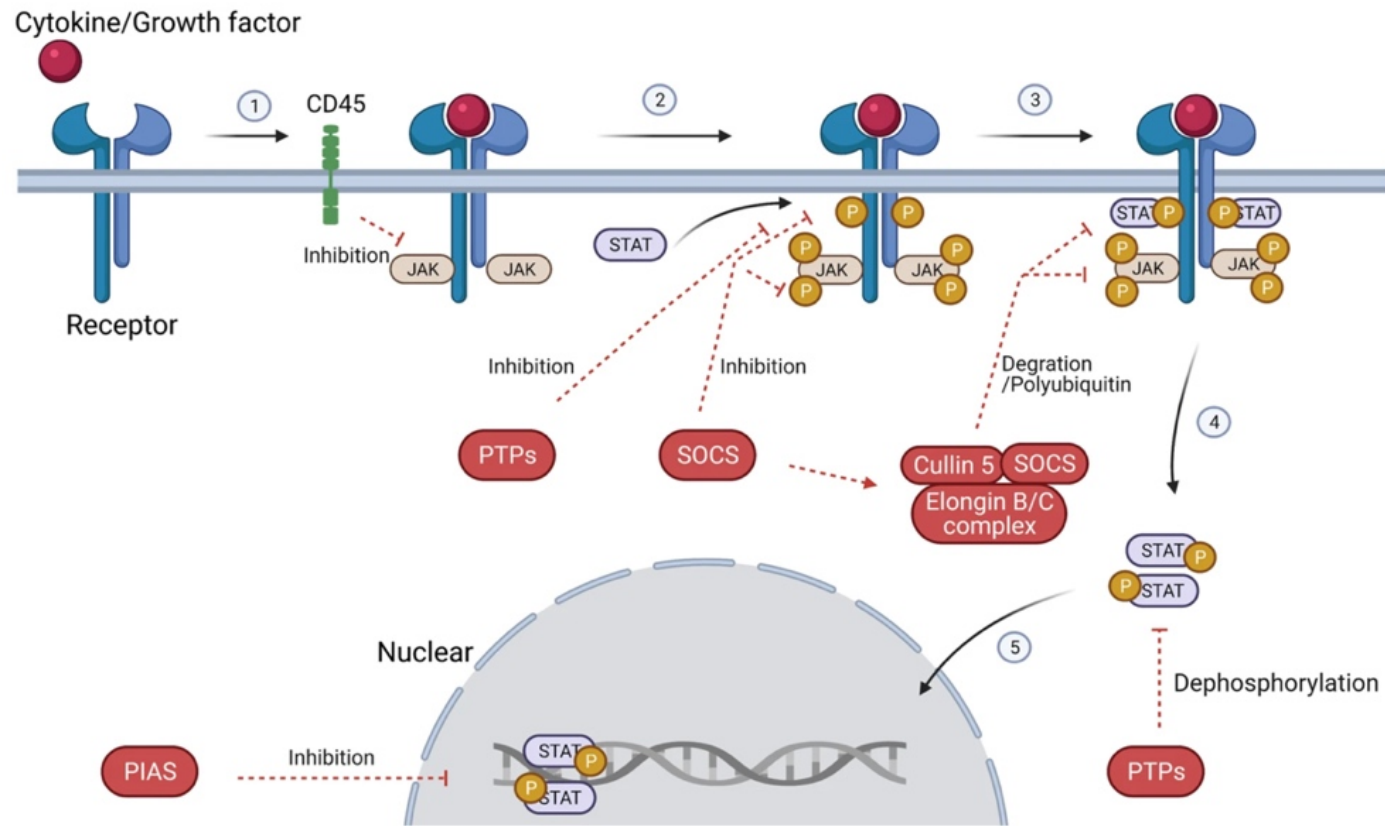
Figure 14. Activation and negative regulation of JAK/STAT signaling pathways. The JAK/STAT signaling pathway is initiated cytokines and growth factors, including hormones, interferons (IFNs), interleukins (ILs), and colony-stimulating factors, leading to receptor dimerization and JAK recruitment. Activated JAKs phosphorylate receptor tyrosine residues, creating docking sites for STATs to be phosphorylated. Subsequently, the phosphorylated STATs dissociate from the receptor, and translocate into the nucleus to regulate gene transcription. The JAK/STAT signaling pathway is negatively regulated by the intracellular SOCS/CIS family, the PIAS family, and protein tyrosine phosphatases (PTPs). JAK/STAT signaling interacts with other vital pathways, such as TGFβ, MAPK, PI3K/AKT/mTOR, and NF-κB (primarily via STAT3), to regulate cellular processes like proliferation, survival, and differentiation.Black arrows indicate the activation process. Red dotted arrows indicated negative regulation (Hu et al., 2021)).

3.5.1 JAK family

Each JAK of the JAKs family is composed of seven homology domains (JH), of which JH1 constitutes the kinase domain; JH2 constitutes the pseudokinase domain; a part of JH3 and JH4 together constitute the SH2 domain; and the FERM domain is composed of the JH5, JH6, and part of the JH4 domains (Hu et al., 2021),**Figure 15**.JAK1 is a conserved tyrosine kinase expressed in various tissues and plays a crucial role in the activation loop, capable of phosphorylating all STAT proteins(O'Shea et al., 2015).It can be activated by cytokines such as interleukin-3 (IL-3), IL-5, IL-7, granulocyte-macrophage colony-stimulating factor (GM-CSF), and granulocyte colony-stimulating factor (G-CSF) to support hematopoietic functions (Ihle et al., 1995). Similarly, JAK2 can be phosphorylated by members of the gp130 receptor family and the class II cytokine-receptor family, and it is involved in signal transduction for the IL-3 receptor family (Schindler and Strehlow, 2000).JAK3 is primarily associated with signal transduction through interleukin receptors including IL-2, IL-4, IL-7, IL-9, IL-15, and IL-21 (Hu et al., 2021).
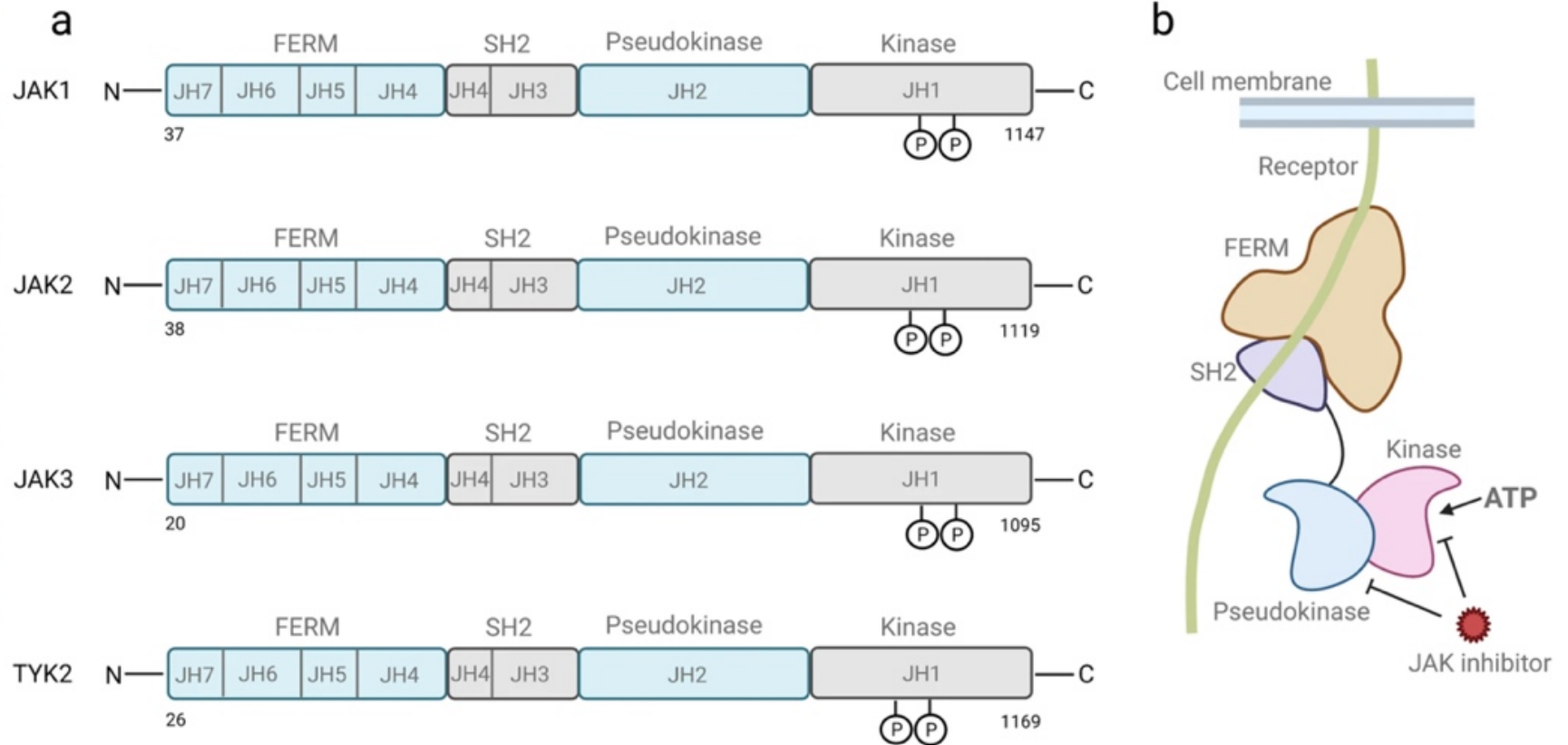
Figure 15. Structure of JAKs. Each JAK of the JAKs family is composed of seven homology domains (JH), of which JH1 constitutes the kinase domain; JH2 constitutes the pseudokinase domain; a part of JH3 and JH4 together constitute the SH2 domain; and the FERM domain is composed of the JH5, JH6, and part of the JH4 domains (Hu et al., 2021)).

3.5.2 STAT family

The STAT family comprises proteins ranging from 750 to 900 amino acids (Hu et al., 2021). Structurally, STATs have distinct domains organized from the N-terminus to the C-terminus: i) an N-terminal domain and coil, helix domain; ii) a DNA-binding domain; iii) a linker domain; iv) an SH2 domain; and a transcription-activation domain (Hu et al., 2021)(Figure 16.) Notably, the SH2 domain in STATs is highly conserved, differing from other SH2 domains, and plays a key role in interacting with activated JAKs. This interaction drives SH2-mediated dimerization of phosphorylated STAT monomers, forming homo- or heterodimers(Gupta et al., 1996, Kawata et al., 1997). STAT family members differ in stability and degradation pathways. STAT4, STAT5, and STAT6 are targeted for ubiquitin-dependent degradation, whereas STAT1, STAT2, and STAT3 are more stable, indicating that the transcriptional activation region also affects protein stability (Hu et al., 2021).

STAT1, with splice isoforms STAT1α (91 kDa) and STAT1β (84 kDa), is activated by cytokines such as IL-2, IL-6, interferons (IFN), epidermal growth factor (EGF), and tumor necrosis factor(Schindler et al., 1992) (Hu et al., 2021)). It is primarily involved in inhibiting cell growth, regulating differentiation, promoting apoptosis, and modulating the immune system (Hu et al., 2021). STAT3, like STAT1, has splice isoforms STAT3α and STAT3β with distinct functions. STAT3α activation is linked to promoting tumor growth, whereas STAT3β inhibits cancer and acts as a tumor suppressor(Dimberg et al., 2003, Avalle et al., 2017, Niu et al., 1999, Hu et al., 2021). STAT3 activation occurs through various molecules, including IL-6 family members (e.g., IL-6, IL-11), IL-10 family members, IL-21, IL-27, G-CSF, leptin, and IFNs, mainly influencing cell growth, differentiation, apoptosis, tumor occurrence, and immune responses(Darnell et al., 1994, Hu et al., 2021).

STAT2, distinct in lacking binding to original gamma-activated sites, plays a key role in immune regulation via IFN-α and IFN-β activation (Hu et al., 2021). STAT4, which consists of 784 amino acids, shares structural similarities with other STATs and is activated by cytokines like IFN, IL-12, and IL-23, playing an essential role in immune differentiation (Miyagi et al., 2007, Thieu et al., 2008).STAT5 and STAT6 are critical in regulating cell

proliferation, apoptosis, and inflammation. STAT5 is involved in the JAK/STAT5 signaling pathway triggered by IL-6, IL-15, and RTKs (Tian et al., 2020), while STAT6 participates in JAK/STAT6 signaling through IL-4 and IL-13 (Duetsch et al., 2002).
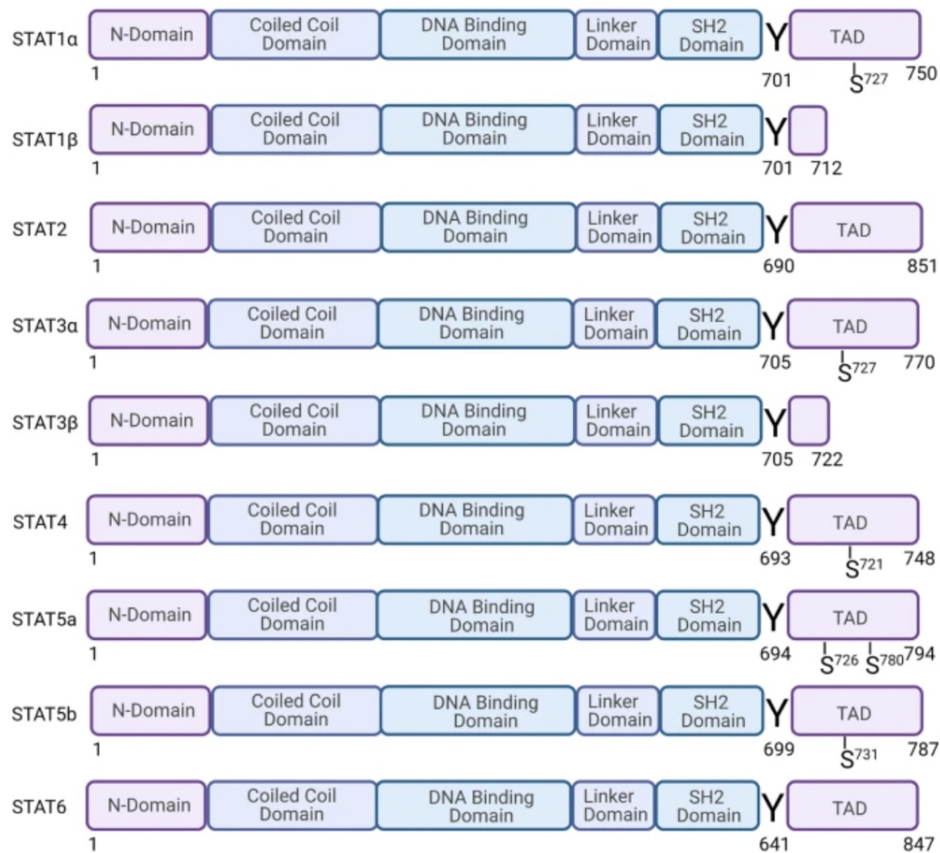

Figure 16. Structure of the STAT protein family. The STAT family comprises proteins ranging from 750 to 900 amino acids. STATs have distinct domains organized from the N-terminus to the C-terminus: i) an N-terminal domain and coil, helix domain; ii) a DNA-binding domain; iii) a linker domain; iv) an SH2 domain; and a transcription-activation domain(Hu et al., 2021)).

4 Aims and objectives

4.1 Aims:

To investigate the effects of CD33 knockout on autophagy flux and the signaling pathways that regulate autophagy in a model cell line, specifically comparing human CD33WT-U937 monocyte-derived macrophages and CD33KO-U937 monocyte-derived macrophages differentiated with PMA.

4.2 Objectives:

1. To identify and validate genes directly and indirectly associated with autophagy, as well as their signaling pathways, through mRNA transcription analysis using RNA deep sequencing, in the presence and absence of CD33.

2. To evaluate the impact of CD33 knockout on the autophagy marker LC3b and to analyze changes induced by inflammatory mediators such as LPS, GW3965, mCRP, and TNF alpha using Western blot analysis.

3. To examine alterations in autophagy-related signaling pathways resulting from CD33 knockout and to confirm these changes under different conditions using inflammatory mediators, namely LPS, GW3965, mCRP, and TNF alpha, through Western blot analysis.

5. Results

5.1 CD33 knockout verification on U937 monocyte

CD33 expression in U937 monocytes was verified using flow cytometry with a PE-conjugated anti-human CD33-WM53 antibody. In CD33WT-U937 monocytes, 99.3% CD33 expression was detected (**Figure 17C**), whereas CD33KO-U937 monocytes exhibited only 0.2% CD33 expression (**Figure 17F**).
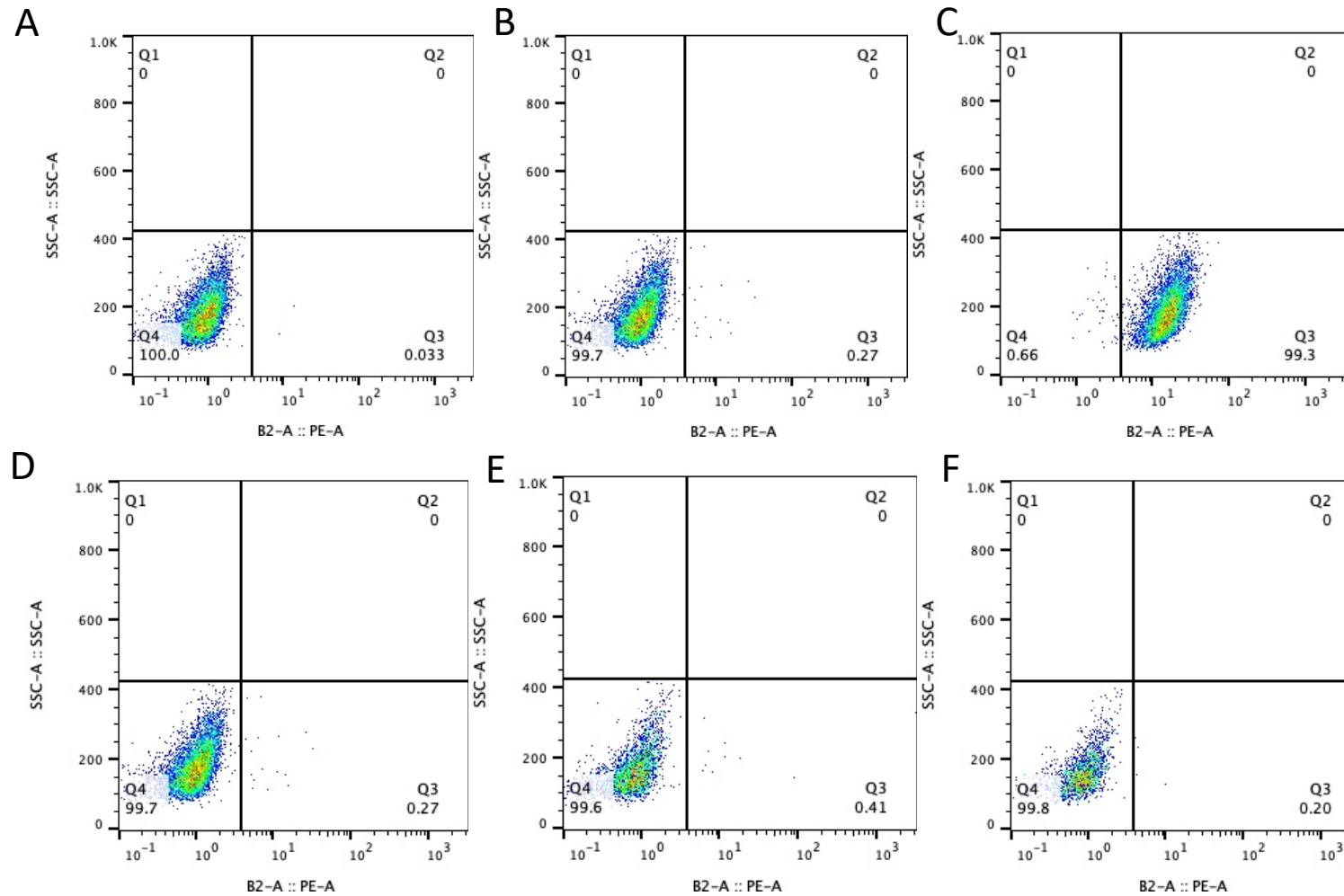
Figure 17. Flow cytometry confirmed CD33 expression on U937 monocytes wild type and CD33 knock out U937 monocytes. The expression level of CD33 on wild type-U937 monocyte and CD33 knockout-U937 monocyte was confirmed by flow cytometry with PE-conjuncted anti-human CD33-WM53 antibody. (A) and (D) represent unstained negative control of WT-U937 and CD33ko-U937 respectively;(B) and (E) represent isotype-PE staining for WT-U937 and CD33KO-U937 respectively;(C) shows the expression of CD33 level detected as 99.3% compared to an expression of 0.20% on CD33ko-U937(F) (n=3).

5.2. Differentiation of CD33WT U937 monocyte and CD33KO U937 monocyte into Macrophages

Previous studies have demonstrated that monocytes, including U937 monocytes, can differentiate into macrophage-like cells through PKC activation stimulated by PMA (Takashiba et al., 1999, Fangradt et al., 2012)).

Figure 18 illustrates morphological alterations in CD33WT-U937 and CD33KO-U937 monocytes following treatment with 50 ng/mL PMA for 24 hours. Both CD33WT-U937 and CD33KO-U937 monocytes, initially round and in suspension, differentiated into adherent cells that formed clusters attached to the culture plate surface. Compared to CD33WT-U937 macrophages (**Figure 18A**), CD33KO-U937 macrophages tended to aggregate into larger clusters (**Figure 18B)** and exhibited more pronounced polarized pseudopodia (**Figure 18B**, red arrows) and cell surface protrusions (**Figure 18D**, red arrows) than CD33WT-U937 macrophages (**Figure 18C**).

The deletion of CD33 led to morphological changes in several parameters, including cell perimeter length (µm) and cell optical volume (µm³), in CD33KO-U937 macrophages compared to CD33WT-U937 macrophages. **Figure 19** presents these changes in cell morphology parameters. The cell perimeter describes the measurement of the outer boundary length, while cell optical volume quantifies the three-dimensional space occupied by the cell based on its appearance, providing insights into overall size and spatial distribution. Both the perimeter and optical volume of CD33KO-U937 macrophages exhibit approximately a threefold increase compared to CD33WT-U937 macrophages.
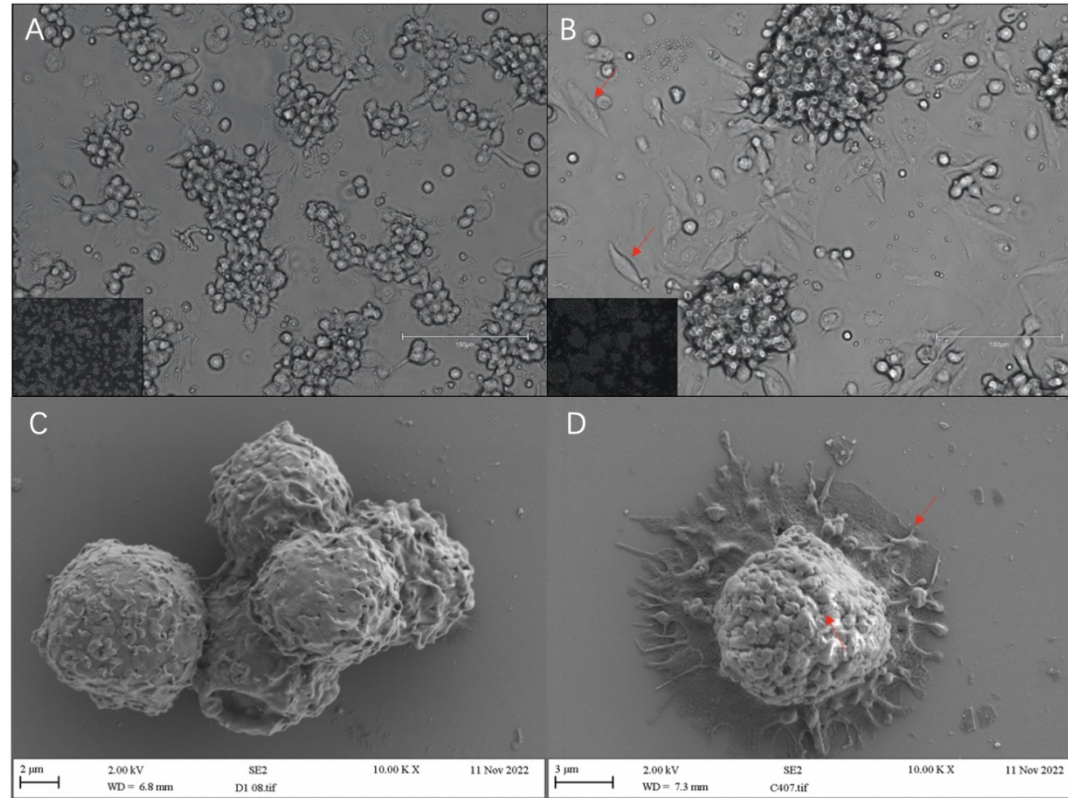
Figure 18. Morphological changes of CD33WT-U937 and CD33KO monocytes after treatment with 50 ng/mL PMA for 24 hours observed under microscope and scanning electron microscope.U937 monocytes were round suspended cells and differentiated into adherent macrophages(A)and(B);(A): CD33WT-U937 macrophage are more likely to aggregate as small and symmetrical clusters compared to large sizes clusters of CD33KO-U937 macrophages aggregated (B).CD33KO-U937 macrophages show polarized changes in morphology and more pseudopodia(D) compared to relatively flat cell surface as shows in CD33WT-U937 macrophages(C). Images were taken with 20X magnification using microscope and 10.00KX magnification with scanning electron microscope. (n=3).

Figure 19. Validation of effect of CD33 knocking out on cell morphology by holomonitor microscope. Deletion of CD33 induce morphology changes in CD33KO-U937 macrophages in cell-morphology parameters of Av. cell perimeter length(um) and Av. cell optical volume(um3) compared to WT-U937 derived macrophages. Data presented as Mean ± SD – t-test (p* = < 0.05 p **= <0.01, p*** = < 0.001, p**** <0.0001. (n=4).

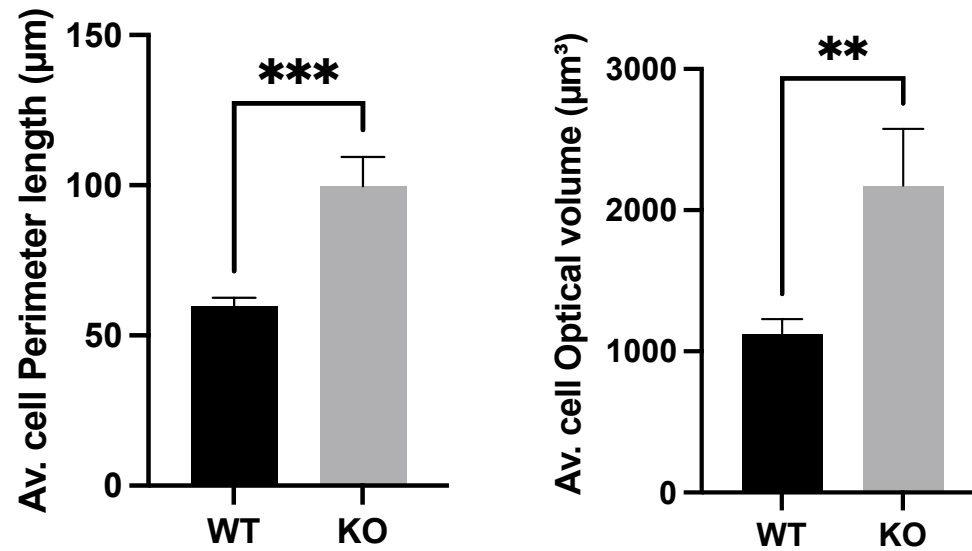**5.3 Validation changes of transcription of key mediators involved in autophagy process related proteins influenced by CD33 knockout by RNA deep sequencing analysis in the presence and absence of LPS**

To assess the effect of CD33 knockout on autophagy-related genes, an RNA deep sequencing assay was conducted. CD33WT-U937 and CD33KO-U937 cells were fully differentiated into macrophages using PMA treatment. Cells were harvested, and RNA was extracted for deep sequencing analysis. The heatmap in **Figure 20A** displays a series of genes directly or indirectly involved in the autophagy process. The deletion of CD33 resulted in increases in gene expression compared to the wild type in PMA-derived macrophages.

Gene analysis focused on autophagy mediators that directly regulate key processes, illustrated in the bar charts in **Figure 20B**. Positive mediators, including BNIP3L (interacting with LC3 to facilitate engulfment), SORL1 (interacting with Beclin-1 for autophagy initiation), and EIF2 alpha (inducing the ISR signaling pathway to upregulate LC3 expression), showed respective increases of 1.5-fold, 5-fold, and 1.5-fold in CD33KO-U937 macrophages compared to CD33WT-U937 macrophages ($P<0.05$). Conversely, IRS2 (activating the mTOR signaling pathway to promote cell survival but inhibit autophagy) and PDK1 (activating the AKT signaling pathway) exhibited twofold and threefold decreases, respectively, in CD33KO-U937 macrophages ($P<0.05$).

Analysis of JAK/STAT signaling-related mediators, specifically JAK2, JAK3, and STAT3, revealed decreases of 2-fold, 5-fold, and 3-fold, respectively, in CD33KO-U937 macrophages compared to CD33WT-U937 macrophages ($P<0.0001$), as shown in **Figure 21**. PI3K/AKT signaling components, such as PDK1 and its downstream factor AKT1, demonstrated transcriptional decreases of threefold and twofold, respectively, following CD33 knockout ($P<0.0001$).

Other notable changes include a twofold upregulation of SOCS3 and a 1.8-fold increase in the lysosome marker LAMP2 in CD33KO-U937 macrophages compared to CD33WT-U937

macrophages (P<0.05). The enzymes INPP4A, INPP4B, INPP5B, and INPP5K, which are involved in degrading PIP3, showed decreases ranging from 1.6-fold to 25-fold in CD33KO-U937 macrophages (P<0.001).
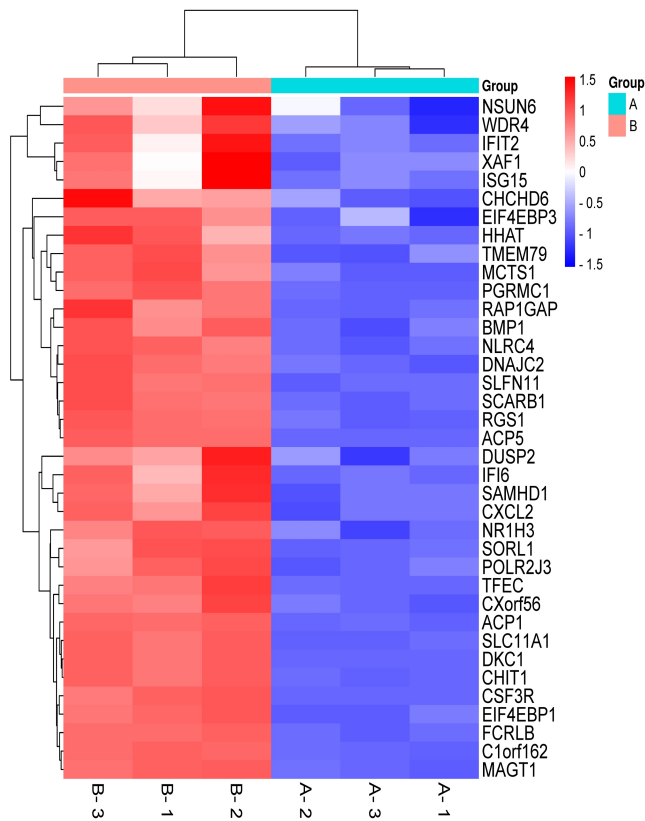
(A)
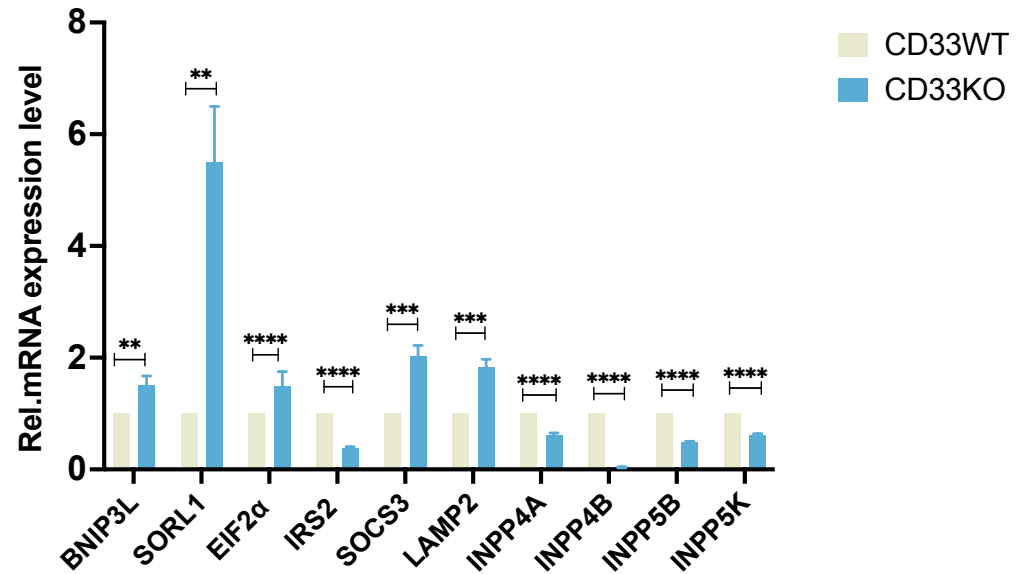
(B)

Figure 20. Gene expression analysis. (A): Heatmap illustrating Autophagy related genes upregulated in CD33KO-U937 derived macrophage compared to CD33WT-U937 derived macrophage, confirming by RNA deep sequencing. Color blue indicates baseline expression of autophagy related genes expressed in CD33WT-U937 derived macrophage; Color red, represents upregulation in expression of autophagy related genes expressed in CD33KO-U937 derived macrophage. Group A (on the Right): CD33WT-U937 derived macrophage, group B (on the left) CD33KO-U937 derived macrophage;(n=3 per genotype). (B): Relative mRNA expression level of autophagy related genes selected as directly involved in autophagy process in CD33WT group and CD33KO group. Data presented as Mean ± SD – t-test (p* = < 0.05 p **= <0.01, p*** = < 0.001, p**** <0.0001. (n=3)

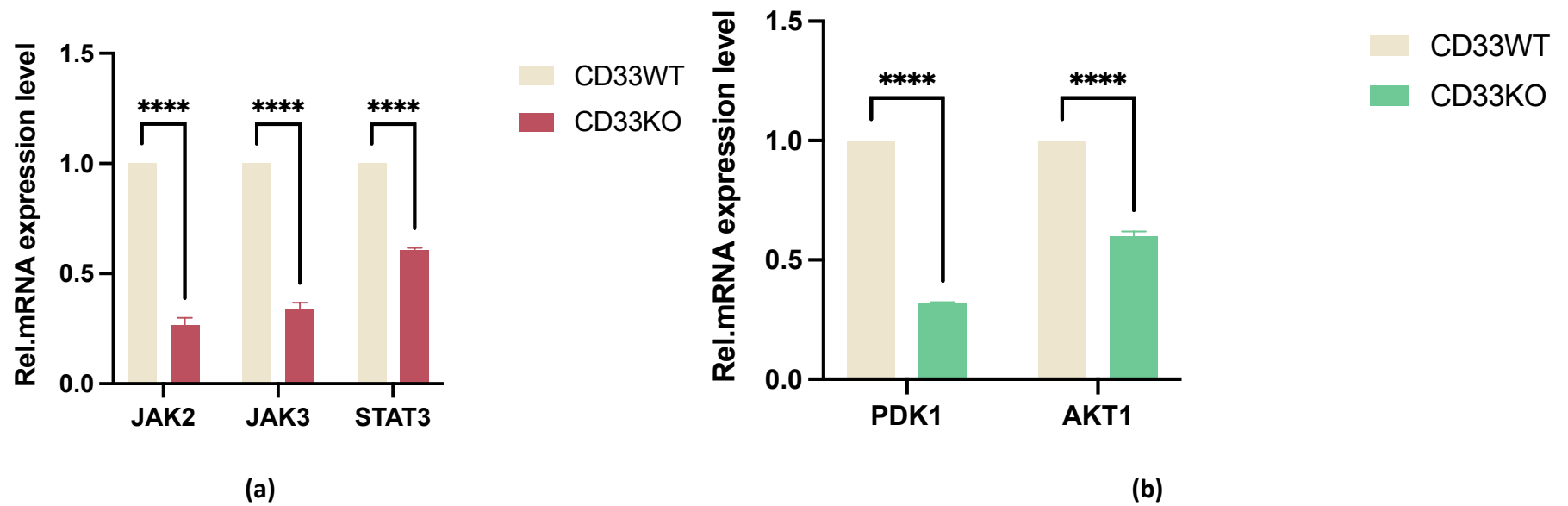**Figure 21. Key factors transcription in PI3K/AKT and JAK/SATA signalling.** CD33 knockout decreased transcription of JAK2, Jak3 and STAT3 with changes of 2-fold,5-fold and 3-fold, respectively (a); and decreased transcription of PDK1 and AKT1 with changes of 3-fold and 2-fold, respectively(b). Data presented as Mean ± SD – t-test (p* = < 0.05 p **= <0.01, p*** = < 0.001, p**** <0.0001. (n=3).

5.4 Validation effect of CD33 knockout on autophagy flux and key factors of signallings by Western blot assays

To further validate changes in autophagy flux and JAK/STAT3 signaling in CD33WT-U937 and CD33KO-U937 macrophages, experiments were conducted as follows: CD33WT-U937 and CD33KO-U937 monocytes were seeded at a density of 1 x 10^6 cells/mL in 6-well plates and differentiated into macrophages using 50 ng/mL PMA, as described in section 2.3. Subsequently, cells were treated with 100 ng/mL LPS and 1 µM GW3965 under both serum and serum-free conditions for 12 hours. Following the treatments, cells were lysed to extract proteins as outlined in section 2.6.2. The autophagy flux marker LC3b and key signaling factors ERK/MAPK and JAK/STAT3 were quantified using Western blot assays, as described in section 2.6.4.

3.4.1 CD33 knockout induces a tremendous increase of LC3b expression

CD33 knockout induced increased expression of the autophagy flux marker LC3b under both nutrient-rich and nutrient-poor conditions, as shown in **Figure 22A** and **Figure 22B**. In nutrient-poor conditions, CD33KO-U937 macrophages exhibited a significant 15-fold upregulation of LC3b expression compared to CD33WT-U937 macrophages (P<0.01), as illustrated in **Figure 25.**

5.4.2 CD33 knockout inhibited phosphorylation of STAT3 but no difference in activating ERK1/2

CD33 knockout resulted in a significant 10-fold decrease in the activation of STAT3, a key component of the JAK/STAT3 signaling pathway, as shown in **Figure 22C** and **Figure 25** (P<0.0001). In contrast, there was no significant difference observed in the phosphorylation of ERK1/2 within the ERK/MAPK signaling pathway in CD33KO-U937 macrophages compared to CD33WT-U937 macrophages (P>0.05), as depicted in **Figure 22D** and **Figure 25**.

5.4.3 LPS and GW3965 can induce autophagy flux marker of LC3b

To evaluate the effects of LPS and the liver X receptor agonist GW3965 on autophagy, Western blot analysis was performed on samples from CD33KO-U937 macrophages cultured under serum-free conditions, as LC3b expression in CD33WT-U937 macrophages was too low to detect. Both LPS and GW3965 individually promoted LC3b expression, showing increases of 1.4-fold and 1.3-fold, respectively, as a result of CD33 knockout (**Figure 26**, P<0.01). When cells were simultaneously treated with LPS and GW3965, the promoting effect on LC3b expression slightly increased to 1.5-fold compared to negative controls (**Figure 26**, P<0.01).

5.4.4 LPS increased STAT3 activation while GW3965 strongly inhibited JAK/STAT3 signalling activation

As shown in **Figure 22C**, STAT3 can be induced by LPS stimulation, resulting in a twofold increase in CD33WT-U937 macrophages (**Figure 27**, P<0.05). A substantial increase in phosphorylated STAT3 was observed in CD33KO-U937 macrophages when treated with LPS under serum-free conditions. However, the activation of STAT3 was significantly inhibited by GW3965 in CD33WT-U937 macrophages compared to the negative control (**Figure 22C**).

5.4.5 LPS induced ERK1/2 activation in the presence of CD33, but no changes were detected in the absence CD33; GW3965 did not contribute to ERK1/2 activation in the presence and absence of CD33

Western blot assays confirmed that LPS induced an average 2.5-fold increase in ERK1/2 activation in CD33-expressing cells (**Figure 22D** and **Figure 28**, P<0.05). However, no significant changes were observed when cells were treated with LPS in the absence of CD33 (**Figure 22D** and **Figure 28**, P>0.05). Additionally, CD33 knockout did not result in significant changes in pERK1/2 expression, as shown in **Figure 22D** (despite a weak band observed in CD33KO-U937 macrophages) and **Figure 25** (P>0.05).

5.4.6 Effect of proinflammatory factors on JAK/STAT3 signalling and ERK1/2/MAPK signalling pathway in the presence and absence of CD33

As shown in **Figure 54**, CD33 knockout induced the transcription of TNFα. To investigate whether proinflammatory mediators affect ERK1/2 and STAT3 signaling, CD33WT-U937

and CD33KO-U937 macrophages were stimulated with mCRP (25 μg/mL) and TNFα (10 ng/mL) under serum-free conditions for 12 hours. Subsequent Western blot assays were conducted as described in section 2.6.

As shown in **Figure 23A** and **Figure 23B**, TNFα induced ERK1/2 activation in the absence of CD33 but strongly inhibited STAT3 activation both with and without CD33 presence. Conversely, mCRP did not significantly alter ERK1/2 activation in either CD33 condition, but it did induce STAT3 activation regardless of CD33 expression.

5.4.7 TNFα and mCRP promote LC3b expression

CD33 knockout strongly inhibited STAT3 activation and was accompanied by a marked increase in LC3b expression, as shown in **Figures 22C** and **22A**. CD33 knockout also induced an increase in TNFα transcription (**Figure 54**), and previous studies have indicated that TNFα stimulates LC3b expression in OCCM-30 cells (Wang et al., 2018).To confirm this effect in our U937 monocyte model, Western blot assays were conducted to verify the impact of TNFα and mCRP on LC3b expression.CD33WT-U937 and CD33KO-U937 macrophages were incubated with mCRP (25 μg/mL) or TNFα (10 ng/mL) under serum-free conditions for 12 hours, and subsequent Western blot assays were performed as described in section 2.6.4.

As potent pro-inflammatory mediators, TNFα and mCRP increased LC3b expression in the presence of CD33 by 3.5-fold (P<0.01) and 6.5-fold (P<0.0001), respectively, as shown in **Figures 24A** and **24B**. However, no significant differences were observed in LC3b expression when cells were stimulated with TNFα and mCRP in the absence of CD33 (P>0.05).

5.5 Observation of LC3b by immunofluorescent staining in the presence and absence of CD33

Autophagy flux was significantly enhanced by CD33 knockout. To further visualize the expression and localization of LC3b in cells, CD33WT-U937 and CD33KO-U937 monocytes were fully differentiated into macrophages as described in section 2.3 and starved for 6 hours. Immunofluorescent staining assays were then performed according to the method outlined in section 2.8.5. LC3b was visualized using a goat anti-rabbit IgG (H+L) Superclonal

Secondary Antibody, Alexa Fluor® 488 conjugate, and images were captured with a confocal microscope at 100X magnification, with a scale bar set at 10 μm using Z-stack imaging.

A marked increase in LC3b expression was observed in CD33KO-U937 macrophages compared to CD33WT-U937 macrophages. LC3b was distributed throughout the cytoplasm, with some areas showing aggregation during autophagic activity, as illustrated in **Figure 29**.
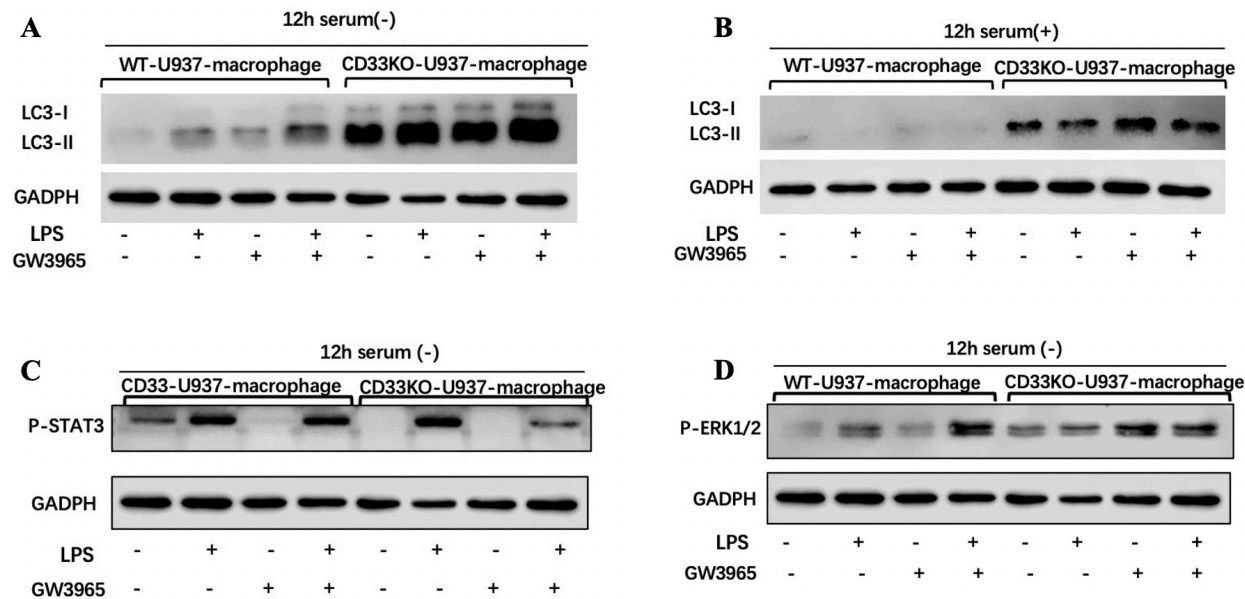
Figure 22. Representative blot images of LC3b, p-ERK1/2 and p-STAT3 in the presence of absence of CD33 with different stimulations for 12 hours.(A) and (B) autophagy flux maker of LC3b expression in CD33WT-U937 macrophages and CD33KO-U937 macrophages with treatments of 100ng/ml LPS and/or 1uM GW3965 under nutrient-rich(A) and nutrient-deprived condition; (C) phosphorylated STAT3 in CD33WT-U937 macrophages and CD33KO-U937 macrophages with treatments of 100ng/ml LPS and/or 1uM GW3965 under nutrient-deprived condition; (D) phosphorylated ERK1/2 in CD33WT-U937 macrophages and CD33KO-U937 macrophages with treatments of 100ng/ml LPS and/or 1uM GW3965 under nutrient-deprived condition. Samples were harvested in serum (+) and/or in serum (-) condition. Images presented one of four independent trials.
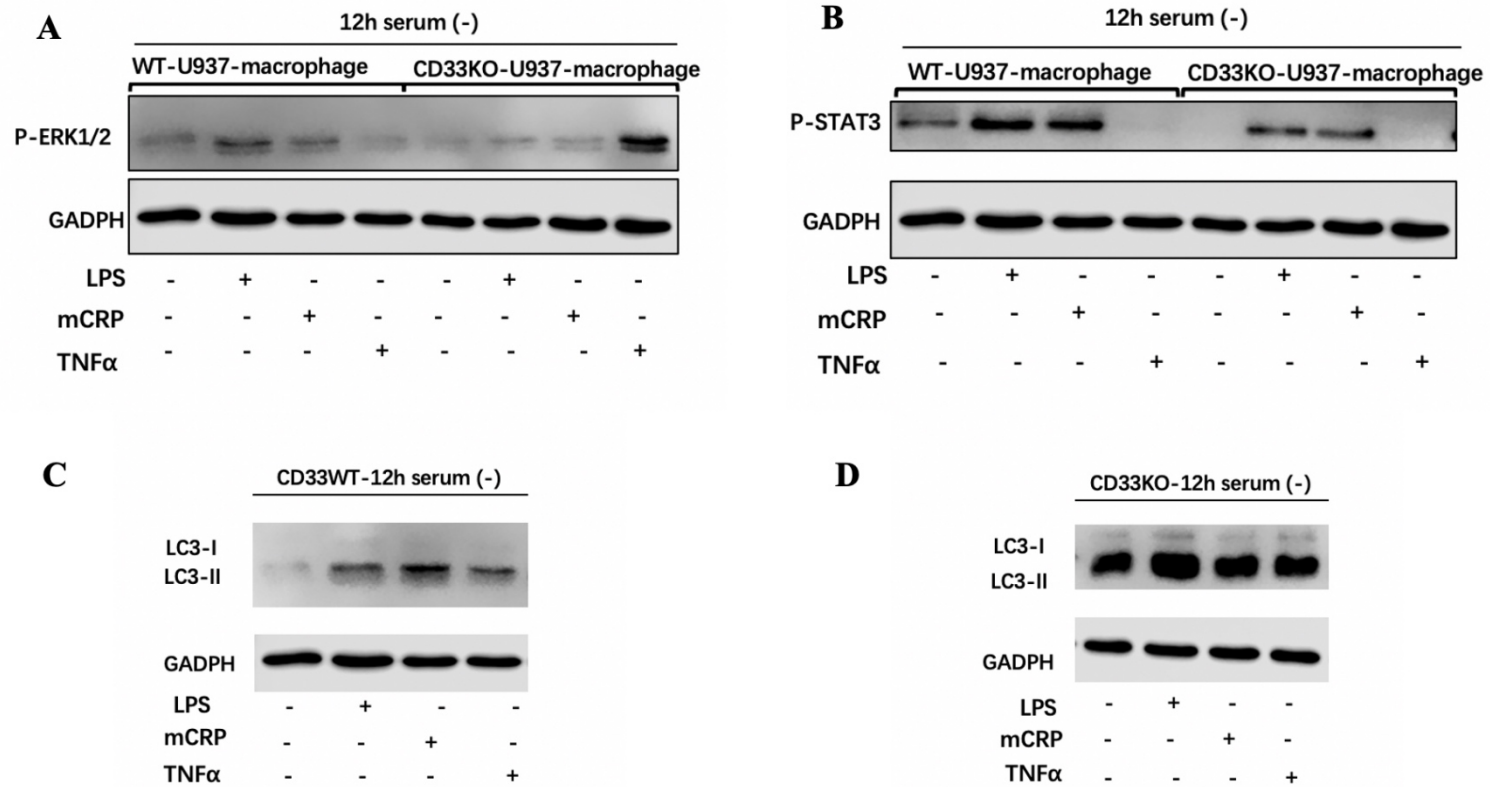
Figure 23. Representatives of ERK1/2 and phosphatase STAT3 expression. (A, B, C, D) represents blot images of pERK1/2, pSTAT3 and LC3b with the corresponding loading control GADPH in CD33WT-U937 macrophages and CD33KO-U937 macrophages with and without stimulation of mCRP and TNFα for 12 hours in serum-free condition. LPS and mCRP induced activation of STAT3, however, TNFα inhibited pSTAT3 in the presence and absence of CD33. (n=3).
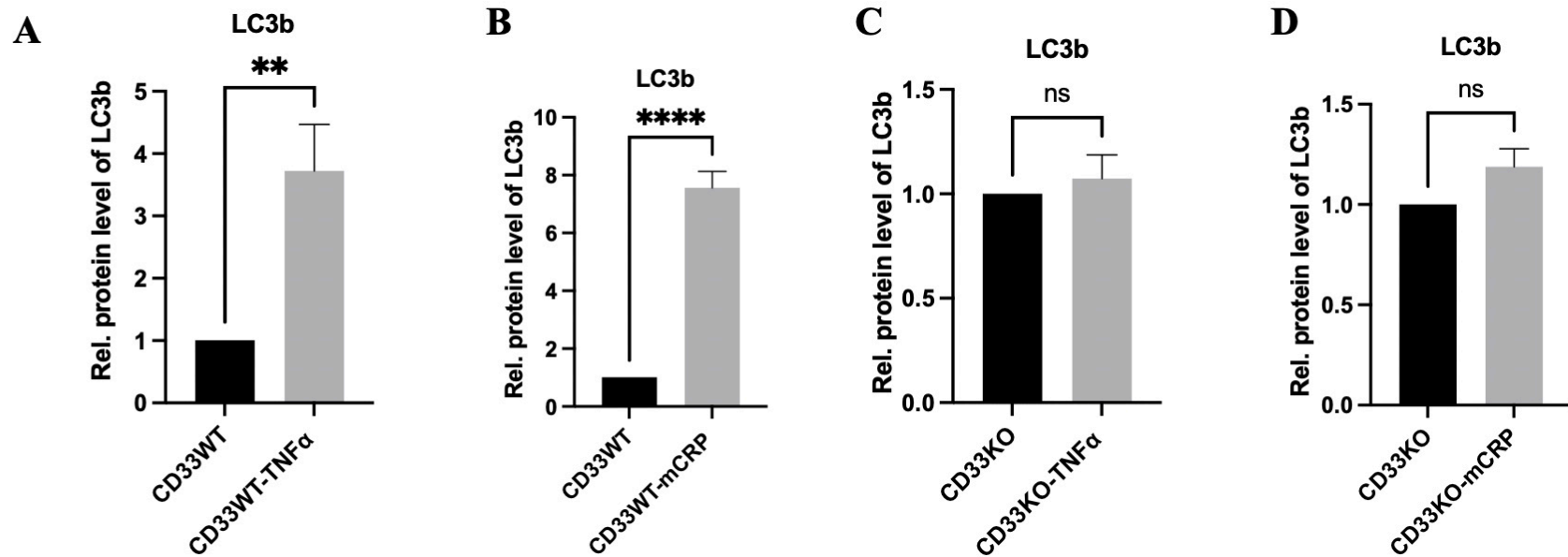
Figure 24. Relative LC3b expression in PMA-differentiated macrophages stimulated by mCRP and TNFα. CD33WT-U937 macrophages and CD33KO-U937 macrophages were treated with drugs for 12 hours in serum-free conditions. In the presence of CD33, TNFα induced a 3.5-fold increase, and mCRP resulted in a 6.5-fold upregulation respectively compared to negative controls (A and B); however, in the absence of CD33, neither TNFα nor mCRP made significant changes in LC3b expression compared to negative controls (C and D). Data presented as Mean ± SD – t-test (p* = < 0.05 p **= <0.01, p*** = < 0.001, p**** <0.0001. (n=3).
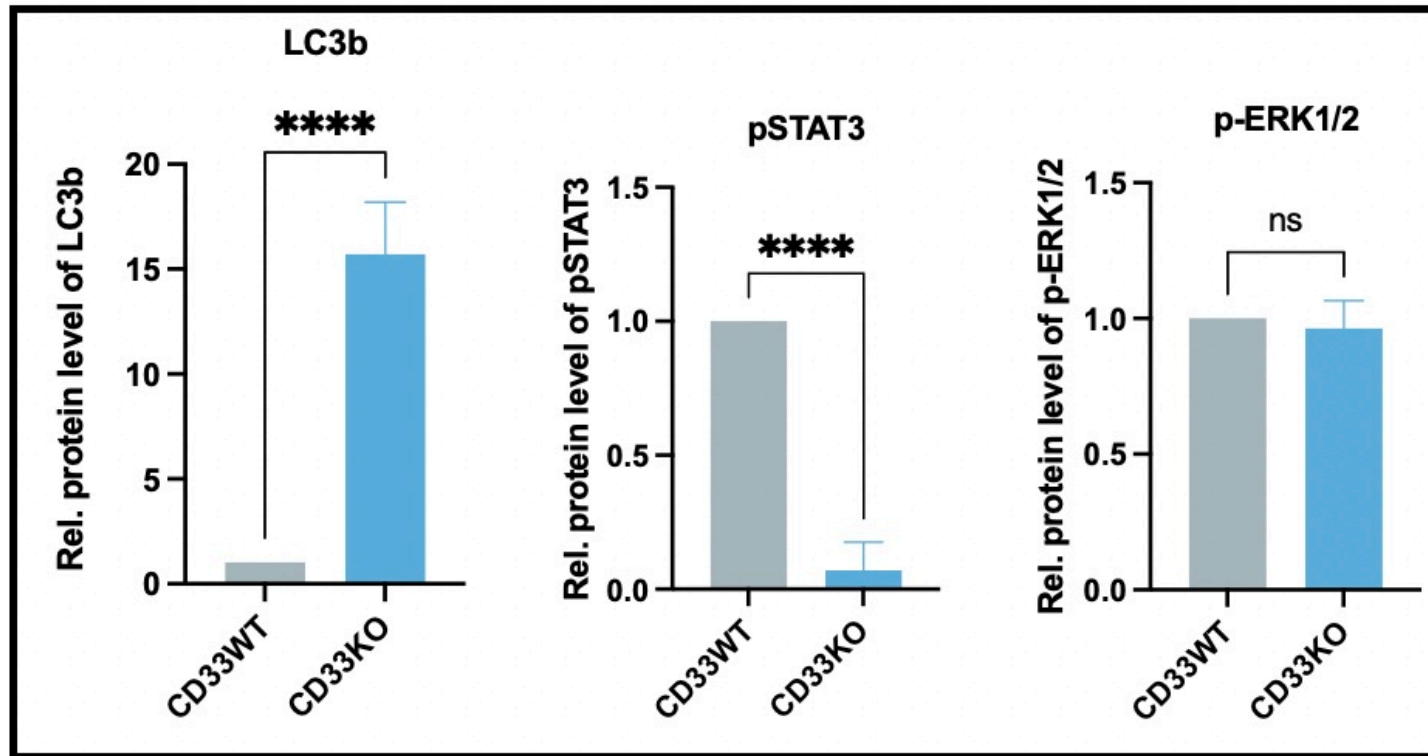
Figure 25. Western blot analysis of the effect of CD33 knockout on LC3b, pSTAT3 and p-ERK1/2. The deletion of CD33 induced a 15-fold increase and a sharp decrease in pSTAT3 (barely undetected in CD33KO-U937 macrophages seen as in Figure 25 and Figure 26), respectively (P < 0.001, mean ± SD, n = 4 independent experiments). No significant changes in activation of ERK1/2 were found between CD33WT-U937 macrophages and CD33KO-U937 macrophages (P>0.05, mean ± SD, n = 4 independent experiments).
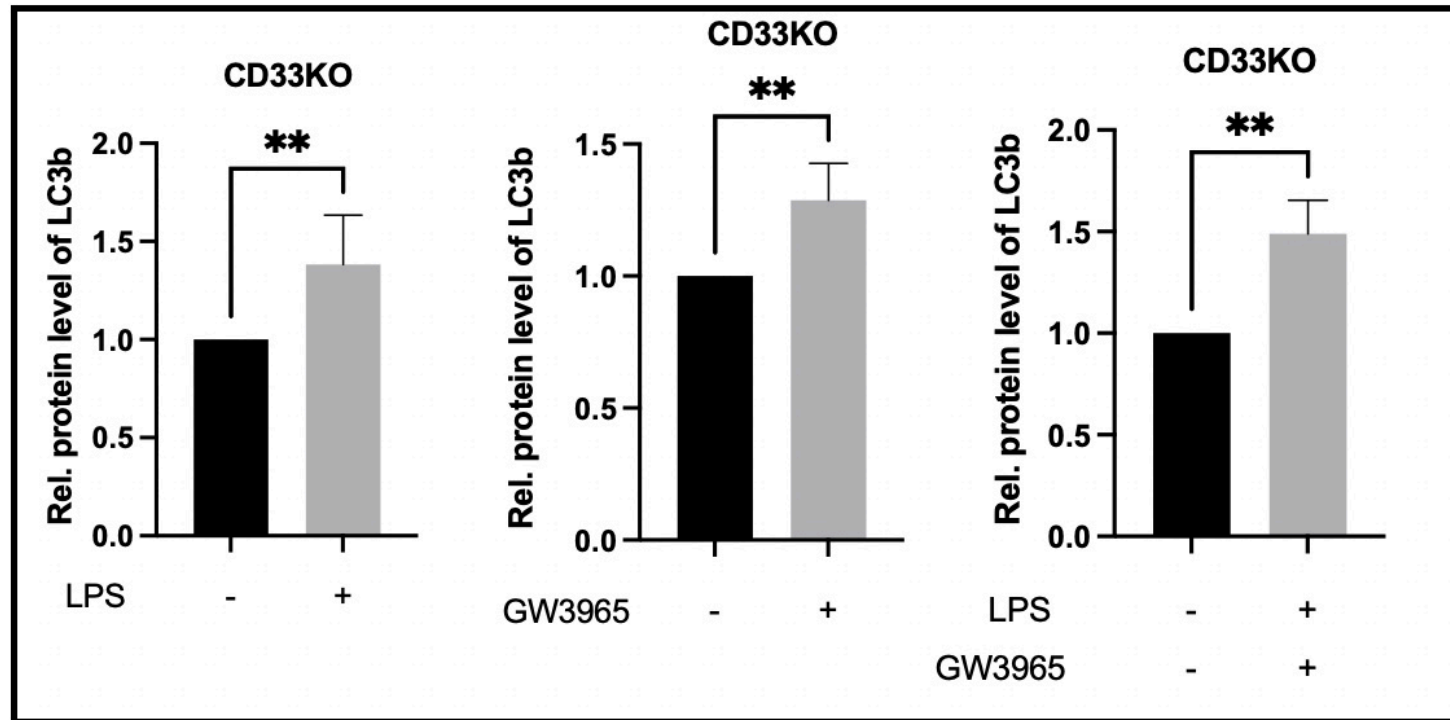
Figure 26.LC3b expression changes with stimulation of LPS and/or GW3965 in the absence of CD33. CD33KO-U937 macrophages were stimulated by LPS and/or GW3965 for 12 hours in serum free condition. LPS induced a 1.4-fold increase in LC3b expression; GW3965 induced 1.3-fold increase in LC3b expression, and a 1.5-fold increase was detected when treated with LPS and GW3965 compared to the negative controls. ($P < 0.01$, mean ± SD, n = 4 independent experiments).
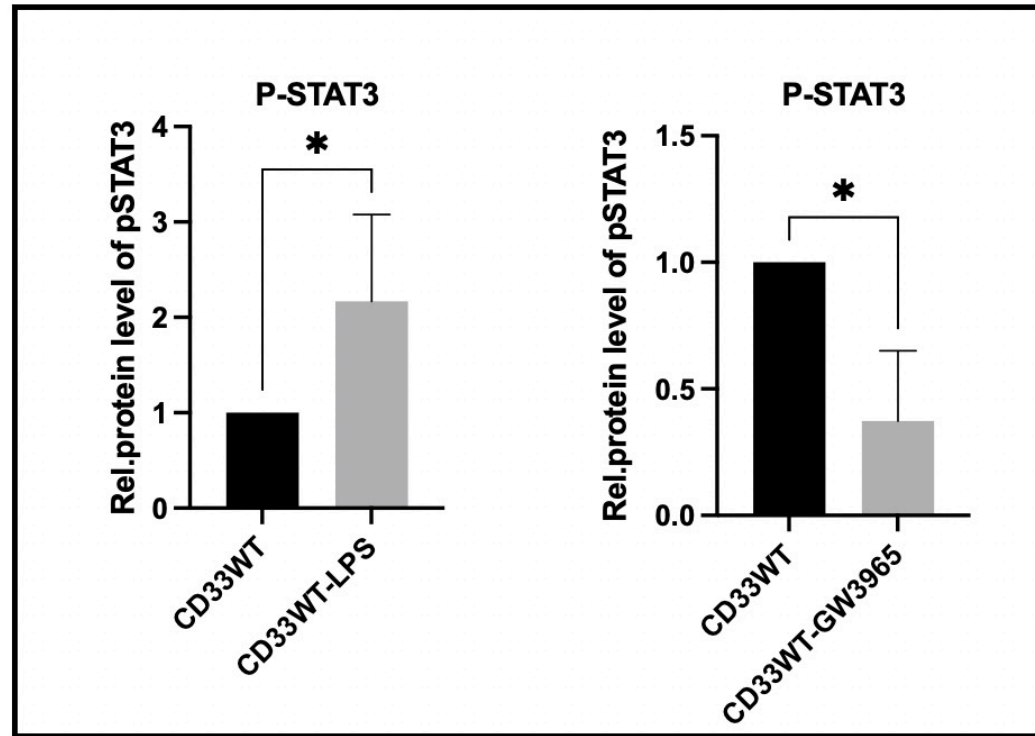
Figure 27.p-STAT3 expression changes by stimulation of LPS or GW3965 in the presence of CD33. CD33KO-U937 macrophages were stimulated by LPS and/or GW3965 for 12 hours in serum free condition. LPS induced a 2-fold increase in pSTAT3 expression, and GW3965 caused a half decrease in pSTAT3 expression, ($P < 0.01$, mean ± SD, n = 4 independent experiments). CD33 knockout strongly inhibited pSTAT3 expression and there were no bands detected in CD33KO-U937 macrophages negative controls.
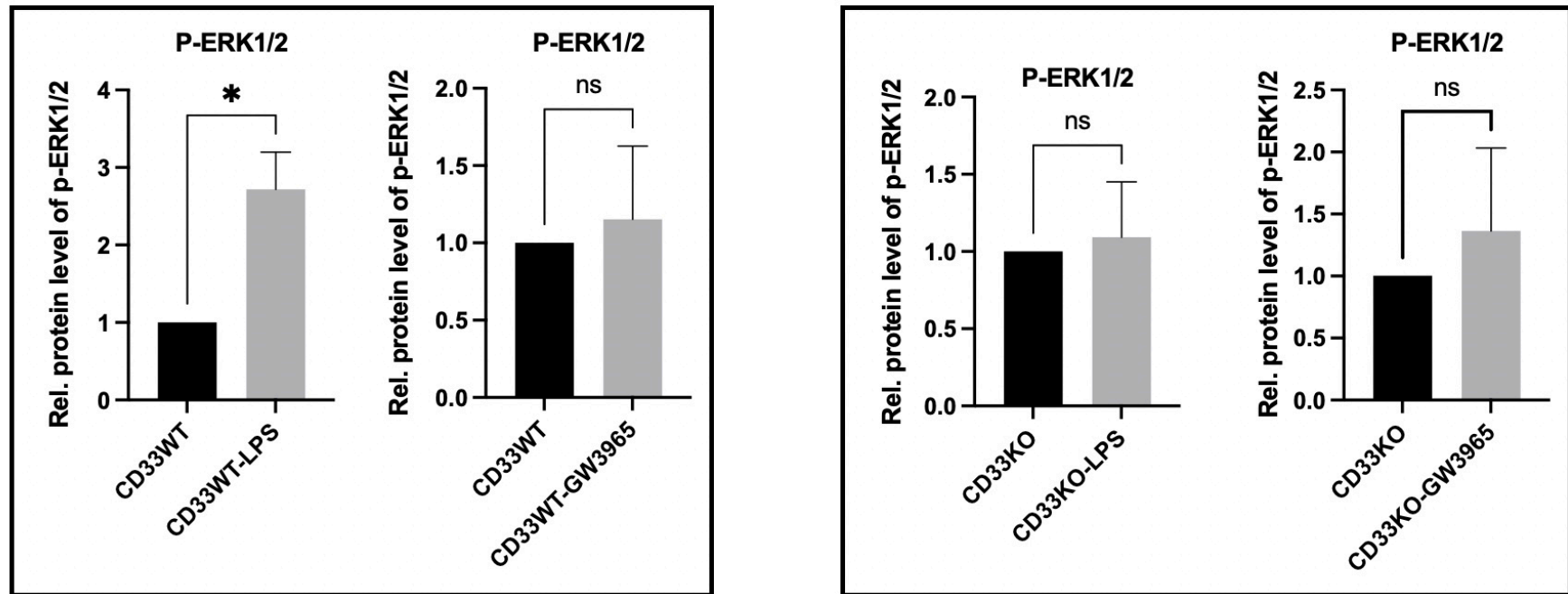
Figure 28.p-ERK1/2 expression changes by stimulation of LPS or GW3965 in the presence and absence of CD33.CD33WT-U937 macrophages and CD33KO-U937 macrophages were stimulated by LPS and/or GW3965 for 12 hours in serum-free condition. In the presence of CD33, LPS induced a 2.5-fold increase in p-ERK1/2 expression ($P < 0.05$) and there were no significant changes caused by GW3965($P > 0.05$) compared to the CD33WT-U937 macrophages negative controls, respectively. Neither LPS nor GW3965 induce significant changes in the expression of p-ERK1/2 in CD33KO-U937 macrophages compared to theirie corresponding negative controls($P > 0.05$). (mean ± SD, n = 4 independent experiments).
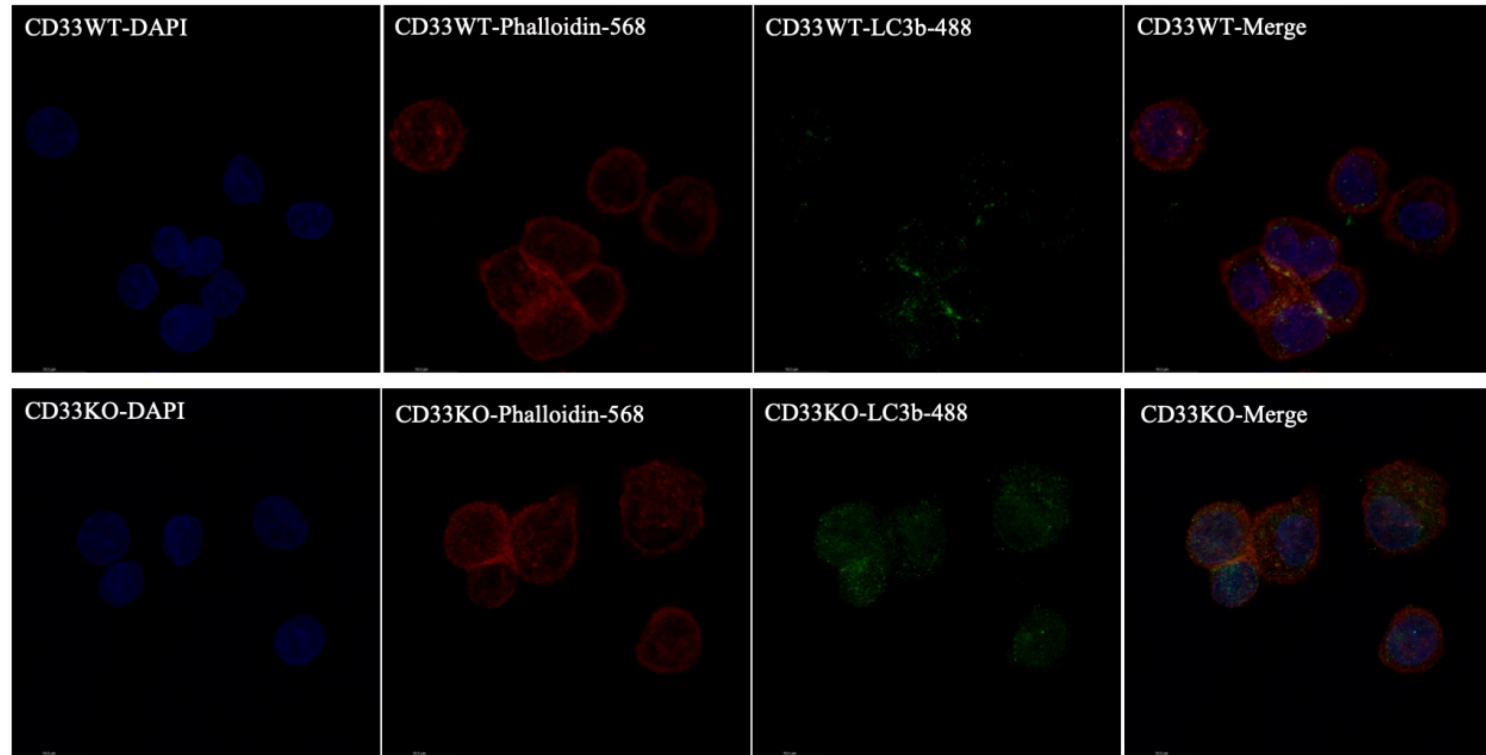
Figure 29. Visualization of LC3b protein expression and localization in CD33WT-U937 and CD33KO-U937 derived macrophages. Immunofluorescent staining for nuclear (blue- DAPI), cell skeleton(red-Phalloidin-568) and LC3(green-488) were observed by confocal microscope. CD33WT-U937 monocytes and CD33KO-U937 monocytes were fully differentiated into macrophages by PMA stimulation. Cells were further cultured in serum free condition for 6 hours to perform immunofluorescent staining. CD33WT-U937 macrophages and CD33KO-U937 macrophages were stained with phallodin-568 to visualize cell skeleton, DAPI to visualize nuclear, and goat anti-rabbit IgG (H+L) superclonal secondary antibody, alexa fluor® 488 conjugate to visualize rabbit anti-human LC3b monoclonal antibody. Z-stack confocal images (100X) were taken with a scale bar of 14.7um.

6.Discussion

Autophagy is a critical cellular process that recycles nutrients and generates energy during periods of starvation, allowing cells to digest misfolded proteins and other damaged components to maintain homeostasis(He and Klionsky, 2009).LC3b is integral to macroautophagy, serving as a key marker due to its presence on autophagosomes, thus facilitating monitoring of autophagy flux(Romao and Münz, 2014).Impaired autophagy has been linked to the accumulation of amyloid beta plaques in Alzheimer's Disease (AD) brains. In this study, the impact of CD33 knockout on autophagy flux was investigated by assessing LC3b expression through Western blot and immunofluorescent assays in CD33WT-U937 and CD33KO-U937 macrophages differentiated with PMA, with or without stimulation by LPS, TNFα, and mCRP. The discussion further explores how CD33 knockout influences the signaling pathways that regulate autophagy.

The deletion of CD33 eliminates ITIMs, leading to significant changes in gene expression at both the mRNA and protein levels. Western blot analysis revealed a substantial increase in LC3b protein in CD33KO-U937 macrophages compared to CD33WT-U937 macrophages after 12 hours in serum-free conditions, regardless of stimulation with LPS, TNFα, mCRP, or GW3965. However, RNA sequencing did not show a significant difference in LC3b mRNA levels following 6 hours of starvation after M0 differentiation.This discrepancy underscores the complex regulation of autophagy through various signaling pathways that interact to ensure a balanced response to different stimuli.

RNA deep sequencing confirmed increased expression of numerous genes associated with autophagy following CD33 knockout, correlating with the elevated LC3b protein levels in CD33KO-U937 macrophages. These changes appear to result from the loss of CD33 and its ITIM signaling. The lack of CD33 removes its associated ITIM motifs, which initiate various downstream signaling cascades. Normally, CD33 ligand binding leads to ITIM phosphorylation by Src family kinases, followed by SHP-1/SHP-2 binding, which is crucial for signal transduction. Without ITIMs, these pathways are disrupted. SHP-2, widely expressed in various cell types, becomes activated upon binding to phosphotyrosines,

while SHP-1, primarily found in hematopoietic cells, is not further discussed here(Xu and Qu, 2008) (Seif et al., 2017) (Neel et al., 2003). The increased autophagy flux observed with CD33 knockout likely alters the signaling network in CD33WT-U937 macrophages. The significant changes in mRNA and protein expressions of key genes suggest that CD33 knockout enhances autophagy flux by inhibiting the JAK/STAT3 and AKT/PI3K signaling pathways.

6.1 CD33 knockout induced autophagy flux via inhibiting activation of JAK/STAT3 signalling

RNA deep sequencing revealed a threefold decrease in JAK2 mRNA expression and a 1.5-fold decrease in JAK3 and STAT3 mRNA levels following CD33 knockout. This reduction was accompanied by a marked decrease in phosphorylated STAT3 expression, confirmed via Western blot analysis. These findings suggest that CD33 knockout may exert an inhibitory effect on JAK/STAT3 signaling. The loss of ITIM motifs reduces the recruitment of SHP1 and SHP2, leading to altered signal transduction in the JAK/STAT3 pathway, which influences autophagy. Previous studies have indicated that SHP-2 can promote JAK2 activation (Yu et al., 2003)(Xu and Qu, 2008). Among JAKs, JAK2 acts as an anchor site for STAT3 activation (Chen et al., 2023, Casanova et al., 2012).Furthermore, SHP2 has been shown to dephosphorylate JAK2 at Y570, enhancing JAK2 and downstream STAT3 activity (Zehender et al., 2018).The decreases in mRNA levels of JAK2, JAK3, and STAT3, along with reduced p-STAT3 protein expression following CD33 knockout, support the notion that SHP-2 positively regulates JAK2, which in turn activates STAT3 signaling. Notably, STAT3 is known to play a role in autophagy regulation(Xu et al., 2022).A study by Shen et al. demonstrated that chemical inhibition of STAT3 enhances autophagy, whereas high STAT3 expression suppresses it both in vitro and in vivo(Shen et al., 2012).STAT3 inhibits autophagy by binding its SH2 domain to the C-terminal region of protein kinase R (PKR), preventing phosphorylation of EIF2a—a crucial step for autophagy initiation via the LC3b and ATG5 cascades (Rouschop et al., 2010).In this project, CD33 knockout induced a 1.5-fold increase in EIF2a mRNA expression in CD33KO-U937 macrophages compared to CD33WT-U937 macrophages. This decrease in STAT3 activation may relieve its inhibitory effect on EIF2a, thus promoting autophagy. Additionally, TNFα was found to inhibit pSTAT3

expression in the presence of CD33, as validated by Western blot, while simultaneously increasing LC3b expression. This observation suggests a negative relationship between autophagy and JAK/STAT3 signaling.

Supporting this notion, Suppressor of Cytokine Signaling 3 (SOCS3) mRNA levels showed a twofold upregulation in CD33KO-U937 macrophages compared to CD33WT-U937 macrophages. It is known that SHP2 shares binding sites with SOCS3 (Nicholson et al., 2000, De Souza et al., 2002).SOCS3 can inhibit JAK2 by binding to its conserved glycine-glutamine-methionine (GQM) motif—unique to JAK2—and can suppress STAT3 activation by interacting with both JAKs and cytokine receptors (Babon et al., 2012)(Carow and Rottenberg, 2014).The increased SOCS3 transcription in CD33KO-U937 macrophages may reflect compensatory feedback due to decreased JAK2 mRNA levels, contributing to reduced STAT3 activation and consequently downregulating autophagy in these cells.

6.2 CD33 knockout induced autophagy flux via PI3K/AKT/mTOR signalling in a JAK/STAT3 dependent and independent mechanism

Phosphoinositide 3-kinase (PI3K) is a crucial enzyme involved in multiple cellular signaling pathways. As a lipid kinase, PI3K mediates the conversion of PIP2 to PIP3, serving as a second messenger to recruit AKT to the cell membrane, where it is activated by PDK1 (Arunsi et al., 2022)(Ziemba et al., 2013). Active AKT subsequently phosphorylates mTOR, regulating processes such as cell survival, growth, and angiogenesis in response to extracellular stimuli (Zhu et al., 2014),while inhibiting autophagy.Similar to STATs, PI3K contains an SH2 domain, allowing it to bind phosphorylated receptors activated by JAKs(Rawlings et al., 2004).The PI3K/AKT/mTOR signaling pathway is well-known for its crucial role in regulating autophagy; it promotes cell growth and survival, but its inhibition induces autophagy. Changes in this signaling pathway shift autophagic activity accordingly. JAK promotes mTOR activation through the induction of PI3K/AKT signaling, leading to autophagy inhibition (Arunsi et al., 2022).In this project, CD33 knockout resulted in reduced mRNA levels of JAK2, JAK3, STAT3, PDK1, and AKT1, ultimately suppressing mTOR activation and promoting autophagy in CD33KO-U937 macrophages. This suggests that reductions in

JAK2 and JAK3 may decrease AKT signaling activation, as depicted in **Figure 30**. A prior study with HUVECs demonstrated that JAK/STAT3 pathway activation induces PI3K/AKT signaling (Zegeye et al., 2018).Additionally, JAK2 can regulate PI3K by binding its P85 regulatory subunit, facilitating crosstalk with PI3K/AKT pathways to influence cellular events(Yamada et al., 2012).Research with EOL-1 cells indicated that JAK2 knockdown significantly reduced the phosphorylation of STAT3, PI3K, and AKT (Li et al., 2012).The observed decreases in JAK2 and JAK3 in CD33KO-U937 macrophages lowered PI3K recruitment and expression. Moreover, the data supports that CD33 knockout enhances autophagy by independently downregulating AKT signaling, as evidenced by a threefold decrease in PDK1 and a twofold decrease in AKT1 mRNA expression. PDK1 is instrumental in phosphorylating and activating AKT signaling(Hoxhaj and Manning, 2020).Consequently, AKT pathway activation is suppressed due to decreased PDK1 in CD33KO-U937 macrophages, aligning with the significant decrease in AKT expression, thereby promoting autophagy.

While a decrease in JAK2 might suggest reduced PI3K activity, PI3K downregulation in CD33KO-U937 macrophages could occur independently of JAK expression changes. The mRNA levels of PIP3-degrading enzymes, namely INPP5B, INPP5K, INPP4A, and the isoenzyme INPP4B, which have been reported to degrade PIP3(Kofuji et al., 2015, Dieterle et al., 2014) were found to decrease in CD33KO-U937 macrophages. This observation suggests a hypothesis where PI3K activity might be intrinsically linked to PIP3 levels, impacted by CD33 knockout.

The decreased expression of these inositol phosphatases could lead to inefficient PIP3 degradation and subsequent accumulation of PIP3. Given PI3K's role in converting PIP2 to PIP3, excess PIP3 may feedback inhibit PI3K expression to prevent further accumulation, thereby reducing both PI3K and PIP3 levels and downregulating the PI3K/AKT signaling pathway. This reduction in PIP3 levels could explain the downregulated transcription of downstream mediators PDK1 and AKT1, ultimately activating autophagy in CD33KO-U937 macrophages.

Additionally, PIP3 accumulation following CD33 knockout might also result from reduced SHIP2 recruitment, as previous studies link SHIP2 knockdown to decreased PIP3 removal rates(Malek et al., 2017).Supporting this, recent studies highlight that reduced INPP5B inhibits PI3K/AKT signaling, with INPP5B significantly enriched in the PI3K/AKT pathway (Deng et al., 2022).However, research on INPP4 and INPP5 in autophagy is limited. Studies in cancer models have shown that depletion of INPP4 and INPP5 can activate AKT signaling (Eramo and Mitchell, 2016), necessitating further investigation to understand their roles in healthy human cell models. Moreover, IRS2, a well-known PI3K activator, also showed reduced expression. IRS2 acts as a critical bridge that recruits and activates PI3K (Fukushima et al., 2012).Its decreased expression may impair PI3K activation, further attenuating downstream AKT signaling and promoting autophagy. This aligns with findings from a mouse model study where reduced IRS2 levels led to increased autophagy in the brain(Sadagurski et al., 2011).
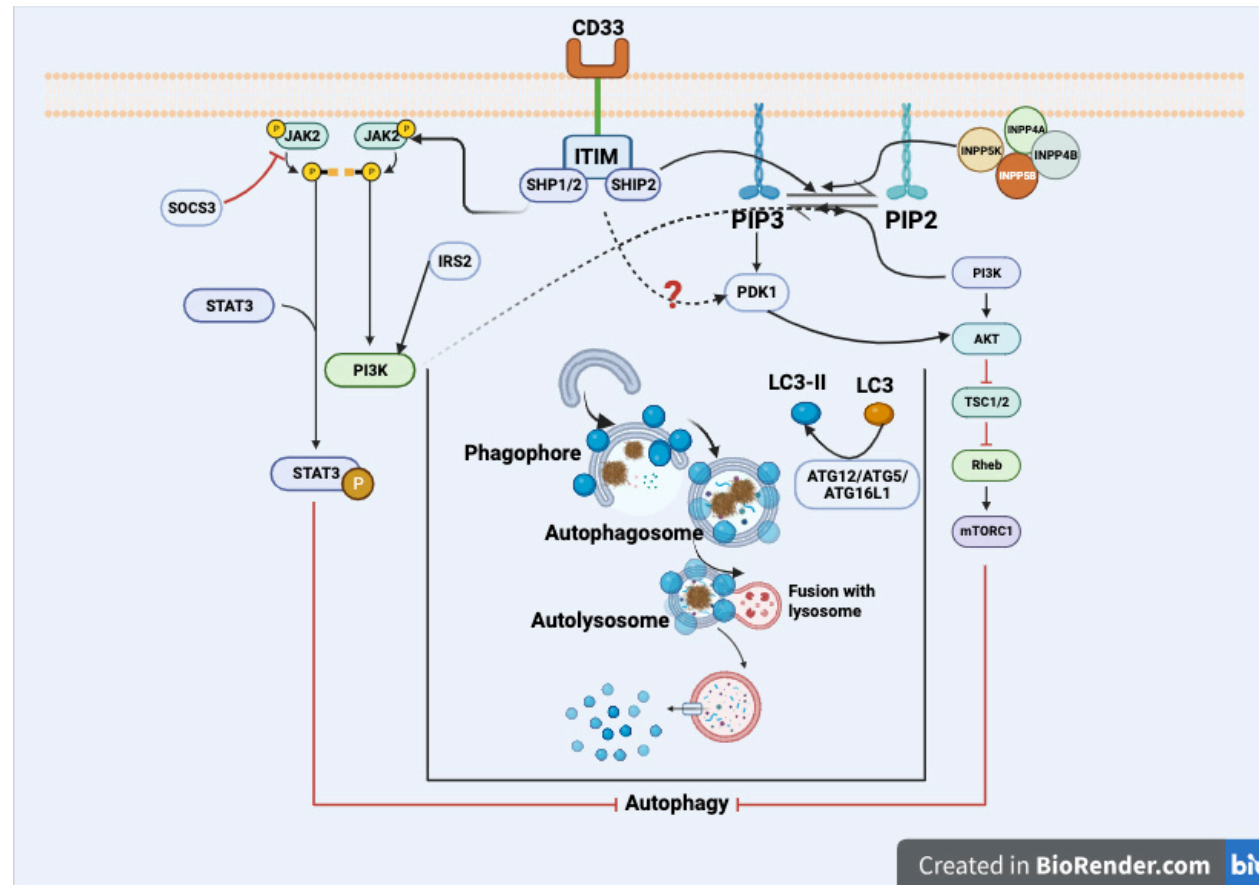
Figure 30. Hypothesis of Regulation of Autophagy by CD33 Signaling through JAK2/STAT3 and PI3K/AKT Pathways.The activation of CD33 leads to the activation of the cytoplasmic ITIM motif, which subsequently recruits downstream molecules such as SHP1, SHP2, or SHIP2, triggering cascades. SHP2 can activate JAK2, resulting in substantial activation of PI3K and STAT3. The activated STAT3 then inhibits the autophagy process. Additionally, PI3K promotes the conversion of PIP2 to PIP3, activating PDK1. The activated PDK1 then activates AKT, which in turn activates mTOR by inhibiting TSC1/2 and subsequently Rheb, ultimately leading to autophagy inhibition. INPP4A, INPP4B, INPP5B, and INPP5K indirectly participate in the regulation of PI3K/AKT signalling by modulating the degradation of PIP3 to PIP2. SHP1 and SHP2 play roles in counter-interacting with the PI3K/AKT signalling, possibly through activating PDK1 or by regulating PIP2 and PIP3 levels via SHIP2. Created with BioRender.com

6.3 Inflammatory mediators contribute to autophagy flux

CD33 knockout results in an imbalance in signaling pathways, leading to the upregulation of autophagy flux, which could potentially benefit AD brains. AD progression is a complex process characterized by disruptions in cytokine production and release, involving both pro-inflammatory and anti-inflammatory cytokines. Inflammatory responses occur throughout all stages of AD, with chronic inflammation playing a central role. Autophagy is recognized as a beneficial cellular process for maintaining homeostasis, and CD33 knockout appears to enhance this beneficial activity.

However, CD33 knockout also results in an imbalance between pro-inflammatory cytokines (e.g., IL-1β and TNFα) and anti-inflammatory cytokines (e.g., IL-10), as discussed extensively in Chapter 5. Consequently, further investigations were conducted to examine whether inflammatory mediators impact autophagy and the ERK1/2 and JAK/STAT3 signaling pathways. Liver X receptors (LXRs) are identified as potent anti-inflammatory molecules in various immune cells, including macrophages(Morales et al., 2008).The LXR agonist GW3965, which inhibited pSTAT3 expression in the presence of CD33 but promoted pSTAT3 in its absence, demonstrated the ability to induce autophagy regardless of CD33 status. Similarly, TNFα inhibited pSTAT3 in the presence of CD33 while inducing LC3b expression. A prior study showed that TNFα stimulation induces autophagy, evidenced by increased LC3b, autophagic vacuoles, autophagosomes, and autolysosomes, in OCCM-30 cells (Wang et al., 2018).These findings support the notion that STAT3 is crucial for autophagy activity, and its inhibition promotes LC3b expression.

Chapter 4 CD33 and Phagocytic Capability

1.Phagocytosis and LOAD

Amyloid beta is a hallmark of late-onset Alzheimer's disease (LOAD). Studies suggest that impaired clearance, rather than overproduction, of amyloid beta contributes significantly to LOAD. Amyloid beta (Aβ) and tau proteins can be degraded by the ubiquitin–proteasome system, autophagy-lysosome system, proteases (Chesser et al., 2013, Miners et al., 2011, Vilchez et al., 2014)), and microglial phagocytosis(Li et al., 2014).Cellular mechanisms for terminating Aβ responses include clearance via phagocytosis, intracellular degradation, and transcytosis across the blood-brain barrier (BBB) (Newcombe et al., 2018).Aβ can be exported from the brain into the bloodstream through routes such as the BBB, blood-cerebrospinal fluid barrier (BCSFB), or lymphatic clearance via cervical lymph nodes (Xin et al., 2018)). In the periphery, circulating $A\beta_{42}$ can be cleared through complement C3b-mediated adherence to erythrocyte CR1, facilitating removal from the bloodstream(Rogers et al., 2006).In the brain, extracellular proteins are degraded by proteases secreted by neurons and astrocytes or by microglial phagocytosis(Lee and Landreth, 2010)(**Figure 31**).Microglia, the resident macrophages in the central nervous system (CNS), form the primary immune defense line. Aβ deposits, which contain sialic acid residues(Salminen and Kaarniranta, 2009)(Szumanska et al., 1987), act as ligands for CD33(Alphey et al., 2003, Taylor et al., 1999, May et al., 1998). There are two subtypes of amyloid beta: amyloid $beta_{1-40}$ and amyloid $beta_{1-42}$. Both proteins can aggregate into insoluble plaques, contributing to LOAD pathology. Intracellular and soluble amyloid beta can be processed and cleared by the ubiquitin–proteasome system and the autophagy-lysosome system, while extracellular amyloid beta is cleared by microglia and astrocytes through phagocytosis or degradation by secreted proteases. Additionally, extracellular amyloid beta present in interstitial fluid (ISF) and cerebrospinal fluid (CSF) can be transported for degradation in peripheral systems, including blood and lymph circulation (Xin et al., 2018).

Transportation of Aβ into peripheral blood and lymphatic systems, or its degradation within CNS tissues, are crucial mechanisms for Aβ clearance(Zuroff et al., 2017).Soluble amyloid beta is transported to the periphery for degradation by the immune system, where hyaline leukocytes play a critical role in Aβ clearance(**Figure 32**). Mononuclear cells derived from bone marrow circulate in the blood and migrate to organs such as the liver, spleen, and

lymph nodes to mature into macrophages. As the brain's key immune cells, microglia significantly influence the physiological processes of Alzheimer's Disease.

Microglial function in AD is complex. On one hand, activated microglia release inflammatory cytokines, contributing to inflammatory cascades that cause neuronal injury and death. On the other hand, phagocytosis can be activated to engulf excess amyloid beta deposits in AD's early stages. Phagocytosis is controlled by various genes, including scavenger receptors, chemokine-like receptor 1, toll-like receptors, and G protein-coupled receptors(Chen et al., 2015). Microglial phagocytosis is significantly influenced by receptors such as TREM2 and CD33, playing pivotal roles in this cellular function(Xin et al., 2018). Genome-wide association studies (GWAS) have strongly linked CD33 to LOAD, and knockout studies have shown that CD33 is involved in Aβ plaque phagocytosis(Griciuc et al., 2013).A 2019 study demonstrated enhanced microglial phagocytosis and increased uptake of Aβ plaques following CD33 gene knockout. In APP/PS1 mice lacking CD33, increased Aβ clearance correlated with decreased Aβ accumulation, underscoring the role of microglia in Aβ phagocytosis (Miles et al., 2019).
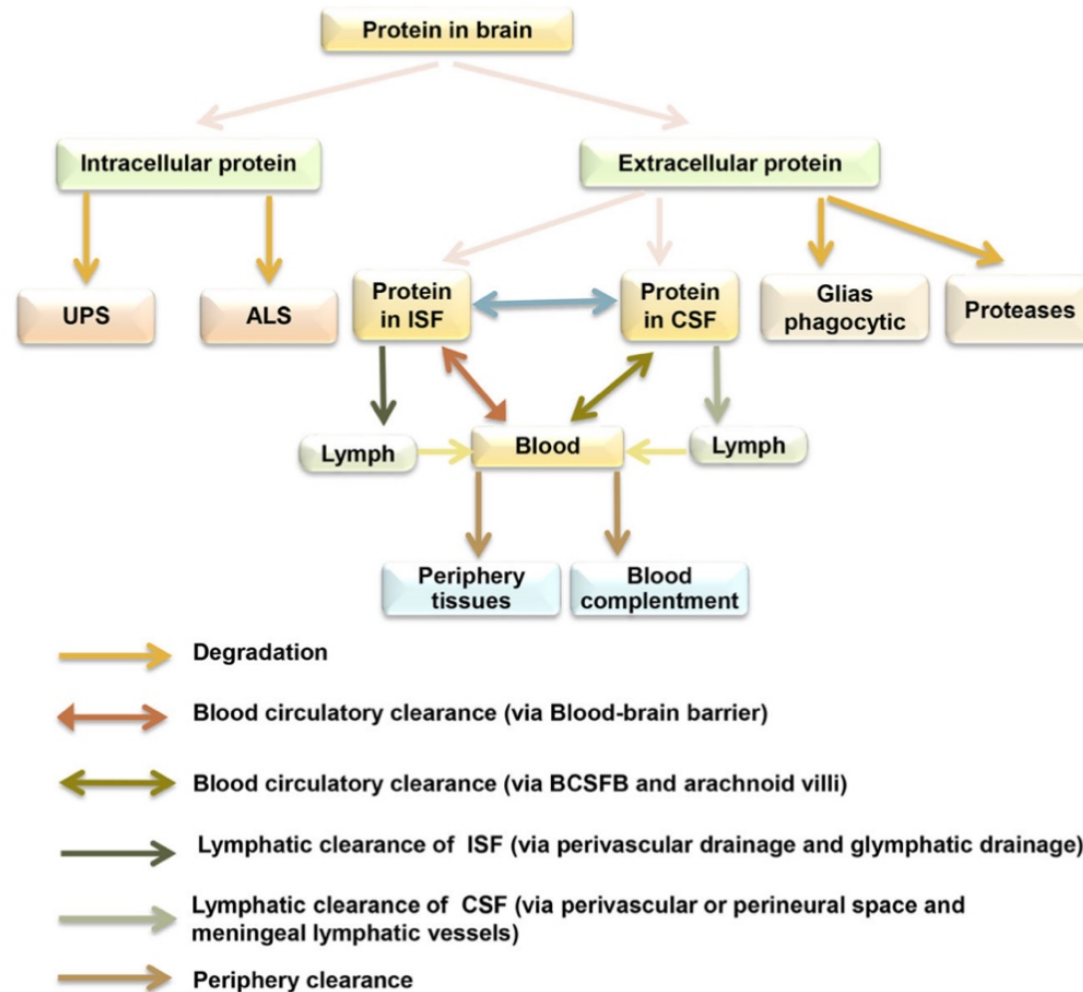
Figure 31. Proteins in brain can be eliminated by various kinds of clearance mechanisms. In the brain, intracellular and soluble amyloid beta can be processed and cleared by the ubiquitin–proteasome system and the autophagy-lysosome system, while extracellular amyloid beta is cleared by microglia and astrocytes through phagocytosis or degradation by secreted proteases. Additionally, extracellular amyloid beta present in interstitial fluid (ISF) and cerebrospinal fluid (CSF) can be transported for degradation in peripheral systems, including blood and lymph circulation (Xin et al., 2018)).
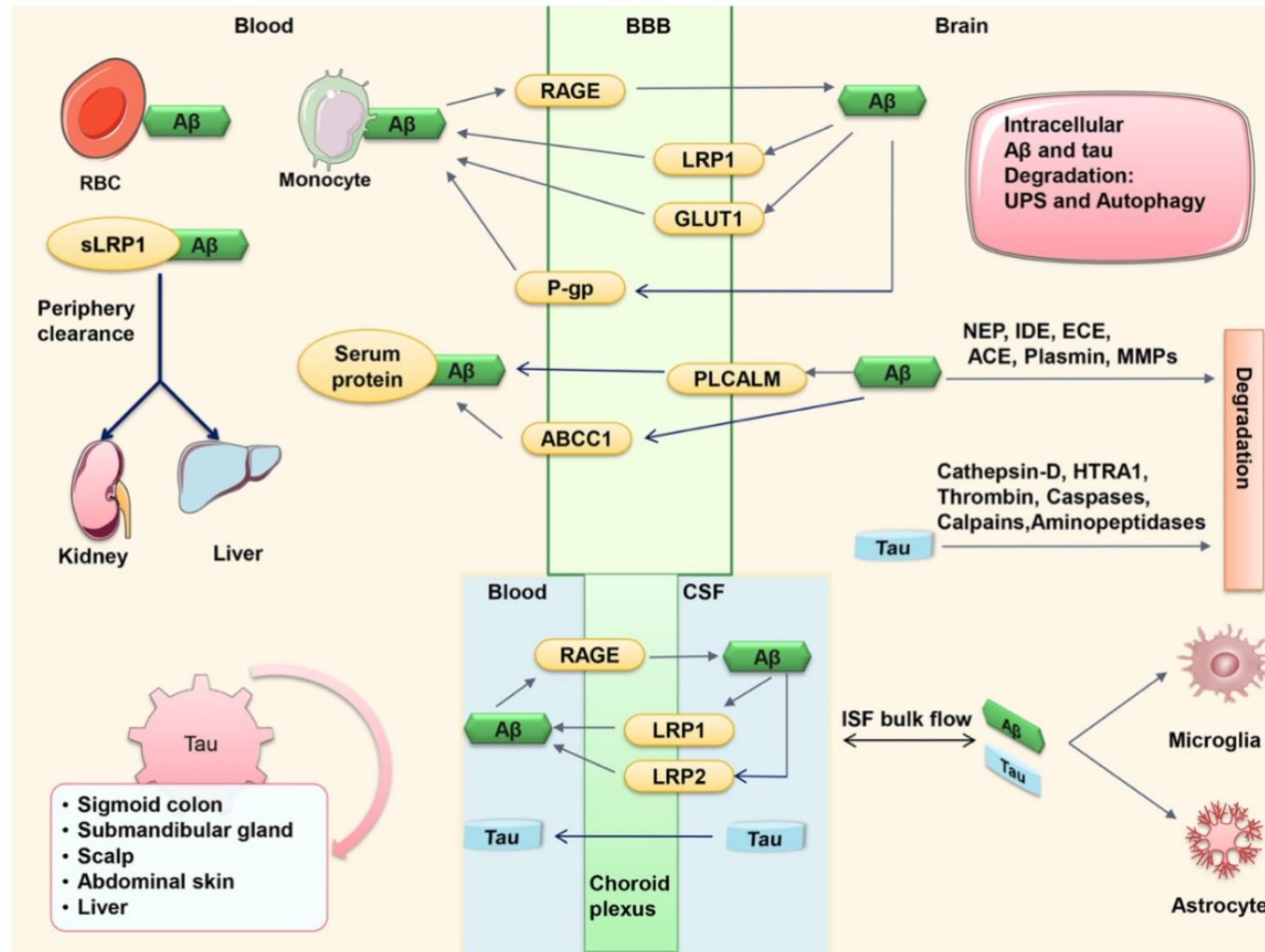
Figure 32. Blood circulatory clearance and periphery clearance of Aβ and tau in AD. Aβ can be exported from the brain into the bloodstream through routes such as the BBB, blood-cerebrospinal fluid barrier (BCSFB), or lymphatic clearance via cervical lymph nodes. In the periphery, circulating Aβ$_{42}$ can be cleared through complement C3b-mediated adherence to erythrocyte CR1, facilitating removal from the bloodstream(Rogers et al., 2006) (Xin et al., 2018)).

2.CD33 and AD

In 2011, two genome-wide association studies (GWAS) identified a single-nucleotide polymorphism (SNP), rs3865444, located upstream of the CD33 gene, as linked to Alzheimer's disease (AD) risk (Hollingworth et al., 2011)). Recent findings have established two risk SNPs within the CD33 gene (Raj et al., 2014)). The SNP rs3865444 is situated in the promoter region of CD33, while the second risk SNP, rs12459419, is located in exon 2 of CD33, exhibiting linkage disequilibrium.

The rs12459419C allele is associated with an increased risk of AD, as it promotes the production of the full-length human CD33 (hCD33M), leading to increased accumulation of amyloid beta (Aβ) plaques. Conversely, the rs12459419T allele is linked to a reduced AD risk, enhancing the production of a shorter isoform (hCD33m) via an alternative expression pathway. The differentiation between rs12459419C and rs1245419T alleles is due to cytidine replacing thymidine near the start of exon 2. Research in brain tissue demonstrated linkage disequilibrium between rs12459419 and rs3865444 (Raj et al., 2014)). The rs3865444 allele results in decreased CD33 expression, thereby reducing Aβ plaque accumulation. Specifically, the rs3865444T allele correlates with decreased Aβ plaque burden in AD patients, while the rs3865444C allele is linked to increased CD33 expression and a corresponding rise in Aβ plaques. Furthermore, reduced CD33 expression correlates with decreased AD susceptibility. Strong causal associations between CD33 and late-onset Alzheimer's disease (LOAD) have been identified by various GWAS (Andrews et al., 2020, Li et al., 2015).The CD33 gene encodes a receptor expressed on various myeloid progenitor cells, including macrophages and mature monocytes. In AD patients, CD33 is notably expressed by microglia in the brain. CD33 knockout studies in mice have shown that CD33 inhibits Aβ plaque phagocytosis by reducing microglial uptake of these plaques (Griciuc et al., 2019, Griciuc et al., 2020).The level of CD33 expression in the brain affects Aβ plaque presence: lower CD33 expression is associated with reduced Aβ aggregation, while higher expression correlates with Aβ accumulation. In AD patients, increased CD33 expression is linked to cognitive decline, corresponding with the extent of Aβ plaque

burden. Elevated brain CD33 expression is thought to modulate microglial activation, thereby inhibiting amyloid beta clearance(Malik et al., 2013, Griciuc et al., 2013).

3. CD33 and phagocytosis

Microglial CD33 expression levels are positively correlated with the presence of amyloid beta and the burden of amyloid beta plaques in AD brains(Griciuc et al., 2013). Furthermore, individuals carrying the polymorphic allele rs3865444(A) of CD33, which is associated with a reduced risk of AD, exhibit lower surface expression of CD33 on microglia and decreased amyloid beta deposition in the brain(Griciuc et al., 2013, Wißfeld et al., 2021). Studies have also reported that the CD33 variant rs3865444(A), linked to a slight decrease in AD risk, is co-inherited with rs12459419(T), which modulates the splicing efficiency of exon 2 in the CD33 gene (Malik et al., 2013, Raj et al., 2014).The full-length form of the CD33 receptor plays a significant role in the clearance of Aβ plaques by inhibiting phagocytosis, whereas the shorter form (lacking exon 2) enhances phagocytosis. Previous CD33 knockout studies have demonstrated that CD33 participates in the phagocytosis of Aβ plaques (Griciuc et al., 2020, Griciuc et al., 2013). Research by Miles et al. confirmed increased microglial Aβ phagocytosis following CD33 knockout (Miles et al., 2019)). However, CD33 knockout also resulted in an increased oxidative burst and inflammation (Claude et al., 2013). This finding is supported by Griciuc et al., in a study that demonstrated increased microglial phagocytosis and Aβ plaque uptake following CD33 gene knockout (Griciuc et al., 2013). Increased Aβ clearance has been observed in APP/PS1 mice lacking CD33, correlating with decreased Aβ accumulation (Wang et al., 2016a). Individuals with the minor rs3865444 allele, leading to a higher proportion of D2-CD33, have peripheral monocytes that exhibit enhanced Aβ phagocytosis compared to individuals producing more full-length CD33(Bradshaw et al., 2013). Hence, it is hypothesized that elevated levels of full-length CD33 in AD brains may hinder microglial phagocytosis, leading to impaired Aβ clearance and its accumulation. Conversely, a reduction in full-length CD33 or an increase in D2-CD33 proportion is associated with decreased normal CD33 function and enhanced Aβ clearance (Zhao, 2019). Areas rich in sialic acid, such as the regions surrounding plaques, can stimulate CD33 signaling, which results in the activation of the CD33 ITIM.This activation triggers SHP1, which inhibits microglial activation, particularly

impacting Syk signaling associated with TREM2 (Malik et al., 2015, Linnartz and Neumann, 2013).These activities converge with the PI3K signaling pathway, regulating microglial processes. PI3K, an intracellular enzyme, plays a crucial role in downstream signaling pathways, including phagocytosis. Upon activation by cell surface receptors, PI3K generates PIP3 from PIP2 at the plasma membrane, recruiting downstream signaling molecules that orchestrate actin rearrangement and membrane remodeling necessary for phagocytic cup formation and target particle engulfment.

Previous analyses of macrophages and microglia indicate that the phagocytic capability for aggregated amyloid beta42 and bacterial particles increases after full or exon 2-specific knockout of CD33, and the knockdown of PTPN6(Tortora et al., 2022).Additionally, the phagocytic oxidative burst observed during the uptake of $A\beta_{1\text{-}42}$ or bacterial particles was elevated in CD33 knockout microglia, though this effect was not seen in microglia lacking exon 2 of CD33 (Wißfeld et al., 2021).

4. Macrophage scavenger receptor 1 (MSR1) and phagocytosis

Macrophage scavenger receptor 1 (MSR1), also known as SCARA1 or CD204, is a type II transmembrane glycoprotein primarily expressed by microglia in the brain (Ishiguro et al., 2001)). MSR1is a member belonging to scavenger receptors which mediate endocytosis of a wide range of ligands including bacterial pathogens, low-density lipoproteins, dead cells, β-amyloid and other molecules (Husemann et al., 2002, Cheng et al., 2019, Li et al., 2021a). The scavenger receptor superfamily plays a crucial role in maintain homeostasis accomplished via its ability to recognize various Damage-associated molecular patterns (DAMPs) and Pathogen-associated molecular patterns (PAMPs). MSR1 is the Class A SRs, composed by composed of 1) cytosol domain, 2) transmembrane domain, 3) spacer domain, 4) alpha-helical coiled-coil domain, 5) collagen-like domain, and 6) cysteine-rich domain (Matsumoto et al., 1990). MSR1 can facilitate the adhesion of microglia to fibrillar Aβ (El Khoury et al., 1996). In AD mice models, MSR1 deficiency impairs clearance of soluble Aβ and results in elevated Aβ deposition, however, Aβ clearance can be enhanced by pharmacological upregulation of MSR1(Frenkel et al., 2013, Sandoval et al., 2019, Li et al., 2021a)). MSR1 also plays an important role in the inflammatory process. MSR1 is of vital

importance of eliminating foreign pathogens (Wang et al., 2021). MSR1 can cooperate with TLR4 to promote phagocytosis of the Gram-negative bacterium Escherichia coli (Amiel et al., 2009).While the elevated phagocytosis of Gram-negative bacterium Staphylococcus aureus can be upregulated due to the cooperation of MSR1 with TLR2(Amiel et al., 2009).

MSR1 induces the synthesis of inflammatory cytokines via NF-κB signaling by interacting with TLR4(Yu et al., 2012). Expressed on CNS phagocytes, MSR1 also plays a neuroprotective role by inhibiting toxic forms of Aβ and slowing disease progression(Zuroff et al., 2017).Activation of MSR1 triggers various downstream signaling cascades, including PTK(Src)/Rac1/PAK/JNK, PTK(Src)/Rac1/PAK/p38 (Hsu et al., 2001), the MSR1/PI3K-Akt/NF-κB pathway (Tian et al., 2022)), and the MAP kinase pathway (Coller and Paulnock, 2001). In AD, activated MSR1 facilitates ligand internalization and engages signaling pathways such as PI3K/NF-κB and MAPK/JNK/p38 (Coller and Paulnock, 2001).These interconnected signaling pathways are involved in regulating inflammation, cell proliferation, cytokine production, and migration.

5.LC3-associated phagocytosis (LAP)

LC3-associated phagocytosis (LAP) is a specialized process where autophagic machinery components conjugate LC3 to phagosomal membranes, forming LC3-positive LAPosomes (Martinez et al., 2015). Initially described in 2007, LAP plays a crucial role in pathogen degradation by macrophages(Romao and Münz, 2014).

LAP is regarded as a non-canonical autophagy.Unlike traditional autophagy, which forms double-membrane autophagosomes, LAPosomes are single-membrane vesicles and do not require a pre-initiation complex(Matsuzawa-Ishimoto et al., 2018)(**Figure 33**). LAP is integral for the degradation of engulfed pathogens and modulation of the innate immune response, with deficiencies linked to increased pathological inflammation and elevated pro-inflammatory cytokine levels (Martinez et al., 2011, Florey et al., 2011, Martinez et al., 2015). It primarily facilitates the clearance of extracellular particles, including pathogens and apoptotic cells, demonstrating its functional intersection with autophagy(Heckmann et al., 2017).Triggered by phagocytosis through Fc receptors, complement receptors, and

Toll-like receptors (TLRs), such as TLR1/2 and TLR4, LAP recruits specific autophagic machinery components to phagosomes, promoting their maturation and the degradation of internalized pathogens(Martinez et al., 2015). Although distinct from traditional autophagy, LAP shares enzymatic components like the Class III PI(3)K complex and ubiquitin-like modifiers.Rubicon (RUN domain Beclin-1 interacting and cysteine-rich protein) is a critical Class III PI(3)K-associated protein necessary for LAP but not for canonical autophagy. It facilitates phagosome maturation and lysosomal fusion by enhancing VPS34 activity and stabilizing the NOX2 complex for reactive oxygen species (ROS) production (Martinez et al., 2015)). ROS generation, crucial for LAPosome maturation, requires the translocation of cytosolic components such as p47PHOX and p67PHOX to the NOX2 complex (Bedard and Krause, 2007)(Suh et al., 2006).NOX2 is implicated in LC3 translocation to phagosomes engaging TLRs or FcγR, playing a signaling role in autophagy machinery recruitment (Huang et al., 2009)). Lipidation of LC3-II is essential for LAPosome maturation and lysosome fusion, involving Atg3, Atg4, and the ATG5–ATG12–ATG16L complex. Additionally, ROS influences autophagy signaling pathways, including AMPK (Mungai et al., 2011) and mTOR(Zhao et al., 2017), impacting ATG4's enzymatic activity crucial for LC3 processing and recycling(Wible and Bratton, 2018).
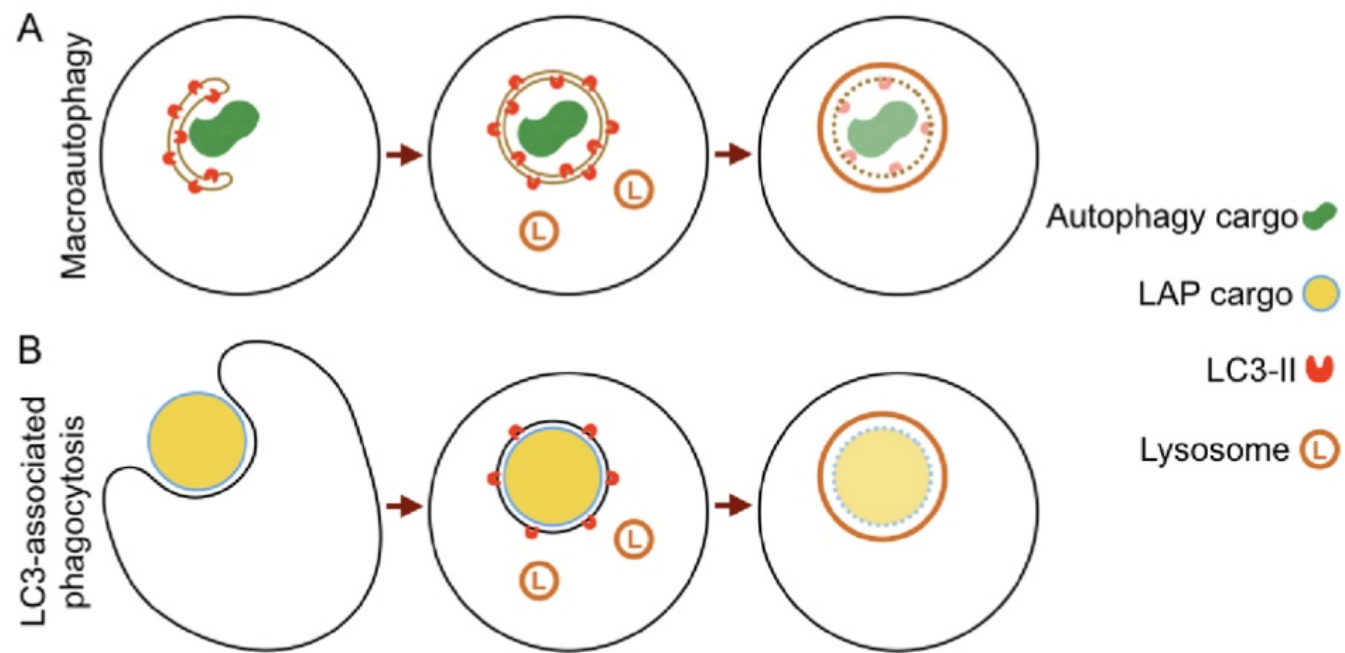
Figure 33. Structure of autophagosome and phagosome. LAP is regarded as a non-canonical autophagy. Unlike traditional autophagy, which forms double-membrane autophagosomes and with LC3b found on both inner and outer autophagosomal membranes, LAPosomes are single-membrane vesicles and do not require a pre-initiation complex(Fazeli and Wehman, 2017).

6. Aims and objectives

6.1 Aims:

To investigate the impact of CD33 knockout on phagocytosis and to validate changes in phagocytosis-related gene expression following CD33 deletion.

6.2 Objectives:

1. Verify changes in phagocytosis-related gene expression resulting from CD33 knockout using qRT-PCR and RNA deep sequencing.

2. Confirm the expression of MSR1 and LAMP2 in CD33WT-U937 and CD33KO-U937 macrophages through Western blot analysis.

3. Validate the influence of CD33 knockout on phagocytic capability using fluorescent beads and the Alzheimer's disease markers amyloid beta$_{40}$ and amyloid beta$_{42}$.

4. Investigate the impact of CD33 knockout on LC3-associated phagocytosis.

7. Results

7.1 Differentiation of Monocytes into M0 Macrophage

Results refer to Chapter 3.

7.2 CD33 knockout upregulated phagocytosis-related gene expression.

CD33WT-U937 and CD33KO-U937 monocytes were seeded in 6-well plates and fully differentiated into M0 macrophages. Subsequently, cells were harvested for RNA extraction and RNA deep sequencing analysis to assess changes in mRNA expression levels across the entire genome.

As shown in the heatmap in **Figure 34**, a range of genes directly and indirectly involved in the positive regulation of phagocytosis exhibited altered expression in CD33KO-U937 macrophages. The bar chart highlights a significant increase in mRNA expression for several phagocytosis-related genes: MSR1 (4-fold), LAMP2 (2-fold), complement C3 (3.5-fold), and various Fcγ receptors, including FCGR1B, FCGR1A, FCGR2A, FCGR2B, FCGR2C, and FCGR3A, with fold changes ranging from 1.5-fold to 13-fold. Notably, SILEC1 receptor and CYBB showed increases of 15-fold and 300-fold, respectively, in CD33KO-U937 macrophages compared to CD33WT-U937 macrophages (P<0.0001 to P<0.05), as depicted in **Figure 35**.
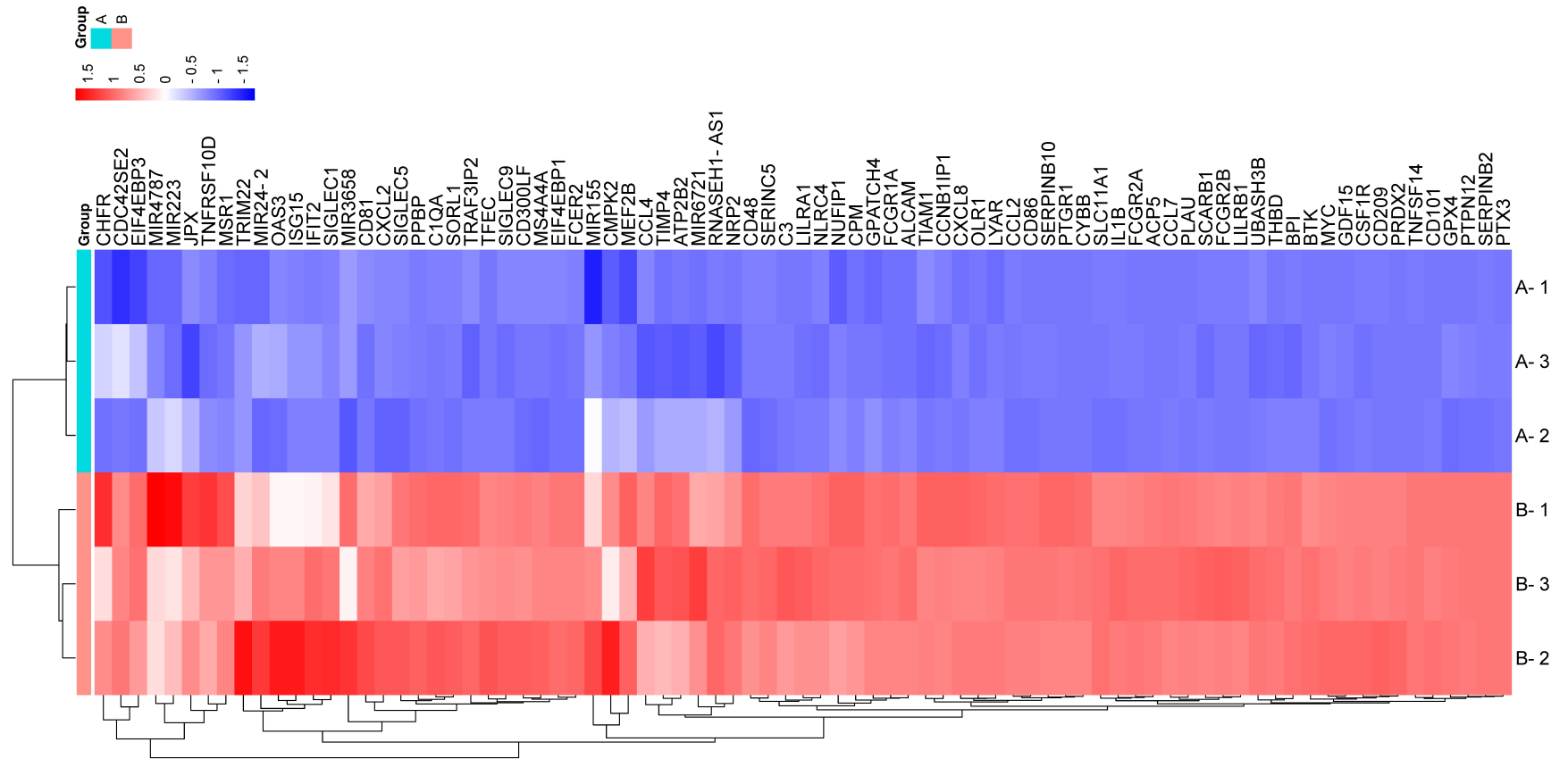
Figure 34. Expression analysis of phagocytosis-Related genes influenced by CD33 knockout. The heatmap illustrates the upregulation of phagocytosis-related genes in CD33KO-U937 macrophages compared to CD33KO-U937 macrophages, confirmed by RNA deep sequencing. Blue bars indicate the baseline expression of phagocytosis-related genes in CD33WT-U937 macrophages, while red bars represent the upregulation in the expression of phagocytosis-related genes in CD33KO-U937 derived macrophages. Group A (1,2,3): CDWT-U937 macrophages; Group B (1,2,3): CD33KO-U937 macrophages; (n=3 per phenotype).

121
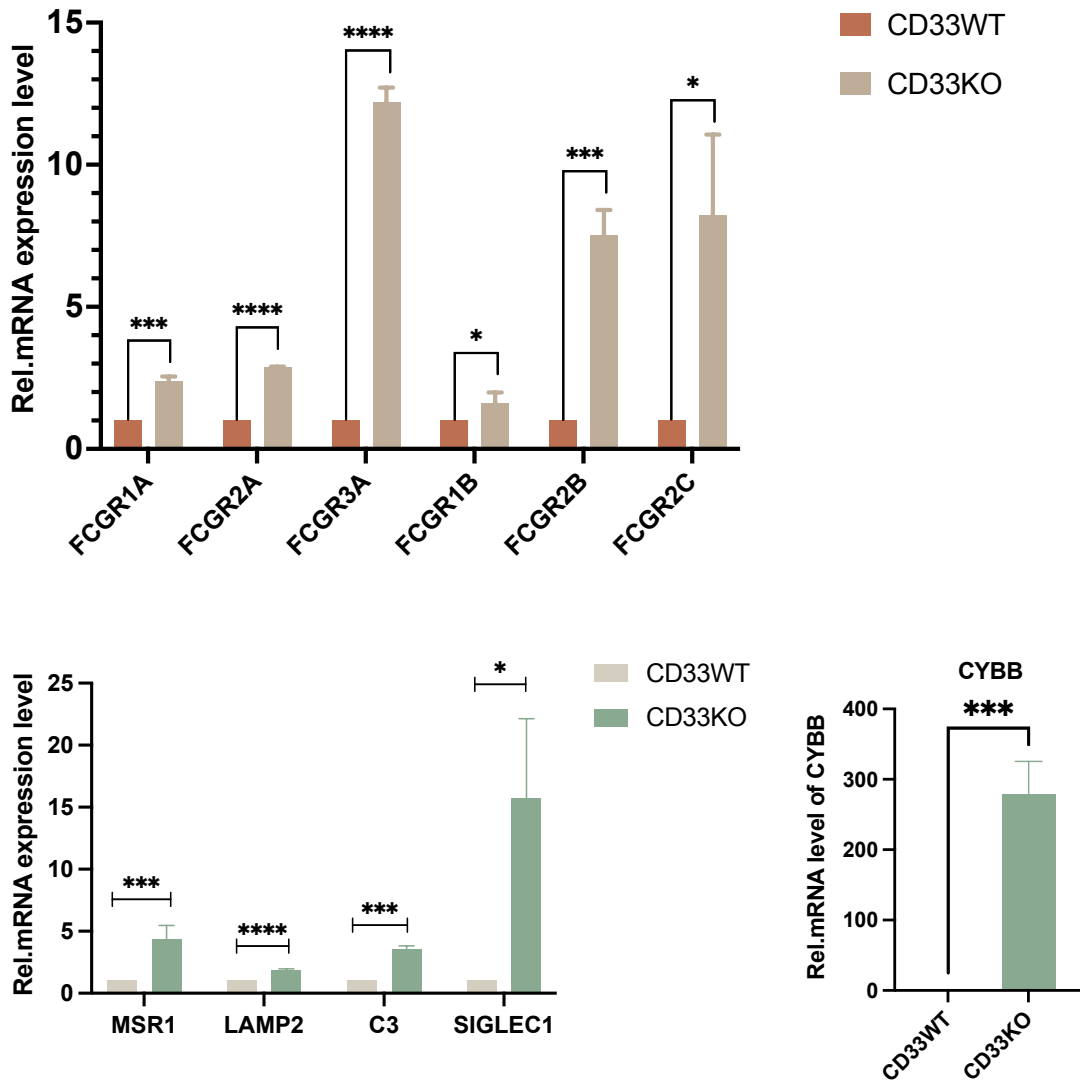
Figure 35. Relative mRNA expression levels of phagocytosis-related genes directly involved in phagocytosis due to CD33 knockout. Bar charts illustrate the relative mRNA level upregulated in CD33KO-U937 macrophages: MSR1 and LAMP2 were increased with changes of 4-fold and 2-fold, respectively due to CD33 knockout. The expression of Fcγ receptors (FCGR1B, FCGR1A, FCGR2A, FCGR2B, FCGR2C, and FCGR3A) exhibited significant increases, ranging from 1.5-fold to 13-fold in CD33KO-U937 macrophages compared to CD33WT-U937 macrophages; additionally, the expression of complement C3, Sialic 1 receptor (SILEC1), and CYBB showed substantial upregulation, with fold changes of 3.5, 15, and 300, respectively in CD33KO-U937 macrophages compared to CD33WT-U937 macrophages. Data are presented as Mean ± SD – t-test (ns = not significant, *p < 0.05, **p < 0.01, ***p < 0.001, ****p < 0.0001; n = 3).

7.3 The effect of CD33 knockout on phagocytic capability

7.3.1 CD33 knockout enhanced the phagocytosis of beads

The impact of CD33 knockout on phagocytic ability was assessed using flow cytometry with

1 μm yellow-green fluorescent beads in both CD33WT-U937 and CD33KO-U937

macrophages. Phagocytosis assays were conducted as described in section 2.4.2, in the presence and absence of a 3-hour treatment with 100 ng/mL of LPS.

Figure 36 and Figure 37 illustrates the mean fluorescence intensity (MFI) of yellow-green beads engulfed by CD33WT-U937 and CD33KO-U937 macrophages under different conditions. Figures 36a and 37a serve as negative controls for CD33WT-U937 and CD33KO-U937 macrophages, respectively. Figures 36b and 37b show bead engulfment by CD33WT-U937 macrophages (1.92%) and CD33KO-U937 macrophages (14.8%). Upon LPS stimulation, the engulfment increased to 4.07% for CD33WT-U937 macrophages and 13.7% for CD33KO-U937 macrophages, as shown in **Figure 36c** and **Figure 37c**.

CD33 knockout resulted in a fivefold increase in phagocytic capability in CD33KO-U937 macrophages compared to CD33WT-U937 macrophages (P<0.05) (**Figure 38g**). However, CD33KO-U937 macrophages exhibited a slight reduction in bead engulfment in response to LPS (P<0.05) (**Figure 38i),** while no significant changes were observed for CD33WT-U937 macrophages in response to LPS (P>0.05) (**Figure 38h**). These findings collectively suggest that CD33 knockout enhances phagocytosis.
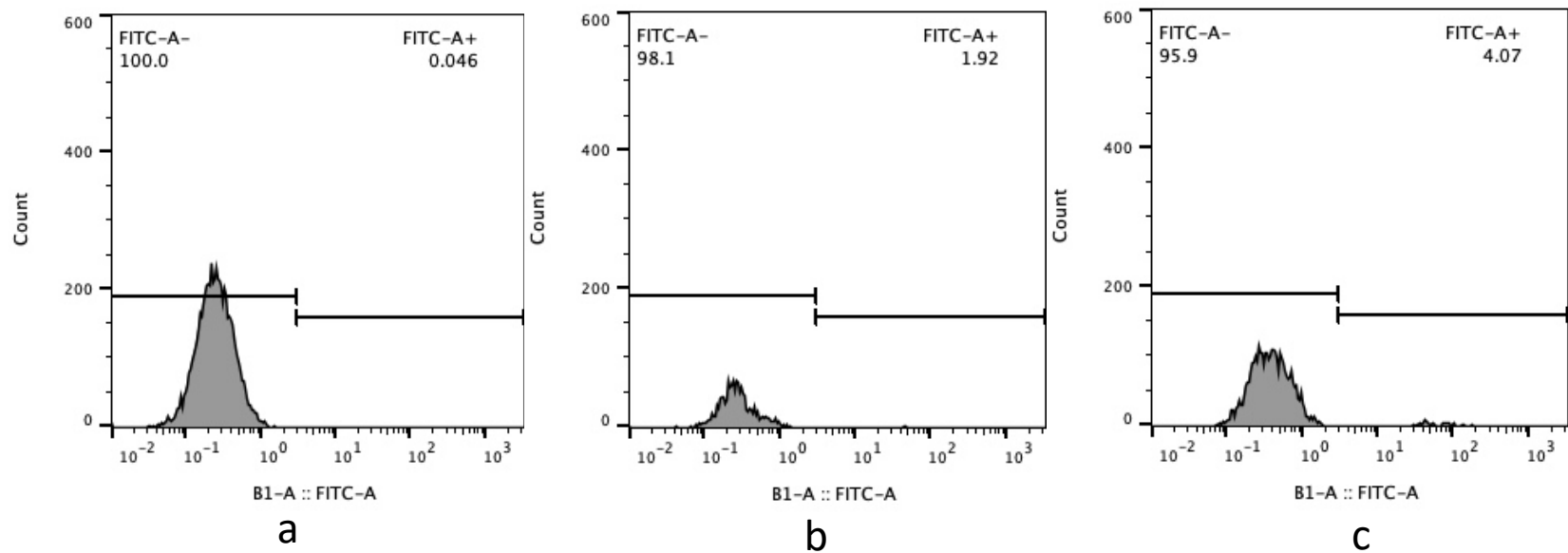
Figure 36. Validation of Phagocytic capability through Fluorescent Bead Engulfment with and without LPS Treatment Confirmed by Flow Cytometry. CD33WT-U937 cells were differentiated into macrophages and treated with yellow-green fluorescent beads (0.05% v/v) in a complete growth medium RPMI-1640 for 3 hours. For LPS stimulation, 100ng/mL of LPS was added 30 minutes prior to the phagocytosis assay setup. (a) Negative control of CD33WT-U937 macrophage (0.046%) ;(b) CD33WT-U937 macrophage with the treatment of yellow-green fluorescent beads indicating an engulfment of 1.92% by CD33WT-U937 macrophages;(c) CD33WT-U937 macrophage with the treatment of yellow-green fluorescent beads and LPS stimulation indicating an engulfment of 4.07%. Data presented as Mean ± SD – t-test (p* = < 0.05 p **= <0.01, p*** = < 0.001, p**** <0.0001, ns=not significant. (n=4).

Figure 37. Validation of Phagocytic capability through Fluorescent Bead Engulfment with and without LPS Treatment Confirmed by Flow Cytometry. CD33KO-U937 cells were differentiated into macrophages and treated with yellow-green fluorescent beads (0.05% v/v) in a complete growth medium RPMI-1640 for 3 hours. For LPS stimulation, 100ng/mL of LPS was added 30 minutes prior to the phagocytosis assay setup. (a) Negative control of CD33KO-U937 derived macrophage (0.087%). (b) CD33KO-U937 derived macrophage with the treatment of yellow-green fluorescent beads indicating an engulfment of 14.8%. (c) CD33KO-U937 derived macrophage with the treatment of yellow-green fluorescent beads and LPS stimulation indicating an engulfment of 13.7%. Data presented as Mean ± SD – t-test (p* = < 0.05 p **= <0.01, p*** = < 0.001, p**** <0.0001, ns=not significant. (n=4).
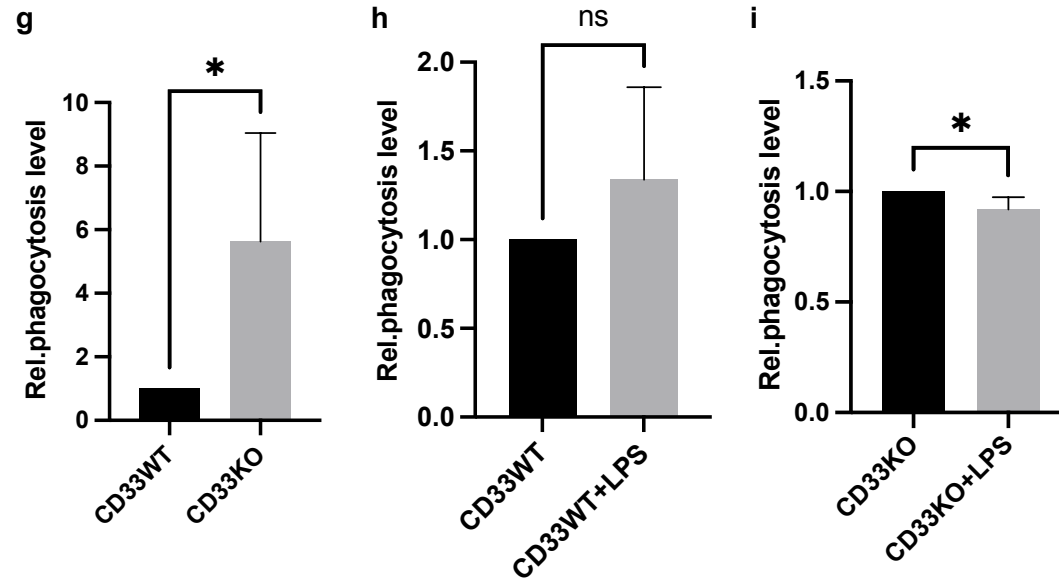
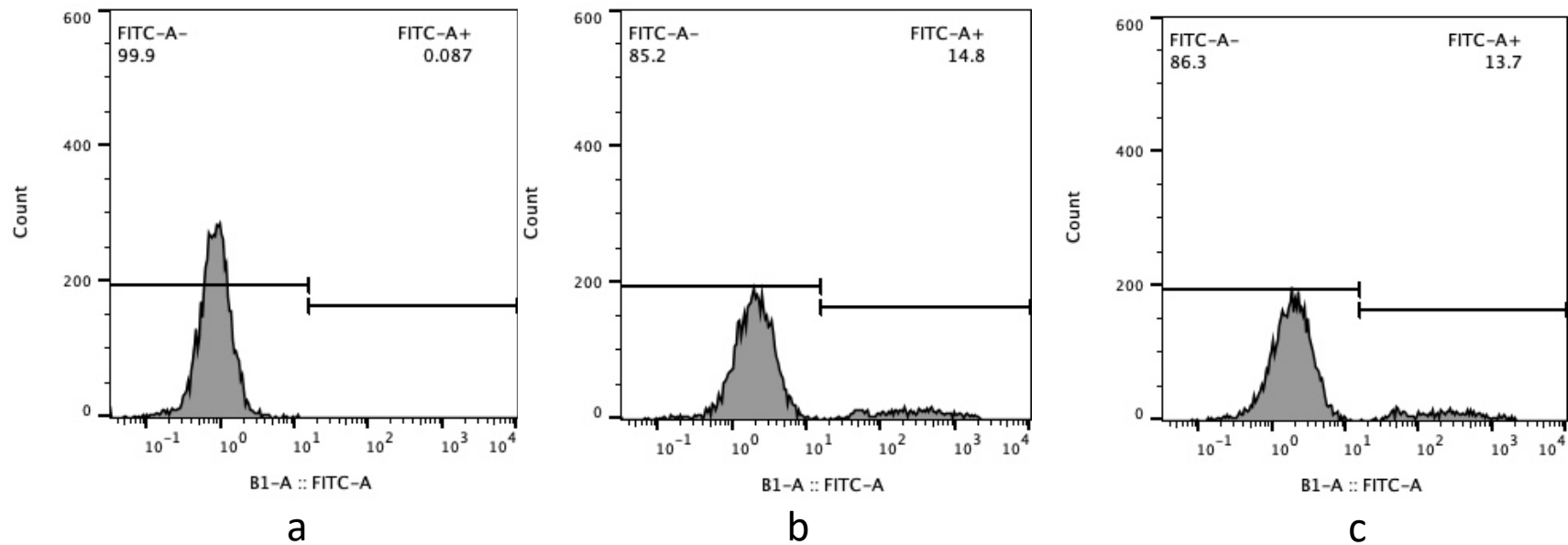**Figure 38. Bar chart analysis of Phagocytic capability through Fluorescent Bead Engulfment with and without LPS Treatment Confirmed by Flow Cytometry.** CD33WT-U937 and CD33KO-U937 were differentiated into macrophages and treated with yellow-green fluorescent beads (0.05% v/v) in a complete growth medium RPMI-1640 for 3 hours. For LPS stimulation, 100ng/mL of LPS was added 30 minutes prior to the phagocytosis assay setup. Bar charts indicated that CD33KO induced a 5-fold engulfment in CD33KO-U937 macrophages compared to CD33WT-U937 macrophages(g). the phagocytic capability was slightly inhibited in CD33KO-U937 macrophages in responses to LPS(i) and there was no significant difference in phagocytosis exhibited in CD33WT-U937 macrophages when exposed to LPS(h). Data presented as Mean ± SD – t-test (p* = < 0.05 p **= <0.01, p*** = < 0.001, p**** <0.0001, ns=not significant. (n=4).

**7.3.2 CD33 knockout resulted in an increased phagocytic ability in a time- and concentration-dependent way.**

Phagocytosis of yellow-green fluorescent beads by CD33WT-U937 macrophages and CD33KO-U937 macrophages were observed under fluorescent microscopy (20X). Cells were seeded with proper density and cultured in 12-well plates to fully differentiated into macrophages using methods as described in 2.3. Subsequently, they were treated with fluorescent beads in a complete growth medium at concentrations of 0.05% (v/v) and 0.1% (v/v) and incubated for 3 hours and 6 hours, respectively. Fluorescent microscopy (20X) was employed to observe the phagocytosis of beads by CD33WT-U937 macrophages and CD33KO-U937 macrophages. Notably, it is noted that CD33KOU937 macrophages exhibited a significant elevated capability of engulfment compared to the CD33WT-U937 counterparts, shown as in both **Figure 39**. Meanwhile, the phagocytic activities observed in the monocyte-PMA derived macrophages performed in a manner of time-dependent and bead concentration-dependent. To validate this, CD33KO-U937 macrophages were incubated with respective bead concentrations of a low concentration of 0.05% (v/v) and a higher concentration of 0.1% (v/v)—over a time span ranging from 3 to 6 hours. At the lower concentration of 0.05% (v/v), the relative phagocytic cells (%) after 6 hours of incubation was 2-fold higher compared to the 3-hour incubation period($P<0.01$), as shown in **Figure 41a**. However, when elevated the bead concentration to 0.1% (v/v), the phagocytic activity after 6 hours exhibited a 1.5-fold increase over the 3-hour incubation($P<0.01$),**Figure 41b**.Furthermore, at the time point of 3-hour exposure, cells incubated with high bead concentration of 0.1% (v/v) exhibited a 1.5-fold increase compared to the lower concentration of 0.05% (v/v) ($P<0.0001$),as shown in **Figure 40**. Additionally, when the incubation was extended to 6 hours, the difference in phagocytic cells (%) between the two concentrations narrowed, with cells under the higher bead concentration showing only a 1.1-fold increase over the lower concentration($P<0.05$),shown in **Figure 40**.These indicated that the upregulated phagocytic capability increased due to CD33 knockout also exhibited a choke point in engulfment, which depends on the cargo concentration and exposure period, similar as the wild type does.
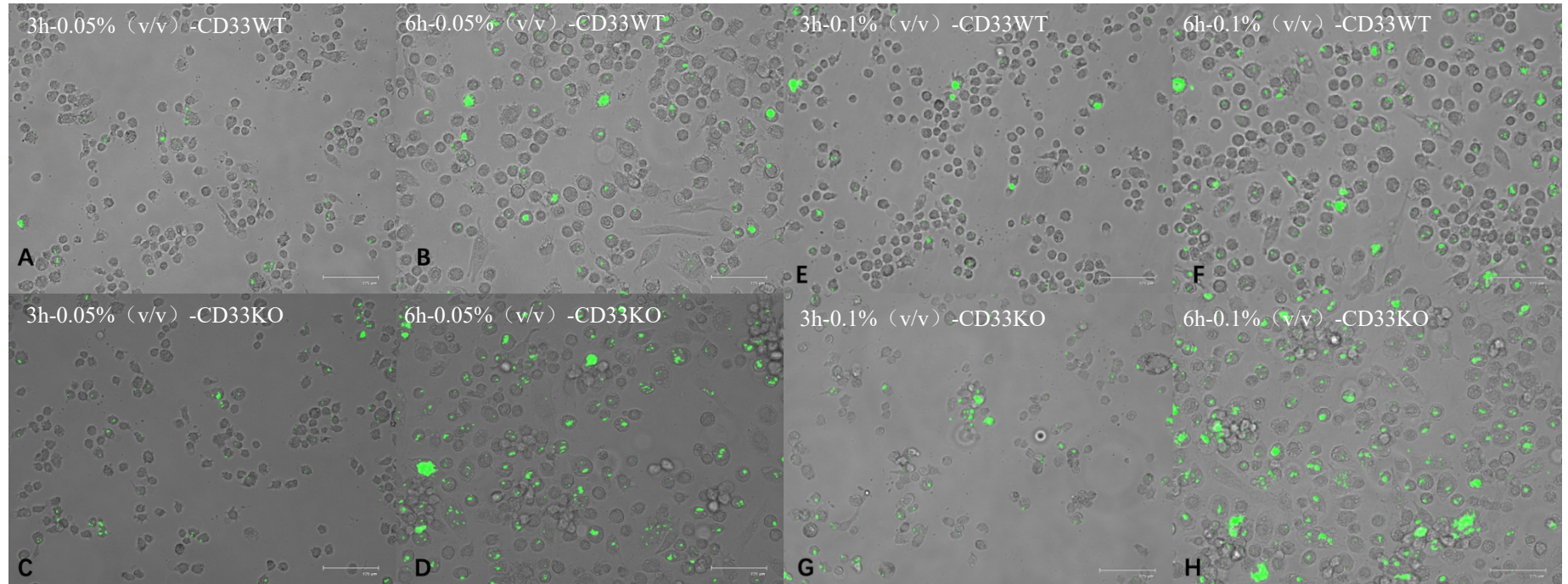
Figure 39. Observation of phagocytic activity using fluorescent beads in the presence and absence of CD33. Phagocytic ability was observed in both CD33WT-U937 macrophages and CD33KO-U937 macrophages using yellow-green fluorescent beads at concentrations of 0.05% (v/v) and 0.1% (v/v). Phagocytosis assays were conducted under respective incubation periods of 3 hours and 6 hours. Images were taken under a fluorescent microscope with a scale bar of 125um. (A, B, E, F): Incubation for 3 to 6 hours in 0.05% (v/v) and 0.1% (v/v) bead-containing RPMI-1640 growth medium in CD33WT-U937 macrophages. (C, D, G, H): Incubation for 3 to 6 hours in 0.05% (v/v) and 0.1% (v/v) bead-containing RPMI-1640 growth medium in CD33KO-U937 macrophages. CD33WT refers to CD33WT-U937 macrophages, and CD33KO refers to CD33KO-U937 macrophages.
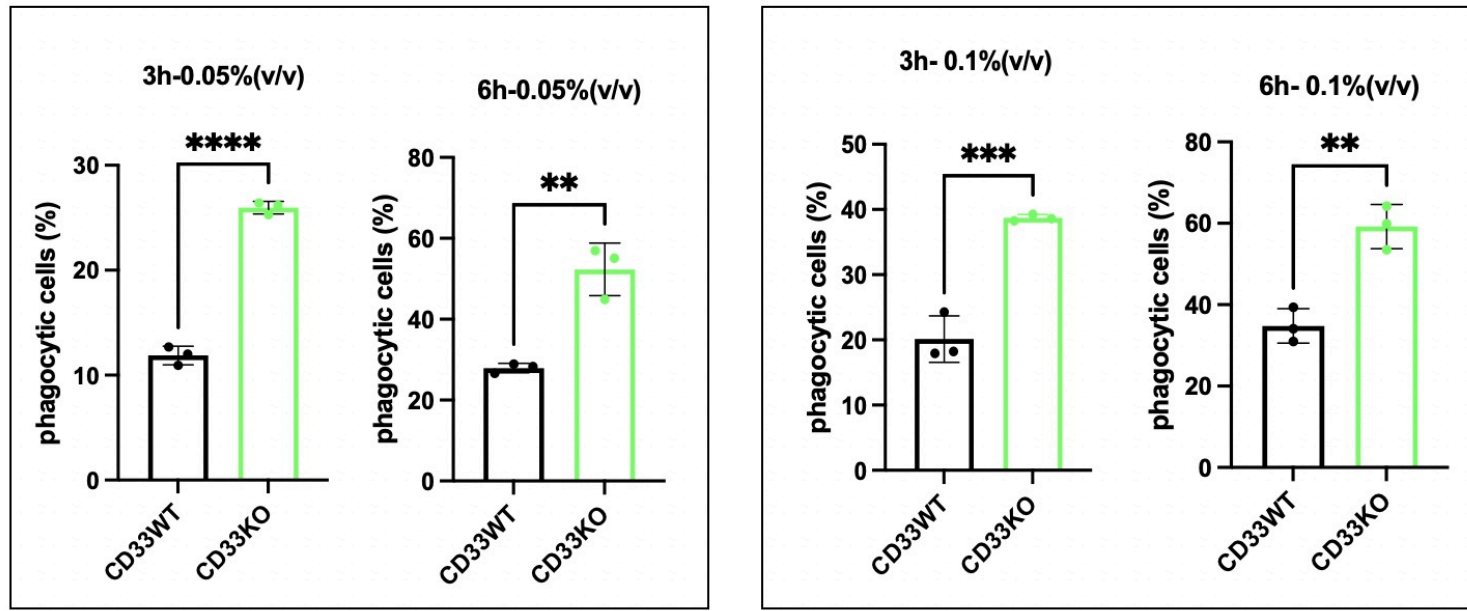
Figure 40. Quantification of phagocytic capability. The impact of CD33 knockout on bead engulfment was assessed at varying concentrations of 0.05% (v/v) and 0.1% (v/v), along with distinct incubation durations of 3 hours and 6 hours, respectively. Data are represented as Mean ± SD and were subjected to t-test analysis (p* = < 0.05, p** = < 0.01, p*** = < 0.001, p**** < 0.0001, ns = not significant). The experiment was conducted with a sample size of n=3.
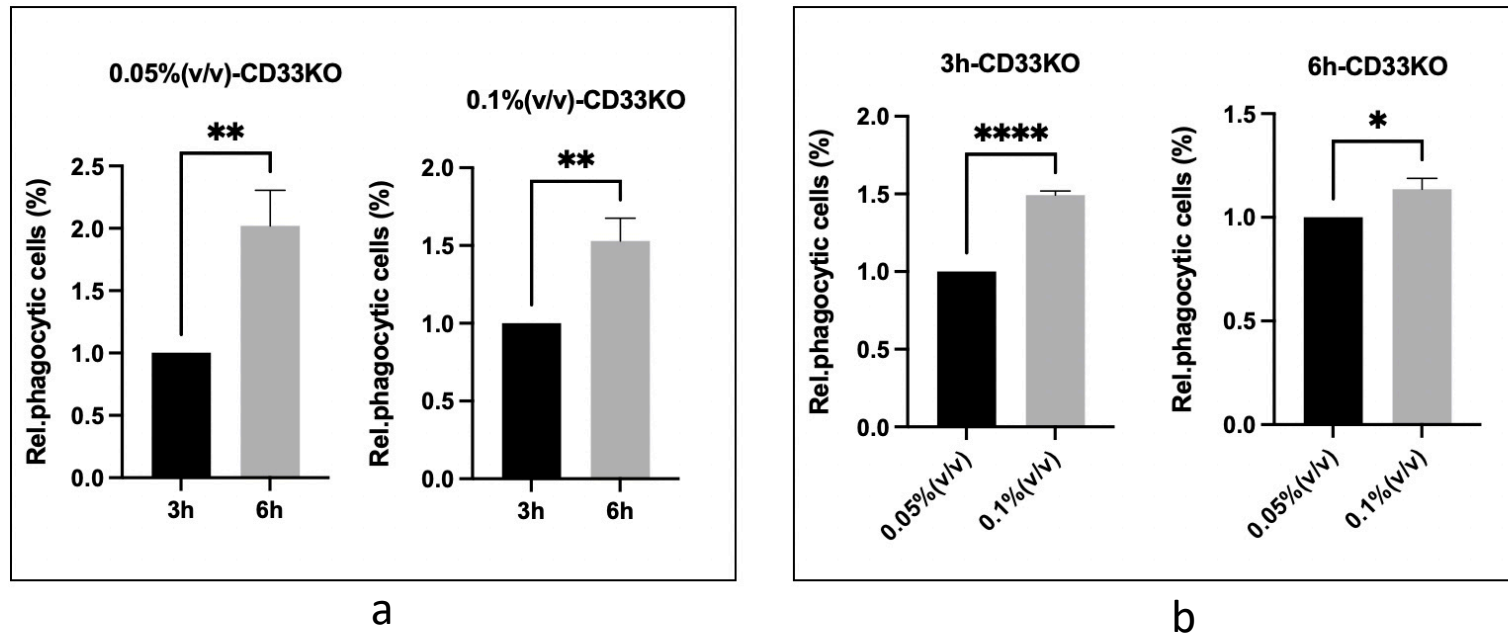
Figure 41.CD33KO-U937 macrophages phagocyte cargos in time-dependent and concentration-dependent manners.(a): CD33KO-U937 macrophages were incubated with beads-containing RPMI-1640 at concentrations of 0.05%(v/v) and 0.1%(v/v) under incubation period from 3 hours to 6 hours: the relative phagocytic cells (%) was 2-fold higher after 6 hours of incubation compared to the 3-hour incubation period at lower concentration of 0.05% (v/v); when elevated the bead concentration to 0.1% (v/v), the phagocytic activity after 6 hours exhibited a 1.5-fold increase over the 3-hour incubation.(**b**) At the time point of 3-hour exposure, cells incubated with high bead concentration (0.1% v/v) exhibited a 1.5-fold increase compared to the lower concentration (0.05% v/v). Additionally, extended incubation to 6 hours, the difference in phagocytic cells (%) between the two concentrations narrowed, with cells under the concentration (0.1% v/v) showing only a 1.1-fold increase over the lower concentration (0.05% v/v). Data are represented as Mean ± SD and were subjected to t-test analysis (p* = < 0.05, p** = < 0.01, p*** = < 0.001, p**** < 0.0001, ns = not significant). The experiment was conducted with a sample size of n=3.

**7.4 Validation effect of CD33 knockout on phagocytic capability on Alzheimer's disease hallmark of amyloid beta plaque**

To further validate the potential positive impact of CD33 knockout on the engulfment of the biological AD hallmark of amyloid beta plaques, phagocytosis assays were conducted using pre-aggregated PE-labeled amyloid beta$_{40}$ and FITC-labeled amyloid beta$_{42}$ by both CD33WT-U937 macrophages and CD33KO-U937 macrophages for a 3-hour incubation.CD33WT-U937 monocytes and CD33-KO-U937 monocytes were seeded with proper cell density in a 24-well plate separately, and cells were fully differentiated into macrophages using the method as described in 2.3. After that, the full differentiated macrophages were incubated with pre-aggregated PE-labeled amyloid beta$_{40}$ (2ug/ml) and FITC-labeled amyloid beta$_{42}$ (2ug/ml) in RPMI-1640 growth medium for 3 hours. IF assays were performed as described in 2.8.4. Phagocytosis was observed under confocal microscopy. Z-stacks were performed on phalloidin-stained phagocytes to visualize a series of layers through the interior of phagocytes and identify intracellular TAMRA-amyloid beta$_{40}$ (**Figure 42** and **Figure 43**) and FITC-amyloid beta$_{42}$ (**Figure 44** and **Figure 45**), using a 100X objective on a Leica STELLARIS 5 confocal microscopy. The TAMRA-amyloid beta$_{40}$ was confirmed inside the green-stained CD33WT-U937 macrophage and CD33KO-U937 macrophages as shown in **Figure 42** and **Figure 43** from multiple perspectives. FITC-amyloid beta$_{42}$ was confirmed inside the yellow-stained CD33WT-U937 macrophages and CD33KO-U937 macrophages as shown in Figure 44 and Figure 45 from multiple perspectives. The size of Z-steps was set at 0.04 μm in this experiment. In line with the increased engulfment observed with beads in CD33WT-U937 macrophages and CD33KO-U937 macrophages, CD33KO-U937 macrophages demonstrated an enhanced capability to engulf both amyloid beta $_{40}$ ($P<0.01$) as well as amyloid beta$_{42}$ ($P<0.001$), as depicted in Figure 46. And CD33WT-U937 macrophages exhibited higher affinity to amyloid beta$_{42}$ than to amyloid beta$_{40}$ compared to that in CD33KO-U937 macrophages as shown in **Figure 46**(P<0.01~0.05).

Figure 42. Verification of Phagocytic Capability in CD33WT-U937 Macrophages Using TAMRA-fAβ$_{1-40}$. CD33WT-U937 and CD33KO-U937 monocytes were differentiated into macrophages. TAMRA-f Aβ$_{1-40}$ (red) was diluted in complete growth medium to a working concentration of 2 μg/mL and incubated at 37 °C for 1 hour to promote aggregation. The macrophages were then incubated with the pre-aggregated Aβ1-40 medium for 3 hours. After incubation, cells were fixed with 4% PFA, and nuclei were stained with DAPI (blue). An anti-mouse Alexa Fluor® 488-conjugated antibody was used to visualize tubulin (green). 3D Z-stack confocal images (100X) with a 50 μm scale bar were captured. (A-F) display 3D images from various perspectives illustrating Aβ$_{1-40}$ engulfment in CD33WT-U937 macrophages.
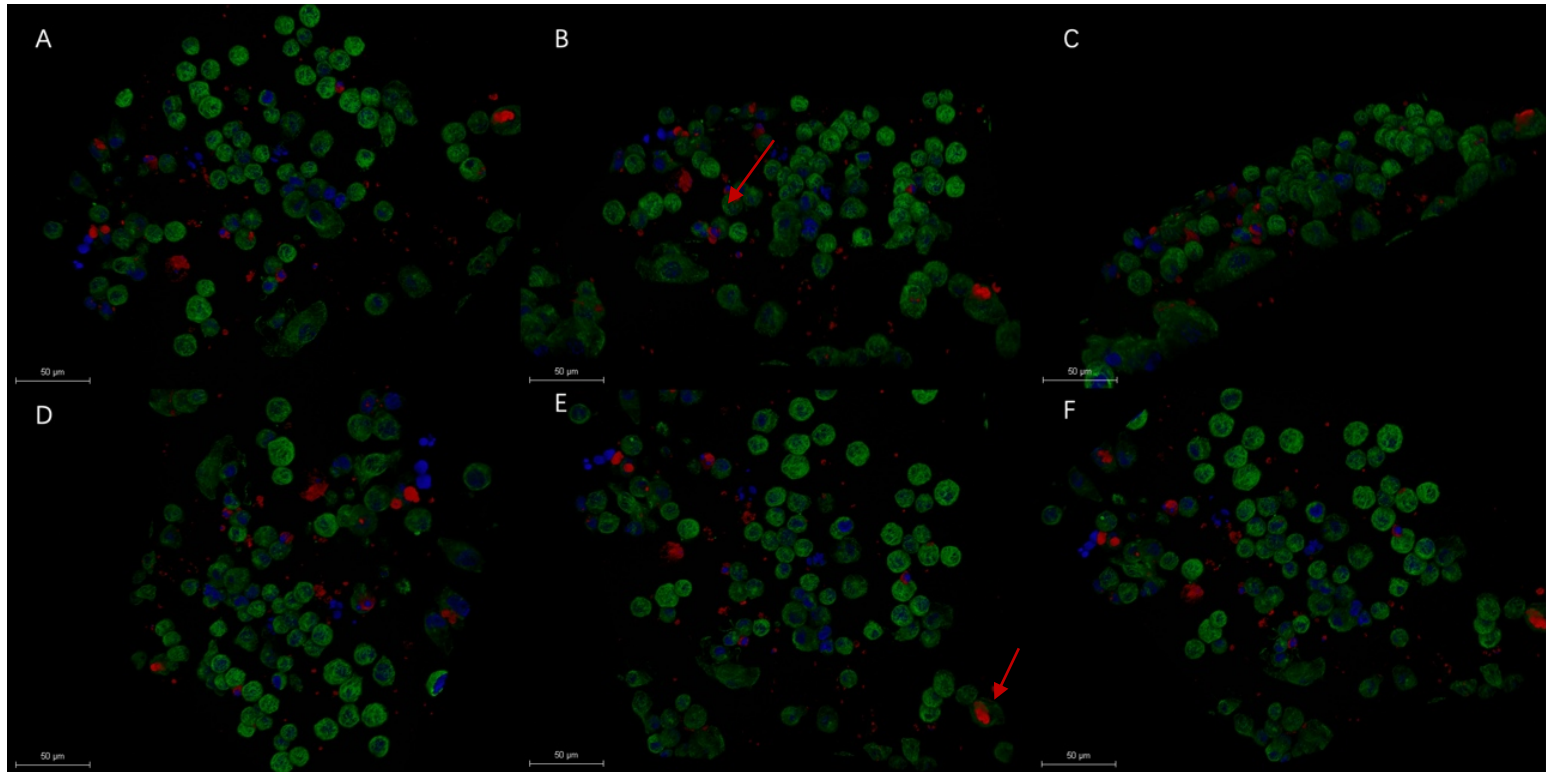
Figure 43. Verification of Phagocytic Capability in CD33KO-U937 Macrophages Using TAMRA-fAβ$_{1-40}$. CD33WT-U937 and CD33KO-U937 monocytes were differentiated into macrophages. TAMRA-f Aβ$_{1-40}$ (red) was diluted in complete growth medium to a working concentration of 2 μg/mL and incubated at 37 °C for 1 hour to promote aggregation. The macrophages were then incubated with the pre-aggregated Aβ1-40 medium for 3 hours. After incubation, cells were fixed with 4% PFA, and nuclei were stained with DAPI (blue). An anti-mouse Alexa Fluor® 488-conjugated antibody was used to visualize tubulin (green). 3D Z-stack confocal images (100X) with a 50 μm scale bar were captured. (G-L) display 3D images from various perspectives illustrating Aβ$_{1-40}$ engulfment in CD33KO-U937 macrophages.
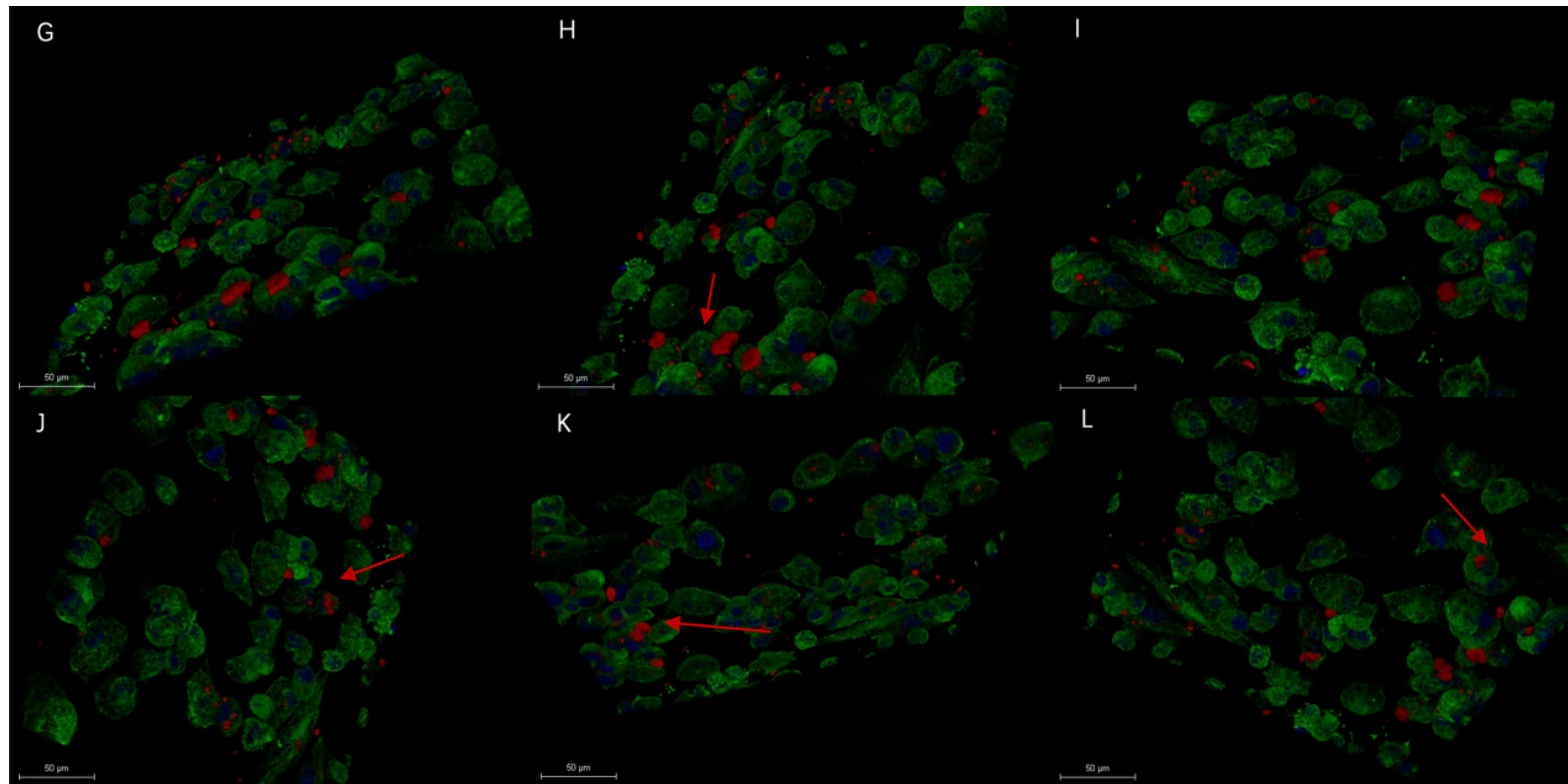
Figure 44. Validation of Phagocytosis in CD33WT-U937 Macrophages Using fAβ$_{1-42}$-FITC. CD33WT-U937 monocytes were differentiated into macrophages. fAβ$_{1-42}$-FITC (green) was diluted in complete growth medium to a working concentration of 2 μg/mL and incubated at 37 °C for 1 hour to facilitate aggregation. The macrophages were then incubated with the pre-aggregated Aβ$_{1-42}$ medium for 3 hours. Following incubation, cells were fixed with 4% PFA, and nuclei were stained with DAPI (blue). Phalloidin (far red) was used to visualize F-actin. 3D Z-stack confocal images (100X) with a 20 μm scale bar were captured. Panels (A-F) show 3D images from various perspectives illustrating the engulfment of Aβ$_{1-42}$ (green) in CD33WT-U937 macrophages;.Images are representative of one of three independent experiments. Red arrows indicate Aβ$_{1-42}$ inside macrophages.
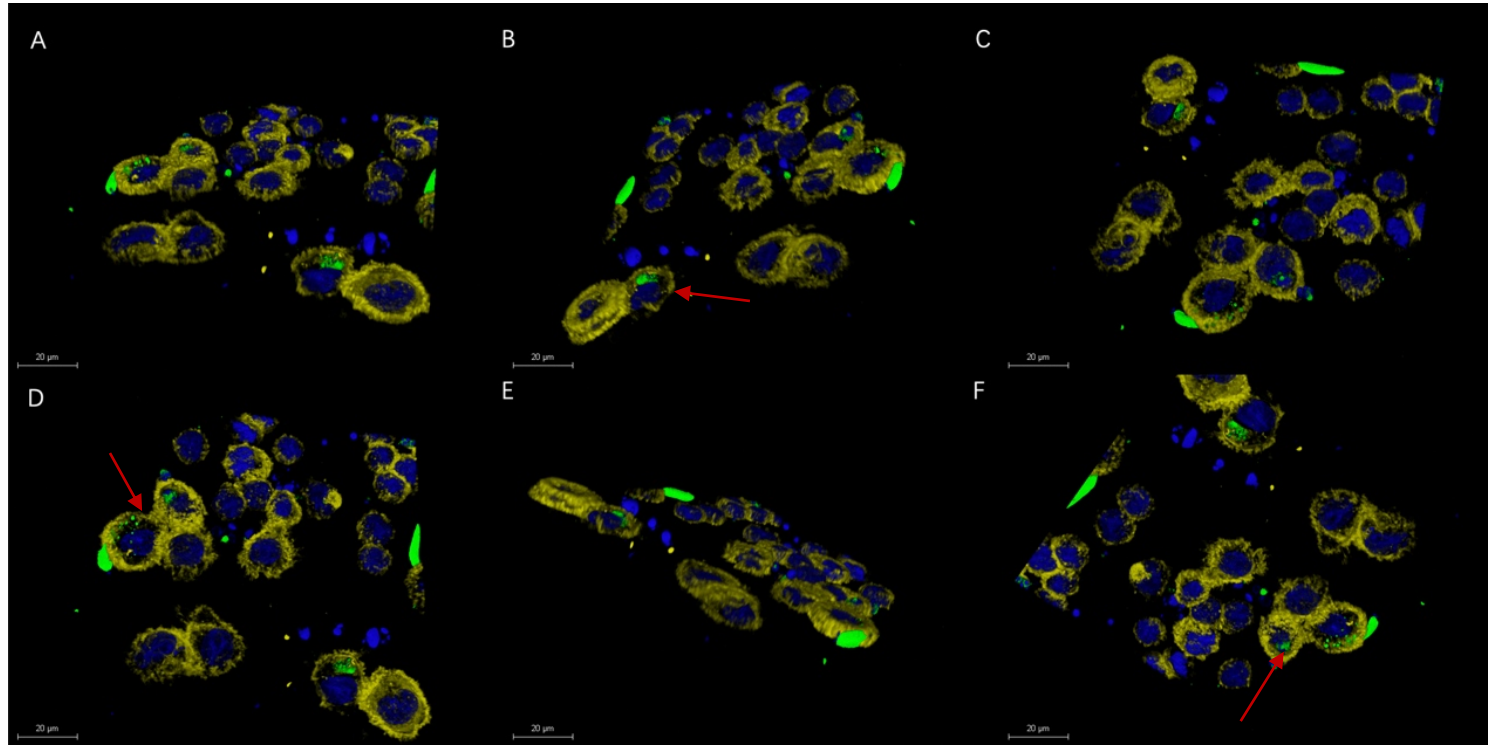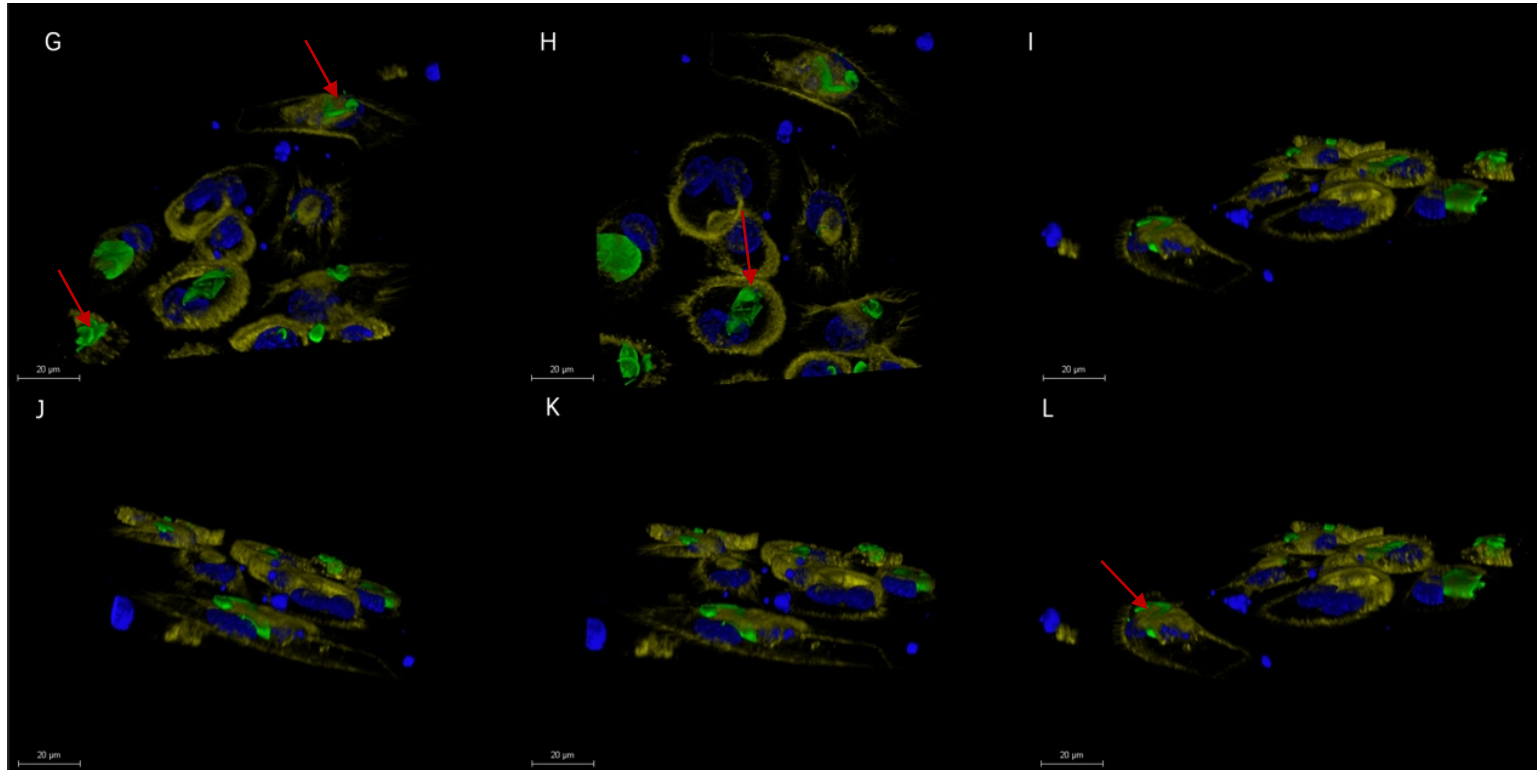
Figure 45. Validation of Phagocytosis in CD33KO-U937 Macrophages Using fAβ$_{1-42}$-FITC. CD33KO-U937 monocytes were differentiated into macrophages. fAβ$_{1-42}$-FITC (green) was diluted in complete growth medium to a working concentration of 2 μg/mL and incubated at 37 °C for 1 hour to facilitate aggregation. The macrophages were then incubated with the pre-aggregated Aβ$_{1-42}$ medium for 3 hours. Following incubation, cells were fixed with 4% PFA, and nuclei were stained with DAPI (blue). Phalloidin (far red) was used to visualize F-actin. 3D Z-stack confocal images (100X) with a 20 μm scale bar were captured. Panels (G-L) depict 3D images from different perspectives demonstrating the engulfment of Aβ$_{1-42}$ (green) in CD33KO-U937 macrophages. Images are representative of one of three independent experiments. Red arrows indicate Aβ$_{1-42}$ inside macrophages.
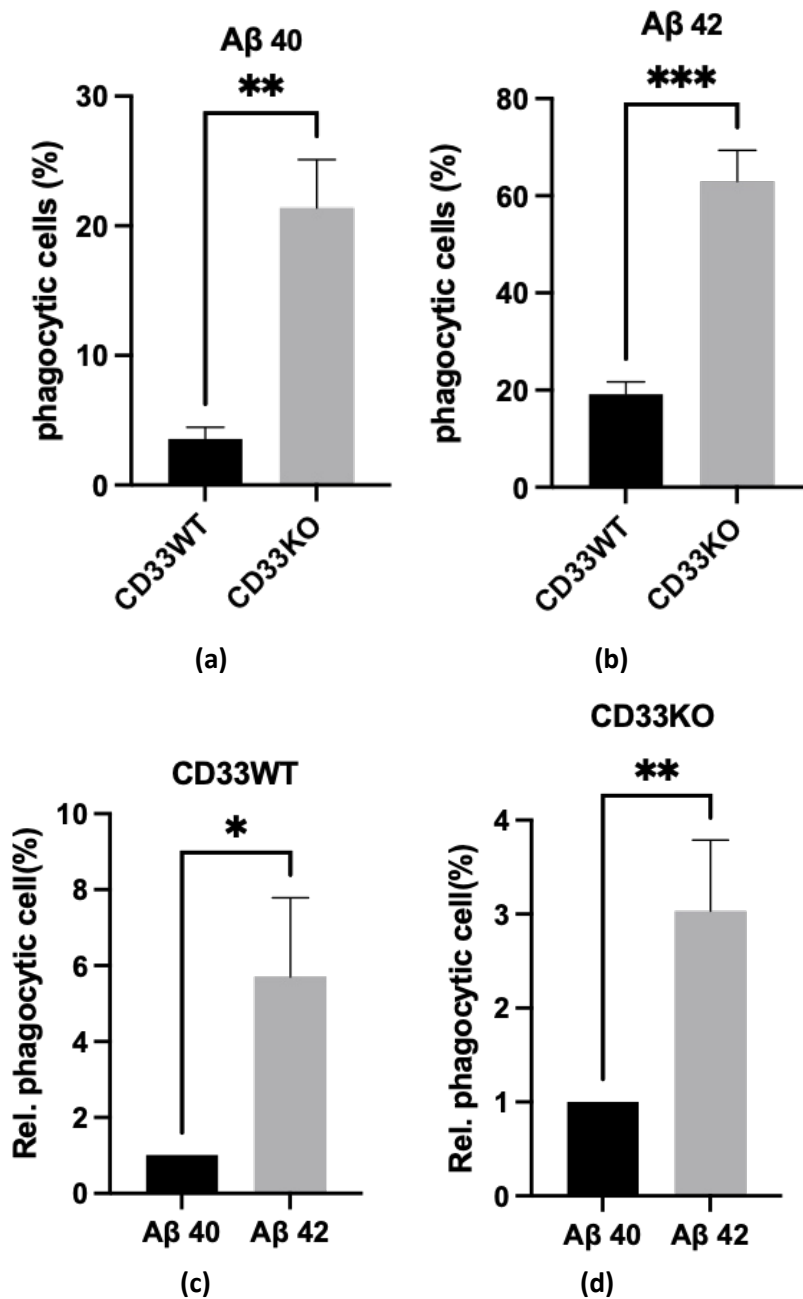
Figure 46. Analysis of the internalization ability of CD33WT-U937 and CD33KO-U937 derived macrophages using Aβ$_{1-40}$ and Aβ$_{1-42}$. An average of 5-fold upregulation of phagocytosis activity in CD33KO-U937 derived macrophages was detected by using Aβ$_{1-40}$(a), and an average of 3-fold increase of phagocytosis in CD33KO-U937 derived macrophages was detected by using Aβ$_{1-42}$(b). both CD33WT-U937 macrophages and CD33KO-U937 derived macrophages tend to have high ability to engulf Aβ$_{1-42}$ than Aβ$_{1-40}$(c)(d). Data presented as Mean ± SD – t-test (p* = < 0.05 p **= <0.01, p*** = < 0.001, p**** <0.0001, ns=not significant. (n=3).

7.5 Validation on the effect of CD33 knock out on MSR1 and lysosome marker LAMP2.

MSR1, as described above, is a scavenger receptor prominently expressed on the surface of various macrophage types, playing a crucial role in regulating phagocytosis and

maintaining homeostasis(Gudgeon et al., 2022). The lysosomal marker LAMP2 is essential for both autophagy and phagocytosis, facilitating the fusion of phagosomes or autophagosomes with lysosomes for efficient cargo degradation. CD33 knockout significantly enhanced phagocytic capability and implicated the upregulation of numerous phagocytosis-related genes. Here, the expression of key phagocytosis genes, MSR1 and LAMP2, was further investigated.

To confirm the expression levels of MSR1 and LAMP2, RT-qPCR and Western blot assays were conducted. CD33WT-U937 and CD33KO-U937 macrophages were treated with or without LPS and amyloid beta42 for 12 hours under serum-free conditions. Samples were collected as described in section 2.5.1. The mRNA expression of MSR1 was further validated through RT-qPCR.

7.5.1 CD33 knockout promotes MSR1 expression from protein level and mRNA level, and LPS inhibits MSR1 transcription in the presence and absence of CD33.

Expression of MSR1 exhibited a significant increase in CD33KO-U937 macrophages compared to CD33WT-U937 macrophages. CD33 knockout induced a fourfold increase in mRNA expression, as confirmed by RNA deep sequencing ($P<0.05$, **Figure 49a**), and a corresponding sixfold increase detected by RT-qPCR ($P<0.05$, **Figure 48a**). Additionally, Western blot analysis showed a significant increase in MSR1 protein levels in CD33KO-U937 macrophages compared to CD33WT-U937 macrophages (**Figure 47**).

When treated with LPS for 6 hours, CD33KO-U937 macrophages exhibited a twelvefold increase in MSR1 transcription compared to CD33WT-U937 macrophages ($P<0.05$, Figure 48d). In the presence of CD33, LPS inhibited both MSR1 transcription and protein expression compared to negative controls, a pattern similarly observed in CD33KO-U937 macrophages (**Figure 47**, **Figure 48b** and **Figure 48c).**

7.5.2 CD33 knockout promotes LAMP2 expression from protein level and mRNA level

RNA deep sequencing revealed an average 1.7-fold increase in LAMP2 transcription in CD33KO-U937 macrophages compared to CD33WT-U937 macrophages (P<0.05, Figure 49b). This transcriptional increase was accompanied by a corresponding rise in LAMP2 protein expression, as confirmed by Western blot analysis (P<0.001, **Figure 47**).

7.5.3 LPS inhibit MSR1 expression both in mRNA and protein expression

Figure 48c and **Figure 48b** indicated approximately a 50% decrease in MSR1 mRNA expression in both CD33WT-U937 macrophages (P<0.01) and CD33KO-U937 macrophages (P<0.05) when compared to their respective negative controls, following a 6-hour LPS treatment, as confirmed by RT-qPCR (P<0.05). Protein expression analysis of MSR1 in CD33WT-U937 macrophages, shown in **Figure 47**, was nearly undetectable. Conversely, MSR1 was significantly expressed in CD33KO-U937 macrophages but exhibited a slight decrease upon 12-hour LPS stimulation compared to its CD33KO-U937 macrophage negative control (**Figure 47**).
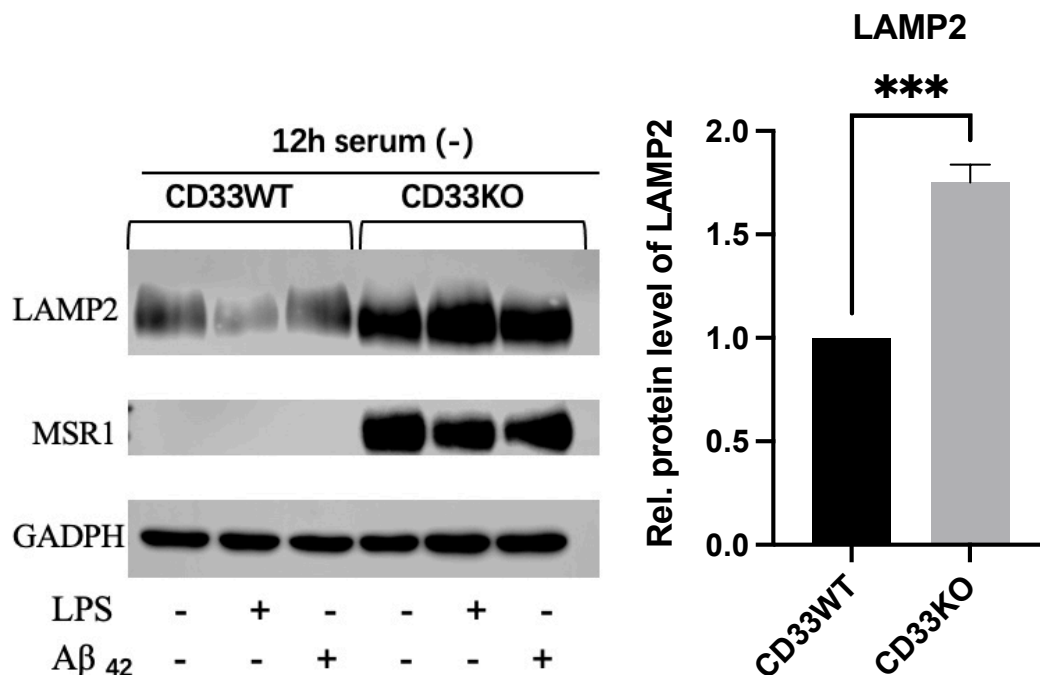
Figure 47. Representative blot images of MSR1 and LAMP2 in the presence of absence of CD33.CD33 knockout tremendously induced protein expression of MSR1 in CD33KO-U937 macrophages and there were no bands detected in CD33WT-U937 macrophages in negative controls, LPS stimulation and amyloid beta42 stimulation groups. LAMP2 expression was upregulated due to CD33 knockout in CD33KO-U937 macrophages compared to CD33WT-U937 macrophages. Images presented one of four independent trials. Samples harvested with treatments of 100ng/ml LPS and amyloid beta42 in serum-free condition for 12 hours.n=3.
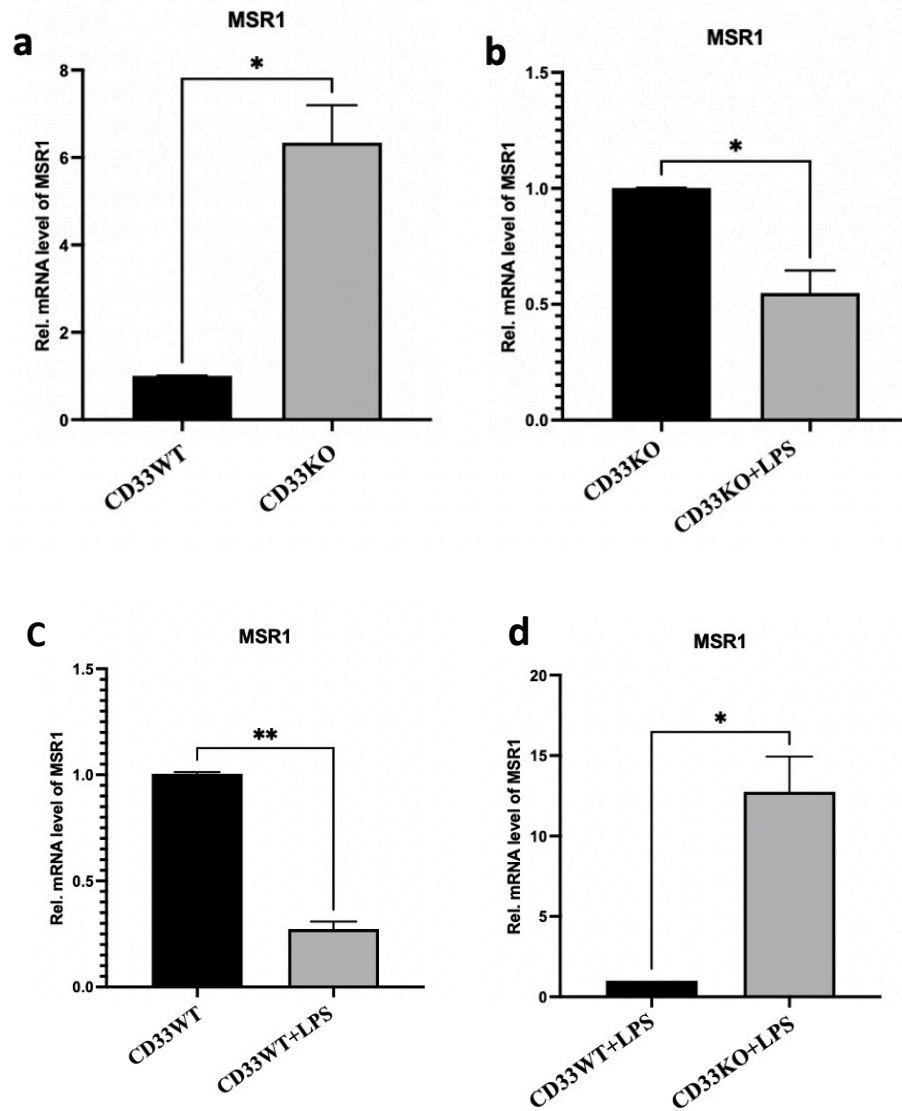
Figure 48. mRNA expression changes of MSR1 after CD33 knockout in the presence and absence of LPS for 6 hours, confirmed by RT-qPCR. CD33 knockout induced a 6-fold increase in transcription of MSR1(a); in response to LPS stimulation, CD33KO-U937 macrophages exhibited high reaction of over 10-fold increase in promoting MSR1 transcription compared to CD33WT-U937 macrophages (d); and LPS inhibited mRNA expression of MSR1 in both presence and absence of CD33(b and c). Data presented as Mean ± SD – t-test (p* = < 0.05 p **= <0.01, p*** = < 0.001, p**** <0.0001, n=3).
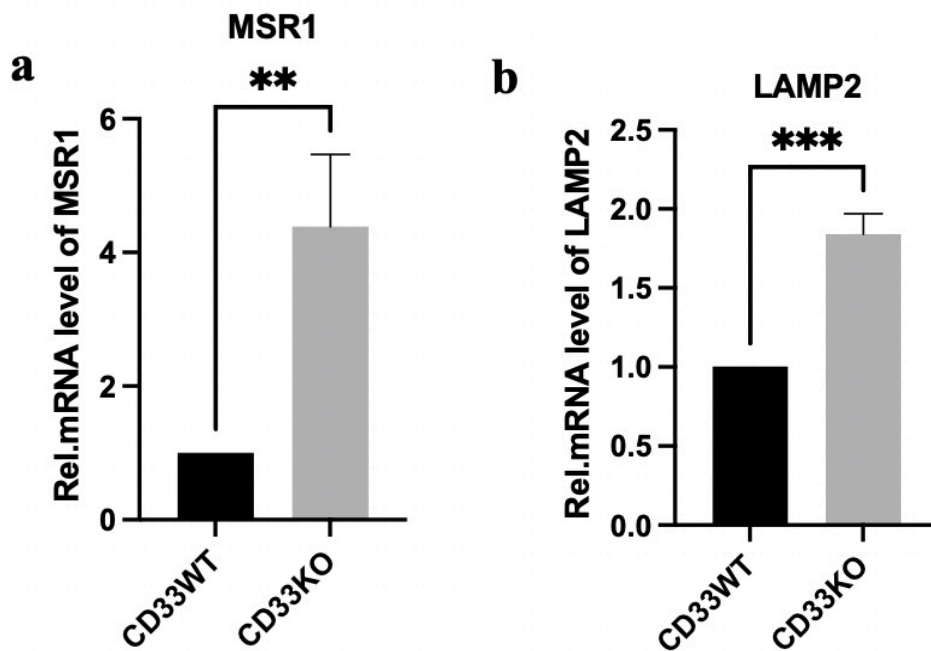
Figure 49. The effect of CD33 knockout on transcription of MSR1 and LAMP2, confirmed by RNA deep sequencing. The deletion of CD33 induced a 4-fold increase in MSR1 transcription(a) and a 1.7-fold increase of LAMP2 transcription(b). Data presented as Mean ± SD – t-test (p* = < 0.05 p **= <0.01, p*** = < 0.001, p**** <0.0001. (n=3).

7.6 Visualization of LAP (LC3-associated phagocytosis) in the presence and absence of CD33 by immunofluorescent staining

CD33 knockout enhanced phagocytic activity and upregulated the expression of phagocytosis-related genes MSR1 and LAMP2, both at mRNA and protein levels. A substantial increase in LC3b expression was also observed post-CD33 knockout (as detailed in Chapter 3). To further explore phagocytosis induced by amyloid beta plaques, CD33WT-U937 and CD33KO-U937 monocytes were fully differentiated into macrophages as described in section 2.3. These macrophages were then incubated with pre-aggregated 2 µg/mL amyloid beta42 under serum-free conditions for 6 hours, and immunofluorescent staining assays were conducted as outlined in section 2.8. **Figure 50** illustrates phagolysosomes (yellow staining) marked by the lysosome marker LAMP2(red staining) in both CD33WT-U937 and CD33KO-U937 macrophages stimulated with pre-aggregated amyloid beta42. Phagosome membranes were detected using phalloidin-568 staining, while LAMP2 was observed using a goat anti-mouse IgG (H+L) Superclonal Secondary Antibody, Alexa Fluor® 647 conjugate.

To investigate whether CD33 knockout facilitates phagocytosis through traditional mechanisms as well as LC3-associated phagocytosis (LAP), CD33WT-U937 and CD33KO-U937 macrophages were further incubated with pre-aggregated 2 μg/mL FITC-amyloid beta42 under serum-free conditions for 6 hours. Immunofluorescent staining assays were performed according to the method described in section 2.8. **Figure 51** demonstrates an increase in LC3b (yellow staining) and LAMP2 (red staining) within the cytoplasm of CD33KO-U937 macrophages compared to CD33WT-U937 macrophages. The co-localization of LC3b and LAMP2 was enhanced in response to FITC-amyloid beta$_{42}$ plaques in the absence of CD33 (**Figure 52**).

These results indicate that CD33 knockout not only boosts phagocytosis via classical mechanisms but also enhances the engulfment and degradation process through an LC3-associated phagocytosis mechanism.
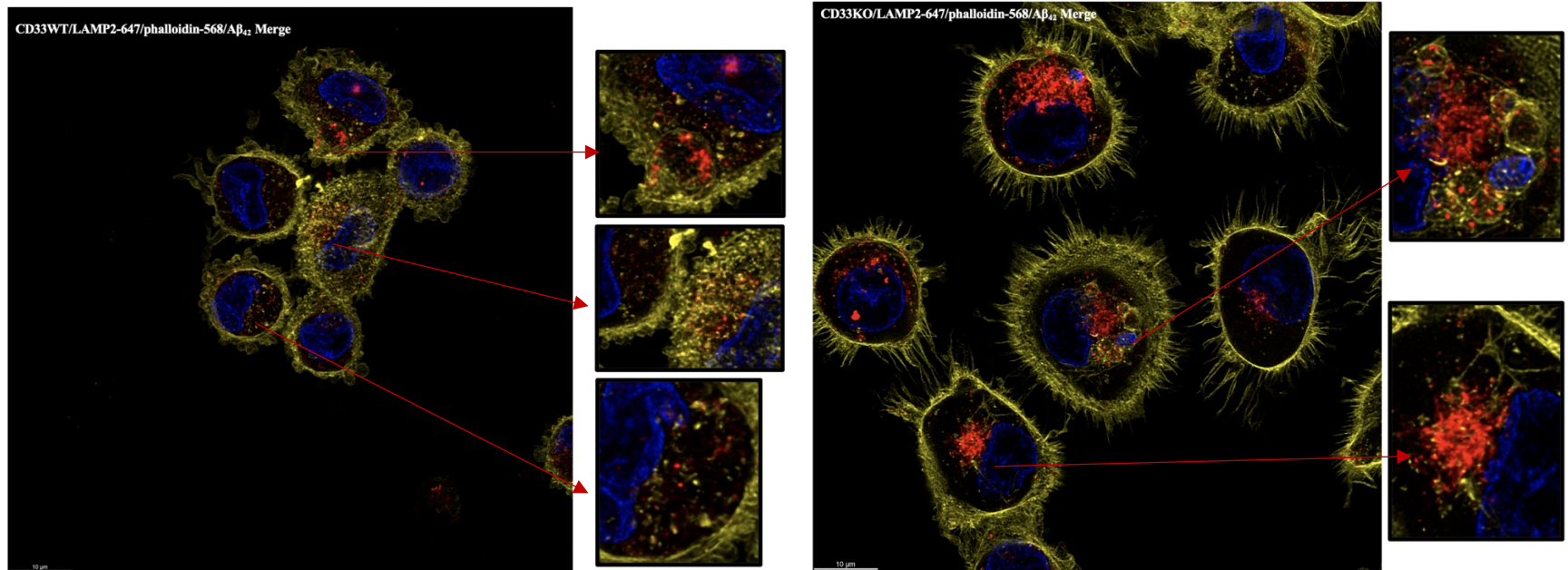
Figure 50. Expression and localization of phagolysosome combined with LAMP2 in CD33WT-U937 macrophages and CD33KO-U937 macrophages.CD33WT-U937 monocytes and CD33KO-U937 monocytes were fully differentiated into macrophages and treated with pre-aggregated amyloid beta$_{42}$(2ug/ml) for 6 hours in serum free condition. The macrophages ramified out to form phagosomes to engulf target cargos.CD33 knockout induced increased expression of phagosomes and phagolysosomes which combined to LAMP2. Red arrows indicate the phagolysosomes combined with lysosome marker of LAMP2. Phagosome membrane derived from cell membranes was stained with phallodin-568(yellow staining). Nuclear was stained by DAPI (blue stanning), lysosomal marker LAMP2 was visualized by goat anti-mouse IgG (H+L) superclonal secondary antibody, alexa fluor® 647 conjugate (red staining). Z-stack confocal images (100X) were taken with a scale bar of 10um.
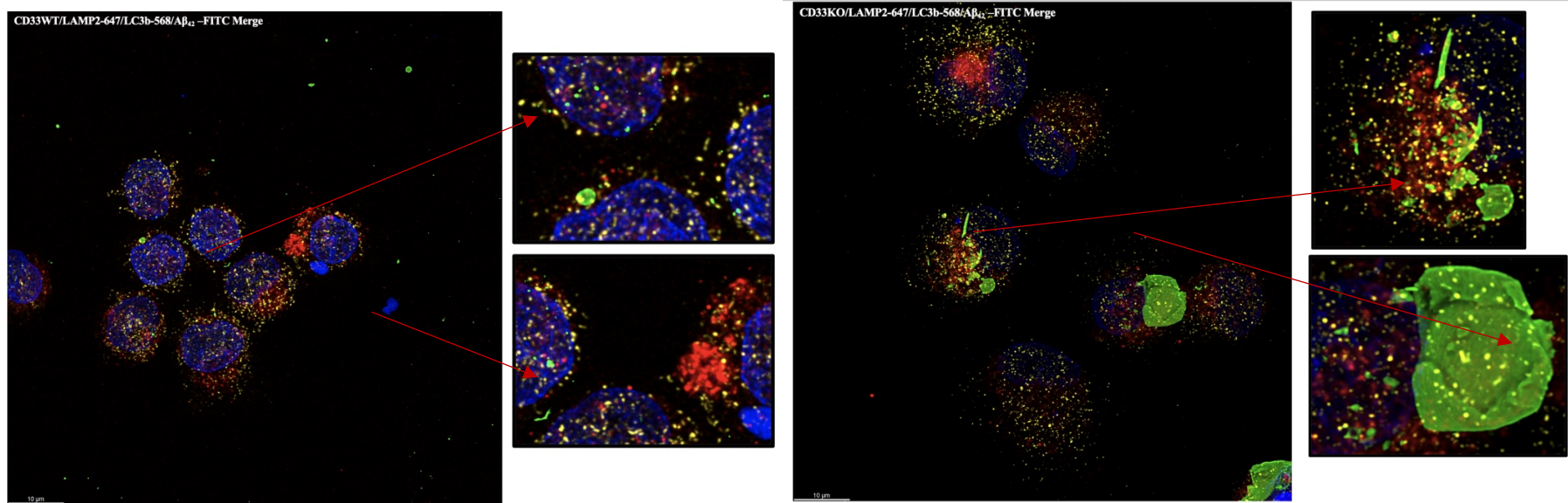
Figure 51. Immunofluorescent colocalization of LC3 and LAMP2 of LC3b-associated phagocytosis in CD33WT-U937 macrophages and CD33KO-U937 macrophages. CD33WT-U937monocytes and CD33KO-U937monocytes were fully differentiated into macrophages and treated with pre-aggregated FITC-amyloid beta42 (2ug/ml) for 6 hours in serum-free condition. The expression of LC3b and LAMP2 were increased stimulated by pre-aggregated FITC-amyloid beta42 as well as co-localization of LAMP2(red staining) and LC3b (yellow staining) was increased in the absence of CD33.Red arrows indicate co-localization of LC3b-associated phagocytic phagolysosomes or classic phagolysosomes combined with the aggregated LAMP2 with FITC-amyloid beta42 plaques wrapped in. DAPI was stained to visualize nuclear, goat anti-rabbit IgG (H+L) superclonal secondary antibody, alexa fluor® 568 conjugate to visualize rabbit anti-human LC3b monoclonal antibody, and goat anti-mouse IgG (H+L) superclonal secondary antibody, alexa fluor® 647 conjugate to visualize mouse anti-human LAMP2 monoclonal antibody Z-stack confocal images (100X) were taken with a scale bar of 10um.
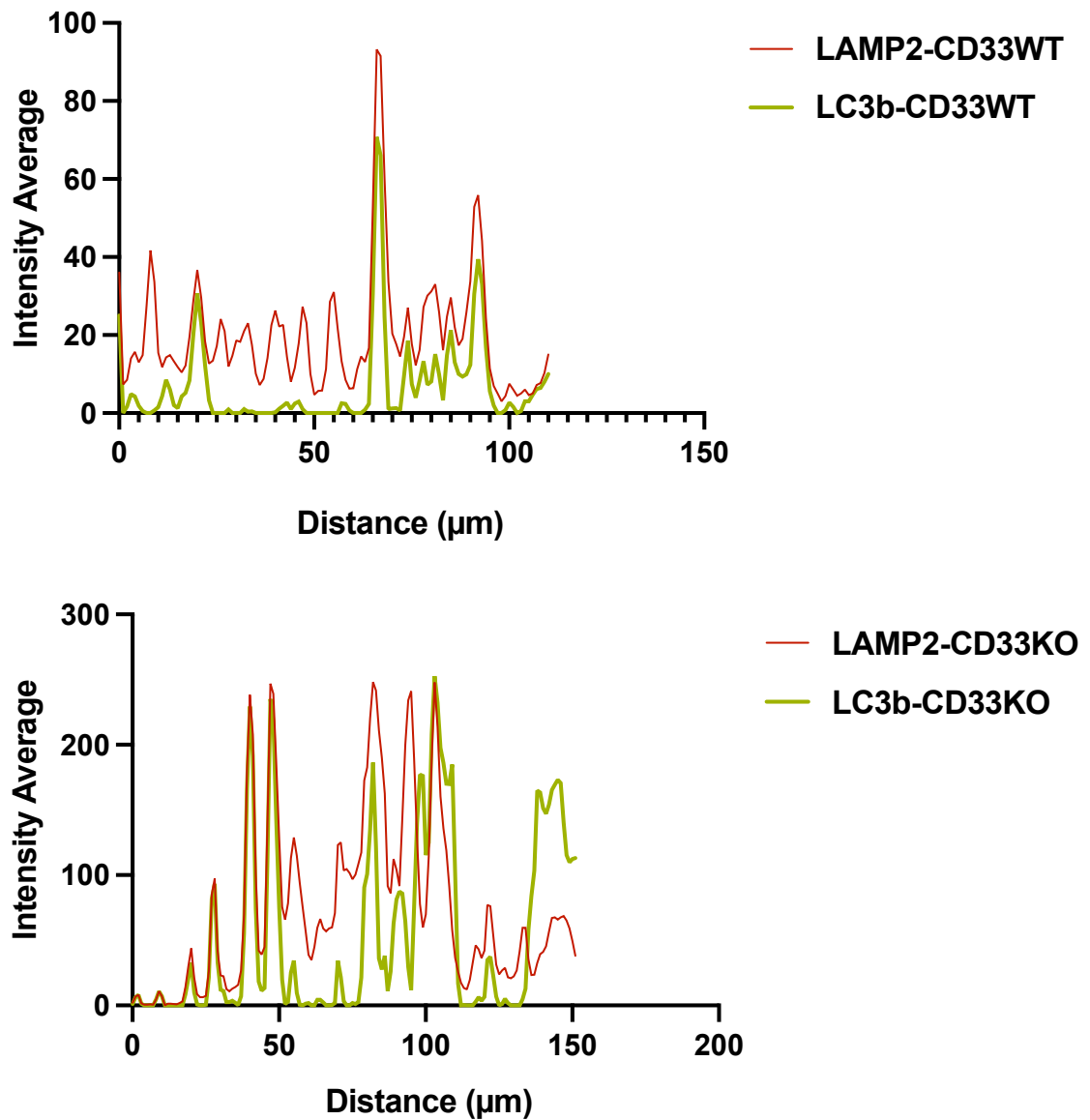
Figure 52. Immunofluorescent colocalization of LC3 and LAMP2. The average intensity of LC3b (green line) and LAMP2 (red line) in CD33WT-U937 macrophages and CD33KO-U937 macrophages. LC3b and LAMP2 were upregulated and tended to be more colocalized in CD33KO-U937 macrophages compared to CD33WT-U937 macrophages.

8.Discussion

The Alzheimer's Disease (AD) brain is marked by the excessive deposition of extracellular amyloid plaques composed of amyloid beta (Aβ) peptides and the accumulation of intracellular neurofibrillary tangles primarily consisting of aggregated hyperphosphorylated tau proteins(Gallardo and Holtzman, 2017). Targeting the clearance of extracellular Aβ plaques has long been a focus for AD therapy development. CD33 has emerged as a top AD risk gene through genome-wide association studies (GWAS), prompting significant research in the relationship between CD33 and Aβ clearance. Numerous in vitro and in vivo studies have demonstrated that CD33 deletion in microglia/macrophages enhances Aβ plaque clearance(Li et al., 2015, Griciuc et al., 2013, Gu et al., 2022).Although CD33's role in inhibiting amyloid beta uptake is well-demonstrated, the downstream signaling mechanisms involved in phagocytosis and whether CD33 deletion aids in further processing post-engulfment remain subjects for debate. This chapter thoroughly examines the impact of CD33 knockout on phagocytosis and the consequent changes in downstream signaling pathways.CD33 knockout induces the transcription of numerous phagocytosis-related genes, including pattern recognition receptors (PRRs) such as MSR1, complement components like C3, Fcγ receptors such as FCGR1B, FCGR1A, FCGR2A, FCGR2B, FCGR2C, and FCGR3A, and various chemokines that directly and indirectly promote phagocytic activity. Consistent with earlier research, CD33 knockout significantly enhances the phagocytic capability of macrophages, albeit in a concentration- and time-dependent manner, resulting in markedly increased phagocytosis in CD33KO-U937 macrophages compared to CD33WT-U937 macrophages. Although the enhancement of phagocytosis following CD33 deletion is established, the precise mechanisms remain under investigation. This discussion will propose hypotheses regarding how CD33 knockout augments phagocytic activity and detail the underlying pathways that may contribute to this phenomenon.

8.1 CD33 knockout induces phagocytosis via the balance of the ITAM-ITIM signalling axis

Cellular functions are tightly regulated by a network of signaling pathways that interact to ensure balanced physiological processes. In the regulation of phagocytosis, the interplay between activating ITAM signaling and inhibitory ITIM signaling is crucial. Receptors like TREM2, a known AD risk factor, possess ITAM motifs to activate downstream DAP12-SYK signaling pathways to enhance phagocytosis. In contrast, CD33, a Siglec receptor, contains ITIMs in its cytoplasm that initiate inhibitory signals by recruiting phosphatases such as SHP-1 and SHP-2.Activation of CD33 leads to the recruitment of SHP-1 and SHP-2, which inhibit Syk signaling, thereby suppressing ITAM-mediated activities including phagocytosis (Malik et al., 2015)). In AD pathology, the extensive aggregation of amyloid beta (Aβ), which contains sialic acid residues(Salminen and Kaarniranta, 2009) (Szumanska et al., 1987) acts as ligands for CD33(Alphey et al., 2003, Taylor et al., 1999, May et al., 1998). This interaction triggers ITIM signaling, recruiting SHP1 and SHP2, and subsequently silencing ITAM signaling, which results in the inhibition of phagocytosis.Consequently, this suppression contributes to the persistent build-up of toxic Aβ plaques that progressively damage neurons and promote chronic inflammatory responses in the brain.Therefore, CD33 knockout promotes phagocytosis by removing inhibition to ITAM signaling, potentially ameliorating plaque accumulation and its detrimental effects.

8.2 CD33 knockout induces phagocytosis via upregulating MSR1, Fc gamma receptors and C3

CD33 knockout significantly enhanced the expression of MSR1 at both the transcriptional and protein levels. MSR1, a type II transmembrane glycoprotein, is a member of the scavenger receptor family that mediates the endocytosis of a diverse range of ligands, including bacterial pathogens, low-density lipoproteins, dead cells, β-amyloid, and other molecules (Ishiguro et al., 2001) (Husemann et al., 2002, Cheng et al., 2019, Li et al., 2021a). In the brain, MSR1 predominantly expresses in microglia (Ishiguro et al., 2001)), it plays a crucial role in amyloid beta clearance by facilitating the adhesion of microglia to fibrillar Aβ, promoting the engulfment of Aβ deposits(El Khoury et al., 1996), which promotes the engulfment of Aβ deposition in the brain. In Alzheimer's Disease (AD) mouse models, MSR1 deficiency is associated with impaired clearance of soluble Aβ and increased Aβ deposition.

Conversely, pharmacological upregulation of MSR1 enhances Aβ clearance, indicating its neuroprotective role in inhibiting toxic Aβ forms (Frenkel et al., 2013, Sandoval et al., 2019, Li et al., 2021a)(Zuroff et al., 2017). The loss of CD33 has been shown to increase MSR1 expression and promote the engulfment of aggregated Aβ40 and Aβ$_{42}$ in CD33KO-U937 macrophages, thus enhancing phagocytic capacity.

RNA deep sequencing further confirmed the upregulation of several genes associated with phagocytosis in CD33KO-U937 macrophages. Besides MSR1, Fc gamma receptors (FcγRs) exhibited increased transcription following CD33 knockout. FcγRs are glycoproteins that specifically bind the Fc region of IgG molecules, facilitating opsonization of target particles (Freeman and Grinstein, 2014, Uribe-Querol and Rosales, 2020).Expressed on macrophages and microglia, FcγRs(Okun et al., 2010) regulate phagocytosis through cytoplasmic ITAM and ITIM signaling (Anthony et al., 2012, Meylan et al., 2006)). Our study found that CD33 deletion led to a significant increase in the transcription of ITAM-containing Fcγs, including FCGR1A, FCGR2A, FCGR3A, and FCGR2C, with fold increases ranging from 3 to 12. Similarly, ITIM-containing FcγRs, FCGR1B and FCGR2B, also exhibited increased transcription, with 1.5-fold and 7-fold changes, respectively. The phagocytic process mediated by FcγRs relies on the balance between activating ITAM and inhibitory ITIM FcγRs(Fuller et al., 2014). In CD33KO-U937 macrophages, the predominant increase in ITAM-FcγRs likely contributes to enhanced phagocytic capability. Elevated IgG levels have been reported in the cerebrospinal fluid (CSF) of AD patients(Blennow et al., 1990). Efforts to enhance Aβ clearance in microglia via Fcγ-mediated phagocytosis using anti-Aβ antibodies have shown promise in reversing cognitive decline in transgenic APP mouse models (Wilcock et al., 2004a, DeMattos et al., 2001)). However, this is associated with side effects such as increased cerebral microhemorrhage (Wilcock et al., 2004).

On the other hand, the deletion of CD33 also led to an increase in C3 transcription. C3, a critical component of the complement system, assists in opsonizing microbial surfaces, facilitating immune recognition and phagocytosis (Li et al., 2007a, Trial et al., 2016). It has been reported to promote amyloid beta plaque clearance through interactions with CR3 receptors, as demonstrated in both in vivo and in vitro studies(Strohmeyer et al., 2002,

Maier et al., 2008, Choucair-Jaafar et al., 2011, Fu et al., 2012). Fu et al. highlighted that CR3 receptors facilitate amyloid beta (Aβ) uptake by interacting with class A scavenger receptors(Fu et al., 2012) such as MSR1 (Matsumoto et al., 1990).Further evidence suggests CR3's colocalization with Aβ plaques in AD brains, supporting the potential for direct CR3-Aβ interactions(Strohmeyer et al., 2002).

In Alzheimer's Disease pathology, complement pathways are crucial for amyloid beta clearance.Evidence indicates that circulating $A\beta_{42}$ adheres to complement C3b on erythrocyte CR1, marking it for removal from the bloodstream(Rogers et al., 2006). Combined with increased MSR1 expression in CD33KO-U937 macrophages, the upregulated C3 transcription may enhance phagocytosis through direct interaction with CR3 or a collaborative MSR1-CR3 mechanism.

8.3 CD33 knockout induced cargo degradation by increasing the lysosomal marker of LAMP2 and through an LC3-associated phagocytosis mechanism

A critical step in phagocytosis is degradation, where phagosomes envelop cargo and fuse with lysosomes to form phagolysosomes, facilitating the breakdown and recycling or disposal of materials. This fusion and degradation process relies on the lysosomal marker LAMP2. CD33 knockout led to increased transcription and protein expression of LAMP2 in CD33KO-U937 macrophages compared to CD33WT-U937 macrophages. To further visualize phagocytosis, immunofluorescence assays were conducted on both CD33WT-U937 and CD33KO-U937 macrophages, using fluorescent-labeled amyloid beta plaques as cargo to observe the engulfment process. Key markers LC3b and LAMP2 were employed to assess and compare autophagy flux and lysosomal activation in the two macrophage types. Results showed a marked increase in LAMP2 expression and aggregation on phagosomes' surfaces in CD33KO-U937 macrophages compared to CD33WT-U937 macrophages. This strongly suggests that CD33 knockout enhances the engulfment process and subsequent degradation of cargo.Interestingly, amyloid beta induced colocalization of LAMP2, LC3b, and amyloid plaques, indicating that CD33 deletion not only facilitates classical phagocytosis but also promotes digestion through an LC3-associated phagocytosis (LAP)

mechanism. LAP involves the conjugation of LC3 to phagosomal membranes (Martinez et al., 2015) and has been suggested to prevent neurodegeneration even without autophagy flux (Plaza-Zabala et al., 2017).Animals deficient in LAP exhibit increased pathological inflammation and pro-inflammatory cytokines (Martinez et al., 2011, Florey et al., 2011, Martinez et al., 2015). LAP facilitates the clearance of extracellular particles and is initiated through phagocytosis via Fc receptors, complement receptors, and TLRs(Heckmann et al., 2017)(Martinez et al., 2015).Therefore, increased LAP activity can be attributed to the upregulation of Fc receptors due to CD33 knockout.The NOX2 enzyme, encoded by the CYBB gene, is the only NADPH oxidase expressed in phagocytes and is primarily found in the membranes of phagosomes' intracellular vesicles(Bedard and Krause, 2007).NOX2 is linked to LC3 translocation to TLR- or FcγR-engaged phagosomes and assists in recruiting autophagy machinery to localized targets(Huang et al., 2009) .In this study, CD33 knockout led to a dramatic (over 300-fold) increase in CYBB transcription, potentially contributing to enhanced phagocytosis and LAP activity.

Chapter 5 The effect of CD33 knockout on Cytokine Production and Cell Movement

1. Inflammation in AD

CD33-related Siglecs are proteins primarily expressed on leukocyte subsets and are involved in regulating leukocyte functions during inflammatory and immune responses (Lock et al., 2004, Zhang et al., 2004).It is predominantly expressed on macrophages and monocytes, alongside Siglec-5, Siglec-7, Siglec-9, and Siglec-10, as depicted in **Figure 53**. Although these Siglecs exhibit functional redundancy, they also display distinct binding patterns, suggesting diverse roles in cellular activation processes. The molecular characteristics and signaling properties of CD33-related Siglecs imply a significant influence on cellular activation within the innate immune system and subsequent inflammatory responses(Crocker et al., 2012a).CD33 acts as an inhibitory receptor on monocytes and macrophages. Its interaction with ligands triggers downstream regulation, leading to the release of various pro-inflammatory cytokines and other inflammatory mediators. Alzheimer's Disease (AD), characterized by neuroinflammation, has been associated with CD33 function, particularly in microglia—the resident macrophages in the brain. During inflammation, activated microglia change phenotype and produce pro-inflammatory mediators such as IL-1, TNFα, and nitric oxide, which can induce neuronal damage and cell death(Ransohoff and Perry, 2009).Conversely, microglia can exert anti-inflammatory effects by releasing cytokines that trigger negative feedback mechanisms to resolve inflammation.

In microglia, Siglec-11 is thought to regulate inhibitory signaling pathways(Wang and Neumann, 2010).The immune cell-expressed ITAM motif, activated by spleen tyrosine kinase (SYK), contrasts with the inhibitory ITIM motif, which recruits SHP1 and SHP2 to trigger downstream inhibitory responses. SHP1 and SHP2 phosphatases can deactivate key signaling molecules by removing phosphate groups, counterbalancing SYK-driven activation when ITAM-containing receptors are involved. They can instead regulate immune cell activation positively by being recruited to ITAM-containing receptors.

Transcriptome analysis of macrophage lines revealed that CD33 knockout and knockdown of the CD33 signaling-associated protein tyrosine phosphatase PTPN6 led to constitutive

activation of inflammation-related pathways(Wißfeld et al., 2021). Moreover, CD33 deletion or expression of Exon 2-deleted CD33 resulted in increased phosphorylation of SYK and ERK1/2 (Wißfeld et al., 2021).

	Mouse		Human
Eosinophil	siglec-F		siglec-8, siglec-10 (low)
Mast cell	siglec-F		CD33, siglec-5, -6, -8, -10 (low)
Basophil	siglec-F (low)		CD33, siglec-3, -5, -6, -8
Neutrophil	CD33, siglec-E		siglec-5,-9,-14
Monocyte	siglec-E		CD33, siglec-5,-7,-9,-10,-11,-14
Macrophage	alveolar – siglec-E,-F peritoneal – siglec-E stimulated BMDM – siglec-E		CD33, siglec-5,-11,-15,-16
Dendritic cells	siglec-E siglec-G (mRNA) pDCs - siglec-H		CD33, siglec-7,-9,-10,-15 pDCs –siglec-5,-14
Microglial cell	siglec-F		siglec-11 (-16?)
T cells	activated T cells –siglec-F		siglec-7, -9 (both subset CD8)
NK cell			siglec-7,-9, -10
B cell	siglec-G		siglec-5,-6,-10

Figure 53.CD33-related siglecs expression on leukocytes in human and mouse(Crocker et al., 2012b).

2. Inflammatory cytokines and AD

Alzheimer's disease (AD) is a complex neurodegenerative disorder, with inflammation playing a crucial role throughout its development and progression. In the AD process, activated microglia release pro-inflammatory cytokines such as IL-1β, IL-6, and TNFα (Babić Leko et al., 2020)),which lead to neuron damage and loss, however, the anti-inflammatory

cytokines such as IL-10(Babić Leko et al., 2020) leading to neuronal damage and loss. However, they also produce anti-inflammatory cytokines like IL-10, which help balance these effects and maintain immune homeostasis. In the early stages of AD, microglia are activated to clear the excessive deposition of amyloid beta. Yet, prolonged activation reduces their phagocytic ability, and the resulting increase in pro-inflammatory cytokines exacerbates neuronal damage. During sustained inflammation, pro-inflammatory cytokines, including IL-1β, IL-6, and TNFα, are released by activated microglia. Meanwhile, anti-inflammatory cytokines like IL-10 are also secreted to maintain immune response balance(Su et al., 2016).Single nucleotide polymorphisms (SNPs) in the genes for IL-1, IL-6, IL-10, and TNFα have been associated with AD (Mun et al., 2016).IL-1β, an isoform within the interleukin 1 family, is a major pro-inflammatory cytokine in the brain and plays a role in acute and chronic inflammatory disorders. IL-6, produced by activated cells such as microglia and astrocytes, potentially triggers a cascade of pro-inflammatory cytokines. TNFα, released by immune cells like microglia/macrophages and monocytes, not only promotes inflammation but also triggers additional pro-inflammatory cytokines, amplifying the inflammatory response. Conversely, interleukin 10 (IL-10) acts as an anti-inflammatory cytokine released by macrophages and B cells, preventing excessive inflammatory responses. IL-10 suppresses the production of pro-inflammatory cytokines like IL-1, IL-6, and TNFα, while promoting other anti-inflammatory cytokines such as IL-4. Given AD's classification as a neuroinflammatory disease, studying related cytokines has been an area of significant focus. This project will investigate the influence of CD33 knockout on the expression of several inflammatory cytokines in PMA-differentiated macrophages under an in vitro inflammatory environment established by LPS.

3. Cell migration

Cell migration is a highly complex process regulated by intricate signaling pathways. To date, the MAPK/ERK(Ridley et al., 2003) and PI3K/AKT/mTOR (Chin and Toker, 2009, Iksen et al., 2021) pathways are recognized as key regulators of cell migration. In mammals, the three isoforms of Akt—Akt1 (PKBα), Akt2 (PKBβ), and Akt3 (PKBγ)—are activated by PI3K signaling. The AKT/mTOR pathway regulates migration through both AKT/mTORC1 and AKT/mTORC2 mechanisms. mTORC1 is involved in ribosome biogenesis, protein translation,

and autophagy, while mTORC2 influences actin dynamics(Chadha and Meador-Woodruff, 2020).mTORC1 phosphorylates p70S6 kinase (S6K) and eukaryotic initiation factor 4E-binding protein 1 (4EBP1), promoting protein synthesis (Holroyd and Michie, 2018).

The matrix metalloproteinase (MMP) protein family is regulated by AKT/mTORC1/S6 signaling. MMPs are calcium-dependent, zinc-containing endopeptidases responsible for tissue remodeling and extracellular matrix (ECM) degradation, produced by a wide range of cells including fibroblasts, endothelial cells, macrophages, neutrophils, and lymphocytes (Verma and Hansch, 2007). In some systems, MMPs are crucial for initiating epithelial–mesenchymal transition (EMT) by predominantly degrading ECM components to facilitate migration and invasion(Savagner et al., 2005).EMT involves a shift from epithelial to mesenchymal phenotypes, leading to changes in cell migration and invasion (Yang et al., 2020).mTORC2 regulates migration by modulating the actin cytoskeleton. In mammals, PKC, PKA signaling, and Rac/RhoA are key regulators of mTORC2-mediated migration(Leve et al., 2008).mTORC2 appears to control neutrophil chemotaxis by regulating F-actin polarization and myosin II phosphorylation, with PKC-dependent cAMP production occurring via a RhoA/ROCK-dependent manner (He et al., 2013).

Besides the AKT/mTOR pathway, the MAPK family, including Jun N-terminal kinase (JNK), p38, and ERK, also plays a significant role in regulating migration through distinct mechanisms(Huang et al., 2004).The MAPK signaling mechanisms in migration regulation are complex and remain under active investigation. Hypothesized mechanisms include extracellular stimuli activating JNK via FAK/Src or Rac/MEKK1/MKK4/7/JNK, leading to the activation of molecules such as Paxillin, Spir, and MAP2 to promote neuronal migration. Additionally, p38 signaling is mediated through MLK3/MKK3/6, ultimately influencing actin dynamics to regulate migration(Huang et al., 2004). The RAS/RAF/MEK1/2/ERK pathway also participates in migration signaling, with ERK activation regulating membrane protrusion and adhesion dynamics to induce cell migration(Huang et al., 2004).

Monocyte chemoattractant protein-1 (MCP-1) is a cytokine that plays a critical role in regulating the migration and infiltration of monocytes and macrophages (Deshmane et al.,

2009). It is released by various cell types in response to oxidative stress, cytokine release, and growth factor release (Yadav et al., 2010). In humans, MCP-1 can bind to at least two receptors, and its production can be triggered by interleukin-4 (IL-4), IL-1, TNF-α, bacterial lipopolysaccharides (LPS), and IFN-γ (Yadav et al., 2010). Increasing evidence suggests that MCP-1 influences T-cell immunity by enhancing IL-4 secretion from T cells and plays a role in leukocyte migration (Deshmane et al., 2009). This regulatory function affects monocytes and macrophages, which are major MCP-1 sources(Yadav et al., 2010).Moreover, mCRP has been shown to increase MCP-1 secretion, leading to pro-inflammatory activity through a p38 MAPK-dependent mechanism(Khreiss et al., 2004).Several studies have demonstrated that CCL2, also known as monocyte chemotactic protein-1 (MCP-1), is induced following various central nervous system (CNS) insults, and its receptor, CCR2, is critical for the attraction and infiltration of mononuclear phagocytes into the brain (Lee and Landreth, 2010, Babcock et al., 2003).

4. Aims and objectives

4.1 Aims

This chapter aims to validate the effects of CD33 knockout on the production of cytokines associated with inflammation and cell movement.

4.2 Objectives

1.Investigate the impact of CD33 knockout on cytokine production.

2.Assess the effect of CD33 knockout on cell movement in the presence and absence of the Alzheimer's disease pathological hallmark, amyloid beta$_{42}$ plaques.

3.Evaluate the effect of CD33 knockout on cell movement in the presence and absence of lipopolysaccharide (LPS).

5. Results

5.1 The effect of CD33 knockout on mediator production

5.1.1 CD33 knockout promotes transcription of IL-1 receptor antagonist (IL-RN) and pro-inflammatory cytokines (IL-1 beta, TNF), however, decreases anti-inflammatory cytokine of IL-10

To investigate the effect of CD33 knockout on inflammatory responses, total RNA was isolated from CD33WT-U937 macrophages and CD33KO-U937 macrophages for RNA deep sequencing. The analysis confirmed a 7-fold increase in IL-1 beta transcription ($P<0.001$) and a 2-fold increase in TNF transcription ($P<0.001$), alongside a 50% decrease in the anti-inflammatory cytokine IL-10 ($P<0.05$) and a 3-fold increase in IL-1 receptor antagonist ($P<0.05$) in CD33KO-U937 macrophages compared to CD33WT-U937 macrophages (**Figure 54A**). These findings were further validated by RT-qPCR, which showed a 4-fold increase in IL-1 receptor antagonist, an 8-fold increase in IL-1 beta, and a 2.5-fold increase in TNFα in CD33KO-U937 macrophages compared to CD33WT-U937 macrophages ($P<0.05$). However, qRT-PCR did not reveal a significant decrease in IL-10 expression due to CD33 knockout (**Figure 54B**).
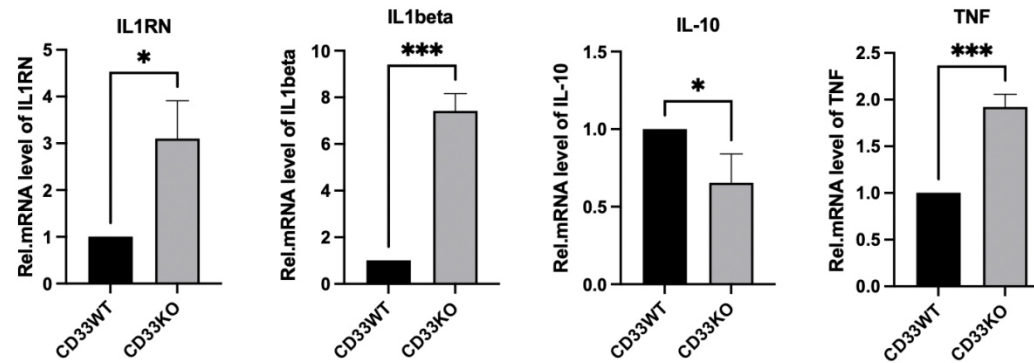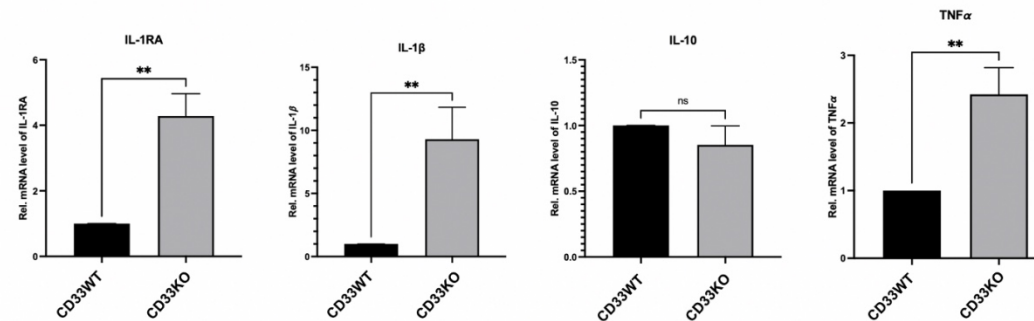
Figure 54. The effect of CD33 knockout on inflammatory mediator expression level verified by RT-qPCR and RNA deep sequencing. Specific inflammation-related genes of IL-1RN, IL-beta, IL-10 and TNF (tumour necrosis factor) were selected from RNA deep sequencing data(A) to be verified by RT-qPCR(B). IL-1RN, IL-beta indicate a 3-fold increase,7-fold increase in RNA sequencing analysis in corresponding to a 4-fold increase and 8-fold increase in RT-q PCR analysis, respectively; TNF(tumour necrosis factor) showed double upregulation in RNA sequencing analysis(A) compared to a 2.5-fold increase in RT-q PCR analysis(B); IL-10 shown a slight decrease of 0.5-fold in RNA sequencing analysis(A), and no significant decrease in IL-10 was detected by RT-q PCR analysis(B). Data presented as Mean ± SD – t-test (p* = < 0.05 p **= <0.01, p*** = < 0.001, p**** <0.0001. (n=3).

5.1.2 CD33 knockout induces chemokine production associated with cell movement

Other key mediators involved in inflammation, such as chemokines from the C-C Chemokine Family—including CCL2, CCL3, CCL4, CCL7, CCL8, CCL18, and CCL20—showed increased mRNA transcription levels ranging from 2-fold to 40-fold (P<0.001 to P<0.05) in CD33KO-U937 macrophages compared to CD33WT-U937 macrophages **(Figure 55)**. Additionally, a broad array of genes associated with mononuclear migration exhibited elevated transcription levels following CD33 knockout (**Figure 56**).
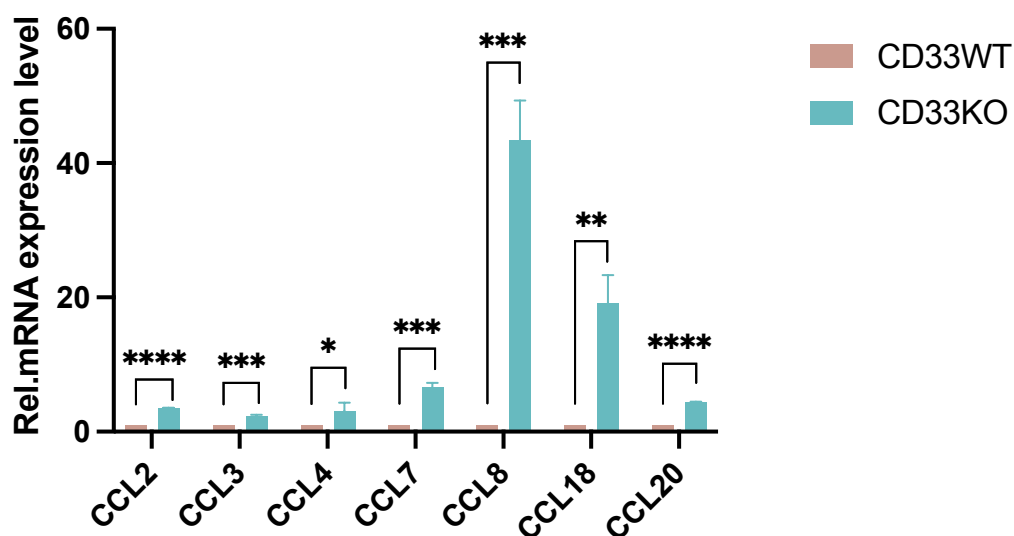
Figure 55. The effect of CD33 knockout on chemokines transcription level RNA deep sequencing.CD33 knockout resulted in the upregulation of several chemokines involved in recruiting and activating immune cells in inflammatory responses. The mRNA levels of CCL2, CCL7, CCL18 and CCL8 were significantly increased, showing fold changes of 5-fold (p<0.0001), 10-fold (p<0.001), 20-fold (p<0.01) and 40-fold (p<0.001), respectively. Additionally, CCL3, CCL4, and CCL20 also exhibited increased expression, with fold changes of 2-fold (p<0.001), 3-fold (p<0.05), and 4-fold (p<0.0001), respectively. Data presented as Mean ± SD – t-test (p* = < 0.05 p **= <0.01, p*** = < 0.001, p**** <0.0001. (n=3).
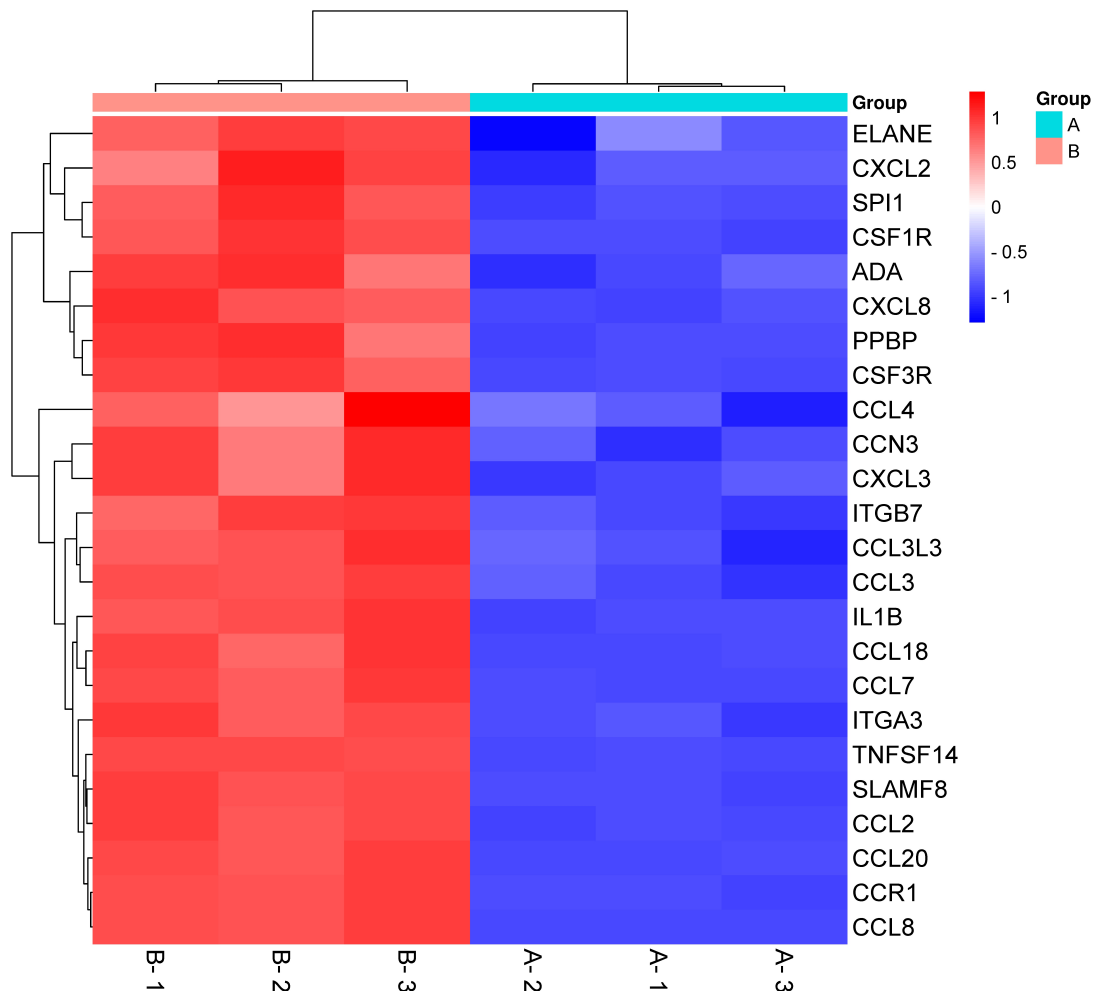
Figure 56. Gene expression of mononuclear migration-related genes. Heatmap illustrates mononuclear migration-related genes upregulated in CD33KO-U937 derived macrophage compared to WT-U937 derived macrophage, confirmed by RNA deep sequencing. Color blue indicates baseline expression of genes expressed in WT-U937 derived macrophage; Color red, represents upregulation in the expression of genes expressed in CD33KO-U937 derived macrophage. Group A represents CD33WT-U937 macrophage, and Group B represents CD33KO-U937 macrophage. (P value <0.05, fold change>2 n=3 per genotype).

5.2 Validation of effect of CD33 knockout on cell movement in PMA differentiated-U937 macrophages

The effect of CD33 knockout on cell movement was analyzed in CD33KO-U937 macrophages compared to CD33WT-U937 macrophages using single-cell tracking assays with holominitor microscopy over a 24-hour observation period. CD33WT-U937 and CD33KO-U937 monocytes were seeded into 24-well plates at appropriate densities and fully differentiated into macrophages, as described in section 2.3. After differentiation, the macrophages were replenished with fresh RPMI-1640 complete growth medium and prepared for single-cell tracking analysis, following the method described in section 2.9.

The movement pathways of CD33WT-U937 and CD33KO-U937 macrophages were visualized in rose plots (**Figure 57**). CD33KO-U937 macrophages exhibited a slight increase in motility speed, from an average of 21 µm/h to 23 µm/h (P<0.0001), as shown in Figure 60. This increased motility speed due to CD33 knockout corresponded to enhanced cell movement paths (**Figure 57**). Specifically, CD33WT-U937 macrophages moved within an X-axis range of -212.9 µm to +130 µm, and a Y-axis range of -130.0 µm to +130.0 µm. In contrast, CD33KO-U937 macrophages exhibited a broader movement range, with X-axis limits of -253.2 µm to +200.0 µm, and Y-axis limits of -150.0 µm to +170 µm.

To further investigate, cells were stimulated with 100 ng/mL LPS and pre-aggregated amyloid beta$_{42}$ for 24 hours. As shown in Figure 60, LPS reduced the motility speed of CD33KO-U937 macrophages from an average of 23 µm/h to 18 µm/h (P<0.001). However, this decreased speed was accompanied by a larger movement range in response to LPS, as depicted in **Figures 58**. Pre-aggregated amyloid beta$_{42}$ did not affect the motility speed of either CD33WT-U937 or CD33KO-U937 macrophages as depicted in **Figure 59** and **Figure 60**.
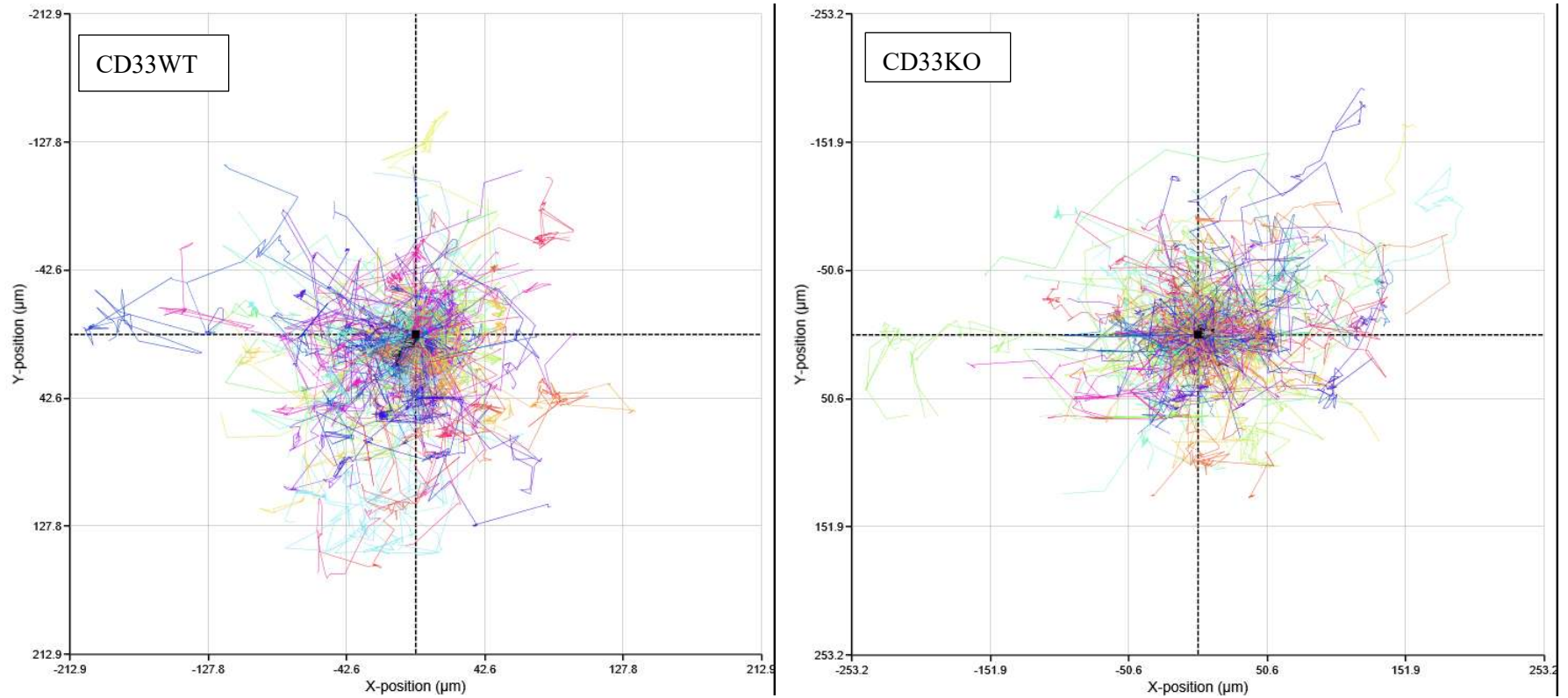
Figure 57. Visualization the effect of CD33 knock out on cell movement validated by holomonitor.CD33WT-U937 monocytes and CD33KO-U937 monocytes were fully differentiated into macrophages by stimulation of 50ng/ml of PMA. Rose plot of CD33WT-macrophage and CD33KO macrophage. Rose plots displayed single cell 2D movement trajectories from 200 cells chosen at random each field. Cell movement pathways are displayed on X and Y axis by means of logarithmic scale. Plots represents the cell motility pathway for 24 hours.
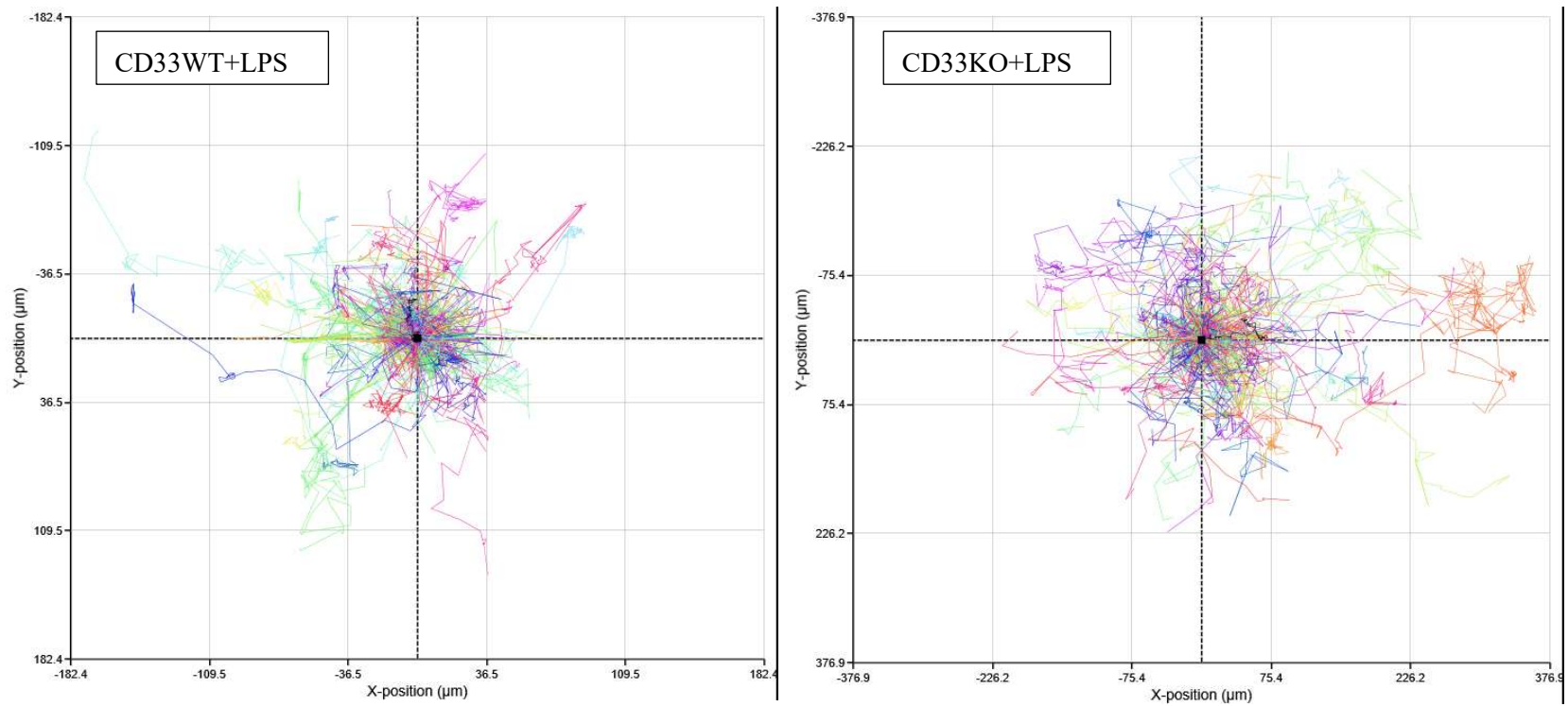
Figure 58. Visualization of the effect of LPS on cell movement pathways in the presence and absence of CD33.CD33WT-U937 monocytes and CD33KO-U937 monocytes were fully differentiated into macrophages by stimulation of 50ng/ml of PMA.Cells were further treated with 100ng/ml LPS in serum (+) condition for 24 hours. Rose plots displayed single-cell 2D movement trajectories from 200 cells chosen at random in each field of CD33WT-macrophage and CD33KO macrophage. Cell movement pathways are displayed on X and Y axis by means of a logarithmic scale.
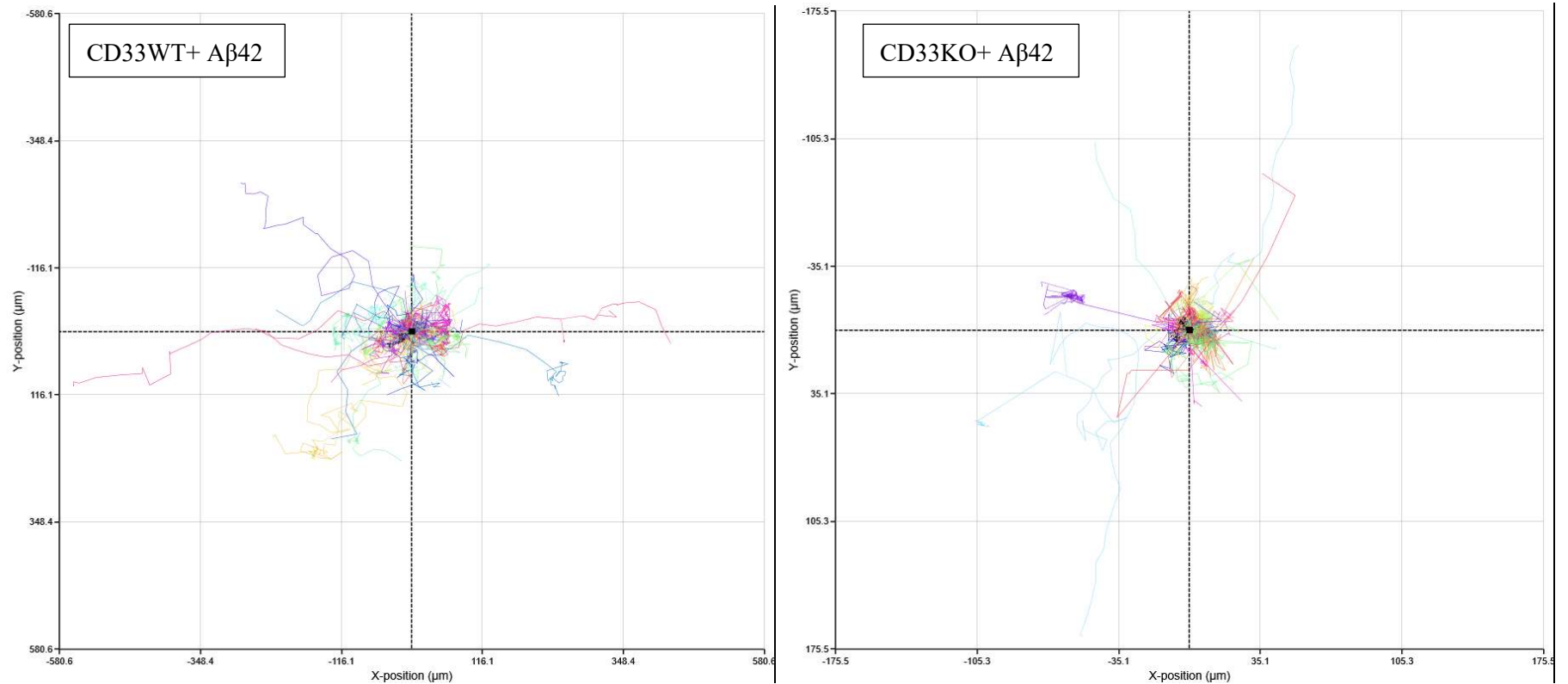
Figure 59. Visualization of the effect of pre-aggregated Aβ42 on cell movement pathways in the presence and absence of CD33.CD33WT-U937 monocytes and CD33KO-U937 monocytes were fully differentiated into macrophages by stimulation of 50ng/ml of PMA. cells were further treated with 2ug/ml of Aβ42 deposition in serum (+) condition for 24 hours. Rose plots displayed single-cell 2D movement trajectories from 100 cells chosen at random in each field of CD33WT-macrophage and CD33KO macrophage. Cell movement pathways are displayed on X and Y axis by means of a logarithmic scale.

164
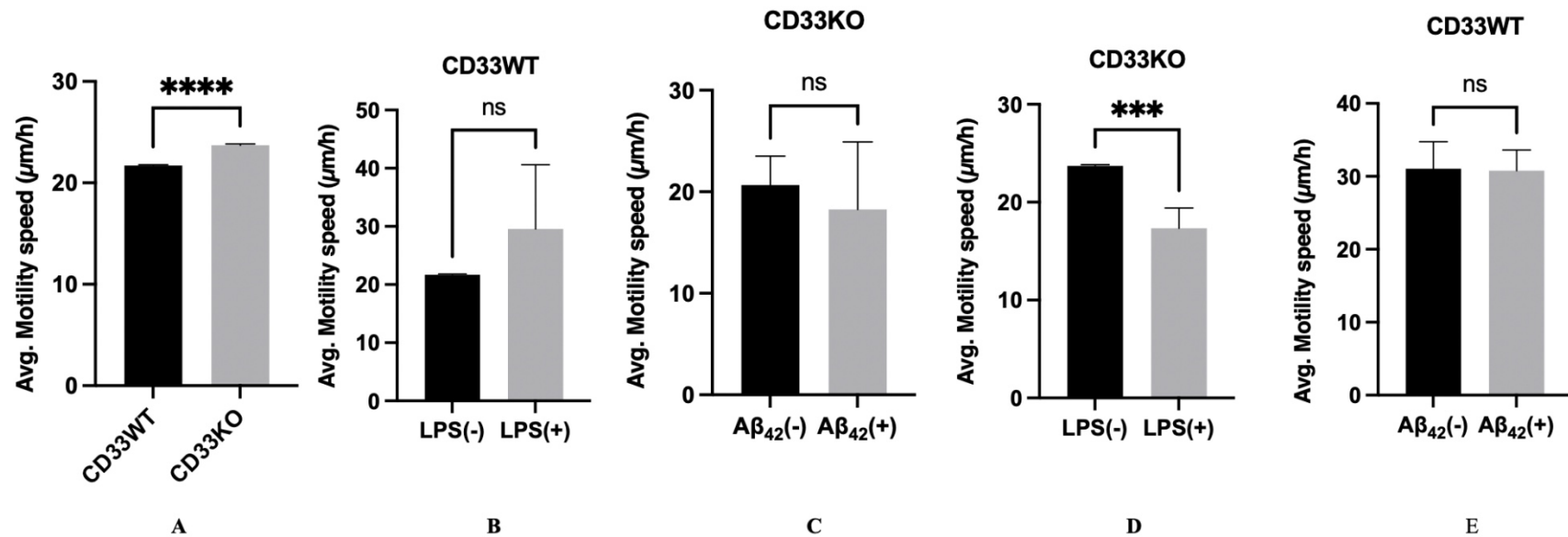
Figure 60. Verification of motility speed in the presence and absence of LPS or pre-aggregated Aβ42 after CD33 knockout. A: Bar chart indicating a slight increase in average motility speed (um/h) due to CD33 knockout. Motility speed was inhibited when CD33KO-U937 macrophages were exposed to LPS (D); however, LPS did not significantly change the motility speed of CD33WT-U937 macrophages (B). The motility speed of both CD33WT-U937 macrophages and CD33KO-U937 macrophages were not influenced by treatment with Aβ42 (C, E). Data presented as Mean ± SD – t-test (p* = < 0.05 p **= <0.01, p*** = < 0.001, p**** <0.0001(n=6).

6. Discussion

Alzheimer's disease (AD) is a complex neurodegenerative disorder characterized by chronic neuroinflammation throughout its stages. Genome-wide association studies (GWAS) have identified CD33 as a key gene associated with the clearance of AD hallmarks, including extracellular amyloid beta (Aβ) deposits(Ransohoff and El Khoury, 2015, Gallardo and Holtzman, 2017).Previous chapters have explored the effects of CD33 knockout on Aβ clearance through phagocytosis and autophagy. This chapter focuses on the impact of CD33 deletion on cytokine production and cell movement, crucial factors for macrophage activation in immune responses and phagocytosis.

Based on previous results, CD33 knockout in CD33KO-U937 macrophages enhanced phagocytic capability compared to CD33WT-U937 macrophages. Cell migration is essential for effective phagocytosis, enabling cells to reach target cargo. A critical component of this process is cell polarization, which is vital for migration. Polarization involves distinct molecular activities at the leading and trailing edges of a moving cell, facilitating directional movement(Ridley et al., 2003). CD33KO-U937 macrophages showed a higher polarization propensity and a motility speed increase to 23 μm/h compared to 21 μm/h in CD33WT-U937 macrophages, as revealed by Holomonitor assays. Other study demonstrated that the full-length isoform of CD33 inhibits migration, proliferation, and phagocytosis in human cells, whereas the short isoform enhances these functions(Butler et al., 2021).Microscope observations suggested that CD33KO-U937 cells proliferated faster and remained viable longer than CD33WT-U937 cells, although further proliferation assays are needed to confirm this finding.

RNA sequencing analysis indicated increased expression of specific Monocyte Chemoattractant Proteins (MCPs) following CD33 deletion. CCL2/MCP-1, CCL7/MCP-3, and CCL8/MCP-3 increased by 3-fold, 5-fold, and over 40-fold, respectively, in CD33KO-U937 macrophages. As part of the C-C chemokine subfamily, MCPs are crucial for immune-cell migration, attracting monocytes and macrophages to inflammation or tissue damage sites. CCL2 and its receptor CCR2 facilitate mononuclear phagocyte infiltration into the brain (Lee

and Landreth, 2010, Babcock et al., 2003).MCP-1 levels in plasma and cerebrospinal fluid are potential biomarkers for AD-related inflammation, with CCL2 often upregulated in AD patients (Pola et al., 2004). Gene variations in MCP-1, such as the -2518 A/G polymorphism, are strongly linked to AD (Pola et al., 2004)previous study found that silencing CCL8 reduces OPN and cyclinD1 expression, downregulating AKT and ERK1/2 phosphorylation(Dai et al., 2020).In this study, SPP1 (encoding OPN), which influences migration, inflammation, and tissue repair (Iida et al., 2017), showed a nearly 2-fold increase in mRNA expression due to CD33 knockout, alongside a 50% decrease in CCND1 (cyclinD1) expression. This suggests that CD33 knockout in PMA-differentiated macrophages significantly induces CCL8/MCP-2 and SPP1 expression. While CCL8 upregulation seems to promote migration, it also potentially enhances migration via SPP1 induction. However, it is not clear if OPN increases due to elevated CCL8 or direct CD33 knockout effects.Previous studies reported CCL2 enhances migration through the Smad3-dependent MEK-ERK1/2 pathway and promotes cell survival via a Smad3-independent MEK-ERK1/2 mechanism(Fang et al., 2012). Additionally, ERK1/2 and p38 play crucial roles in increasing CCL1 and CCL8 expression (Hintzen et al., 2008).

Another cytokine subgroup within the C-C chemokine family is the macrophage inflammatory protein family (MIPs), which plays a crucial role in regulating cell migration, particularly in immune responses and inflammation. RNA deep sequencing revealed significant upregulation of MIPs in CD33KO-U937 macrophages: a 4-fold increase in CCL20, a 3-fold increase in CCL4, and a 2-fold increase in both CCL3 and CXCL2. As chemokines, MIPs attract immune cells by binding to specific chemokine receptors on immune cells, thereby activating migration-related signaling pathways that facilitate cell migration and immune-cell interactions.Chronic inflammation persists throughout all stages of AD as continuous activation of microglia releases pro-inflammatory cytokines, such as IL-1, IL-6, and TNF-α, triggering inflammatory cascades and leading to neuronal damage and loss (Perry et al., 2010, Streit et al., 2004, Jiang et al., 2012). Early studies indicate that Aβ fibrils can initiate inflammatory processes by binding to and activating microglia(Heneka et al., 2015, Mosher and Wyss-Coray, 2014) and peripheral monocytes(Fiala et al., 2005, Saresella et al., 2014). Microglia and macrophages are critical in AD pathology. Microglia, as the

predominant immune cells in the CNS, directly interact with Aβ plaques and tau pathology, whereas peripheral macrophages contribute by migrating to Aβ plaque sites and engulfing soluble Aβ in the periphery. However, the activation of these immune cells acts as a double-edged sword, as prolonged activation during chronic inflammation can exacerbate neuronal damage through the production of pro-inflammatory cytokines.

CD33, primarily expressed on leukocyte subsets, is associated with immune responses and inflammation, with high expression levels identified in peripheral monocytes of AD patients. Throughout AD progression, macrophages and microglia shift between different activation states, generally classified as pro-inflammatory M1 and anti-inflammatory M2 phenotypes. In systemic immune responses, immune cells are recruited to sites of insult via pro-inflammatory signaling pathways(Newcombe et al., 2018). Activated pro-inflammatory cascades produce various molecules that mediate inflammation by recruiting additional immune cells or inducing phagocytosis to clear pathogens and debris. Key mediators include transcription factors (e.g., STAT3), cytokines (e.g., TNF-α, IFN-γ, IL-1β, IL-6, IL-18), chemokines (e.g., CCL2, CCL3, CXCL8), complement components (e.g., C5), enzymes, and reactive oxygen species (ROS) (Newcombe et al., 2018, Wang et al., 2015). As inflammation progresses, the M1 phenotype shifts towards the anti-inflammatory M2 phenotype via anti-inflammatory signaling pathways, leading to reduced production of pro-inflammatory mediators and increased expression of anti-inflammatory mediators such as IL-4, IL-10, and IL-13 (Czeh et al., 2011, Newcombe et al., 2018). While acute inflammatory events resolve quickly with inflammation levels returning to baseline, chronic inflammation as seen in AD lacks resolution(Newcombe et al., 2018).In the brains of AD patients, chronic inflammation causes microglia and macrophages to shift from a neuroprotective M2 phenotype to a more classically activated phenotype in later stages, contributing substantially to progressive neurodegeneration(Wang et al., 2015).

In CD33KO-U937 macrophages, RNA deep sequencing revealed notable changes in cytokine expression levels: pro-inflammatory mediators TNF alpha, IL-1β, and CXCL8 (IL-8) were upregulated by approximately 2-fold, 7-fold, and 4-fold, respectively, while the anti-inflammatory mediator IL-10 showed a 2-fold decrease compared to CD33WT-U937

macrophages. Previous studies in AD mouse models indicated elevated levels of M1 markers such as IL-1β, TNF-α, and IL-6, alongside increases in the M2 marker IL-10 compared to age-matched wild-type controls(Wang et al., 2015). RT-PCR further validated these findings, showing a 9-fold increase in IL-1β and over a 2-fold increase in TNF alpha mRNA in CD33KO-U937 macrophages, though IL-10 mRNA levels did not significantly change. Earlier research has documented elevated transcripts of pro-inflammatory markers TNF and IL-1β in AD(Wang et al., 2010, Klein et al., 2010). IL-1β, a potent pro-inflammatory cytokine, plays a critical role in initiating and amplifying pro-inflammatory cascades by inducing other cytokines such as TNF alpha. Notably, CD163, a biological marker for the M2 phenotype, decreased 10-fold following CD33 knockout. Although RNA deep sequencing indicated a halved expression of IL-10, RT-qPCR did not show a significant decrease, suggesting that CD33KO-U937 macrophages may adopt an M1-like phenotype.

Conversely, IL-1 receptor antagonist (IL-1Ra), which neutralizes IL-1β signaling, showed a 3-fold increase in expression according to RNA deep sequencing and a 4-fold increase as confirmed by RT-qPCR. Previous in vivo and in vitro evidence has highlighted increased synthesis of pro-inflammatory cytokines—including IL-1β, IL-6, IL-18, TNF-α, and IFN-γ—in AD brains(Sastre et al., 2006, Ojala et al., 2009, Abbas et al., 2002, Benzing et al., 1999). Chronic Aβ accumulation in brains drives neuroinflammation by activating microglia, a primary source of pro-inflammatory cytokines in AD(Prinz et al., 2011).The interaction of Aβ with microglial cell surfaces induces pro-inflammatory gene expression, elevating cytokines such as TNF-α, IL-1β, IL-6, and IL-18, which contribute to tau hyperphosphorylation and neuronal loss(von Bernhardi et al., 2010). Chronic activation of microglia and macrophages by extracellular Aβ plaques exacerbates AD pathology, resulting in sustained neuroinflammation. Dysfunctional and imbalanced production of pro-inflammatory and anti-inflammatory cytokines may be detrimental to AD brains.

IL-1β is a potent pro-inflammatory mediator in the brain and plays a crucial role in the progression of AD. Early studies have shown that blocking or neutralizing IL-1β activity can potentially prevent cognitive deficits and reduce tau pathology, S100 synthesis, and fibrillar amyloid beta (fAβ) in AD mouse models (Kitazawa et al., 2011).fAβ can activate microglia,

leading to increased production of pro-inflammatory cytokines and neurotoxic secretory products such as IL-1β and reactive oxygen species(ROS)(Heneka et al., 2010).As mentioned in previous chapters, the mRNA expression of CYBB (also known as NOX2), a key component of the NADPH oxidase complex involved in ROS production, showed a 300-fold increase in CD33KO-U937 macrophages. In an early study, Parajuli et al. demonstrated that soluble oligomeric amyloid beta (oAβ) upregulates the maturation of pro-IL-1β to IL-1β in microglia through ROS-dependent activation of the NLRP3 inflammasome(Parajuli et al., 2013). Evidence suggests that excessive IL-1β can impair microglial Aβ clearance functions (Heneka et al., 2010)) and increase the permeability of the blood-brain barrier (BBB), promoting Aβ deposition in the brain (Wang et al., 2014). However, other studies have highlighted the potential benefits of elevated IL-1β in limiting AD pathology. High levels of IL-1β may reduce Aβ-related pathology by promoting microglia-dependent plaque degradation in vitro and in vivo(Tachida et al., 2008, Shaftel et al., 2007, Ghosh et al., 2013). Overall, while CD33 knockout enhances macrophage phagocytic capability and upregulates several beneficial phagocytosis-related genes, such as MSR1, it appears to shift macrophages toward a pro-inflammatory phenotype. This shift may lead to sustained overexpression of pro-inflammatory mediators, which can exacerbate AD pathology.

Chapter 6 Discussion and Future Work

1.Discussion

Alzheimer's disease (AD) is the most common form of dementia(Ballard et al., 2011),with late-onset AD (LOAD) accounting for approximately 90% of all cases. Unlike familial AD, LOAD does not follow a Mendelian inheritance pattern but involves multiple risk genes identified through genome-wide association studies (GWAS) (Griciuc et al., 2013). Among these, CD33 has gained considerable attention due to its association with LOAD susceptibility and its strong negative correlation with the phagocytic capabilities of microglia and macrophages (Miles et al., 2019) (Andrews et al., 2020, Li et al., 2015). These cells are crucial for clearing amyloid-beta (Aβ) plaques, a hallmark of AD pathology. Macrophages and microglia act as main phagocytes, responsible for clearing the excessive Aβ plaques, composed of $A\beta_{40}$ and $A\beta_{42}$, as well as tau tangles, which are key pathological features of AD(Ballard et al., 2011). The chronic accumulation of Aβ plaques triggers neuroinflammation throughout all stages of AD (**Figure 61**). During this process, the release of pro-inflammatory cytokines (such as IL-1β and TNFα) and anti-inflammatory cytokines (such as IL-10) by microglia, macrophages, and astrocytes plays a vital role in disrupting homeostasis. CD33, a member of the Siglec family and identified as a significant AD risk gene by GWAS, not only inhibits phagocytosis but also plays an important role in modulating inflammatory responses (Griciuc et al., 2020, Wißfeld et al., 2021 ,Claude et al., 2013). The aim of this project is to investigate how CD33 signaling influences the clearance of Aβplaques in human macrophages. Instead of using a mouse model, which is structurally different from humans(Bhattacherjee et al., 2021, Butler et al., 2021).CRISPR/Cas9 gene-editing technology was performed to knock out CD33 in U937 human monocytes as a cell model line. Both CD33 wild-type (CD33WT-U937) and CD33 knockout (CD33KO-U937) monocytes were differentiated into macrophages with PMA stimulation. Total RNA from these PMA-differentiated macrophages underwent RNA deep sequencing followed by bioinformatics analysis. The deletion of CD33 altered the transcription of genes involved in a broad range of cellular functions, including phagocytosis, autophagy, cell movement, and cytokine synthesis, which were subsequently validated at mRNA and protein levels using RT-qPCR and Western blot assays. In this study, we investigated the impact of CD33 deletion on macrophages, particularly focusing on the clearance of amyloid beta(Aβ)

through phagocytosis, autophagy, and LC3-associated phagocytosis. While previous studies have highlighted the enhanced phagocytic capability following CD33 knockout, the specific signaling pathways driving this process remain largely unexplored.

Our findings demonstrated that CD33 knockout led to significant inhibition of JAK/STAT3 signaling at both the RNA and protein levels in CD33KO macrophages, coinciding with increased expression of the autophagy marker LC3b. Consistent with earlier studies, elevated STAT3 levels have been shown to suppress autophagy both in vitro and in vivo (Shen et al., 2012).This effect may be attributed to the loss of the ITIM motif, which serves as a docking site for SHP2, facilitating JAK2 dephosphorylation and promoting STAT3 activity(Zehender et al., 2018). As a vital cellular process for nutrient recycling and energy regeneration(He and Klionsky, 2009).Autophagy is regulated by complex signaling pathways, including PI3K/AKT/mTOR, which are detailed in the introduction. Our hypothesis suggests that CD33 deletion may lead to decreased expression of PDK1 and AKT, thereby suppressing these pathways to induce autophagy. The interplay between the JAK/STAT3 and PI3K/AKT/mTOR pathways may further contribute to autophagy induction, as JAK could promote mTOR activation via PI3K/AKT, ultimately inhibiting autophagy(Arunsi et al., 2022).In addition to autophagy, phagocytosis was significantly increased after CD33 deletion. Aβ deposits interacting with CD33 were previously shown to activate the inhibitory ITIM motif via their salic residues(Alphey et al., 2003, Taylor et al., 1999, May et al., 1998), reducing phagocytic efficiency(Salminen and Kaarniranta, 2009) (Szumanska et al., 1987).In our study, CD33KO macrophages exhibited increased expression of MSR1, a pattern recognition receptor primarily expressed by microglia in the brain (Ishiguro et al., 2001) and elevated lysosomal activity marker LAMP2 at both RNA and protein levels, indicating enhanced degradation capabilities. Endocytosis of β-amyloid and other molecules mediated by MSR1 has been confirmed in other studies (Husemann et al., 2002, Cheng et al., 2019, Li et al., 2021a). In this study, when treated with pre-aggregated Aβ, CD33KO macrophages exhibited an upregulated phagocytic capability to engulf Aβ compared to wild-type macrophages. Following the increased engulfment, the upregulation of LAMP2 expression indicates that degradation activity in CD33KO macrophages was also induced. In AD, activated MSR1 facilitates ligand internalization and

engages signaling pathways MSR1/PI3K-Akt/NF-κB pathway (Tian et al., 2022, Coller and Paulnock, 2001).The changes in the expression of MSR1 and AKT resulting from CD33 deletion may indicate a crosstalk that contributes to the increased autophagy observed in CD33KO macrophages. The research revealed that in the absence of CD33, macrophages may undergo a complete process of phagocytosis and autophagy, supported by changes in various degradation pathways, including the JAK/STAT3 signaling pathway and the PI3K/AKT/mTOR signaling pathway. Although the precise degradation stages were not directly monitored in this study, the increased LAMP2 expression strongly supports this enhanced activity. In the meanwhile, morphological changes expressed in CD33KO macrophages, including more polarization and increased size, together with the increased motility (including an increased expression of chemokines such as CCL2, CCL3, and CCL7) potentially indicated the enhanced engulfment and degradation capabilities in CD33KO macrophages.Other persuasive evidence in the study to support the upregulated phagocytosis found in the study are the upregulating RNA expression in CD33KO macrophages of substrate receptors like complement receptors such as C3, and Fcγ receptors, which in assists in facilitating immune recognition and phagocytosis(Li et al., 2007a, Trial et al., 2016), and in recruiting autophagy(Huang et al., 2009) by serving as opsonins to coat target particles (Freeman and Grinstein, 2014, Uribe-Querol and Rosales, 2020).

However, CD33 knockout presented a double-edged sword. Albeit the deletion enhanced phagocytic capability, autophagy, lysosome activation, and cell movement, it potentially increases the production of pro-inflammatory cytokines like IL-1β and TNFα, while decreasing anti-inflammatory markers such as IL-10 and CD163. The reduced expression of IL-10 corresponds with the diminished expression of STAT3 in CD33KO macrophages. A previous study by Takeda et al. (Takeda et al., 1999) indicated that the suppressive effects of IL-10 on the production of pro-inflammatory cytokines are entirely absent in macrophages and neutrophils deficient in STAT3. More importantly, the high expression of MSR1 in CD33KO macrophages may indicate an increased capability of macrophages to engage in inflammatory activities. MSR1 is crucial for eliminating foreign pathogens (Wang et al., 2021) and can cooperate with other receptors, such as TLR4 or TLR2, to promote the

phagocytosis of the bacterium(Amiel et al., 2009) and to induce production of inflammatory cytokines via NF-κB signaling by interacting with TLR4(Yu et al., 2012). Although IL-1 antagonism was elevated in CD33KO-U937 macrophages, which may partially neutralize the pro-inflammatory effects, however the overall consequence of CD33 knockout seemed to be a shift toward a more pro-inflammatory M1-like phenotype.

2.Limitations and future work

Acquiring a detailed understanding of CD33 is crucial for developing new therapies for Alzheimer's disease. In this project, we demonstrated that low expression of CD33 in human monocyte-derived macrophages can induce increased phagocytosis (including LC3-phagocytosis) and autophagy activities, along with changes in the gene expression of key factors related to these induced biological activities. Human U937 monocytes were used to create a CD33-knockout macrophage model to study the effects of CD33 knockout on autophagy, phagocytosis, and inflammation. The absence of CD33 led to increased expression of the autophagy flux marker LC3b, phagocytosis receptors such as MSR1, the Fc gamma receptor family, and other mediators, including the lysosomal marker LAMP2, at both transcriptional and/or protein levels. This confirmed the induced effects of autophagy and phagocytosis, as well as changes in some key factors related to their associated signaling pathways. However, it is clear that there are key limitations in this project, and these issues require further exploration.

Firstly, all results reported in this study are based on a U937-PMA-differentiated macrophage model. Although this cell line provides strong evidence that CD33 knockout increases phagocytosis and autophagy related to the Alzheimer's disease hallmark, amyloid beta42 plaques, it is crucial to note that there are significant biological and functional differences when compared to human microglia. To further investigate novel therapies for treating Alzheimer's disease, future studies are necessary to replicate this work using CD33KO-iPSC-derived microglia. This approach would complement the use of monocytes in studying this disease.

We partially demonstrated an induced expression of pSTAT3, indicating a change in the JAK/STAT3 signaling pathway. However, we have not yet determined the key signaling mediators, such as PI3K, PDK1, and AKT, at the protein level. These factors are known to be vital in regulating phagocytosis and autophagy. Therefore, additional research is needed in the future to gain a deeper understanding of the relationship between the changes in these factors and CD33 deletion. This would involve investigating how CD33 deletion influences the JAK/STAT and PI3K/AKT signaling pathways.

In this study, strong evidence suggests that CD33 knockout induces MSR1, LAMP2, and LC3b, accompanied by increased phagocytosis and autophagy activities. However, to obtain more convincing results regarding the degradation of engulfed cargo, particularly amyloid beta$_{42}$ plaques, a substantial amount of research is needed to clarify the degradation process. This could be accomplished through ELISA assays or Western blot analysis to test for degraded molecules of amyloid beta plaques.

Furthermore, the deletion of CD33 in monocyte-derived macrophages exhibits a pro-inflammatory effect, which may result from the complete knockout of the outer IgV and IgC domains. This full-length deletion has shown a pro-inflammatory effect; even though RNA deep sequencing indicated an increase in some anti-inflammatory cytokines in CD33KO macrophages compared to CD33WT macrophages, the CD33KO macrophages still displayed an induced functional and biological phenotype characteristic of M1-like macrophages. These changes were accompanied by increased phagocytosis and autophagy, but the upregulation of pro-inflammatory cytokine release is not a favorable phenomenon in Alzheimer's disease pathology.Therefore, future work should further explore this by using CD33KO short isoform microglia, which have also been reported to exhibit a gain-of-function in phagocytosis(Butler et al., 2021).The CD33 short isoform is also naturally expressed in human microglia(Bhattacherjee et al., 2019)).Consequently, future efforts for this project will involve using CRISPR-Cas9 to establish CD33-short-isoform iPSC-derived microglia and verify their functional activities and biological features.

Overall, these approaches may shed valuable insights into the pathophysiological mechanisms underlying the absence of CD33 in Alzheimer's disease and potentially identify novel therapeutic targets.
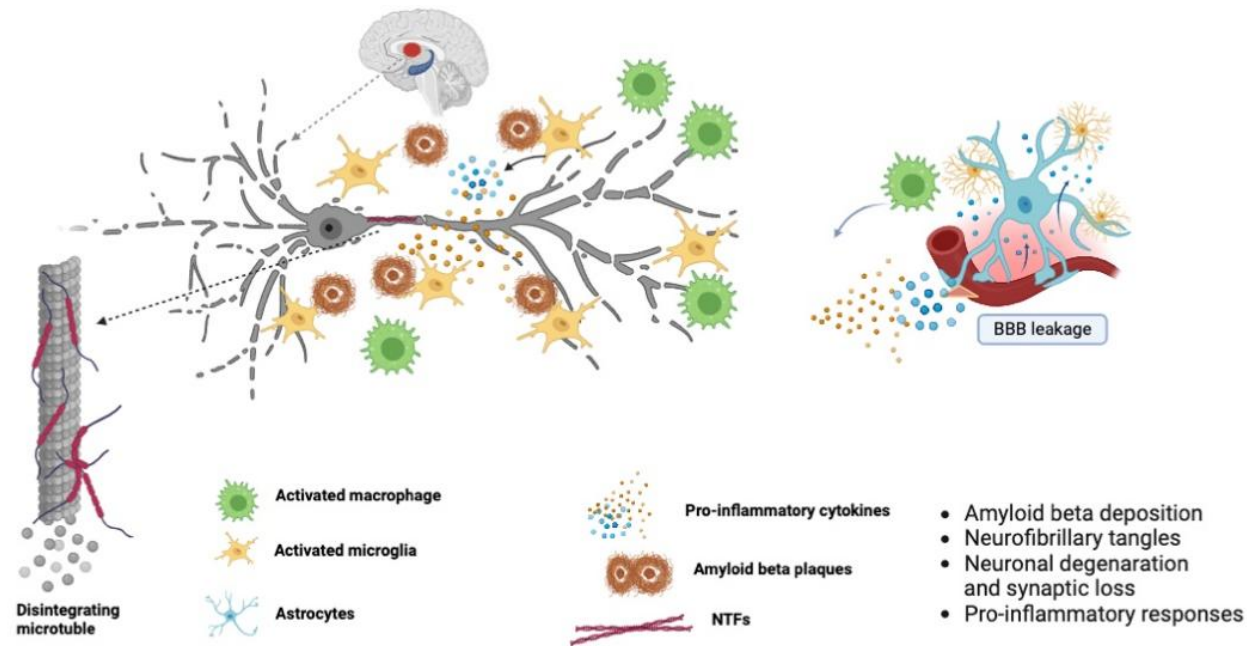
Figure 61. Pathology of Alzheimer's disease. AD is a chronic neurodegenerative disease characterized by a wide range of pathological changes in the brain. The excessive amyloid beta plaques consisting of $A\beta_{40}$ and $A\beta_{42}$, as well as neurofibrillary tangles composed of hyperphosphorylated tau protein, are AD hallmarks that lead to neuronal death and the activation of inflammatory responses. This persistent presence of risk factors contributes to the progression of neuronal damage and neuroinflammation, resulting in the acceleration of pathological changes spreading from one region to other regions. Ultimately, this leads to widespread brain damage with multiple symptoms, such as cognitive impairment.

3.Conclusion

The key findings of the study include upregulated phagocytosis and autophagy activities resulting from CD33 knockout, as well as significant effects on several signaling pathways that regulate these activities. Increased expression of MSR1, LC3b, and LAMP2 indicates the activation of engulfment and degradation processes due to CD33 knockout. Changes in the expression of JAK2, JAK3, STAT3, PDK1, and AKT1 reveal the underlying mechanisms of the molecular cascades involved in phagocytosis and autophagy signaling that are influenced by the deletion of CD33. Furthermore, this study demonstrates that these cellular processes are interconnected, functioning as a network to regulate cellular activities especially phagocytosis and autophagy. The upregulated clearance of amyloid beta caused by CD33 knockout could lead to the discovery of more effective therapeutic modalities for eliminating the amyloid beta plaque burden, providing a promising treatment for patients with Alzheimer's disease in the future.

Chapter 7 References

AL-BARI, M. A. A. & XU, P. 2020. Molecular regulation of autophagy machinery by mTOR-dependent and -independent pathways. *Ann N Y Acad Sci*, 1467, 3-20.

AMIEL, E., ALONSO, A., UEMATSU, S., AKIRA, S., POYNTER, M. E. & BERWIN, B. 2009. Pivotal Advance: Toll-like receptor regulation of scavenger receptor-A-mediated phagocytosis. *J Leukoc Biol*, 85, 595-605.

ANNICOTTE, J. S., SCHOONJANS, K. & AUWERX, J. 2004. Expression of the liver X receptor alpha and beta in embryonic and adult mice. *Anat Rec A Discov Mol Cell Evol Biol*, 277, 312-6.

ANTHONY, R. M., WERMELING, F. & RAVETCH, J. V. 2012. Novel roles for the IgG Fc glycan. *Ann N Y Acad Sci*, 1253, 170-80.

BALLARD, C., GAUTHIER, S., CORBETT, A., BRAYNE, C., AARSLAND, D. & JONES, E. 2011. Alzheimer's disease. *Lancet*, 377, 1019-31.

BAUD, V. & KARIN, M. 2001. Signal transduction by tumor necrosis factor and its relatives. *Trends Cell Biol*, 11, 372-7.

BEDARD, K. & KRAUSE, K. H. 2007. The NOX family of ROS-generating NADPH oxidases: physiology and pathophysiology. *Physiol Rev*, 87, 245-313.

BILLADEAU, D. D. & LEIBSON, P. J. 2002. ITAMs versus ITIMs: striking a balance during cell regulation. *J Clin Invest*, 109, 161-8.

BJERKE, M. & ENGELBORGHS, S. 2018. Cerebrospinal Fluid Biomarkers for Early and Differential Alzheimer's Disease Diagnosis. *J Alzheimers Dis*, 62, 1199-1209.

BLENNOW, K., WALLIN, A., DAVIDSSON, P., FREDMAN, P., GOTTFRIES, C. G. & SVENNERHOLM, L. 1990. Intra-blood-brain-barrier synthesis of immunoglobulins in patients with dementia of the Alzheimer type. *Alzheimer Dis Assoc Disord*, 4, 79-86.

BOURNAZOS, S., WANG, T. T., DAHAN, R., MAAMARY, J. & RAVETCH, J. V. 2017. Signaling by Antibodies: Recent Progress. *Annu Rev Immunol*, 35, 285-311.

BREIJYEH, Z. & KARAMAN, R. 2020. Comprehensive Review on Alzheimer's Disease: Causes and Treatment. *Molecules*, 25.

BRUHNS, P., IANNASCOLI, B., ENGLAND, P., MANCARDI, D. A., FERNANDEZ, N., JORIEUX, S. & DAËRON, M. 2009. Specificity and affinity of human Fcgamma receptors and their polymorphic variants for human IgG subclasses. *Blood*, 113, 3716-25.

BURNS, K., MARTINON, F. & TSCHOPP, J. 2003. New insights into the mechanism of IL-1beta maturation. *Curr Opin Immunol*, 15, 26-30.

CALLAGHAN, J., NIXON, S., BUCCI, C., TOH, B. H. & STENMARK, H. 1999. Direct interaction of EEA1 with Rab5b. *Eur J Biochem*, 265, 361-6.

CAO, W., LI, J., YANG, K. & CAO, D. 2021. An overview of autophagy: Mechanism, regulation and research progress. *Bull Cancer*, 108, 304-322.

CAROW, B. & ROTTENBERG, M. E. 2014. SOCS3, a Major Regulator of Infection and Inflammation. *Front Immunol*, 5, 58.

CHADHA, R. & MEADOR-WOODRUFF, J. H. 2020. Downregulated AKT-mTOR signaling pathway proteins in dorsolateral prefrontal cortex in Schizophrenia. *Neuropsychopharmacology*, 45, 1059-1067.

CHEN, Q., CHEN, Y. Q., YE, H. Y., YU, J. Q., SHI, Q. Q. & HUANG, Y. 2015. [The mechanism of tenuigenin for eliminating waste product accumulation in cerebral neurons of Alzheimer's disease rats via ubiquitin-proteasome pathway]. *Zhongguo Zhong Xi Yi Jie He Za Zhi*, 35, 327-32.

CHRISTOFORIDIS, S., MCBRIDE, H. M., BURGOYNE, R. D. & ZERIAL, M. 1999. The Rab5 effector EEA1 is a core component of endosome docking. *Nature*, 397, 621-5.

CROCKER, P. R., MCMILLAN, S. J. & RICHARDS, H. E. 2012a. CD33-related siglecs as potential modulators of inflammatory responses. *Ann N Y Acad Sci*, 1253, 102-11.

CROCKER, P. R., MCMILLAN, S. J. & RICHARDS, H. E. 2012b. CD33‑related siglecs as potential modulators of inflammatory responses. *Annals of the New York Academy of Sciences,* 1253, 102-111.

CROCKER, P. R., PAULSON, J. C. & VARKI, A. 2007. Siglecs and their roles in the immune system. *Nat Rev Immunol,* 7, 255-66.

CROTZER, V. L. & BLUM, J. S. 2008. Cytosol to lysosome transport of intracellular antigens during immune surveillance. *Traffic,* 9, 10-6.

DARNELL, J. E., JR. 1997. STATs and gene regulation. *Science,* 277, 1630-5.

DESHMANE, S. L., KREMLEV, S., AMINI, S. & SAWAYA, B. E. 2009. Monocyte chemoattractant protein-1 (MCP-1): an overview. *J Interferon Cytokine Res,* 29, 313-26.

DETER, R. L. & DE DUVE, C. 1967. Influence of glucagon, an inducer of cellular autophagy, on some physical properties of rat liver lysosomes. *J Cell Biol,* 33, 437-49.

DORSZEWSKA, J., PRENDECKI, M., OCZKOWSKA, A., DEZOR, M. & KOZUBSKI, W. 2016. Molecular Basis of Familial and Sporadic Alzheimer's Disease. *Curr Alzheimer Res,* 13, 952-63.

DUETSCH, G., ILLIG, T., LOESGEN, S., ROHDE, K., KLOPP, N., HERBON, N., GOHLKE, H., ALTMUELLER, J. & WJST, M. 2002. STAT6 as an asthma candidate gene: polymorphism-screening, association and haplotype analysis in a Caucasian sib-pair study. *Hum Mol Genet,* 11, 613-21.

EDWARDS, S. W. & WATSON, F. 1995. The cell biology of phagocytes. *Immunol Today,* 16, 508-10.

EISHINGDRELO, H. & KONGSAMUT, S. 2013. Minireview: Targeting GPCR Activated ERK Pathways for Drug Discovery. *Curr Chem Genom Transl Med,* 7, 9-15.

FAZELI, G. & WEHMAN, A. M. 2017. Safely removing cell debris with LC3-associated phagocytosis. *Biol Cell,* 109, 355-363.

FULLER, J. P., STAVENHAGEN, J. B. & TEELING, J. L. 2014. New roles for Fc receptors in neurodegeneration-the impact on Immunotherapy for Alzheimer's Disease. *Front Neurosci,* 8, 235.

GALLARDO, G. & HOLTZMAN, D. M. 2017. Antibody Therapeutics Targeting Aβ and Tau. *Cold Spring Harb Perspect Med,* 7.

GLICK, D., BARTH, S. & MACLEOD, K. F. 2010. Autophagy: cellular and molecular mechanisms. *J Pathol,* 221, 3-12.

GORDON, S. 2016. Phagocytosis: An Immunobiologic Process. *Immunity,* 44, 463-475.

GUDGEON, J., MARÍN-RUBIO, J. L. & TROST, M. 2022. The role of macrophage scavenger receptor 1 (MSR1) in inflammatory disorders and cancer. *Front Immunol,* 13, 1012002.

HE, C. & KLIONSKY, D. J. 2009. Regulation mechanisms and signaling pathways of autophagy. *Annu Rev Genet,* 43, 67-93.

HECKMANN, B. L., BOADA-ROMERO, E., CUNHA, L. D., MAGNE, J. & GREEN, D. R. 2017. LC3-Associated Phagocytosis and Inflammation. *J Mol Biol,* 429, 3561-3576.

HERRUP, K. 2010. Reimagining Alzheimer's disease--an age-based hypothesis. *J Neurosci,* 30, 16755-62.

HUANG, C., JACOBSON, K. & SCHALLER, M. D. 2004. MAP kinases and cell migration. *J Cell Sci,* 117, 4619-28.

IHLE, J. N., WITTHUHN, B. A., QUELLE, F. W., YAMAMOTO, K. & SILVENNOINEN, O. 1995. Signaling through the hematopoietic cytokine receptors. *Annu Rev Immunol,* 13, 369-98.

JIE, C., TREYER, V., SCHIBLI, R. & MU, L. 2021. Tauvid™: The First FDA-Approved PET Tracer for Imaging Tau Pathology in Alzheimer's Disease. *Pharmaceuticals (Basel),* 14.

KAWAI, T. & AKIRA, S. 2010. The role of pattern-recognition receptors in innate immunity: update on Toll-like receptors. *Nat Immunol,* 11, 373-84.

KHREISS, T., JÓZSEF, L., POTEMPA, L. A. & FILEP, J. G. 2004. Opposing effects of C-reactive protein

isoforms on shear-induced neutrophil-platelet adhesion and neutrophil aggregation in whole blood. *Circulation,* 110, 2713-20.

KIBAYASHI, E., URAKAZE, M., KOBASHI, C., KISHIDA, M., TAKATA, M., SATO, A., YAMAZAKI, K. & KOBAYASHI, M. 2005. Inhibitory effect of pitavastatin (NK-104) on the C-reactive-protein-induced interleukin-8 production in human aortic endothelial cells. *Clin Sci (Lond),* 108, 515-21.

KRAUSE, C. D., MEI, E., MIROCHNITCHENKO, O., LAVNIKOVA, N., XIE, J., JIA, Y., HOCHSTRASSER, R. M. & PESTKA, S. 2006. Interactions among the components of the interleukin-10 receptor complex. *Biochem Biophys Res Commun,* 340, 377-85.

LAI, K. S., JIN, Y., GRAHAM, D. K., WITTHUHN, B. A., IHLE, J. N. & LIU, E. T. 1995. A kinase-deficient splice variant of the human JAK3 is expressed in hematopoietic and epithelial cancer cells. *J Biol Chem,* 270, 25028-36.

LEE, C. Y. & LANDRETH, G. E. 2010. The role of microglia in amyloid clearance from the AD brain. *J Neural Transm (Vienna),* 117, 949-60.

LEE, I. H. & FINKEL, T. 2009. Regulation of autophagy by the p300 acetyltransferase. *J Biol Chem,* 284, 6322-8.

LENG, F. & EDISON, P. 2021. Neuroinflammation and microglial activation in Alzheimer disease: where do we go from here? *Nat Rev Neurol,* 17, 157-172.

LEVE, F., DE SOUZA, W. & MORGADO-DÍAZ, J. A. 2008. A cross-link between protein kinase A and Rho-family GTPases signaling mediates cell-cell adhesion and actin cytoskeleton organization in epithelial cancer cells. *J Pharmacol Exp Ther,* 327, 777-88.

LEVINE, B. & KROEMER, G. 2008. Autophagy in the pathogenesis of disease. *Cell,* 132, 27-42.

LI, J., SHUI, X., SUN, R., WAN, L., ZHANG, B., XIAO, B. & LUO, Z. 2021. Microglial Phenotypic Transition: Signaling Pathways and Influencing Modulators Involved in Regulation in Central Nervous System Diseases. *Front Cell Neurosci,* 15, 736310.

LI, K. & UNDERHILL, D. M. 2020. C-Type Lectin Receptors in Phagocytosis. *Curr Top Microbiol Immunol,* 429, 1-18.

LI, Q. & BARRES, B. A. 2018. Microglia and macrophages in brain homeostasis and disease. *Nat Rev Immunol,* 18, 225-242.

LI, Q., LIU, Y. & SUN, M. 2017. Autophagy and Alzheimer's Disease. *Cell Mol Neurobiol,* 37, 377-388.

LI, Y., TAN, M.-S., JIANG, T. & TAN, L. 2014. Microglia in Alzheimer's Disease. *BioMed Research International,* 2014, 437483.

LIANG, Y., BUCKLEY, T. R., TU, L., LANGDON, S. D. & TEDDER, T. F. 2001. Structural organization of the human MS4A gene cluster on Chromosome 11q12. *Immunogenetics,* 53, 357-68.

LINNARTZ-GERLACH, B., KOPATZ, J. & NEUMANN, H. 2014. Siglec functions of microglia. *Glycobiology,* 24, 794-9.

LIU, M., GAO, S., ELHASSAN, R. M., HOU, X. & FANG, H. 2021. Strategies to overcome drug resistance using SHP2 inhibitors. *Acta Pharm Sin B,* 11, 3908-3924.

LIVNAH, O., STURA, E. A., MIDDLETON, S. A., JOHNSON, D. L., JOLLIFFE, L. K. & WILSON, I. A. 1999. Crystallographic evidence for preformed dimers of erythropoietin receptor before ligand activation. *Science,* 283, 987-90.

MA, J., YU, J. T. & TAN, L. 2015. MS4A Cluster in Alzheimer's Disease. *Mol Neurobiol,* 51, 1240-8.

MCGEER, E. G. & MCGEER, P. L. 2010. Neuroinflammation in Alzheimer's disease and mild cognitive impairment: a field in its infancy. *J Alzheimers Dis,* 19, 355-61.

MEIJER, A. J. & CODOGNO, P. 2007. AMP-activated protein kinase and autophagy. *Autophagy,* 3, 238-40.

MENDIOLA, A. S. & CARDONA, A. E. 2018. The IL-1β phenomena in neuroinflammatory diseases. *J*

Neural Transm (Vienna), 125, 781-795.

MIKITA, T., DANIEL, C., WU, P. & SCHINDLER, U. 1998. Mutational analysis of the STAT6 SH2 domain. *J Biol Chem,* 273, 17634-42.

MIZUSHIMA, N. 2005. A(beta) generation in autophagic vacuoles. *J Cell Biol,* 171, 15-7.

MONTGOMERY, S. L. & BOWERS, W. J. 2012. Tumor necrosis factor-alpha and the roles it plays in homeostatic and degenerative processes within the central nervous system. *J Neuroimmune Pharmacol,* 7, 42-59.

MOSMANN, T. R. & COFFMAN, R. L. 1987. Two types of mouse helper T-cell clone Implications for immune regulation. *Immunol Today,* 8, 223-7.

NAISMITH, J. H., DEVINE, T. Q., BRANDHUBER, B. J. & SPRANG, S. R. 1995. Crystallographic evidence for dimerization of unliganded tumor necrosis factor receptor. *J Biol Chem,* 270, 13303-7.

NAKAGAWA, Y. & CHIBA, K. 2014. Role of microglial m1/m2 polarization in relapse and remission of psychiatric disorders and diseases. *Pharmaceuticals (Basel),* 7, 1028-48.

NAKATOGAWA, H., SUZUKI, K., KAMADA, Y. & OHSUMI, Y. 2009. Dynamics and diversity in autophagy mechanisms: lessons from yeast. *Nat Rev Mol Cell Biol,* 10, 458-67.

NAUSEEF, W. M. 2014. Myeloperoxidase in human neutrophil host defence. *Cell Microbiol,* 16, 1146-55.

NEEL, B. G., GU, H. & PAO, L. 2003. The 'Shp'ing news: SH2 domain-containing tyrosine phosphatases in cell signaling. *Trends Biochem Sci,* 28, 284-93.

NIXON, R. A., WEGIEL, J., KUMAR, A., YU, W. H., PETERHOFF, C., CATALDO, A. & CUERVO, A. M. 2005. Extensive involvement of autophagy in Alzheimer disease: an immuno-electron microscopy study. *J Neuropathol Exp Neurol,* 64, 113-22.

O'SHEA, J. J., SCHWARTZ, D. M., VILLARINO, A. V., GADINA, M., MCINNES, I. B. & LAURENCE, A. 2015. The JAK-STAT pathway: impact on human disease and therapeutic intervention. *Annu Rev Med,* 66, 311-28.

OKUN, E., MATTSON, M. P. & ARUMUGAM, T. V. 2010. Involvement of Fc receptors in disorders of the central nervous system. *Neuromolecular Med,* 12, 164-78.

OUYANG, W., RUTZ, S., CRELLIN, N. K., VALDEZ, P. A. & HYMOWITZ, S. G. 2011. Regulation and functions of the IL-10 family of cytokines in inflammation and disease. *Annu Rev Immunol,* 29, 71-109.

OWEN, K. L., BROCKWELL, N. K. & PARKER, B. S. 2019. JAK-STAT Signaling: A Double-Edged Sword of Immune Regulation and Cancer Progression. *Cancers (Basel),* 11.

PARAJULI, B., SONOBE, Y., HORIUCHI, H., TAKEUCHI, H., MIZUNO, T. & SUZUMURA, A. 2013. Oligomeric amyloid β induces IL-1β processing via production of ROS: implication in Alzheimer's disease. *Cell Death Dis,* 4, e975.

PARZYCH, K. R. & KLIONSKY, D. J. 2014. An overview of autophagy: morphology, mechanism, and regulation. *Antioxid Redox Signal,* 20, 460-73.

POWIS, K. & DE VIRGILIO, C. 2016. Conserved regulators of Rag GTPases orchestrate amino acid-dependent TORC1 signaling. *Cell Discov,* 2, 15049.

PRINZ, M., PRILLER, J., SISODIA, S. S. & RANSOHOFF, R. M. 2011. Heterogeneity of CNS myeloid cells and their roles in neurodegeneration. *Nat Neurosci,* 14, 1227-35.

QU, L., MATZ, A. J., KARLINSEY, K., CAO, Z., VELLA, A. T. & ZHOU, B. 2022. Macrophages at the Crossroad of Meta-Inflammation and Inflammaging. *Genes (Basel),* 13.

R, A. A. 2019. Risk factors for Alzheimer's disease. *Folia Neuropathol,* 57, 87-105.

RABANAL-RUIZ, Y., OTTEN, E. G. & KOROLCHUK, V. I. 2017. mTORC1 as the main gateway to autophagy. *Essays Biochem,* 61, 565-584.

RABINOVICH, G. A., VAN KOOYK, Y. & COBB, B. A. 2012. Glycobiology of immune responses. *Ann N Y Acad Sci,* 1253, 1-15.

RANE, S. G. & REDDY, E. P. 1994. JAK3: a novel JAK kinase associated with terminal differentiation of

hematopoietic cells. *Oncogene,* 9, 2415-23.

RANSOHOFF, R. M. & PERRY, V. H. 2009. Microglial physiology: unique stimuli, specialized responses. *Annu Rev Immunol,* 27, 119-45.

RAVETCH, J. V. & LANIER, L. L. 2000. Immune inhibitory receptors. *Science,* 290, 84-9.

RAWLINGS, J. S., ROSLER, K. M. & HARRISON, D. A. 2004. The JAK/STAT signaling pathway. *J Cell Sci,* 117, 1281-3.

RE, F., MUZIO, M., DE ROSSI, M., POLENTARUTTI, N., GIRI, J. G., MANTOVANI, A. & COLOTTA, F. 1994. The type II "receptor" as a decoy target for interleukin 1 in polymorphonuclear leukocytes: characterization of induction by dexamethasone and ligand binding properties of the released decoy receptor. *J Exp Med,* 179, 739-43.

REZAI-ZADEH, K., GATE, D., GOWING, G. & TOWN, T. 2011. How to get from here to there: macrophage recruitment in Alzheimer's disease. *Curr Alzheimer Res,* 8, 156-63.

RIDLEY, A. J., SCHWARTZ, M. A., BURRIDGE, K., FIRTEL, R. A., GINSBERG, M. H., BORISY, G., PARSONS, J. T. & HORWITZ, A. R. 2003. Cell migration: integrating signals from front to back. *Science,* 302, 1704-9.

ROGERS, J., LI, R., MASTROENI, D., GROVER, A., LEONARD, B., AHERN, G., CAO, P., KOLODY, H., VEDDERS, L., KOLB, W. P. & SABBAGH, M. 2006. Peripheral clearance of amyloid beta peptide by complement C3-dependent adherence to erythrocytes. *Neurobiol Aging,* 27, 1733-9.

ROMAO, S. & MÜNZ, C. 2014. LC3-associated phagocytosis. *Autophagy,* 10, 526-8.

ROSALES, C. & URIBE-QUEROL, E. 2017. Phagocytosis: A Fundamental Process in Immunity. *Biomed Res Int,* 2017, 9042851.

ROSSET, C., NETTO, C. B. O. & ASHTON-PROLLA, P. 2017. TSC1 and TSC2 gene mutations and their implications for treatment in Tuberous Sclerosis Complex: a review. *Genet Mol Biol,* 40, 69-79.

SALMINEN, A. & KAARNIRANTA, K. 2009. Siglec receptors and hiding plaques in Alzheimer's disease. *J Mol Med (Berl),* 87, 697-701.

SAVAGNER, P., GILLES, C., NEWGREEN, D. F., SATO, H. & THOMPSON, E. W. 2005. Matrix metalloproteases and epithelial-to-mesenchymal transition: implications for carcinoma metastasis. *Rise and fall of epithelial phenotype: concepts of epithelial-mesenchymal transition,* 297-315.

SCHINDLER, C. & STREHLOW, I. 2000. Cytokines and STAT signaling. *Adv Pharmacol,* 47, 113-74.

SCHÜLKE, S. 2018. Induction of Interleukin-10 Producing Dendritic Cells As a Tool to Suppress Allergen-Specific T Helper 2 Responses. *Front Immunol,* 9, 455.

SCHWAB, C. & MCGEER, P. L. 2008. Inflammatory aspects of Alzheimer disease and other neurodegenerative disorders. *J Alzheimers Dis,* 13, 359-69.

SEIF, F., KHOSHMIRSAFA, M., AAZAMI, H., MOHSENZADEGAN, M., SEDIGHI, G. & BAHAR, M. 2017. The role of JAK-STAT signaling pathway and its regulators in the fate of T helper cells. *Cell Commun Signal,* 15, 23.

SPROSTON, N. R. & ASHWORTH, J. J. 2018. Role of C-Reactive Protein at Sites of Inflammation and Infection. *Front Immunol,* 9, 754.

STROHMEYER, R., RAMIREZ, M., COLE, G. J., MUELLER, K. & ROGERS, J. 2002. Association of factor H of the alternative pathway of complement with agrin and complement receptor 3 in the Alzheimer's disease brain. *J Neuroimmunol,* 131, 135-46.

SU, F., BAI, F. & ZHANG, Z. 2016. Inflammatory Cytokines and Alzheimer's Disease: A Review from the Perspective of Genetic Polymorphisms. *Neurosci Bull,* 32, 469-80.

SUZUKI, K. & TERRY, R. D. 1967. Fine structural localization of acid phosphatase in senile plaques in Alzheimer's presenile dementia. *Acta Neuropathol,* 8, 276-84.

SZUMANSKA, G., VORBRODT, A. W., MANDYBUR, T. I. & WISNIEWSKI, H. M. 1987. Lectin histochemistry

of plaques and tangles in Alzheimer's disease. *Acta Neuropathol,* 73, 1-11.

TAKAI, T. 2002. Roles of Fc receptors in autoimmunity. *Nat Rev Immunol,* 2, 580-92.

TENHUMBERG, S., SCHUSTER, B., ZHU, L., KOVALEVA, M., SCHELLER, J., KALLEN, K. J. & ROSE-JOHN, S. 2006. gp130 dimerization in the absence of ligand: preformed cytokine receptor complexes. *Biochem Biophys Res Commun,* 346, 649-57.

THINAKARAN, G. & KOO, E. H. 2008. Amyloid precursor protein trafficking, processing, and function. *J Biol Chem,* 283, 29615-9.

TIAN, M., QI, Y., ZHANG, X., WU, Z., CHEN, J., CHEN, F., GUAN, W. & ZHANG, S. 2020. Regulation of the JAK2-STAT5 Pathway by Signaling Molecules in the Mammary Gland. *Front Cell Dev Biol,* 8, 604896.

TIAN, Y., CHANG, J. C., GREENGARD, P. & FLAJOLET, M. 2014. The convergence of endosomal and autophagosomal pathways: implications for APP-CTF degradation. *Autophagy,* 10, 694-6.

TILLETT, W. S. & FRANCIS, T. 1930. SEROLOGICAL REACTIONS IN PNEUMONIA WITH A NON-PROTEIN SOMATIC FRACTION OF PNEUMOCOCCUS. *J Exp Med,* 52, 561-71.

TRACY, K. & MACLEOD, K. F. 2007. Regulation of mitochondrial integrity, autophagy and cell survival by BNIP3. *Autophagy,* 3, 616-9.

VERMA, R. P. & HANSCH, C. 2007. Matrix metalloproteinases (MMPs): chemical-biological functions and (Q)SARs. *Bioorg Med Chem,* 15, 2223-68.

VOLANAKIS, J. E. 2001. Human C-reactive protein: expression, structure, and function. *Mol Immunol,* 38, 189-97.

VON BERNHARDI, R., TICHAUER, J. E. & EUGENÍN, J. 2010. Aging-dependent changes of microglial cells and their relevance for neurodegenerative disorders. *J Neurochem,* 112, 1099-114.

WALSH, D., MCCARTHY, J., O'DRISCOLL, C. & MELGAR, S. 2013. Pattern recognition receptors--molecular orchestrators of inflammation in inflammatory bowel disease. *Cytokine Growth Factor Rev,* 24, 91-104.

WANG, W. Y., TAN, M. S., YU, J. T. & TAN, L. 2015. Role of pro-inflammatory cytokines released from microglia in Alzheimer's disease. *Ann Transl Med,* 3, 136.

WANG, Y. & ZHANG, H. 2019. Regulation of Autophagy by mTOR Signaling Pathway. *Adv Exp Med Biol,* 1206, 67-83.

WEGMANN, S., BIERNAT, J. & MANDELKOW, E. 2021. A current view on Tau protein phosphorylation in Alzheimer's disease. *Curr Opin Neurobiol,* 69, 131-138.

WEIDBERG, H., SHVETS, E. & ELAZAR, Z. 2011. Biogenesis and cargo selectivity of autophagosomes. *Annu Rev Biochem,* 80, 125-56.

WIBLE, D. J. & BRATTON, S. B. 2018. Reciprocity in ROS and autophagic signaling. *Curr Opin Toxicol,* 7, 28-36.

WIDMANN, C., GIBSON, S., JARPE, M. B. & JOHNSON, G. L. 1999. Mitogen-activated protein kinase: conservation of a three-kinase module from yeast to human. *Physiol Rev,* 79, 143-80.

WILCOCK, D. M., ROJIANI, A., ROSENTHAL, A., SUBBARAO, S., FREEMAN, M. J., GORDON, M. N. & MORGAN, D. 2004. Passive immunotherapy against Abeta in aged APP-transgenic mice reverses cognitive deficits and depletes parenchymal amyloid deposits in spite of increased vascular amyloid and microhemorrhage. *J Neuroinflammation,* 1, 24.

WILLCOCKS, L. C., SMITH, K. G. & CLATWORTHY, M. R. 2009. Low-affinity Fcgamma receptors, autoimmunity and infection. *Expert Rev Mol Med,* 11, e24.

WU, L., ROSA-NETO, P., HSIUNG, G. Y., SADOVNICK, A. D., MASELLIS, M., BLACK, S. E., JIA, J. & GAUTHIER, S. 2012. Early-onset familial Alzheimer's disease (EOFAD). *Can J Neurol Sci,* 39, 436-45.

XU, D. & QU, C. K. 2008. Protein tyrosine phosphatases in the JAK/STAT pathway. *Front Biosci,* 13, 4925-

32.

YADAV, A., SAINI, V. & ARORA, S. 2010. MCP-1: chemoattractant with a role beyond immunity: a review. *Clin Chim Acta,* 411**,** 1570-9.

YAZDI, A. S. & GHORESCHI, K. 2016. The Interleukin-1 Family. *Adv Exp Med Biol,* 941**,** 21-29.

YIN, R. H., YU, J. T. & TAN, L. 2015. The Role of SORL1 in Alzheimer's Disease. *Mol Neurobiol,* 51**,** 909-18.

YORIMITSU, T. & KLIONSKY, D. J. 2005. Autophagy: molecular machinery for self-eating. *Cell Death Differ,* 12 Suppl 2**,** 1542-52.

ZEGEYE, M. M., LINDKVIST, M., FÄLKER, K., KUMAWAT, A. K., PARAMEL, G., GRENEGÅRD, M., SIRSJÖ, A. & LJUNGBERG, L. U. 2018. Activation of the JAK/STAT3 and PI3K/AKT pathways are crucial for IL-6 trans-signaling-mediated pro-inflammatory response in human vascular endothelial cells. *Cell Communication and Signaling,* 16**,** 55.

ZELOVÁ, H. & HOŠEK, J. 2013. TNF-α signalling and inflammation: interactions between old acquaintances. *Inflamm Res,* 62**,** 641-51.

ZHANG, J. & NEY, P. A. 2009. Role of BNIP3 and NIX in cell death, autophagy, and mitophagy. *Cell Death Differ,* 16**,** 939-46.

ZHANG, W. & LIU, H. T. 2002. MAPK signal pathways in the regulation of cell proliferation in mammalian cells. *Cell Res,* 12**,** 9-18.

ZHAO, L. 2019. CD33 in Alzheimer's Disease - Biology, Pathogenesis, and Therapeutics: A Mini-Review. *Gerontology,* 65**,** 323-331.

ZHOU, F., VAN LAAR, T., HUANG, H. & ZHANG, L. 2011. APP and APLP1 are degraded through autophagy in response to proteasome inhibition in neuronal cells. *Protein Cell,* 2**,** 377-83.

ZIEMBA, B. P., PILLING, C., CALLEJA, V., LARIJANI, B. & FALKE, J. J. 2013. The PH domain of phosphoinositide-dependent kinase-1 exhibits a novel, phospho-regulated monomer-dimer equilibrium with important implications for kinase domain activation: single-molecule and ensemble studies. *Biochemistry,* 52**,** 4820-9.

ZUROFF, L., DALEY, D., BLACK, K. L. & KORONYO-HAMAOUI, M. 2017. Clearance of cerebral Aβ in Alzheimer's disease: reassessing the role of microglia and monocytes. *Cellular and Molecular Life Sciences,* 74**,** 2167-2201.